Hillslope and Climatic Controls on Hydrologic Fluxes

by

Guido Daniel Salvucci

B.S. in Atmospheric Fluid Mechanics
New York University (1989)

B.E. in Civil Engineering
The Cooper Union for the Advancement of Arts and Science (1989)

S.M. in Civil and Environmental Engineering
Massachusetts Institute of Technology (1992)

Submitted to the Department of Civil and Environmental Engineering in Partial Fulfillment of the Requirements for the Degree of

Doctor of Philosophy

at the
Massachusetts Institute of Technology

May, 1994

Author _____
Department of Civil and Environmental Engineering
April, 1994

Certified By _____
Dara Entekhabi
Assistant Professor of Civil and Environmental Engineering
Thesis Supervisor

Accepted By _____
Joseph M. Sussman
Chairman, Departmental Committee on Graduate Studies

Hillslope and Climatic Controls on Hydrologic Fluxes
by
Guido Daniel Salvucci

Submitted to the Department of Civil and Environmental Engineering in April, 1994
in Partial Fulfillment of the Requirements for the Degree of
Doctor of Philosophy

Abstract

Hydrologic fluxes display strong spatial variability related to the physiographic characteristics of drainage basins. Understanding the processes and couplings which determine this relationship is critical to effective use of measured (e.g. Digital Elevation Maps) or parameterized (e.g. stream ordering) descriptions of physiographic properties in characterizing hydrologic response.

The position and shape of the water table has long been considered to be a useful diagnostic both for field analysis of the spatial structure of hydrologic behavior and for initializing hydrologic forecasting models. Water tables near the surface often indicate areas which contribute strongly to surface runoff generation, yield evaporation at climate demanded rates, and discharge saturated zone groundwater. Deeper water tables typically indicate drier areas where evaporation is suppressed and infiltration enhanced, therefore promoting groundwater recharge. The long time integral of these fluxes over an area forms the local climatic hydrologic cycle.

This cycle is driven by the interaction of atmospheric forcing with the partially saturated soils at the land-atmosphere boundary, the direct effects of which are the surface hydrologic fluxes of infiltration, evapotranspiration and surface runoff. Under the action of capillary and gravitational forces, the unsaturated (vadose) zone responds by filtering the fluxes and by balancing them, in the long term, through the recharging of moisture to or lifting of moisture from the saturated zone. In the saturated zone, where hydraulic conductivities are much larger and capillary gradients are eliminated, the groundwater is free to respond to the lateral pressure gradients that result from topographic and geologic variations. The dependence of these fluxes on the position of the water table is shown to yield a negative feedback between changes in elevation and flow convergence. One result of this behavior is the potential to develop a continuously adjusting but stable water table in equilibrium with the climatic forcing.

This thesis develops a methodology for coupling saturated and unsaturated flows which allows analytic determination of the equilibrium water table and the corresponding

spatial structure of recharge, discharge, evaporation and runoff. The coupling is accomplished by using the equivalent steady state soil moisture profile, i.e. the steady vadose zone moisture profile which transmits the mean unsaturated zone flux, as an approximation of the mean pre-storm and pre-interstorm moisture profiles. In this way the soil's infiltration, exfiltration and storage capacity, which partly determine the response of the landsurface to atmospheric forcing, are related to the water table depth and the mean moisture flux. This simple parameterization of the highly dynamic unsaturated zone moisture state by the equivalent steady profile is shown to be satisfactory through both analytic perturbation analysis of the governing equations and by comparison of analytic results with full numerical flow simulation. Following *Eagleson* [1978], the mean surface hydrologic fluxes (infiltration, runoff and evaporation) are derived analytically by integrating the system's infiltration and exfiltration capacity over probability distributions of storm and interstorm atmospheric forcings.

Continuity (throughout a hillslope) of the mean moisture flux between the land-atmosphere interface, the unsaturated zone, and the saturated zone provides closure to the system. The equilibrium water table and the corresponding spatial structure of climatic mean recharge, discharge, evaporation and surface runoff production are thereby determined. This method of analysis provides a tool for the systematic study of how characteristics of the atmospheric forcing (e.g. mean precipitation, evaporative demand, and storm intermittency and intensity), soil properties, and geologic features (e.g. topographic and lithographic) interact to yield observed spatial patterns of distinct hydrologic behavior within watersheds.

Application to simplified and idealized hillslope geometries reveals spatial patterns in good qualitative agreement with field observations. The case studies demonstrate that the wide range of behavior observed in nature are reproducible within the observed range of climatic, geologic and soil parameters. Partial analysis of the full system yields a few dimensional parameter groups, the relative values of which are indicative of transitions between geologic, soil and climate controlled conditions and the presence or absence of characteristic hydrologic zones such as seepage faces, recharge areas, hinges, transition zones, discharge areas, and partial areas of surface runoff production.

Thesis Supervisor: Dara Entekhabi
Title: Assistant Professor of Civil and Environmental Engineering

ACKNOWLEDGMENTS

I thank Dara Entekhabi for his mentoring, support and friendship. His sense of humor and perspective on life and academics, which he has shared freely even as a thesis supervisor, has made this journey one of enjoyable play rather than distressing work. I hope to carry with me his unique ability to be both (extremely) successful and at the same time light-hearted. The research accomplishments and findings of Professor Peter S. Eagleson are the source of inspiration for this work. He is a true giant in this field (and gentleman and friend), and I thank him for sharing his work and insight with me. The work in these pages owes its approach and philosophy to him. I thank Ignacio Rodriguez-Iturbe, Rafael Bras, and Ted Engman for serving on my thesis committee and sharing their insights, motivations and experience. I also thank the faculty at the Parsons lab (Mei, Harleman, McLaughlin, Gelhar, Stolzenbach...) and at EAPS (Stone, Rosen, Lindzen, Williams...) for their excellent teaching of not only methodology but also of the context of their research. I thank my colleagues at the Parsons lab and in the "Entekhabi Group" for their friendship and support (and for the great defense party).

The greatest support of course has come from my fiancé Amy. She is the love of my life and my best friend. She has always believed in me, understood me, and encouraged me. She has made me truly happy, has filled my life with fun and newness, and has kept my life in balance throughout my stay at MIT. I thank Chris for his absolute and unconditioned friendship throughout every stage of my life from elementary school through defending this thesis. I thank my friends outside the lab for keeping things fun. I thank my mother and father for their support, guidance and all that they have taught me through their incredible parenting. I thank them and my grandparents, sisters, aunts, and uncles for a great family life of love, support and fun.

In addition, I would like to thank the National Aeronautics and Space Administration (NASA) for supporting this research through subcontract NAS 5-31721.

TABLE OF CONTENTS

Abstract 3

Acknowledgments 7

Table of Contents 9

List of Figures 15

List of Tables 23

Notation List 25

1. Introduction 37
    a. Scope and Relevance 37
    b. Overview of Problem, Analytic Approach, and Assumptions 43
        1. The Equilibrium Water Balance at a Point 43
        2. The Equilibrium Water Table 45
        3. Basin Geometry 49
        4. Influence of Physiographic Factors on Hydrologic Response 49
    c. Relevant Literature 51
        1. Running Water Balance Models 54
        2. Equilibrium Water Balance Models 57

2. Tools for Equilibrium Water Balance Model Building 61
    a. Background and Assumptions 61
    b. Hydrologic Processes and Atmospheric Forcing 62
    c. Analysis of Moisture Profiles 66
        1. Moisture Profiles under Deep Water Table Conditions 68
        2. Moisture Profiles under Shallow Water Table Conditions 72
    d. The Time Compression Approximation 77
        1. Test of the TCA under Uniform Initial Conditions 80

2. Test of the TCA under Mean Initial Conditions 83
3. Test of the TCA under Equivalent Steady Initial Conditions 89
e. Implications for Event Based Water Balance Models 94
f. Conclusions 98

3. Modification and Testing of a Statistical-Dynamical Model of the Equilibrium Water Balance for Soils Bounded by Deep Water Tables 101
a. Background 101
b. Model Review 102
1. General Framework 102
2. Climate Forcing 102
3. Soil Moisture Processes 104
4. Mean Annual Infiltration 106
5. Mean Annual Bare Soil Evaporation 108
6. Recharge 109
7. Equilibrium Water Balance Partitioning 109
c. Modifications 110
d. Tests and Discussion 112
1. The Equilibrium Soil Moisture and the Equivalent Steady State Moisture Profile 117
e. Requirements for Extension to Near Surface Water Table Conditions 123
f. Conclusions 124

4. Process Studies 127
a. Background 127
b. The Steady State Moisture Profile 127
1. Derivation 129
2. Inversion 137
c. The Storage Capacity of the Unsaturated Zone at Equilibrium With the Water Table 141
d. Infiltration into Soils Bounded by a Water Table 143
1. Derivation of Approximate Solution 145

2. Example Applications of Approximate Infiltration Equations 154
3. Explicit Approximation of the Infiltration Capacity 159
4. Two Term Solution for Application to Current Model 167
e. Exfiltration from Soils Bounded by a Water Table 171
f. Summary 172

5. Expected Value of Hydrologic Fluxes under Conditions of Shallow Water Table 173
a. Background 173
b. Bare Soil Evaporation 174
c. Infiltration Excess Runoff 176
d. Storage Excess Runoff 181
e. The Equilibrium Water Balance in the Presence of a Water Table 183
f. Summary 187

6. The Spatial Structure of Surface Fluxes under the Influence of Saturated-Unsaturated Zone Coupling, Climate Forcing and Geological Constraints 189
a. Background 189
b. Coupling the Saturated and Unsaturated Zones 190
c. Case Studies and Supporting Field Evidence 195
1. Equilibrium Coupled Saturated-Unsaturated Flow on Inclined Surfaces 195
2. Influence of Hydrogeologic and Climatic Factors on Hillslope Hydrologic Fluxes 201
3. Supporting Field Evidence 216
d. Conclusions and an Index of Geological, Climatic and Soil Control 219

7. Key Findings and Planned Research Extensions 223
a. Key Findings 223
b. Planned Research Extensions 224

Appendix A. Soil Hydraulic Models 227
Appendix B. Infiltration into Unbounded Soils 229
References 233

LIST OF FIGURES

Fig. 1.1	Spatial structure of recharge and discharge in Canadian prairie [Toth, 1966]	40
Fig. 1.2	Distribution of saturated areas during storm [Kirkby, 1978]	41
Fig. 1.3	Scaling of mean annual runoff with area [Moore and Morgan, 1969]	42
Fig. 1.4	Idealized hillslope hydrology and sub-process boundaries	46
Fig. 1.5	Mathematical model for representing converging and diverging drainage patterns	50
Fig. 1.6	Classification of water balance models	53
Fig. 2.1	Characteristic moisture profiles: Deep water table case	69
Fig. 2.2	Cumulative power spectra of flow variability at various depths: Deep water table case	73
Fig. 2.3	Characteristic moisture profiles: Shallow water table case	75
Fig. 2.4	Cumulative power spectra of flow variability at various depths: Shallow water table case	76
Fig. 2.5	Illustration of time compression approximation (TCA) for infiltration	81
Fig. 2.6	Illustration of time compression approximation (TCA) for exfiltration	82
Fig. 2.7	Test of time compression approximation for infiltration using mean initial conditions: Deep water table case	85
Fig. 2.8	Test of time compression approximation for infiltration using mean initial conditions: Shallow water table case	86
Fig. 2.9	Test of time compression approximation for exfiltration using mean initial conditions: Deep water table case	88
Fig. 2.10	Test of time compression approximation for infiltration using equivalent steady state initial conditions: Deep water table case	90
Fig. 2.11	Test of time compression approximation for exfiltration using equivalent steady state initial conditions: Deep water table case	91

Fig. 2.12	Test of time compression approximation for infiltration using equivalent steady state initial conditions: Shallow water table case	92
Fig. 2.13	Test of time compression approximation for infiltration using hydrostatic initial conditions: Deep water table case	96
Fig. 2.14	Test of time compression approximation for exfiltration using hydrostatic initial conditions: Deep water table case	97
Fig. 3.1	Simplified hydro-climate system [*Eagleson*, 1978a]	103
Fig. 3.2	Comparison of finite-element simulated mean water balance and analytic equilibrium model estimates	115
Fig. 3.3	Soil moisture representation [*Eagleson*, 1978a]	118
Fig. 3.4	Characteristic soil moisture profiles for silt-loam, arid climate case study	122
Fig. 4.1	Comparison of Brooks-Corey (soiid lines) and Gardner type model (pluses and circles) of hydraulic conductivity as a function of capillary tension head	130
Fig. 4.2	Comparison of approximate capillary tension head profiles (solid lines) and numerical solution (circles) for clay (n=3.3)	134
Fig. 4.3	Comparison of approximate capillary tension head profiles (solid lines) and numerical solution (circles) for silt-loam (n=5.64)	135
Fig. 4.4	Comparison of approximate capillary tension head profiles (solid lines) and numerical solution (circles) for sand-loam (n=11.88)	136
Fig. 4.5	Definition sketch for approximating the storage capacity of the steady state soil moisture profile	142
Fig. 4.6	Definition sketch for linear wetting front model	146
Fig. 4.7	Definition sketch for wetting front control volume	151
Fig. 4.8	Wetting fronts in clay soil: analytic model vs. finite-element simulation	155
Fig. 4.9	Wetting fronts in silt soil: analytic model vs. finite-element simulation	156
Fig. 4.10	Wetting fronts in sand soil: analytic model vs. finite-element simulation	157
Fig. 4.11	Infiltration capacity into clay soil: analytic model vs. finite-element simulation	160

Fig. 4.12	Infiltration capacity into silt soil: analytic model vs. finite-element simulation	161
Fig. 4.13	Infiltration capacity into sand soil: analytic model vs. finite-element simulation	162
Fig. 4.14	Infiltration capacity into clay soil: comparison of approximate analytic models	168
Fig. 4.15	Infiltration capacity into silt soil: comparison of approximate analytic models	169
Fig. 4.16	Infiltration capacity into sand soil: comparison of approximate analytic models	170
Fig. 5.1	Definition sketch for infiltration excess runoff generation	177
Fig. 5.2	Comparison of mean finite-element simulated (circles) and analytic equilibrium estimated hydrologic fluxes for a range of depths to water table	186
Fig. 6.1	Definition sketch of simple planar hillslope for analysis of coupled flow saturated-unsaturated flow analysis	192
Fig. 6.2	Definition sketch of converging and diverging hillslopes for coupled saturated-unsaturated flow analysis	194
Fig. 6.3	Schematic showing required climate, soil and geology parameters	196
Fig. 6.4	Sensitivity of point equilibrium water balance to distance to water table for silt soil and semi-humid climate	197
Fig. 6.5	Modeled equilibrium hillslope fluxes: Base case	199
Fig. 6.6	Modeled equilibrium hillslope fluxes: Effect of reduced soil depth	202
Fig. 6.7	Modeled equilibrium hillslope fluxes: Effect of increased soil depth	204
Fig. 6.8	Modeled equilibrium hillslope fluxes: Effect of increased hillslope length	206
Fig. 6.9	Modeled equilibrium hillslope fluxes: Effect of reduced slope	207
Fig. 6.10	Modeled equilibrium hillslope fluxes: Effect of increased slope	208
Fig. 6.11	Modeled equilibrium hillslope fluxes: Humid climate	209
Fig. 6.12	Modeled equilibrium hillslope fluxes: Arid climate	211

Fig. 6.13	Modeled equilibrium hillslope fluxes: Clay soil	212
Fig. 6.14	Sensitivity of point equilibrium water balance to distance to water table for clay soil and semi-humid climate	213
Fig. 6.15	Modeled equilibrium hillslope fluxes: Effect of hillslope convergence	214
Fig. 6.16	Modeled equilibrium hillslope fluxes: Effect of hillslope divergence	215
Fig. 6.17	Spatial structure of recharge and discharge within a prairie environment [Toth, 1966]	217
Fig. 6.18	Relation of hillslope evapotranspiration to distance from channel [*Helvey et al.* ,1972]	220
Fig. 6.19	Simplified spatial structure of hydrologic fluxes and an index of climatic and geologic control	222
Fig. B.1	Infiltration capacity of an unbounded silt soil: comparison of four term explicit expression and finite-element simulation	231

LIST OF TABLES

2.1	Climate Parameters	67
2.2	Soil Parameters	67
2.3	Simulated Mean Annual Water Balance	68
3.1	Representative Brooks-Corey Soil Parameters	113
3.2	Representative Climate Parameters	113
3.3	Comparison of Simulated Mean Water Balance and Analytic Equilibrium Model Estimates	114
3.4	Sensitivity of Mean Hydrologic Fluxes to Soil Moisture at Equilibrium	121
3.5	Equilibrium and Equivalent Steady Soil Moisture	123
4.1	Representative Values of the Brooks-Corey Soil Parameters and Representative Climatic Limits of Normalized Flow Rate (q')	131
4.2	Comparison of Relative Error of Limiting Evaporation Formulae	139

NOTATION

(Dimensions given in brackets, L=length, T=time)

A_o	Second term of Philip infiltration equation, [L/T]
c	Pore disconnectedness index of Brooks-Corey soil hydraulic model, [dimensionless]
d	Exponent of soil moisture for Brooks-Corey unsaturated diffusivity, [dimensionless]
$D(\cdot)$	Unsaturated dimensional diffusivity [L^2/T]
E	Dimensionless parameter group appearing in the expression of mean annual bare soil evaporation, an index of the relative ability of soil to evaporate at the climate limiting rate
E_{p_A}	Annual (or seasonal) potential evaporation, [L]
E_{s_A}	Annual (or seasonal) bare soil evaporation, [L]
e_p	Annual average bare soil potential evaporation rate, [L/T]
$F_{e,event}$	Cumulative exfiltration up to current time during event (i.e. interstorm), [L]
$F_{i,event}$	Cumulative infiltration up to current time during event (i.e. storm), [L]
F_e^*	Potential cumulative exfiltration capacity, the time integral of the potential exfiltration capacity, [L]
F_i^*	Potential cumulative infiltration capacity, the time integral of the potential infiltration capacity, [L]
f_e^*	Potential exfiltration capacity, the exfiltration capacity of a soil with surface boundary condition at Ψ_{min} from time zero, [L/T]
f_i^*	Potential infiltration capacity, the infiltration capacity of a soil with surface boundary condition ponded from time zero, [L/T]

f_e^{TCA}	The exfiltration rate estimated using the time compression approximation, [L/T]
f_i^{TCA}	The infiltration rate estimated using the time compression approximation, [L/T]
$f_{e,event}$	The actual infiltration rate during an event (i.e. interstorm), [L/T]
$f_{i,event}$	The actual infiltration rate during an event (i.e. storm), [L/T]
$f_{e,event}^*$	Event exfiltration capacity, the exfiltration capacity of a soil whose surface has not been at Ψ_{min} from time zero, but instead started out with flux boundary condition, [L/T]
$f_{i,event}^*$	Event infiltration capacity, the infiltration capacity of a soil whose surface has not been ponded from time zero, but instead started out with flux boundary condition, [L/T]
H	Soil depth of modeled hillslope domains, [L]
I_A	Annual (or seasonal) infiltration, [L]
i	Rainfall intensity, [L/T]
$K(\cdot)$	Unsaturated hydraulic conductivity, [L/T]
K_S	Saturated hydraulic conductivity, [L/T]
m	Pore size distribution index of Brooks-Corey soil hydraulic model, [dimensionless]
m_v	Mean number of storms per year (season)
n	Exponent parameter of the Gardner model relating unsaturated conductivity to capillary tension head, [dimensionless]
n_e	Effective porosity, fraction of soil available to flow, [dimensionless]
P_A	Annual (or seasonal) precipitation, [L]
q	Moisture flux in vertical direction, positive for q in direction of z, i.e. evaporation, [L/T].

$q_o(t)$	Climate forcing at soil surface, positive for evaporation, [L/T]
R_{g_A}	Annual (or seasonal) groundwater recharge, [T]
R_{se}	Event storage excess surface runoff for water table bounded soils, [L]
$R_{ie,bounded}$	Event infiltration excess surface runoff for water table bounded soils, [L]
$R_{ie,unbounded}$	Event infiltration excess surface runoff for unbounded soils, [L]
$R_{ie_{A,bounded}}$	Annual (or seasonal) infiltration excess surface runoff for water table bounded soils, [L]
$R_{ie_{A,unbounded}}$	Annual (or seasonal) infiltration excess surface runoff for unbounded soils, [L]
R_{se_A}	Annual (or seasonal) storage excess surface runoff for water table bounded soils, [L]
S_e	Exfiltration desorptivity, [L/T$^{1/2}$]
S_i	Sorptivity, [L/T$^{1/2}$]
s	Relative soil saturation equal to the volume of water divided by the pore volume available to moisture flow, ranges from zero to one, [dimensionless]
$s(z)$	Vertical profile of soil saturation, [dimensionless]
$\hat{s}$	Average soil saturation of the linearly approximated wetting front during infiltration, [dimensionless]
s_*	Value of soil saturation at the ground surface, [dimensionless]
s_o	Equilibrium soil moisture, the value of soil saturation for which the analytical model mean fluxes are in balance, [dimensionless]
$s_{pi}(z)$	Vertical profile of soil saturation *p*rior to *i*nterstorm, [dimensionless]
$s_{ps}(z)$	Vertical profile of soil saturation *p*rior to *s*torm, [dimensionless]

$s_s(z)$	Vertical profile of steady state soil saturation, [dimensionless]
$s_s(z; q_{st} = \langle q \rangle)$	Vertical profile of equivalent steady state soil saturation corresponding to mean flux <q>, [dimensionless]
$s_s(z; q_{st} = 0)$	Vertical hydrostatic profile of soil saturation, [dimensionless]
T	Time in one year (season), [T]
t	Time variable, [T]
t_b	Interstorm duration, [T]
t_c	Concentration time, the time at which potential infiltration (exfiltration) capacity is equal to the storm intensity (interstorm potential evaporation), [T]
t_d	Drying time, the time from the beginning of an interstorm at which the soil surface dries to Ψ_{min} and the surface flux becomes soil controlled.
t_p	Ponding time, the time from the beginning of a rainstorm event at which surface ponding first occurs and the surface flux becomes soil controlled, [T]
t_r	Storm duration, [T]
t_s^*	Approximated time to column saturation assuming soil-controlled infiltration history, [T]
t_s^{**}	Approximated time to column saturation assuming atmosphere-controlled infiltration history, [T]
v_f	Velocity of descent of the tension saturated zone, [L]
w	Potential rate of capillary rise from water table to dry ground surface, [L/T]
Z^*	Depth to saturated zone for which the mean flux between the saturated and unsaturated zones is zero, [L]
Z_j	Vertical Cartesian location of the intersection of the steady-state soil moisture profile expansions around the ground surface and tension-saturated zones, [L]

Z_w	Vertical Cartesian location of the water table, [L]
z	Vertical Cartesian coordinate, positive upward, [L].
z_c	Length of wetting front excluding the tension saturated zone, [L]
z_{ts}	Length of the tension saturated zone at some time during infiltration, [L]
α	Inverse of the approximated wetting front slope, [dimensionless]
β	Inverse of mean time between storms,.[T]
χ	Time constant appearing in the derivation of the infinite series expansion of infiltration capacity, [T]
Ω	Dimensionless parameter group appearing in the expression of mean annual bare soil evaporation
Λ	Dimensionless parameter group appearing in the expression of mean annual bare soil evaporation
δ	Inverse of mean storm duration, [T^{-1}]
Φ	Total energy head, sum of elevation head and capillary tension head, [L]
ϕ	Slope of the steady-state soil moisture profile evaluated at the start of the tension-saturated zone, [dimensionless]
ϕ_i	Dimensionless sorption diffusivity
Γ	Dimensionless parameter group appearing in the derivation of the infinite series expansion of infiltration capacity
η	Inverse of mean storm intensity, [T/L]
λ	Slope of the steady-state soil moisture profile evaluated at the ground surface, [dimensionless]
Θ	Volumetric soil moisture content, [dimensionless]
θ	Slope of bedrock of modeled hillslope domains, [dimensionless]

τ	Bounded nondimensional index of time used in infiltration power series, bounded between zero and one, [dimensionless]; *OR* dummy variable for time integrals, [T]
Ψ	Capillary tension head (negative), [L]
Ψ_{min}	Value of capillary tension head at which soil water is in near thermodynamic equilibrium with surface atmospheric humidity [L]
Ψ_s	Bubbling head of Brooks-Corey soil hydraulic model, the value of the capillary tension head (negative) at which the soil first de-saturates, [L]
Ψ_1	Scale parameter of the Gardner model relating unsaturated conductivity to capillary tension head, [L]
$\forall_e$	Storage capacity of the unsaturated zone under conditions of steady state equilibrium with a water table, [L]
$\forall$	Control volume of approximated infiltration wetting front, [L]
$\langle\cdot\rangle$	Temporal mean value operator, expected value operator
a'	Nondimensionalized variable "a"; *OR* perturbation of variable "a" from its mean value
$\Gamma(\cdot)$	Gamma function
$\gamma(\cdot,\cdot)$	Incomplete gamma function
$K_2(\cdot)$	Bessel function of second type

Chapter 1: Introduction

1.a Scope and Relevance

Predicting the partitioning of precipitation into runoff and evapotranspiration is a central problem in hydrology. Due to the strong coupling of heat and moisture budgets by the latent heat of evaporation, the partitioning is also important to climatology. Understanding the sensitivity of these fluxes to catchment properties and atmospheric forcing is a prerequisite for the construction of sensible forecasting models, for the ability to transfer observation and understanding from experimental sites to other (perhaps larger) areas, and for the reliable assessment of the environmental impact caused by natural and man-made actions.

The scale of human alteration of the environment and the scope of its effect on hydrologic systems have, through history, increased from the environmental impacts of small dams and urbanization, to the effects of large scale agriculture on runoff and erosion, and finally to the possible global impact on the water balance and climate by continental scale deforestation and changing composition of the atmosphere. Concurrently, the desire to transfer observations and understanding of the hydrologic processes has grown from the laboratory soil sample and first order catchment to the scale of resolution of global circulation models (10^5 km^2). Likewise the time scale of interest has grown to include not only single events (e.g. floods) but also changes in the long term average state of natural systems (e.g. the sustainable yield of an aquifer). These issues involve increases (decreases) in space and time scales which necessitate the aggregation (disaggregation) of processes understood at one scale to a larger (smaller) one. Inferring a larger scale behavior from a known smaller scale behavior, or relating large scale integrated observations (e.g., streamflow) to small scale measurements (e.g., soil hydraulic conductivity) is often greatly complicated by nonlinear dependencies of the process physics on properties varying at the smaller scale. This complication tends to be the rule rather than the exception in the study of natural systems.

Sometimes the scales are disparate enough that stochastic methods provide a rigorous and fruitful means of approach. A common example from thermodynamics is the combination of the (molecular scale) kinetic theory of gases with stochastic methods to

arrive at the larger scale "laws" relating pressure, temperature and volume. Most critical for the applicability of this type of approach is for the scales to be disparate enough for single realizations (observations of temperature, for example) to be near the ergodic limit due to abundant sampling.

Disparities in scale (spatial and/or temporal), which allow various hydrologic processes relevant in this study to be treated separately and viewed "stochastically" from the larger scale to the smaller, have been exploited successfully in the past. Some relevant examples are: 1) In *Eagleson's* [1978c] model of unsaturated flow, the filtering out (by diffusion) of high-frequency temporal variations in the landsurface boundary conditions such that the quasi-steady moisture state deep in the soil can be matched to the expected value of the highly variable moisture state near the surface; 2) In *Bakr et al.* [1978], the use of spectral perturbation methods in aggregating the effects of variability in soil conductivity to derive an effective conductivity which is valid when applied over many correlation scales; and 3) In *Rodriguez-Iturbe and Valdes* [1979], the interpretation of the instantaneous unit hydrograph as a probability density function (p.d.f.) of travel times integrated from the smaller scale (random) channel branches up to the basin outlet scale.

The temporal scale of interest of the various hydrologic fluxes in this work is the climatic mean. As such, the stochastic approach of *Eagleson* [1978c] is perfectly suited to this analysis.

The spatial scale addressed, however, is of an intermediate size relative to the crucial hydrologic processes: the hillslope scale. Central to this work is the belief that in order to transfer well understood hydrologic point processes such as infiltration and exfiltration to the typical scale of measurement and/or prediction, which may be a first or higher order catchment if streamflow is being measured, the "footprint" of a satellite remote sensing scan, or a General Circulation model (GCM) grid, the deterministic variations of hydrologic behavior that occur along a hillslope must be incorporated. There is simply not a large enough disparity in scale between the level of aggregation and the scale of variations of, for example, the moisture field to treat the variations as purely random. Often the failure of simple point process models to predict integrated measurements has been attributed to a lack of incorporating the essentially random component of the heterogeneity of the physical parameters (e.g. hydraulic conductivity) appearing in point models. While this is clearly a source of error, a possibly more serious problem with point models is their inability to account for the deterministic heterogeneity of

things like water table position and moisture state as caused, for example, by topographic variations. Various approaches to accounting for parameter and state variable heterogeneity are contrasted in the review of literature that follows this introduction.

There is ample field evidence of this sort of deterministic variation in moisture state, water table depths, and hydrologic behavior. An example is given in Figure 1.1 from [*Toth*, 1966]. This figure shows regions of groundwater recharge (down arrow), discharge (up arrow) and transition zones (dashes) inferred from geochemical (e.g. concentrations of salt precipitates), geobotanical, and other field characteristics across a prairie in Saskatchewan Canada. In general, topographic lows have water tables near the surface, contribute strongly to surface runoff generation, yield evaporation at climate demanded rates, and discharge saturated zone groundwater. Likewise topographic highs are associated with deeper water tables, drier surface moistures, suppressed evaporation, enhanced infiltration and groundwater recharge [*Freeze and Cherry,*, 1979, esp. pp. 193-211]. As another example, consider the map of Figure 1.2, reproduced from *Kirkby* [1978], which demonstrates a high correlation between areas of surface saturation during a storm and a topographic index representing both the relative water table elevation and the lateral convergence of groundwater flow (contributing area divided by slope, a/s).

Indirect effects of the role of deterministic spatial variations in moisture state and hydrologic behavior are evident in the way area integrated hydrologic responses, for example basin yield and surface runoff, scale with geometric basin properties. Two examples are:

1.) the scaling of average annual streamflow with catchment area: If pointwise hydrologic response were either homogeneous or dependent only on heterogeneous properties which varied over small scales, average annual streamflow would increase linearly with area. There would be scatter due to heterogeneities, but the scatter would be unbiased. Instead, Figure 1.3 from [*Moore and Morgan*, 1969] shows that average annual streamflow may increase or decrease with area, in a nonlinear manner, depending on regional climate;

2.) attempts at discerning a representative elementary area (R.E.A.) of hydrologic response [*Wood et al.*, 1988]. At the R.E.A. scale of aggregation, the variance of response should be minimized and there should be no deterministic trend. Field analysis often yields R.E.A.'s greater than the hillslope scale, indicating that deterministic variation may exist

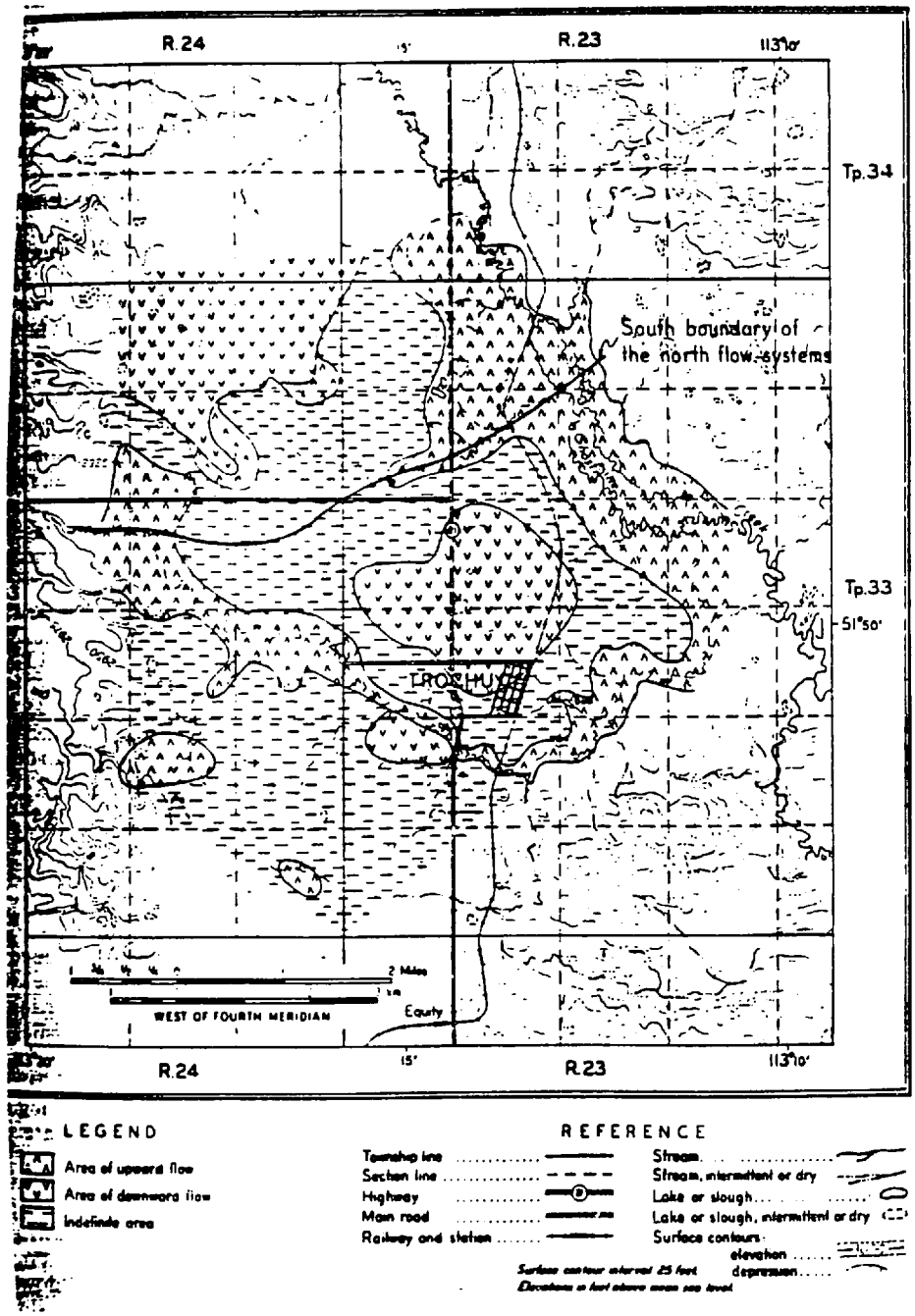

Figure 1.1 Spatial structure of recharge and discharge in Canadian prairie [Toth, 1966]

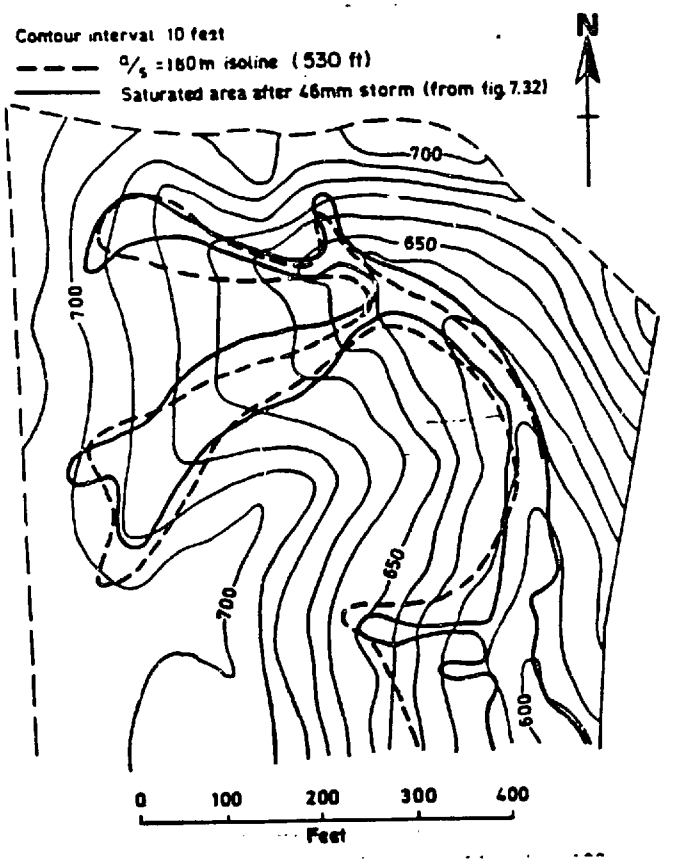

Figure 1.2 Distribution of saturated areas during storm [Kirkby, 1978]

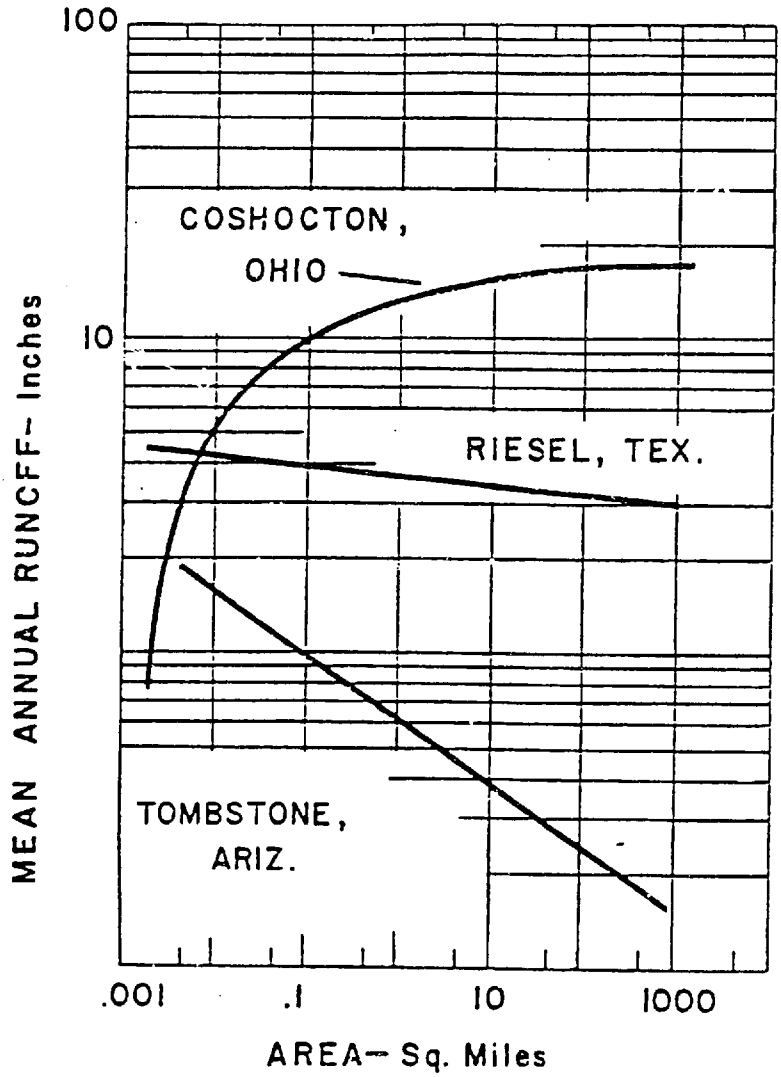

Figure 1.3 Scaling of mean annual runoff with area [Moore and Morgan, 1969]

within the hillslope scale.

In this thesis a statistical-dynamical methodology is developed for coupling the flows in the saturated and unsaturated zones within a hillslope. This yields a tool with which the preceding phenomena related to the spatial structure and scaling of hydrologic fluxes may be systematically studied. In the following the overall approach and major assumptions are discussed. Reference to the chapters in which aspects of the methodology are discussed are given.

1.b Overview of Problem, Analytic Approach, and Basic Assumptions

The focus of this research is the coupling, by the water table, of the (primarily) vertical unsaturated flows and the (primarily) lateral saturated flows that the former supply. This coupling arises from the joint dependency of these flows on the water table elevation. In summary: 1) at each location along the water table, the magnitude and sign of the vertical moisture flux which recharges (percolation) or drains (capillary rise) the saturated zone depends, in part, on the elevation of the water table relative to the surface; and 2) the elevation of the water table at any location depends on the lateral flow it transmits and thus on the net uphill recharge

1.b.1 Equilibrium Water Balance at a Point

To analyze this coupling, first consider a hypothetical "point" long-term average water balance. The continuously changing atmospheric boundary conditions (precipitation and evaporative demand) at the soil surface induce a diffusion of moisture into and out of the soil column and temporal variability in the moisture profile. Depending on the near surface moisture profile at a given time, the soil may be unable to infiltrate or exfiltrate moisture at the rates demanded by the atmospheric forcing. In these instances, the flux into or out of the soil is determined by the soil instead of the atmosphere. These "soil controlled" periods are responsible for surface runoff production and evaporation at less than the potential (atmospheric limited) rate. These soil controlled maximum flux rates are termed the infiltration and exfiltration capacities. Their exact mathematical definition, application, and a discussion of their utility in the partitioning of hydrologic fluxes are discussed in detail in Chapter 2

The event fluxes into and out of the soil are balanced by storage changes along the profile which cause the magnitude of variation of the fluxes to attenuate with depth. High frequency variability (the "weather") penetrates less deeply than low frequency variations (e.g. seasonality). Depending on the soil properties, unsaturated zone depth, and the frequency of variation in the boundary conditions, a quasi-steady flux and corresponding quasi-steady moisture profile may occur deep in the soil profile. The rate and sign of this resulting deep soil flux depends upon the steady (or quasi-steady) moisture profile, which is fixed to saturation at the water table. This attenuation of the atmospheric forcing and its implications for model construction are explored through spectral analysis in Chapter 2.

The unsaturated zone may thus be conceptually divided into a near surface region in which the moisture profile and fluxes are highly variable, and a deep soil region where a quasi-steady condition persists [*Eagleson* , 1978c]. Assuming that the climatic boundary conditions are stationary, the temporal mean of the storage changes in the near surface region will be zero. An equilibrium condition will thus be reached for which the mean of the fluxes in the near surface (or at the ground surface, i.e. the infiltration and exfiltration) equals the steady flux deep in the soil [*Eagleson* , 1978a].

Eagleson [1978a-g] focused mainly on conditions of deep water tables and analytically characterized the equilibrium condition by the effective vertically averaged soil moisture at which the steady percolation to the groundwater would balance the mean of the surface fluxes. In Chapter 3 Eagleson's purely analytical model is shown, after minor modification, to yield excellent estimates of the water balance partitioning when compared with numerical simulation. In this work his general approach is extended to apply to both deep and shallow water table conditions. Under shallow water table conditions the moisture profile shows considerable deterministic variation with depth (and thus may not be approximated by a depth average) and may, in the long term mean, either percolate water to or lift water from the saturated zone.

In Chapter 2 it is shown through perturbation analysis that the equivalent steady profile, i.e. the moisture profile which transmits the mean unsaturated zone flux, forms a sufficient proxy of the actual soil moisture distribution for use in initializing infiltration and exfiltration capacities. A simple analytic expression for this steady moisture profile was derived by *Salvucci* [1993]. The expression is presented in Chapter 4 and used as the basis for deriving the infiltration capacity and storage capacity of soils bounded by a water table. As a rule, wet, shallow moisture profiles yield small infiltration and storage

capacities and large exfiltration capacities. Expressing the dependence of these surface flux capacities on the equivalent steady moisture profile provides the critical teleconnection between the water table and fluxes at the land-atmosphere interface.

Because the equivalent steady profile depends on the water table position, the "equilibrium" point water balance will itself depend on the water table depth. In general, shallow water tables promote wet surfaces causing an excess of evaporation over infiltration and a compensating discharge (capillary rise) from the saturated zone, while deep water tables promote infiltration over evaporation, leading to groundwater recharge (percolation). The reasons for this behavior are discussed in detail in Chapter 5, where the analytic expressions for components of the point water balance of a soil column bounded by water table and forced with intermittent precipitation are derived.

An important property of the climatic mean water balance is that it is a stable equilibrium [*Eagleson*, 1985] This stability is a result of the fact that: 1) wet near-surface moisture conditions reduce the net (unsteady) flow into the soil surface (e.g. by lengthening the atmosphere-controlled period of an exfiltration event and the soil-controlled period of an infiltration event) while increasing the steady flow through the soil column, thus drying the soil profile; and 2) dry near surface conditions increase the net flux into the surface (e.g. by lengthening the atmosphere-controlled period of infiltration events and the soil-controlled period of interstorm evaporation events) but decrease the flow out of the column, and thus wet the soil column. Thus the feedbacks between changes in the moisture content and changes in the flux rates are such that the system is driven toward stable equilibrium.

1.b.2 The Equilibrium Water Table

In the schematic Figure 1.4, "point" water balance concepts are illustrated in the context of a hillslope. Now these average fluxes of percolation or capillary rise are sources and sinks of moisture along the phreatic water table. The (primarily) lateral flow in the saturated region redistributes these fluxes, in this case draining the net accretion to the channel. The rate of lateral flow in this region depends primarily on the thickness of the saturated zone and the slope of the water table.

With both the vertical unsaturated fluxes and the saturated lateral flux dependent on the water table shape, an equilibrium condition may be reached for which the difference in

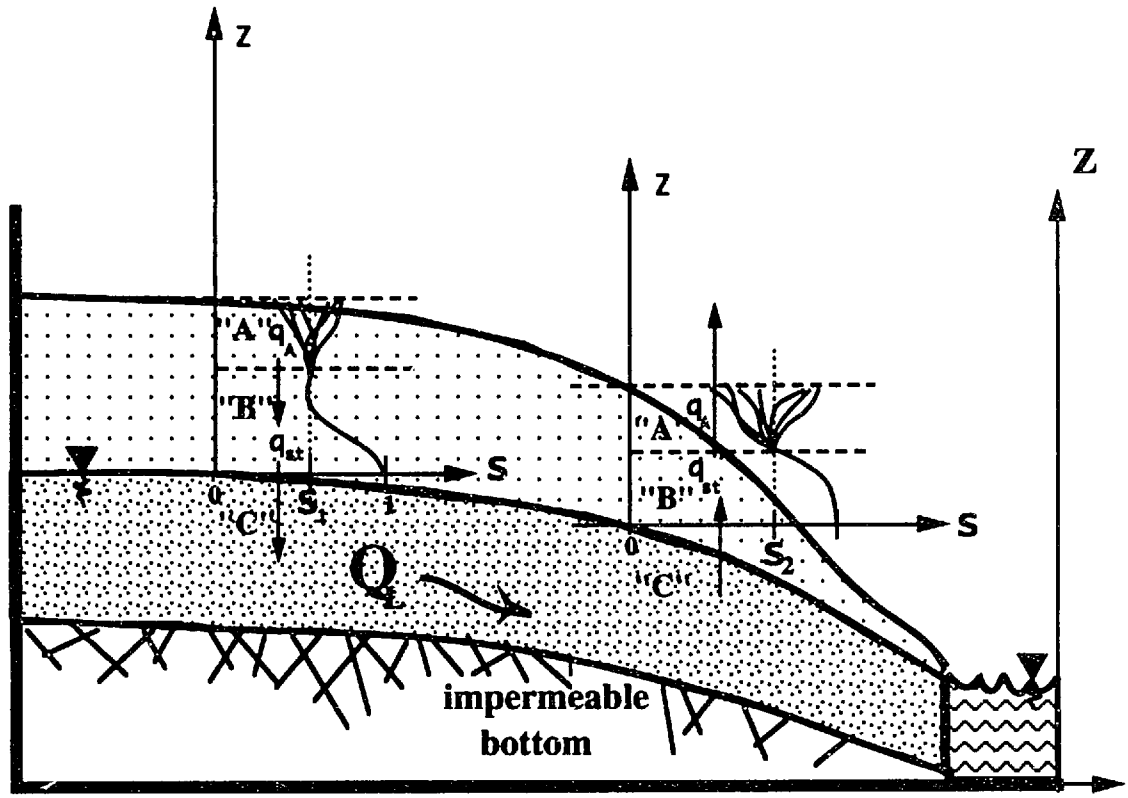

legend

"A" unsteady, unsaturated vertical flow

"B" steady, unsaturated vertical flow

"C" steady, saturated lateral flow

Figure 1.4 Idealized hillslope hydrology and sub-process boundaries

the lateral flow rate between two positions along the water table will be equal to the net vertical flux added along that segment.

This concept of a water table in equilibrium with the unsaturated zone and from which the long term average basin yield and recharge-discharge characteristics may be inferred was introduced by *Toth* [1962 and 1963] and extended by *Freeze and Witherspoon* [1966]. In both of these works the water table was treated as a measurable diagnostic from which the saturated flow field (and thus recharge and discharge) could be inferred by application of the mathematics describing steady state saturated flow. Analysis of the unsaturated zone was not necessary in these studies, as the unsaturated zone was assumed to be in equilibrium with the saturated groundwater flow. *Freeze and Cherry* [1979, p. 194] assert that this equilibrium condition is approximated in many hydrogeologic basins. The supposition of this dynamic equilibrium is used in this thesis as the final closure condition in solving the full hillslope problem.

An important distinction between the above cited work and the effort undertaken here is that those researchers measured the existing water table depths (or assumed that it follows the surface topography directly) and used mathematical models to infer, solely from the saturated zone, the regional flow, basin yield, and spatial distribution of recharge and discharge. Here the question of why the water table should be where it is in the first place is considered. By relating the mean unsaturated zone fluxes to the water table depth, an attempt is made to break what *Freeze and Witherspoon* [1968, p. 585] call the vicious circle of groundwater recharge analysis:

> " ...existing water-table configurations, which controls the nature of the ground water flow pattern, will influence the quantity of groundwater recharge. But it is also true that the nature and amount of rainfall will control, to a certain degree, the configuration of the water-table.....Future studies should consider the effect of climatic patterns on water-table configurations."

The nature of this feedback is used in conjunction with the previous discussion of the unsaturated zone equilibrium condition to understand why the equilibrium water table is also stable to perturbations. Consider that when the water table at any point is lower (higher) than the equilibrium position, two processes will tend to restore it: 1) the lateral

flow will converge to (diverge from) it due to the induced gradient along the phreatic surface; and 2) as the unsaturated zone equilibrates with the lower (higher) water table drier (wetter) surface conditions will prevail which reduce (increase) evaporation and promote (reduce) infiltration, thus causing the net recharge to increase (decrease) and the water table to rise (fall).

Following his early work on steady state, saturated zone modeling, *Freeze* [1969 and 1971] carried out numerical analyses of the dynamic hydrologic factors of the saturated and unsaturated zones which lead to groundwater recharge. In the first of these publications he succinctly summarizes the equilibrium condition as follows [*Freeze* , 1969, p. 156]:

> In nature, a dynamic equilibrium exists whereby the groundwater flow pattern, the resulting rate of groundwater recharge or discharge, the water table position, and the unsaturated flow conditions are in harmony, and the water table fluctuations are kept within relatively narrow bounds"

Note that it is not assumed that the water table is actually at steady state. Rather it is assumed that the effect of fluctuations around the equilibrium water table are small. Clearly this assumption can break down under some conditions. *Freeze and Witherspoon* [1968] give two conditions for its applicability: 1.) that the fluctuations be small in comparison with the total saturated depth of the basin and 2.) that the relative configuration of the water table remains the same throughout cycles of fluctuations.

To avoid confusion in this thesis, the equilibrium condition will be referred to as a condition of statistical dynamical equilibrium, i.e. one in which the *mean* unsaturated zone recharge and discharge are in equilibrium with the *mean* saturated zone flow divergence. In the same way that the "equivalent steady state" moisture profile is used to parameterize the unsaturated zone, the equilibrium water table is assumed to describe the saturated zone and is herein called the "equivalent steady state" water table. With this assumption the saturated zone is analyzed using the steady state equations of flow. Following *Freeze and Witherspoon* [1968], this is accomplished by applying the method of relaxation to the Laplacian of the groundwater potential. These conceptual and related numerical issues are discussed in Chapter 6.

1.b.3 Basin Geometry

The lateral saturated flows that redistribute water table recharge and losses are driven by variations in water table elevation caused in part by land surface and bedrock topography. In this thesis two situations are considered in characterizing basin geometry. In one it is assumed that symmetry exists along a channel (or valley) and the domain of analysis is taken as a two-dimensional planar hillslope slice (as in Figure 1.4). This choice however is incapable of incorporating the near channel convergence of lateral flows. The importance of convergence in determining the hydrologic response of the surface has been noted by many researchers (e.g. *Beven* [1989]; *Band*, [1991]) and is the critical process in some hydrologic models (e.g., TOPMODEL, *Beven and Kirkby* [1979]) and in some modeling and analyses of catchment evolution (e.g. *Montgomery and Dietrich* [1989], *Tarboton et. al.* [1989], *Willgoose et. al.* [1991]). To approximate the effect of topographically driven convergence in the simplest manner possible, the second situation considers sectors of an idealized circular domain (Figure 1.5) consisting of a circular line sink (a "channel") surrounded by a circular, downward sloping hillslope area.

In this idealized domain, the degree of convergence of lateral flow is parametrically controlled by the radius locating the basin divide (r_d) and the radius locating the circular channel (r_c). For a fixed r_d, when the channel is at position A, there is little convergence and the model behavior would simulate drainage of a planar hillslope to a channel (dominant in a well drained basin). When the channel is at position B , on the other hand, there is much convergence, as might be expected near the head of a first-order catchment's channel (dominant in a poorly drained basin). By switching the location of channel and divide, flow divergence is induced. Figure 1.5 shows how elements of a drainage basin can be approximated by this simple two-and-one-half dimensional basin geometry.

The many other heterogeneities of basins (e.g. undulations, bedrock fractures etc.) are not accounted for in this analysis, but will be addressed in future research extensions of this thesis (see Chapter 7). Here the focus is on the most basic (and potentially scalable) geometrical properties of basins.

1.b.4 Case Studies of the Influence of Physiographic Factors on Hydrologic Response

This thesis reports on an analytic, statistical-dynamical methodology for

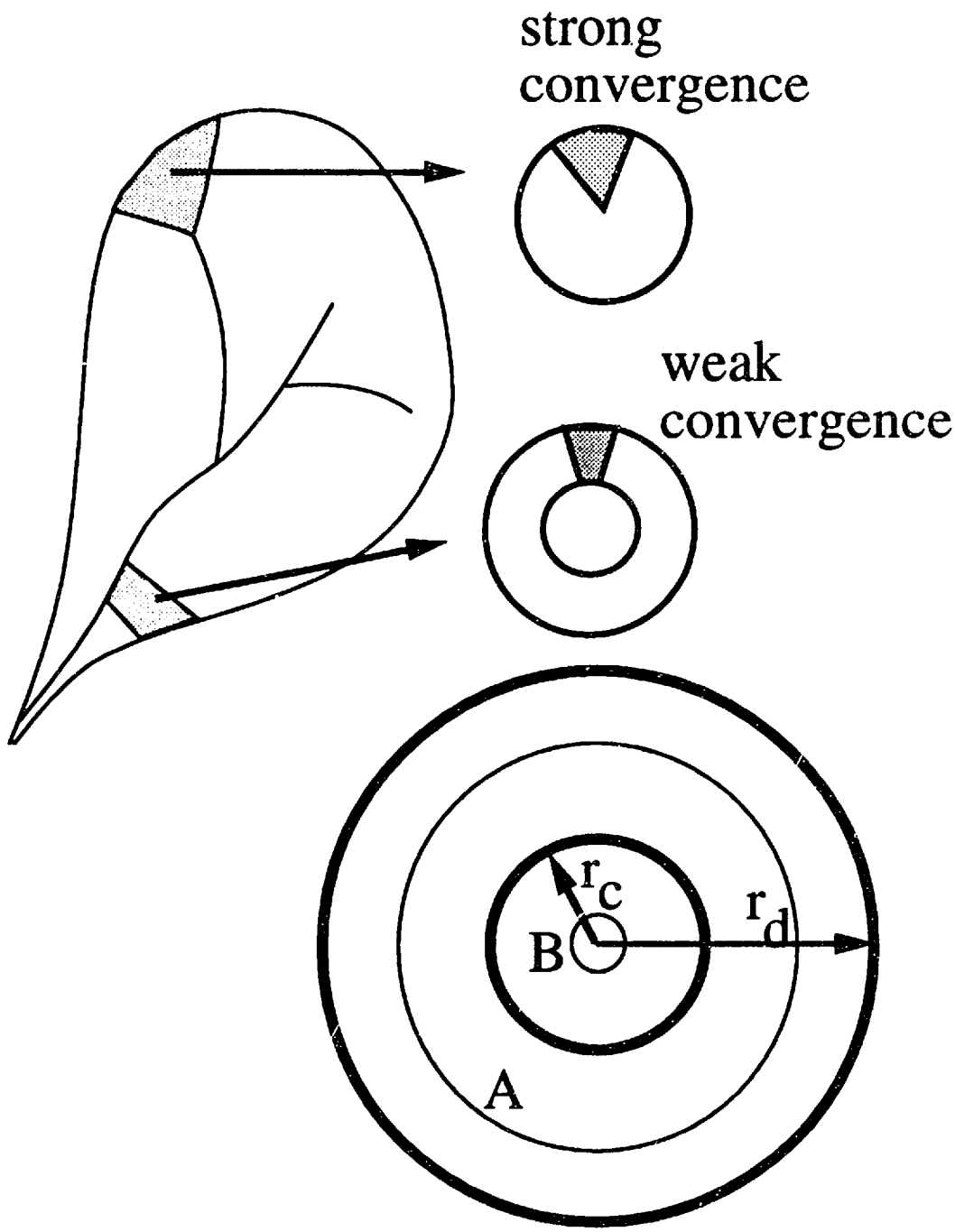

Figure 1.5 Mathematical model for representing converging and diverging drainage patterns

parameterizing the complex saturated-unsaturated flow coupling. The combined effects of the catchment physiographic properties and atmospheric forcing of the landsurface on the climatic mean spatial structure of hydrologic fluxes are studied. The key to the analysis is the supposition of an equilibrium condition between the saturated and unsaturated zones. At this equilibrium condition the equivalent steady water table: 1) serves as the lower boundary of the equivalent steady moisture profile and thus affects the spatial distribution of near surface moisture conditions, thereby determining the spatial distribution of mean evaporation, runoff generation, recharge to and loss from the water table; and 2) simultaneously redistributes these fluxes laterally to achieve basinwide water balance. In Chapter 6 the results of applying this methodology to simple model hillslopes are analyzed and they are compared with field observations of hydrologic spatial variability.

1.c Relevant Literature

Water balance modeling that incorporates many different physical processes (with a variety of length and time scales) may be used for a variety of purposes ranging from water supply and irrigation to climate modeling and ecological stability analysis. Depending on the choice of boundaries, it can incorporate the study of groundwater flows, overland flows, snow and ice physics, and the atmospheric phenomena associated with evaporation. There is, therefore, a myriad of related research addressing individual hydrologic processes, methods of analysis, and the interpretations and implications of results.

In the following, the primary goal is to demonstrate how this thesis relates to and builds upon some of the previous work in this field. In the process some important and relevant aspects of the past studies are discussed.

The emphasis of the review is on water balance models, as opposed to models of individual processes. References to relevant research on individual hydrologic processes are made in the appropriate chapters of the thesis. The term "water balance model" in this survey is restricted to analyses which incorporate one or more hydrologic processes and either: 1) update storage changes of moisture (in the atmosphere, unsaturated zone, groundwater, or surface water) over some time increments such that these storage states serve as initial conditions for processes occurring in the next time increment; or 2) view the equilibrium system in which the mean storage changes may be zero, but for which the mean storage serves as a state variable which the individual processes are jointly dependent

upon. The former may be referred to as "running" water balance models and the latter as "equilibrium" models. By either of these criteria, a water balance model serves to relate the individual hydrologic processes to each other such that, for example, the fraction of yield that is derived form surface runoff vs. groundwater flow may be estimated. A process model, on the other hand, relates the individual process to the system state such that, for example, recharge to an aquifer could be estimated from soil moisture measurements.

Figure (1.6) categorizes some existing water balance models and illustrates where the proposed research fits in relation to them. The two major categories, which form the axes in the figure, are the degree of coupling of the hydrologic processes and the time scales considered. Roughly this forms four general categories of: simple models for the purpose of short range ("event") forecasting; daily to monthly water balance models with varying degrees of atmospheric and landsurface couplings; equilibrium water balance/climate models; and models for estimating long term evaporation and yield

The analysis in this thesis incorporates the equilibrium point water balance concepts of *Eagleson* [1978a-f] and *Lettau* [1969], the equilibrium water table concepts of *Toth* [1962] and *Freeze and Witherspoon* [1966] and the laterally distributed effects which distinguish TOPMODEL [*Beven and Kirkby*, 1979]. In addition, it takes the reductionist view of the dependence of water balance on channel network as, for example, in *Carlston's* [1963, 1966] reformulation of *Jacob's* [1943] groundwater model to depend simply on drainage density, although a negative review of this reductionist approach (and of Carlston's work in particular) was made by *Dingman* [1978]. Dingman's two main conclusions were that: 1) a better descriptor than *Horton's* [1932] drainage density (D = total stream length/area) is effective drainage density (D_e = total valley length/area), since the latter neglects sinuosity, which on average doesn't affect the length of flow paths to streams; and 2) so many other factors (e.g. soil type, basin slope, surface roughness, evaporation) influence both storm runoff production and mean annual yield that the effect of D (or De) could be secondary.

In the following, comments are made on some of the models in Figure 1.6 and on the issues relevant to the model developed in this thesis (e.g. spatial aggregation from point to area). The comments are organized into: 1) Running water balance models; 2) Equilibrium water balance models.

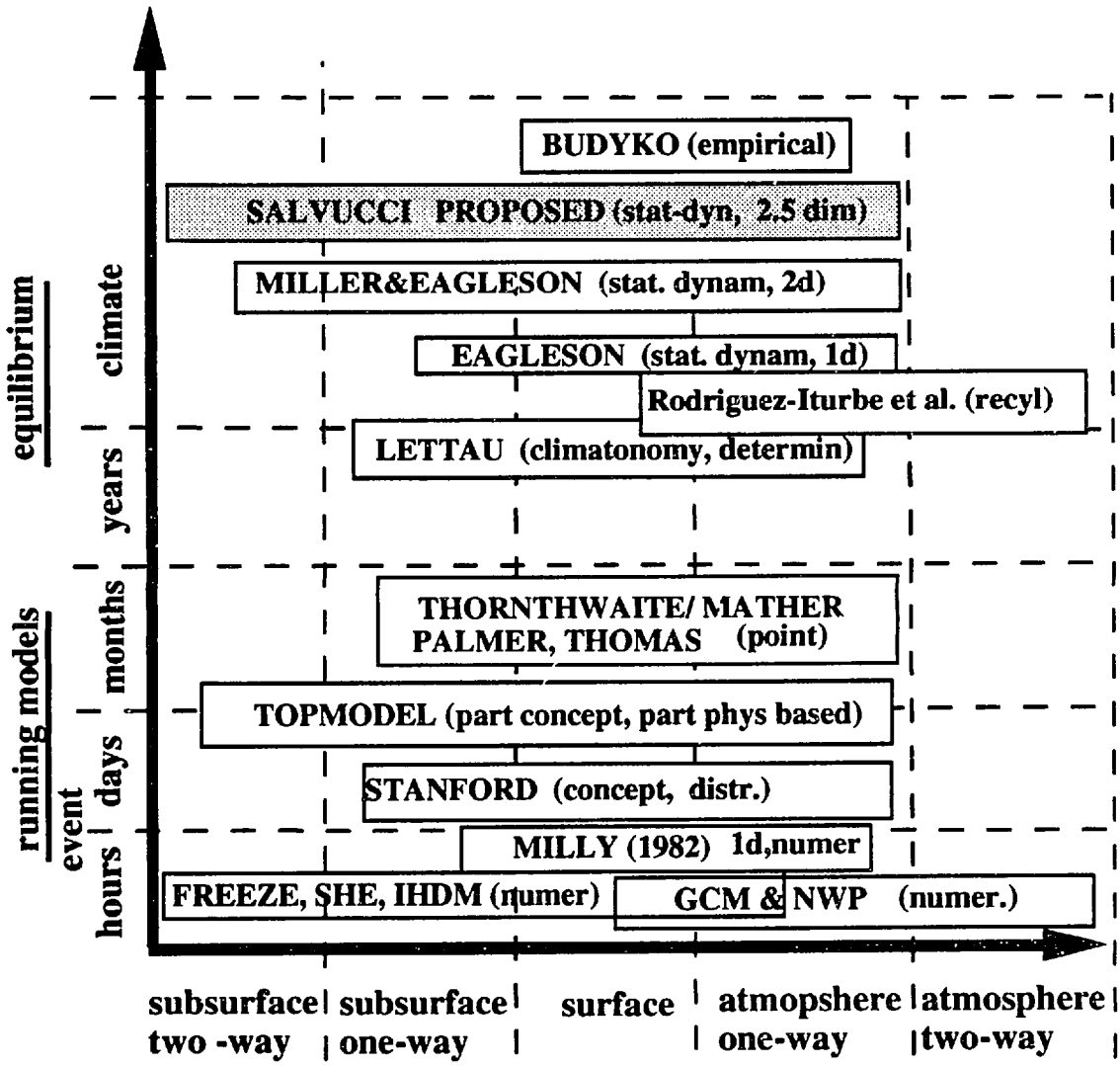

Figure 1.6 Classification of water balance models

1.c.1 Running Water Balance Models

The importance of soil moisture storage as both a result of and regulator of the relation between actual evaporation, potential evaporation and precipitation formed the basis of the first continuous accounting water balance models (e.g. *Thornthwaite* [1946 and 1948] and *Thornthwaite and Mather* [1955]). Since then, a very large number of models have been developed which are conceptually similar , insofar as they perform a running balance, at a point, of some number of hydrologic processes (i.e. input, output, and storage change) which may be modeled in a conceptual, physical, empirical or stochastic way

Stochastic point models, started by *Yevjevich* [1963, referenced in *Parlange et al.* 1992], may for example treat the atmospheric forcing as a random process or the water balance procedure itself as stochastic (as in Auto-Regressive (AR) models). These models have been used for a variety of purposes. Examples geared toward irrigation scheduling include *Cordova and Bras* [1981] and *Ramirez and Bras* [1985], while *Rodriguez-Iturbe, Entekhabi and Bras* [1991] were able to plausibly explain drought persistence through a stochastic model which included climatic feedback between the soil moisture state and precipitation. More recently *Parlange et al.* [1992] derived a stochastic AR model from simplified solutions of unsaturated flow equations. Their model predictions preserved the mean, variance, and skew of field measurements, as well as the cumulative evaporation.

Deterministic point models whose sub processes fit one or more of the descriptions of conceptually, physically or empirically based include, for example: The Palmer Model [*Palmer*, 1965, referenced in *Alley*, 1984]; the abcd model [*Thomas*, 1981, referenced in *Alley*, 1984]; the Stanford Watershed Model [discussed by *Linsley and Franzini*, 1979]; and more recently *Gleick's* [1987] modeling of the Sacramento River Basin. *Alley* [1984] tested and reviewed the first two and the Thornthwaite/Mather model and found that while flows were predicted reasonably well and were mutually consistent (e.g. fifteen percent error for annual yield), the state variable predictions differed widely. He also noted that the fitted values of parameters of the models were often at odds with their definitions, calling into question their physical significance. *Gleick* [1987], on the other hand, found success in predictions of both the timing and magnitude of (monthly) runoff and of changes in soil

moisture conditions.

With all point models however, there is by definition a lack of physical realism which calls into question how well the model can serve to extrapolate from the conditions under which its parameters were chosen to new conditions (caused by, for example, climate change or land surface alteration). The models have tunable parameters that are calibrated by analyzing how the fluctuations in the inputs and outputs of the model are related.

The point water balance concept has been also spatially extended to conceptually balance inputs and outputs at hydrologically connected points over a partitioned area. *Penman* [1951, referenced in *Kuhnel et al.*, 1991] introduced this method by conceptually dividing a basin into riparian areas of high water table and non riparian areas of deep water table. *Engman and Rogowski* [1974] found promising results in modeling runoff generation by subdividing watersheds along similar guidelines. Existing models of the total water balance (as opposed to just runoff production) which are laterally distributed include HYFOR, which includes elevation dependent freeze/thaw and snow effects [*Fox*, 1992] and TOPMODEL [*Beven and Kirkby*, 1979]. TOPMODEL has also been extended to account for variability in both atmospheric forcing (e.g. rainfall) and soil parameters [*Famiglietti and Wood*, 1991a]. Point models have also been stochastically spatially extended without being hydrologically "connected", as in the water balance modeling work of *Milly and Eagleson* [1982]. In the above works the authors have found, in general, that the area-integrated fluxes are not well represented by a single point in space. For example, *Milly and Eagleson* [1982, p. 3] found that "a particular feature of the averaged response is that increased spatial variability of soil type or storm depth almost invariably leads to decreased infiltration and increased runoff".

The method of treating an area as an ensemble of non-interacting columns (i.e. the "unconnected" method) has been partially justified through numerical comparison and mathematical analysis by *Dagan and Bresler* [1983] and *Protopapas and Bras* [1991a]. Both methods of aggregation (i.e. connected or not connected) are widespread in the literature, and it is difficult to determine which "works" better. In part this is because both tend to have the same augmenting effect on the area averaged runoff (which is usually the check on the model), but for different reasons. When spatially aggregating a point runoff model over a statistical distribution of soil parameters, *Milly and Eagleson* [1982, and also, for the equilibrium water balance, 1987] found that the mean areal runoff is larger

than that found by applying the model to the mean of the soil parameters, i.e. the variability itself leads to more predicted runoff. In part this is because the point runoff model used increases nonlinearly with decreasing hydraulic conductivity and thus may not be evaluated at the mean value of its input parameters. In a laterally connected model (e.g. TOPMODEL), on the other hand, the area-averaged runoff increases because the topographically-driven lateral convergence of saturated groundwater flows creates partial areas of runoff-enhancing high water table [*Wood et al.*, 1988]. When the level of aggregation is very large, however, as in the water balance of G.C.M. grid squares, these topographic effects themselves may exist as a statistical ensemble and be incorporated parametrically by assuming a spatial statistical distribution of soil moisture, as in *Entekhabi and Eagleson* [1989].

From the assumptions of lateral flow and hydrologic connectedness made in the various studies, it appears that the favorable results found in the independent aggregation method by, for example, *Bresler and Dagan* [1983], *Protopapas and Bras* [1991b], and *Milly and Eagleson* [1987] are most applicable: 1) at the catchment scale only when the water table is so deep that the saturated and unsaturated regions are de-coupled; and 2) at the very large scale of *Entekhabi and Eagleson's* [1989] work. The related issue of whether or not a laterally inhomogeneous area can be represented by a single point with "effective" soil properties is directly addressed for the equilibrium water balance by *Milly and Eagleson* [1987]. They conclude that it is possible, under certain constraints of the degree of variability (i.e. for small variance).

Another basic model type is the numerical simulation model, which solves the saturated and unsaturated flow equations by finite element or difference techniques over a three dimensional grid. These models were pioneered by *Freeze* [1969,1971,1972a, 1972b] and newer models include SHE [*Abbot et al*, 1986] and IHDM (*Beven et al.*, 1987, referenced in *Binley et al.*, 1989a]. While the advantages of pure, numerical simulation would seem clear, the tremendous amount of parameter evaluation required is problematic. Also, *Beven* [1989] has argued that even these (numerical) models are really conceptual models if the scale of discretization is greater than the scale of heterogeneity in the soil parameters.

As with the point model and distributed point models, the numerical models have included stochastic theory in the specification of parameter values [*Binley et al.*, 1989a] In this work Binley et al. found that for heterogeneous hillslope runoff production the spatial

variability of hydraulic conductivity enhanced runoff production (which is consistent with the previously cited analytic work). *Binley et al.* [1989b], however, found that it was not possible to define an equivalent effective conductivity which, when homogeneously assigned to all points on the hillslope, would reproduce the flow response for the heterogeneous case. Again, this discrepancy with the results of *Eagleson and Milly* [1987] is probably attributable, in part, to the role of the water table in hydrologically "connecting" neighboring soil columns.

Falling somewhere in between the mainly conceptual distributed models like TOPMODEL and the fully physically based numerical models like SHE, are simplified numerical models in which the differential equations of flow and the separation of and interaction of saturated and unsaturated regions have been simplified [*Stagnitti et al.*, 1992 and *Blain and Milly*, 1991, and others]. These models thus benefit from a combination of reasonable computation time and physically realistic hillslope simulation. Even with these models calibration (as opposed to measurements) of soil properties are required. Also, in the latter model, actual evapotranspiration is assumed as a constant (i.e. moisture state independent) proportion of precipitation and in the former it is assumed to occur at the potential rate (which is probably a reasonable assumption as the model is designed for wet, forested watersheds). These assumptions make the models more useful in the study of runoff generation than for water balance studies.

1.c.2 Equilibrium Water Balance Models

While the above models could be integrated for many years to study the equilibrium water balance, they were not, in general, designed for this purpose. Even before Thornthwaite's observations on the relation of precipitation, actual evaporation, and potential evaporation, the equilibrium water balance was expressed by empirical relations between these three quantities [*Schrieber*, 1904 and *Ol'dekop*, 1911, both referenced in *Kuhnel et al.*, 1991]. These empirically derived relations implicitly obey the mean water balance in that the actual evaporation is less than the precipitation, with the difference assumed to be yield. They also display the reasonable asymptotic behavior that the actual evaporation approaches the precipitation when there is little precipitation and approaches the potential evaporation when there is much. *Kuhnel et al.* [1991] review these relations and point out that *Budyko* [1974] found that more than a thousand catchments in the Soviet

Union fell within ten percent of the geometric mean of the two relations of *Schrieber* [1904] and *Ol'dekop* [1911].

The equilibrium water balance concept, in which storage changes average zero but the storage itself is crucial in determining the magnitude of the hydrologic fluxes, were advanced further and derived more physically by *Lettau* [1969] and *Eagleson* [1978a-g] and are discussed with regard to very large scale water balance/climate interaction by *Entekhabi and Eagleson* [1991].

Lettau's [1969] climatonomy model relates evaporation and runoff losses to the soil moisture state and is integrated until the mean annual storage is zero. This model was used successfully in the Phillipines [*Lettau and Baradas*, 1973] and in the central U.S. [*Pinker and Corio*, 1987], though it is difficult to determine if this success was the result of extensive parameter "tuning", or if the parameters were actually physically representative of the watersheds' characteristics.

Eagleson's [1978a-g] model decouples the energy and water budgets by collapsing the energy budget into a potential evaporation atmospheric forcing parameter. The other atmospheric forcing, the precipitation, is treated as a stochastic process. These forcings are taken as the boundary conditions on a one dimensional mathematical description of unsaturated flow and soil transpiration, the solution of which (again after considering long term storage to average zero) yields the mean evapotranspiration and groundwater yield and the statistical distribution of surface runoff events. This model has been used successfully to reproduce the statistical distribution of annual streamflow in climates ranging from humid to arid [*Eagleson*, 1978g, *Chan and Eagleson*, 1980, *Salvucci and Eagleson*, 1992], which is a stringent test on any model and vouches for the model's physical basis. As the model is one dimensional however, the soil physical properties must usually be interpreted as effective parameters. These parameter values may be estimated through corresponding ecological relations [*Eagleson*, 1982 and 1985] which depend on the resulting water balance state (e.g. the soil moisture or evaporation).

In a recent application of this model in a semi-arid setting, *Salvucci and Eagleson* [1992] found that in order to simulate the behavior of the studied watersheds it was necessary to approximately account for the effects of lateral transmissivity on the vertical flow. The coupling discussed in this thesis incorporate these effects directly.

Miller and Eagleson [1982] explored saturated-unsaturated zone coupling using a numerical model of the groundwater flow (in two dimensions) and a model [*Eagleson*,

1978c] of vertical, unsaturated flow. Based on this work, but using analytic solutions at the modeled area's flow boundaries, *Eagleson and Miller* [1983] were able to estimate certain properties of the equilibrium climatic water table shape between the White and Blue Nile rivers in the Gezira region of the Sudan and also to deduce the existence of leakage into an underlying aquifer.

In many ways, the work undertaken here is an extension of the analytic, physically based, and stochastically forced "equilibrium" water balance modeling of *Eagleson* [1978a-g] and *Miller and Eagleson* [1982] into a quasi-three dimensional domain (i.e. 3-d, but radially symmetrical). The important differences between the work contained herein and the above work are: 1) Miller and Eagleson focus on large, deep aquifers with horizontal bedrock boundaries whereas here the focus is on the hillslope scale; 2) Miller and Eagleson do not account for storage excess runoff production; and 3) by virtue of its three-dimensionality, this work incorporates the important effect of lateral flow convergence in creating partial areas of enhanced runoff generation (as in TOPMODEL).

Chapter 2: Tools for Equilibrium Water Balance Model Building

2.a Background and Assumptions

Equilibrium water balance describes models and calculations that result in the determination of the partitioning of atmospheric forcing at the land surface. Atmospheric forcing refers to precipitation intensity during storm events and atmospheric evaporative demand (potential, or climate limited evaporation) during interstorm periods. The landsurface partitions this atmospheric forcing into infiltration, surface runoff, bare soil evaporation, transpiration, groundwater runoff and changes in storage. This partitioning depends on the state of the landsurface and the characteristics of the atmospheric forcing events.

Since the landsurface water and energy balances are coupled through the latent heat of vaporization and thermal inertia, the water balance partitioning has a strong influence on the determination of seasonal land climatology. The heat and moisture balance at the surface in turn influences the climatology and general circulation of the overlying atmosphere. Thus both hydrologists and climatologists have focused effort on improving water balance estimation at the landsurface.

Depending on their particular goals, hydrologists have studied moisture fluxes both on short time scales (as in prediction of flood events) and also on longer time scales (particularly for water resources planning). Climatologists have traditionally been concerned only with long term means (and their trends). Recent use of numerical models to simulate climate however, has focused their interest in hydrology on much smaller temporal scales (e.g. hours). Furthermore, hydrologists have begun to recognize that some important water resources problems, such as drought persistence, may best be understood in the framework of coupled hydrology-climate models [*Entekhabi et al.*, 1993].

In this thesis, the climate water balance is considered in terms of a long term average of event time-scale additions to, and subtractions from, the moisture stored in the land surface. Because these exchanges depend both on the atmospheric forcing at the land-atmosphere interface and on the moisture stored in the unsaturated zone soil matrix, and because wetter moisture states cause the soil to evaporate and drain more readily, while drier states cause the opposite, the system is driven to a long term intermediate equilibrium

state. The fluxes associated with this equilibrium moisture state form the climate water balance [*Eagleson*, 1978a]. Note that this state dependence of the landsurface's response to atmospheric forcing introduces memory and nonlinearity into the system, making solutions of the balance equation non-trivial. Even for systems governed by linear equations, state dependent boundary conditions can make the system nonlinear.

The purpose of this chapter is to develop insight into the relation of: 1) soil moisture profile dynamics, 2) the position of the water table, 3) the flux partitioning at the landsurface, and 4) the time compression approximation, which allows analytic solution under complex boundary conditions. The simulation experiments and the analyses are meant to serve as illustrative examples of physical processes. Throughout, the numerical and analytical results are interpreted with respect to their implications for such issues as: efficient parameterizations of soil moisture processes; conceptual divisions of the soil column according to hydrologic behavior; and initializing flood forecasting models. In the following chapters, the results and findings of these analyses are used: 1) to understand and justify assumptions made by *Eagleson* [1978a-g] in the construction of his water balance model; and 2) as a guide in the extension of the Eagleson model to account for shallow (i.e. near surface) water tables.

2.b Hydrologic Processes, Atmospheric Forcing and the Equilibrium Water Balance

In the following, the hydrologic system and atmospheric forcing are represented as in *Eagleson* [1978a,b], except that vegetation is not considered. This simplification is made in order to focus the current investigation, not to diminish the importance of vegetation in water balance determination. The focus is on a single, representative one-dimensional soil moisture profile, instead of a fully multidimensional and spatially inhomogeneous domain. This one-dimensional representation is assumed to be the simplest one which still captures the critical processes responsible for the system's response to atmospheric forcing. This assumption may be justified by noting that over the typical scale of variation of soil properties (e.g. O(1 meter)), the atmospheric forcing will show very little spatial variation. This leads to a situation in which the unsaturated zone dynamics are dominated by gravity and by moisture gradients whose steepest changes occur in the vertical (i.e. between the surface and the water table). The one dimensional

approximation, in which lateral unsaturated flows are by definition neglected, has been partly supported by the work of *Protopapas and Bras* [1991a], who compared unsaturated flow solutions in a one dimensional domain to solutions in a multidimensional domain of spatially non-uniform soil properties.

The case of modeling landsurface-atmosphere response may be contrasted with the case of point source contaminant transport. In the latter a three dimensional representation of flow and parameter variation is critical because the resulting differential advection of fluid can be the dominant source of dispersion.

In addition the soil properties are taken as homogeneous throughout the column. This assumption is made in order to keep the focus of this analysis on the role of temporal variability. As the flow analysis in this chapter is carried out using a numerical flow simulation model capable of handling layered soils, the procedures outlined here could be extended to heterogeneous soils. The results should not be particularly sensitive to this assumption because the spatial scale of variations in saturation (e.g. moisture fronts) are on the order of ten centimeters or less, whereas the heterogeneity correlation scale is generally at this scale or larger.

Scaling the results from a one dimensional analysis to laterally-hydrologically connected and spatially inhomogeneous areas in order to yield information on the dynamics of area-averaged fluxes is a nontrivial task. As discussed in the literature review of Chapter 1, a variety of approaches exist (cf. *Milly* [1988]), their applicability depending mostly on the size of the area in question (e.g. *Dagan and Bresler*, [1983]; *Milly and Eagleson*, [1987]; *Entekhabi and Eagleson* [1989]; *Famiglietti and Wood*, [1991a]).

With the above assumptions, the land surface at a point is represented by a one dimensional soil column bounded by a water table at some depth ($-Z_w$). Modeling the dynamic behavior of the water table would require a coupled saturated-unsaturated two dimensional dynamic flow simulation. This type of analysis is beyond the scope of this thesis and therefore the water table is fixed throughout all simulations. In the case studies presented here this depth is fixed at different values so that the effect of the presence of a shallow water table on the surface partitioning and profile dynamics are made apparent.

Flow through this characteristic soil column is modeled with Darcy's law:

$$q = -K(\Psi)\frac{d\Phi}{dz} \tag{2.1}$$

where

z = vertical Cartesian coordinate (cm), positive upward

q = flow rate (cm/sec) (positive for q in direction of z, i.e. evaporation)

$K(\Psi)$ = unsaturated hydraulic conductivity (cm/sec)

$\Psi(s)$ = capillary tension head (negative), (cm)

s = relative soil saturation (dimensionless) equal to the volume of water divided by the pore volume available to moisture flow $(0 \leq s \leq 1)$.

Φ = total energy head

The total energy head (Φ) in the unsaturated zone is taken as the sum of the capillary pressure head (Ψ) and the gravitational head. Equation (2.1) then yields:

$$q = -K(\Psi)\left(\frac{d\Psi(s)}{dz} + 1\right) \tag{2.2}$$

Applying continuity for a soil of effective porosity n_e yields *Richards'* [1931] Equation:

$$n_e \cdot \frac{ds(\Psi)}{dt} = -\frac{d}{dz}\left(-K(\Psi)\cdot\left(\frac{d\Psi(s)}{dz} + 1\right)\right) \tag{2.3}$$

which is taken as the governing equation describing moisture flow.

There are a multitude of models for relating capillary tension, unsaturated conductivity, and soil saturation. In this analysis the *Brooks and Corey* [1966] model, which is simple in form and represents the behavior well over a large range of soil textures, is incorporated. The model equations are given in Appendix A. Note that, as pointed out by *Philip* [1969], the governing equation should be left in this Ψ-based form if the soils being modeled have tension-saturated zones, as in the Brooks-Corey model.

Equation (2.3) is solved using the numerical finite element program developed by *Milly* [1982], subject to stationary event-based atmospheric forcing. This forcing ($q_o(t)$) acts in conjunction with tension state at the soil surface to yield the following (state dependent) boundary conditions:

for $q_o(t)$ negative (rainfall):

$$-K(\Psi(s)|_{z=0})\cdot\left(\frac{d\Psi(s)}{dz}|_{z=0}+1\right)=q_o(t) \qquad if \quad \Psi(s)|_{z=0}<0 \tag{2.4}$$

$$\Psi(s)|_{z=0}=0 \qquad if \quad -K(0)\cdot\left(\frac{d\Psi(s)}{dz}|_{z=0}+1\right) \; > \; q_o(t) \tag{2.5}$$

for $q_o(t)$ positive (evaporation):

$$-K(\Psi(s)|_{z=0})\cdot\left(\frac{d\Psi(s)}{dz}|_{z=0}+1\right)=q_o(t) \quad if \quad \Psi(s)|_{z=0}>\Psi_{min} \tag{2.6}$$

$$\Psi(s)|_{z=0}=\Psi_{min} \qquad if \quad -K(\Psi_{min})\cdot\left(\frac{d\Psi(s)}{dz}|_{z=0}+1\right) \; < \; q_o(t) \tag{2.7}$$

Summarizing equations (2.4) and (2.5), the switching of the boundary condition from a flux condition to a Ψ concentration condition occurs whenever Ψ at the soil surface reaches zero, at which time any added precipitation above the infiltration capacity is partitioned to runoff. Likewise in equations (2.6) and (2.7), the switching occurs whenever Ψ at the surface reaches the (large) negative value (Ψ_{min}) at which it is in near thermodynamic equilibrium with the near surface atmospheric moisture [*Gardner*, 1959].

When the soil can absorb (or yield) moisture at the rate which the overlying atmosphere provides (or demands), as in Equation (2.4) and (2.6), the system is said to be climate controlled. This condition occurs at the onset of a rainfall or evaporation period, and applies until the surface either dries to Ψ_{min} , or wets to Ψ =0. This switching may or may not ever occur, depending on the sequence and nature of the forcing, the antecedent moisture state, and the soil characteristics. If and when it does occur, equations (2.5) and (2.7) govern at the boundary and the system is referred to as soil controlled or profile controlled. The soil controlled periods are responsible for infiltration-excess Hortonian surface runoff production and for actual-less-than-potential evaporation.

Note that if the boundary conditions were not state dependent, the solution of the long term mean water balance would be trivial, i.e. the mean annual yield would simply equal the mean annual precipitation minus the mean annual potential evaporation. Absent the effects of vegetation and snow, this nonlinear interaction of the forcing and the surface

moisture state to form the soil-atmosphere boundary condition is the key to the partitioning of the climatic forcing of precipitation and evaporative demand into infiltration, runoff, recharge and evaporation.

The climate forcing, $q_0(t)$, is modeled as a stochastic process consisting of the Poisson arrivals of storm pulses which last for an exponentially distributed duration (t_r). Over this duration, it rains at an intensity (i), also taken as an exponentially distributed random variable. The Poisson storm arrivals imply an exponential distribution of the time between storms (t_b), during which the mean potential rate of evaporation (e_p) defines the atmospheric forcing at the landsurface. These storm pulses and interstorm evaporation periods are referred to as "events".

This is essentially the event based stochastic forcing used in *Eagleson's* [1978c] equilibrium water balance model. While clearly an approximation, this forcing process retains those variables which are important to the dynamics of runoff production and interstorm exfiltration. Most importantly, it realistically models intermittency, event variability and the extremes which often place the system under soil control.

In what follows, conclusions are drawn regarding different statistical and dynamical properties of the moisture profile, flux rates and water balance as derived from solutions to the above described unsaturated flow system under Monte-Carlo realizations of atmospheric forcing. These conclusions relate to the utility and accuracy of various approximations commonly used in event-based water balance modeling.

2.c Analysis of Moisture Profiles

Two case studies are presented corresponding to deep and shallow water table conditions. For both cases, the climate is characteristically semi-humid. The storm structure parameters (Table 2.1) are estimated based on *Hawk and Eagleson's* [1992] storm climatological results for Savannah, Georgia and the potential evaporation is estimated based on regional lake evaporation [*Bras*, 1990]. The Brooks-Corey soil parameters (Table 2.2) listed are typical of clay soils [*Bras*, 1990]. This combination was found to yield enough "soil controlled" events to be illustrative of the interactive nature of the atmospheric forcing on the land surface.

Table 2.1: Climate Parameters

representative climate	Savannah, Georgia
mean storm intensity (m_i)	5.07 (cm/day)
mean storm duration (m_{tr})	0.25 (days)
mean annual potential evaporation (e_p)	112.3 (cm)
mean interstorm duration (m_{tb})	3.44 (days)
mean annual precipitation (mP_a)	125.4 (cm)

Source: *Hawk and Eagleson* [1992]

Table 2.2: Soil Parameters

representative soil	Clay
saturated hydraulic conductivity (K_S)	2.94 (cm/day)
bubbling tension head (Ψ_S)	-90 (cm)
porosity (n_e)	0.45
pore size distribution parameter (m)	0.44

Source: *Bras* [1990]

For the two cases, *Milly's* [1982] unsaturated flow code was used to simulate twenty years of moisture profiles. Each twenty year simulation contained approximately 4,000 events (2,000 rainstorms and 2,000 interstorms). In these simulations, the moisture profile at the end of one event (e.g. a period of rain) was used as the initial condition for the next event (e.g. an interstorm period of evaporation).

The long term mean water balance for each case is presented in Table 2.3. The mean annual surface fluxes (evaporation and infiltration) and bottom flux (recharge or capillary rise) were found by integrating the surface and bottom flux rates throughout the simulation.

Table 2.3: Simulated Mean Annual Water Balance

(all values in centimeters)

	CASE I	CASE II
water table depth (Z_w)	750	150
mean annual precipitation	124.65	124.65
annual bare soil evaporation	88.29	112.36
mean annual surface runoff	4.73	23.99
mean annual exchange with saturated zone (<q>)	-31.84	12.02

For the deep water table case, which might represent a point in the watershed far from a channel, the actual evaporation is approximately eighty percent of the potential evaporation and about four percent of the precipitation is partitioned to surface runoff. For the shallow water table case the near surface moisture state is much wetter, yielding more surface runoff, and actual evaporation equal to the potential evaporation. In this shallow water table case, which might be representative of a near-channel point in a watershed, the vadose zone profile is extracting moisture from the saturated zone in the mean. In a watershed or along a hillslope this would correspond to a region of groundwater discharge, in which case the saturated zone's losses would be replenished by recharging areas (e.g. the far-channel, deep water table point in case 1).

2.c.1 *Moisture Profiles under Deep Water Table Conditions*

In Figure 2.1, five important characteristics of the simulated moisture profile are plotted: 1.) the temporal mean profile (<s(z)>, solid line); 2.) the mean of all the profiles at the beginning of each storm event (<s_{ps}(z)>, diamonds); 3.) the mean of all the profiles at the end of each storm event (<s_{pi}(z)>, beginning of interstorm event; circles); 4.) the hydrostatic profile ($s_s(z;q_{st}=0)$, dashed line; i.e. the steady zero-flow profile); and 5.) the equivalent steady state profile ($s_s(z;q_{st}=<q>)$, dotted line, i.e. the steady state profile that

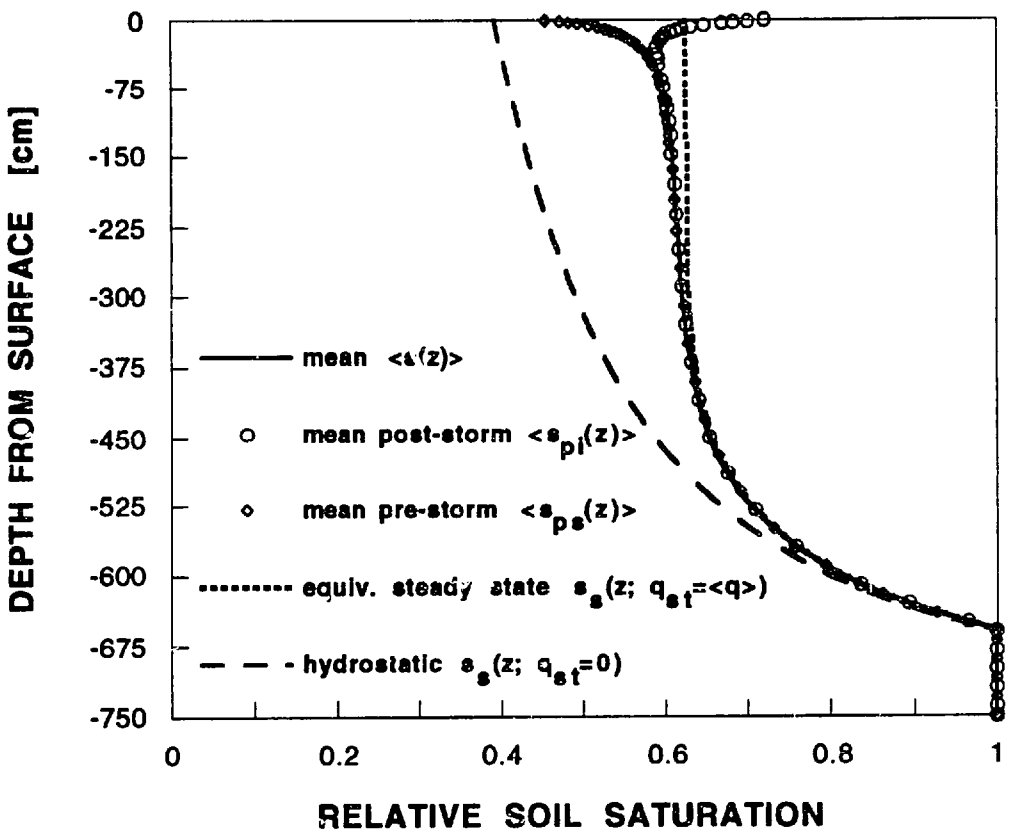

Figure 2.1 Characteristic moisture profiles: Deep water table case

transmits the mean recharge rate, e.g. 31.8 cm/yr, Table 2.3).

The significance of the mean pre-storm and mean post-storm profiles is that they represent the mean initial condition for storm infiltration and interstorm evaporation events, and thus influence the runoff and evaporation partitioning of the soil. As expected the mean profile after rainstorms is wetter than the profile that serves as the mean initial condition for the storm event. The major differences are contained in the top tens of centimeters (in this case, less than fifty).

Most importantly the equivalent steady profile, which may be analytically parameterized in terms of the mean flow and water table depth (e.g. *Salvucci* [1993] and Chapter 4), well approximates the overall mean profile (<s(z)>) and the mean initial condition profiles, particularly in the deeper soil. As will be shown later, the dependence of the surface fluxes on the initial moisture profiles is such that the equivalent steady profile may be used as a surrogate for the actual initial conditions without introducing serious error. The hydrostatic profile, which is a special case of the steady profile corresponding to zero flow, will be discussed in the final section of this chapter.

To illustrate the relation between the equivalent steady profile and the temporal mean profile, consider the case of exponential (linear) soils (see Appendix A). For this representation of soil properties the Darcy flux equation is linear (the diffusivity is constant and the gravity term depends on s linearly) :

$$q = -\frac{K_s}{\alpha}\left(\frac{ds}{dz}\right) - K_s \cdot s \tag{2.8}$$

If the soil moisture and flux rate are expressed as a temporal mean (<( )>) plus a perturbation (( )'), Equation (2.8) may be written:

$$\langle q \rangle + q' = -\frac{K_s}{\alpha}\left(\frac{d\langle s \rangle}{dz} + \frac{ds'}{dz}\right) - K_s \cdot \left(\langle s \rangle + s'\right) \tag{2.9}$$

Because of the linearity of (2.8), taking the mean of Equation (2.9) yields no covariance terms, i.e. the mean equation is simply:

$$\langle q \rangle = -\frac{K_s}{\alpha}\left(\frac{d\langle s \rangle}{dz}\right) - K_s \cdot \langle s \rangle \tag{2.10}$$

For the linear case then, the mean moisture profile will be identical to the steady state solution for the mean flow through the column.

For the Brooks-Corey soil model, the Darcy flux is a nonlinear function of soil moisture:

$$q = \frac{K_s \cdot \Psi_s}{m} s^{(c+1)/2}\left(\frac{ds}{dz}\right) - K_s \cdot s^c \tag{2.11}$$

Expressing the soil moisture and flux as a temporal mean, <( )>, plus a perturbation, ( )', expanding the nonlinear terms around <s> and averaging the resulting equation yields a mean and perturbation equation coupled by covariance terms $\left\langle s' \frac{ds'}{dz} \right\rangle$ and $\left\langle s'^2 \right\rangle$:

$$\begin{aligned} \langle q \rangle &= K_s \cdot \Psi_s \frac{c-3}{2} \langle s \rangle^{(c+1)/2}\left(\frac{d\langle s \rangle}{dz}\right) - K_s \cdot \langle s \rangle^c \\ &+ \frac{1}{4} K_s \cdot \Psi_s (c+1)(c-3) \langle s \rangle^{(c-1)/2} \left\langle s' \cdot \frac{ds'}{dz} \right\rangle \\ &+ \frac{c(c-1)}{2} K_s \langle s \rangle^{c-2} \left\langle s'^2 \right\rangle \end{aligned} \tag{2.12}$$

Note that a perturbation that increases q (e.g. a strong evaporation event) dries the soil, making s' < 0, and from the surface down ds'/dz < 0. A perturbation decreasing q (e.g. an infiltration event) wets the soil (s'>0) from the surface down (ds'/dz >0). Both the variance and covariance terms in Equation (2.12) are thus positive and therefore the mean profile is always drier than the equivalent steady state profile. In Figure 2.1 the deviation between the mean and steady state profiles increases closer to the surface where the magnitudes of the q and s fluctuations and covariances are largest.

In summary, for a linear soil, the equivalent steady moisture profile is identical to the mean profile, while for a nonlinear soil the equivalent steady profile forms a zeroth order (i.e. disregarding the covariance term) estimate of the mean. The magnitude of the neglected covariance terms will be considered next.

The damping of fluctuations by the diffusive process can be seen in the temporal

variance of the flux around the mean state at various depths. The cumulative variance of q is shown for perturbations with period two hours to approximately one year, at a range of depths, in Figure 2.2. The asymptotic values of these cumulative power spectra curves are the total variance of the flow for various depths. The sharply decreasing asymptotic values indicate rapid total variance reduction with depth. For example, flow at the 72 cm depth shows two orders of magnitude less variance than at the surface. More importantly, the near surface variability in the cumulative power spectra is mostly contained in the high-frequency event scale range, while the flow variability in the deeper soil comes from low-pass filtered fluctuations. At the event time scale for example, the variability is reduced by two orders of magnitude over only 31 centimeters, less than half the distance required for the total variance. For the purpose of event time scale modeling, one may then reasonably assume that the moisture state and moisture flow below the near surface is in a quasi-steady state. This approximation leads to a tractable formulation of the water balance problem [*Eagleson*, 1978c].

This structure of moisture and flux profile variability suggests that the deep water table column can be broken up conceptually and for modeling purposes, into two characteristic zones: a highly unsteady near surface zone and a deeper quasi steady zone. In the lower zone the equivalent steady state profile is an adequate estimate of the actual profile at any time. In the upper zone it gives a zeroth order estimate of the temporal mean, mean pre-storm, or mean post-storm profile. If the value of this estimate is measured in terms of its bias and variance, then the equivalent steady profile estimate is seen to improve with depth on both accounts. Note also that the equivalent steady profile ($s_s(z;q_{st}=<q>$) tends to estimate the mean profile prior to interstorm ($<s_{pi}(z)>$) better than the mean profile prior to storm ($<s_{ps}(z)>$), since the former like the equivalent steady profile, is always wetter than the mean ($<s(z)>$).

2.c.2 Moisture Profiles under Shallow Water Table Conditions

For a soil column bounded by a shallow water table, the moisture profiles display some different properties. Note in Figure 2.3 that the equivalent steady profile (close-spaced dots) is a much better estimate of the temporal mean profile (solid line) than in the deep water table case. Beyond the tension saturated zone the mean, steady state, and pre-

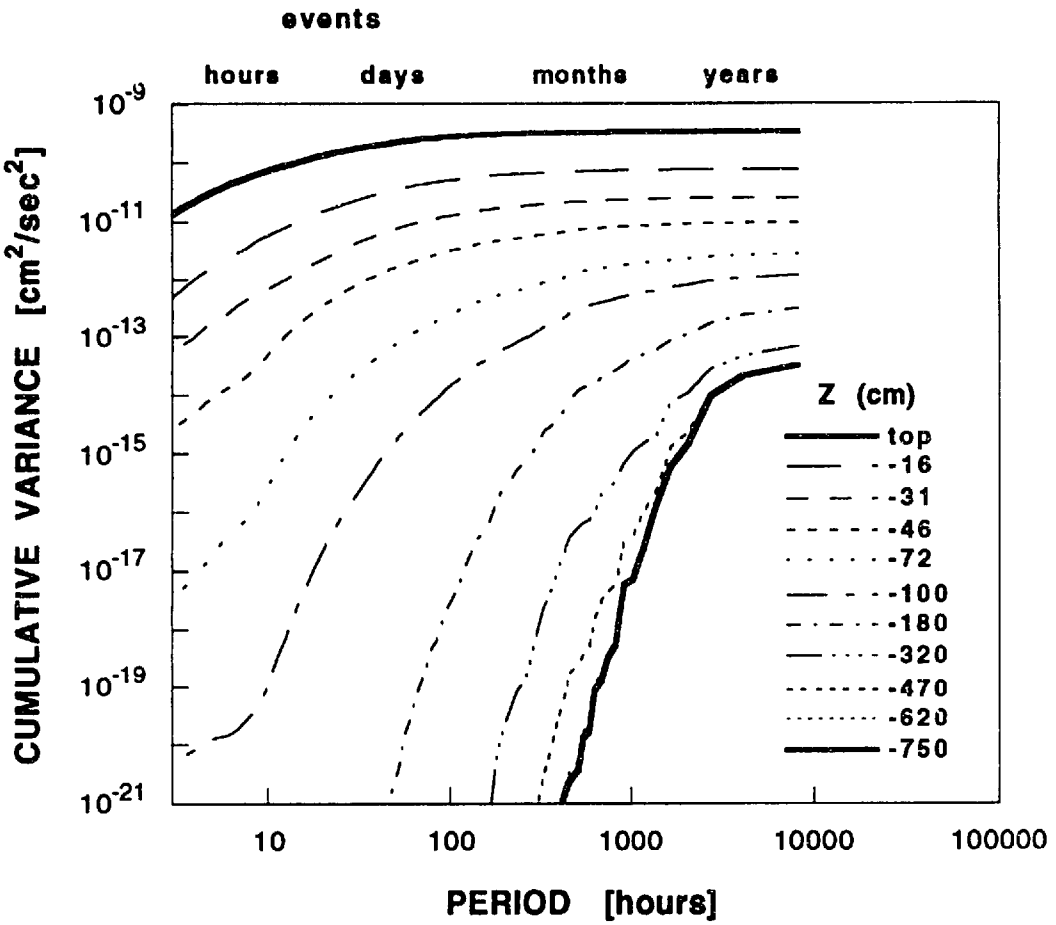

Figure 2.2 Cumulative power spectra of flow variability at various depths: Deep water table case

storm moisture profiles are approximately linear. This is because near the water table, where the soil is relatively wet and near saturation, the soil has high unsaturated conductivity relative to typical forcing rates (e.g. $e_p/K_s \sim 0.1$). Darcy's law (eq. 2.2) then implies that only small deviations from a hydrostatic profile are necessary to balance typical perturbations in the atmospheric forcing. Thus for nearly saturated soils, in which the moisture content locally scales near linearly with Ψ, the moisture profile increases linearly with z.

In summary, either the equivalent steady profile or the hydrostatic profile form an accurate estimate of the temporal mean and mean pre-storm profiles for soil moisture profiles constrained by shallow water table. The mean post-storm profile (circles, Figure 2.3) deviates by a considerable amount, but since the soil is thoroughly moist in this shallow water table case, the interstorm evaporation will proceed at the potential climate-controlled rate, making specification of the pre-interstorm initial condition profile irrelevant.

Note that the profile in this shallow case can no longer be conceptually divided into a highly unsteady zone and quasi-steady zone. This is also evident in the cumulative power spectra (Figure 2.4). For this case, there is less reduction in total variance with depth and more importantly, the reduction is not dependent on frequency. For example the zero depth and bottom depth curves run roughly parallel over most frequencies, indicating that they are accumulating variance from perturbations at similar frequencies. The importance of these differences will be discussed in the final section of this chapter.

A central conclusion of this chapter is that even for soils with nonlinear diffusivity, the equivalent steady flow moisture profile, by way of its relation to the temporal mean profile, is a sufficient estimate of the mean initial condition profile for randomly arriving storm and interstorm events. Utilization of this equivalent steady profile to characterize mean initial condition profiles provides a useful simplification in water balance modeling. In the following the validity of this approximation is demonstrated, for selected precipitation and potential evaporation atmospheric forcings, using time compression analysis. In chapters 3 and 5, its validation is extended to a wide range of soil textures, climates and atmospheric forcings.

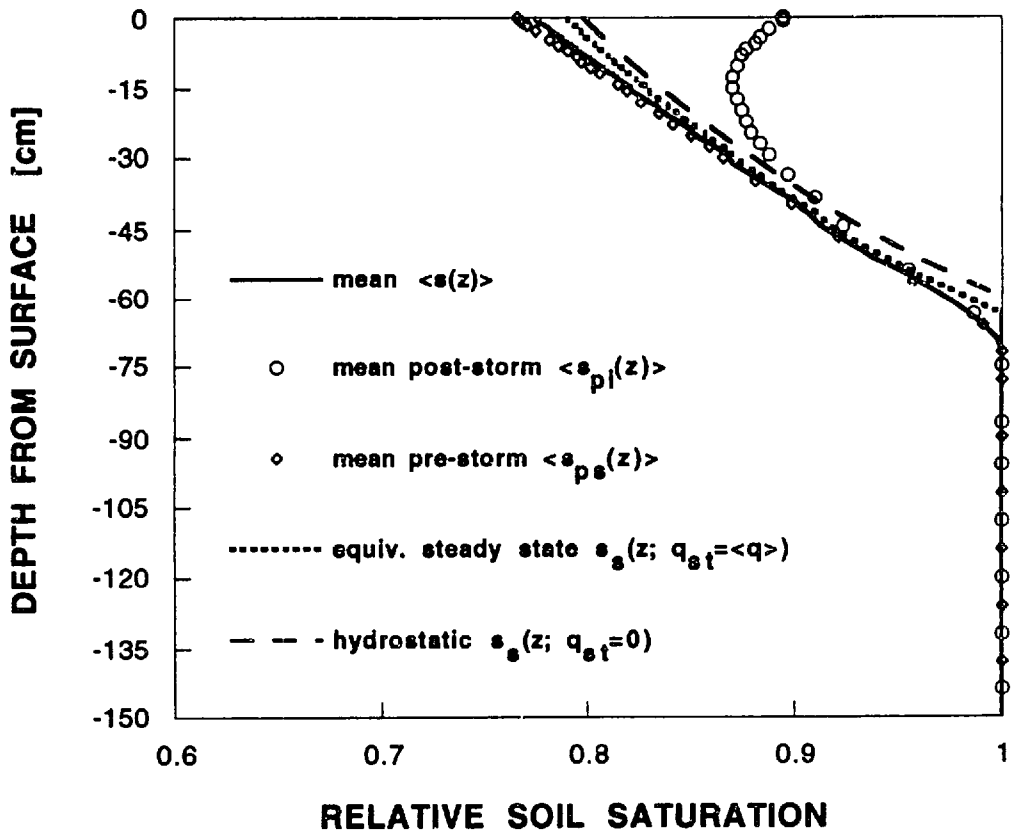

Figure 2.3 Characteristic moisture profiles: Shallow water table case

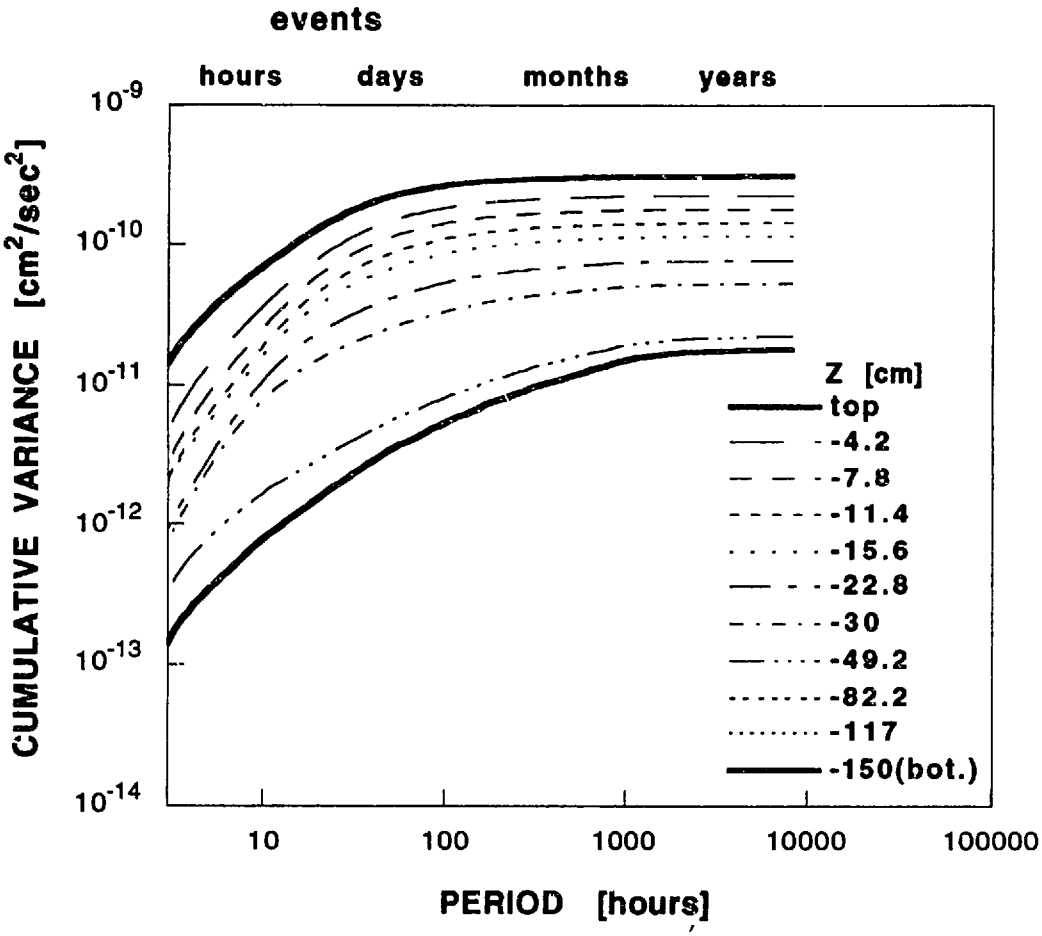

Figure 2.4 Cumulative power spectra of flow variability at various depths: Shallow water table case

2.d Time Compression Analysis

Time compression analysis (TCA) is a commonly used approximation in water balance modeling (e.g. *Reeves and Miller* [1975]; *Eagleson* [1978d,e]; *Milly* [1986]; *Smith and Hebert* [1983]; and *Smith et al.* [1993]). It is derived from an assumption that the maximum rate at which a soil column can infiltrate or exfiltrate water (the infiltration/exfiltration capacity) at any given time during an event depends only on the initial moisture state of the column and the cumulative moisture exchange up to that time. The concept was first used in the context of infiltration by *Sherman* [1943; referenced in *Sivapalan and Milly*, 1989] and in the context of exfiltration by *Philip* [1957b].

The utility of the approximation is that for a given initial moisture state, one can use a single characteristic capacity curve derived as the solution to the infiltration (or exfiltration) rate under flooded (or extremely dry) surface concentration boundary conditions to model the surface flux rate, even if the boundary is actually governed by a combination of flux (i.e. rainfall intensity, before ponding) and head (i.e. $\Psi = 0$, after ponding) conditions. *Sivapalan and Milly* [1989] discuss the relation of this approximation to the more rigorously defined flux concentration relation and use the latter to demonstrate the errors associated with the TCA. In general, they found that the validity of the approximation increases for soils whose diffusivities are highly nonlinearly dependent on soil moisture, becoming exact for Green-Ampt (delta function diffusivity) soils.

The following discussions apply to both infiltration (subscripted "i" and with initial condition moisture profile $s_{ps}(z)$) and exfiltration (subscripted "e", initial moisture profile $s_{pi}(z)$) but will be illustrated for infiltration only. First define the potential infiltration capacity as the maximum rate of infiltration into a given soil with some initial moisture profile $s_{ps}(z)$, i.e. it is the rate of infiltration resulting from a continuously ponded surface. Denote this potential capacity by $f_i^*(t; s_{ps}(z))$, and its time integral, the potential cumulative infiltration, by $F_i^*(t; s_{ps}(z))$. The infiltration capacity during an event which has not had a continuously ponded surface is denoted the event infiltration capacity, $f_{i,event}^*(t;s_{ps}(z))$. This is the rate at which infiltration would occur if, at some time during an event under flux boundary conditions, the surface were ponded.

The time compression approximation states that the relation defined by mapping the potential infiltration capacity $f_i^*(t; s_{ps}(z))$ to the potential cumulative infiltration $F_i^*(t;$

$s_{ps}(z)$), will be approximately the same as the relation between the event infiltration capacity $f_{i,event}^*(t; s_{ps}(z))$ and the cumulative event infiltration ($F_{i,event}(t; s_{ps}(z))$). If this mapping is expressed as G^{tca}, defined by:

$$f_i^*\left(t; s_{ps}(z)\right) = G^{tca}\left(F_i^*\left(t; s_{ps}(z)\right)\right) \tag{2.13}$$

then, by the time compression approximation, the event infiltration capacity and cumulative infiltration are related by:

$$f_{i,event}^*\left(t; s_{ps}(z)\right) \equiv G^{tca}\left(F_{i,event}\left(t; s_{ps}(z)\right)\right) \tag{2.14}$$

Because the surface flux rate that will occur at the moment of ponding will be equal to the event infiltration capacity, the surface boundary conditions given by equations (2.4) and (2.5) are equivalent to stating that the actual surface flux during an event $f_{i,event}$ (t; $s_{ps}(z)$) will be the lesser of the event infiltration capacity ($f_{i,event}^*$(t; $s_{ps}(z)$)) and the event rainstorm intensity (i), i.e.:

$$f_{i,event}\left(t; s_{ps}(z)\right) = MIN\left(f_{i,event}^*\left(t; s_{ps}(z)\right), i\right) \tag{15}$$

With (15), the cumulative event infiltration may be expressed as:

$$F_{i,event}\left(t; s_{ps}(z)\right) = \int_0^t f_{i,event}\left(\tau; s_{ps}(z)\right) d\tau \tag{16}$$

For a given initial condition ($s_{ps}(z)$), equations (2.13) through (2.16) implicitly relate the actual infiltration rate under any rainstorm intensity (i) to the single characteristic potential infiltration capacity curve found under continuously ponded conditions.

All that remains is to determine the mapping f_i^*(t; $s_{ps}(z)$)=G^{tca} (F_i^*(t; $s_{ps}(z)$). This can be found either by field experiment, by numerical simulation, or analytically, if one has an exact or approximate infiltration equation for the continuously flooded boundary condition. For the semi-infinite initial condition $s_{ps}(z)$ constant with depth, many such expressions exist (e.g. for infiltration: *Philip* [1957a]; *Green and Ampt* [1911], referenced

in *Hillel* [1980]; and *Haverkamp et al.* [1990]; and for exfiltration: *Eagleson* [1978c]). In Chapter 4 an expression is derived for Brooks-Corey soils and $s_{ps}(z)$ equal to the equivalent steady state profile.

With one of the above numerical, experimental, or analytic solutions, the time compression approximation may be simplified into either a time-based equation, by eliminating the dependence on cumulative infiltration, or as a cumulative infiltration-based equation, by eliminating time (e.g. *Milly* [1986]). Here the time-based method is chosen.

First note that the event infiltration capacity is by definition equal to the forcing (i) at the time of ponding (t_p):

$$f^*_{i,event}\left(t_p; s_{ps}(z)\right) = i \tag{2.17}$$

Now define a compression time t_c as the time when the potential infiltration capacity is also equal to the forcing, i.e:

$$f^*_i\left(t_c; s_{ps}(z)\right) = i \tag{2.18}$$

By the TCA postulate (equations 2.13 and 2.14), these two capacities are only dependent on the cumulative infiltration and the initial condition, thus:

$$F_{i,event}\left(t_p; s_{ps}(z)\right) \cong F^*_i\left(t_c; s_{ps}(z)\right) \tag{2.19}$$

Because the two capacities only depend on the cumulative infiltration, and because their cumulative infiltrations are identical at time t_p and t_c, the flux capacity at equal increments after these times will also be identical, i.e.:

$$f^*_{i,event}\left(t_p + \tau; s_{ps}(z)\right) \cong f^*_i\left(t_c + \tau; s_{ps}(z)\right) \tag{2.20}$$

Defining the time (t) to start at the beginning of an event, (2.20) and (2.15) yield the final expression for the time compression approximation of the event flux :

$$f_{i,event}(t;s_{ps}(z)) \cong f_i^{tca}(t;s_{ps}(z)) = \begin{cases} i & t<t_p \\ f_i^*\left((t-(t_p-t_c));s_{ps}(z)\right) & t \geq t_p \end{cases} \quad (2.21)$$

In the above, t_c may be found from (2.18) and t_p may be found from (2.19) by noting that for $t < t_p$, $F_{i,event}$ is simply equal to the product of i and t_p and thus:

$$t_p \approx \left(\frac{1}{i}\right) \cdot \int_0^{t_c} f_i^*\left(\tau;s_{ps}(z)\right) d\tau \quad (2.22)$$

Equations (2.18), (2.21) and (2.22) form the TCA approximation to the actual surface flux for any flux boundary condition i (or e_p), in terms of a single solution for the flooded (or extremely dry) concentration boundary condition. In summary, the capacity $f_{i,event}^*(t)$, which changes from event to event and has no general form (because it depends on cumulative infiltration resulting from a mixture of boundary conditions), has been replaced by the well defined f_i^*, which depends only on the initial soil moisture profile and soil properties.

Note that this set of equations (2.18, 2.21 and 2.22) retains the dependence of the surface flux on the initial condition moisture profile $s_{ps}(z)$. The role of the initial condition in governing the potential for runoff and evaporation is therefore incorporated. For example, under conditions of wet initial moisture profile: 1.) the potential infiltration capacity ($f_i^*(t; s_{ps}(z))$) is lower and the ponding time is shortened, thus enhancing infiltration excess runoff production; and 2.) the potential exfiltration capacity is larger and the drying time (t_d) is lengthened, thereby increasing the climate controlled fraction of the interstorm and increasing evaporation. Through this dependence two important factors in determining water balance are preserved, that of memory and that of state dependent, threshold switching of surface flux control from climate to soil.

2.d.1 Test of the TCA Approximation under Uniform Initial Conditions

The accuracy of the time compression approximation for conditions of uniform initial moisture content is illustrated for both infiltration and exfiltration in Figures (2.5) and (2.6). The infiltration example was found using the clay soil of Table 2.1 and a (constant)

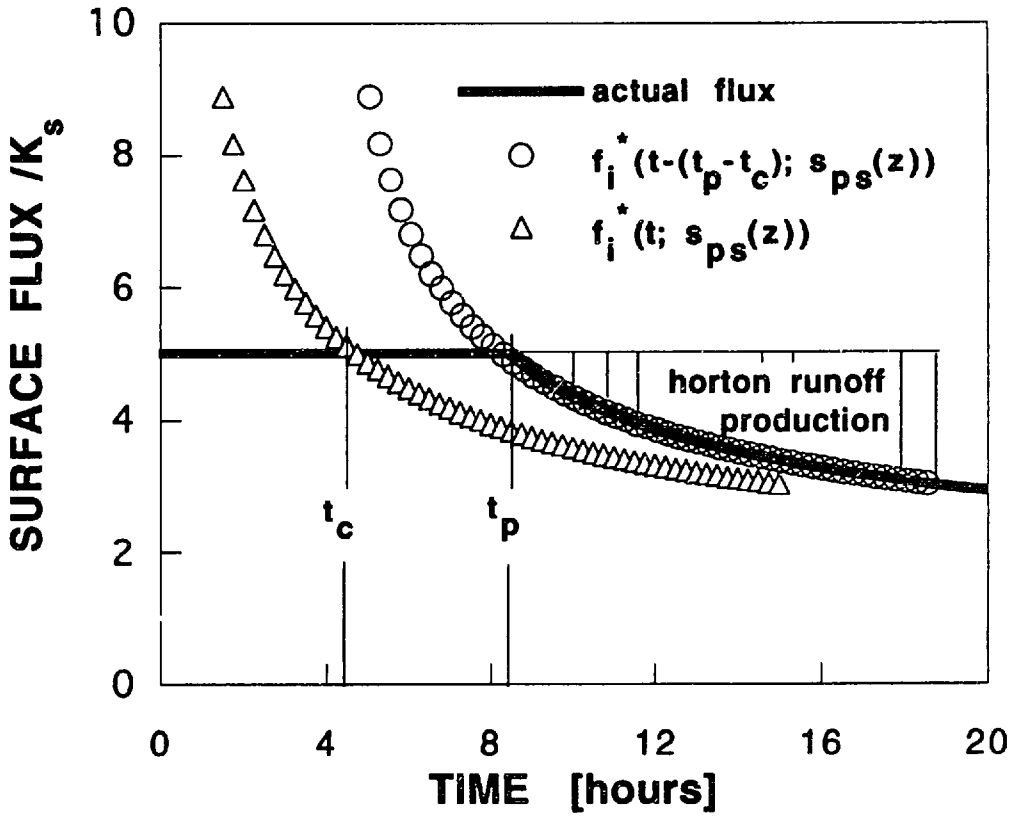

Figure 2.5 Illustration of time compression approximation (TCA) for infiltration

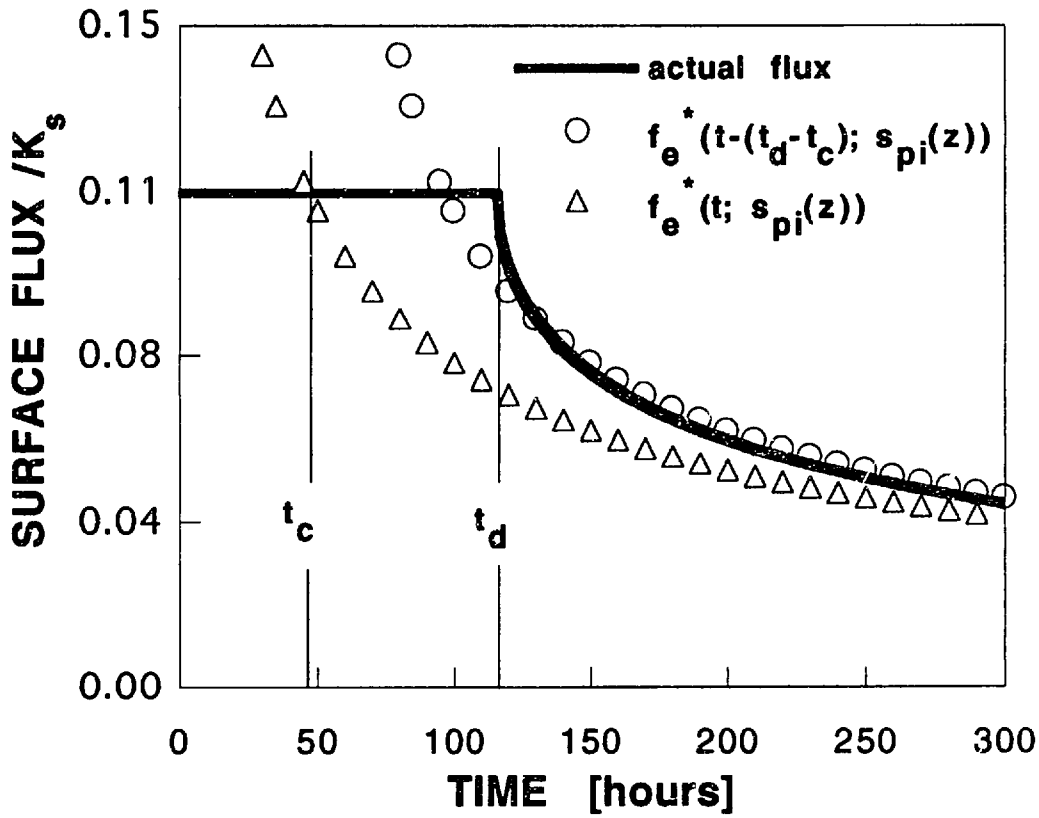

Figure 2.6 Illustration of time compression approximation (TCA) for exfiltration

intensity rainfall of five times the saturated conductivity, or approximately 0.6 cm hr^{-1}. The evaporation example uses the same soil and the potential evaporation from the case studies (Table 2.1). The results show how well the TCA flux rates approximate the actual (mixed boundary condition) flux rate for the given atmospheric forcing. In each case the actual surface flux rate (solid line, found by numerical simulation) is shown with a time origin of zero, while the capacity (also found by numerical simulation) is shown both with a time origin of zero (triangles) and with its origin shifted by t_p-t_c (circles) (as determined by equations (2.18) and (2.22)). The TCA flux rate solution is the rainfall intensity for $t < t_p$, and the shifted capacity curve (circles) for $t > t_p$, while for exfiltration it would be the potential evaporation (e_p) for $t < t_d$, and the shifted capacity curve for $t > t_d$. The approximation is remarkably accurate for infiltration.

Recently *Poulovassilis et al.* [1991] suggested that the approximation is exact for conditions of infiltration into a soil of uniform initial soil moisture. This is inconsistent with the findings of *Sivapalan and Milly* [1989]. In addition, *Dooge and Wang* [1993] have analytically demonstrated that the TCA cannot be exact, but it is an excellent approximation for a large class of soil hydraulic property models.

Regardless of whether the TCA, under these conditions, is exact or just a very good approximation, the existence of a uniform moisture content at the beginning of a storm or interstorm is improbable and unrealistic. An important question then is: how well does the TCA holds up under various estimates of pre-event initial conditions? In the following section, the results of the two case studies are used to address this issue.

2.d.2 Test of the TCA Under Mean Initial Conditions

For testing the applicability of the TCA to equilibrium water balance modeling and for determining its sensitivity to the initial condition moisture profile, the simulated moisture profiles from the previous two case studies are used as initial conditions. Because the model stochastic atmospheric forcing reasonably captures the important dynamics of real atmospheric forcing [*Eagleson*, 1978b], the variability of the simulated moisture profiles from one event to the next should be representative of the scale of (temporal) variability in the field.

For modeling the equilibrium water balance, an important test is to determine whether or not the infiltration or exfiltration capacity curves can be based on the mean

initial condition of all events, and then used in a TCA analysis to reproduce the mean of the soil controlled surface fluxes. In essence, if the TCA behaves as a linear operator, one would expect this approximation to be adequate.

To test this for infiltration, one hundred pre-storm moisture profiles are sampled from the numerical simulations and used as the initial condition for simulating a characteristic infiltration-excess runoff producing event. The average of the one hundred profiles ($<s_{ps}(z)>$) is then used as the initial condition to numerically simulate the capacity curve, f_i^* (t; $<s_{ps}(z)>$). The average of all the simulated flux rate histories are then compared with the TCA approximated solution, using this mean initial condition capacity curve in (2.18), (2.21) and (2.22).

Figures 2.7 and 2.8 illustrate the results for the infiltration case under deep and shallow water table conditions. The applied flux rate for these examples is the same as that used in the uniform initial moisture profile test (i.e. 0.61 cm/hr). This rainfall intensity is chosen to illustrate the important concepts during transitions from climate-controlled to soil controlled conditions and not because it is typical. It is in fact relatively high in comparison with the mean intensity used in the case study (0.21 cm/hr, Table 2.1), and would thus, on the basis of the assumed exponential distribution, occur for only about 6 percent of the storms. These extremes (i.e. $i>>K_S$) however, produce infiltration-excess runoff, and thus determine the departure of infiltration from mean precipitation.

The circles in the figures (2.7 and 2.8) represent the TCA solution formed using the mean initial condition profile in the determination of the capacity curve. The solid lines represent the ensemble average of the (numerically simulated) flux histories, and the dashed lines show plus and minus one standard deviation of the flux rate around this mean. Note that the variation around the mean is least at early and late times. This is to be expected because: 1) few post-evaporation moisture profiles (i.e. the infiltration initial conditions) are so wet as to cause very early ponding, and thus the early time solutions are soil independent (climate controlled); and 2) at very late times, the near surface initial condition has been passed over by the infiltration front, leaving the flow dynamics dominantly governed by the deep soil moisture profile. Because this deep soil moisture state is less variable from event to event than the near surface (see Figures 2.2 and 2.4), the long time flux rate is less variable (note earlier discussion on deep water table moisture profiles). In fact, for the shallow case, there is no variability after ~ 9 hours, because the soil column is saturated and the initial condition has been completely erased. Note that the larger variation

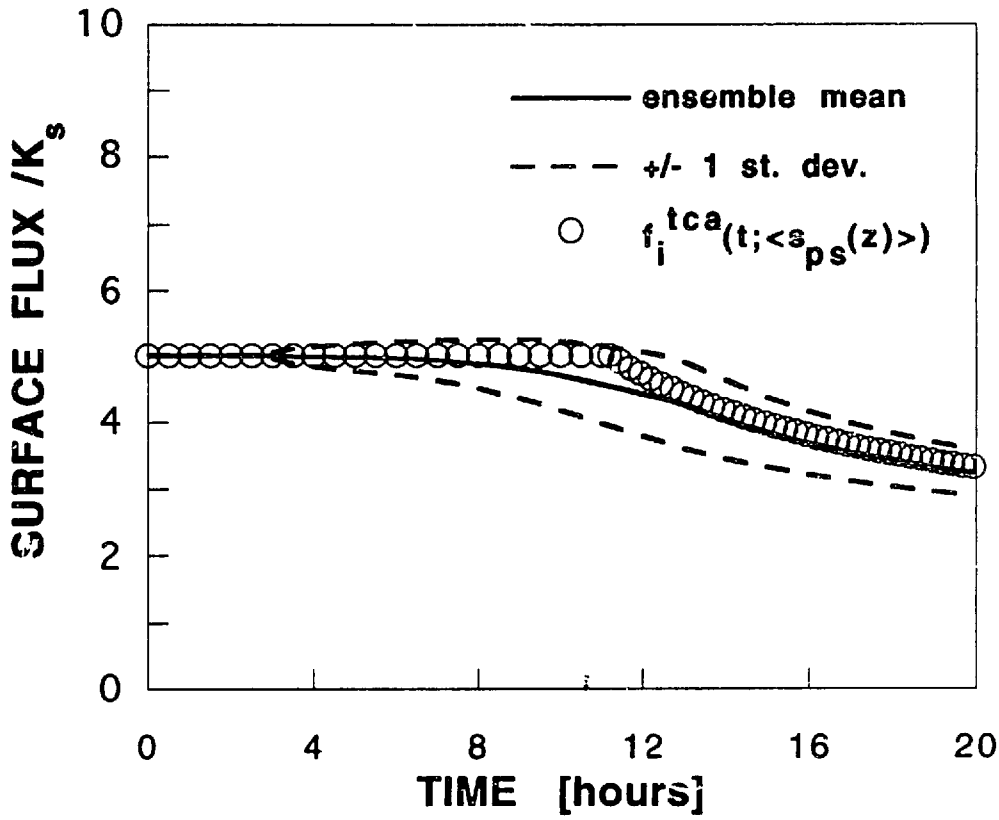

Figure 2.7 Test of time compression approximation for infiltration using mean initial conditions: Deep water table case

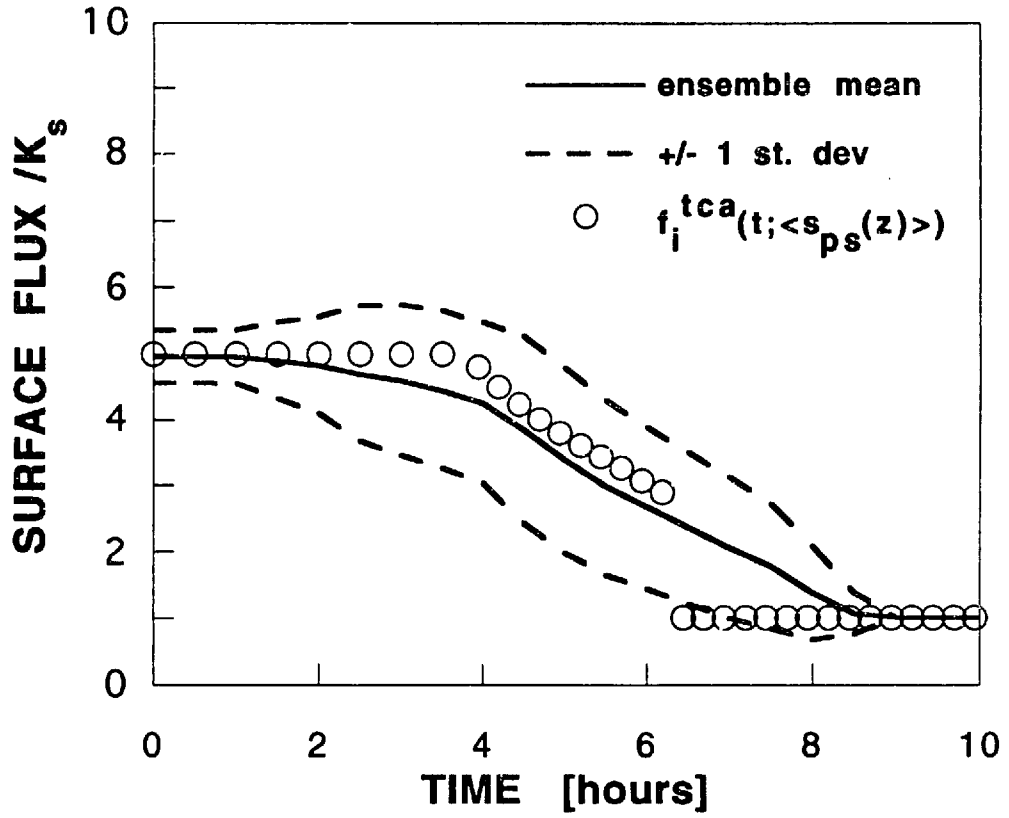

Figure 2.8 Test of time compression approximation for infiltration using mean initial conditions: Shallow water table case

at the intermediate times smoothes out the kink in the flux rate that occurs at the moment of ponding. The kink is smoothed out because each realization of the initial condition profile results in a slightly different ponding time.

To a very good approximation the TCA appears to apply for infiltration in this mean sense. For example, if one knew the non-uniform mean initial moisture profile at a location in a watershed then one could use this mean profile to initialize the infiltration capacity curve and use the TCA expressions to estimate the infiltration for a given storm event. The infiltration capacity curve for each event may thus be generalized and a single infiltration capacity curve for a season and location may be defined. In fact, the historical success of engineering flood forecasting practices (e.g. SCS curves and regionalized empirical infiltration equations) is partly owed to this physical characteristic of the vadose zone moisture dynamics.

Any one infiltration prediction could contain significant scatter, as indicated by the standard deviation envelope. For long term mean water balance however, any given storm intensity will occur many times and thus be exposed to the full ensemble of initial condition profiles. Thus to the degree that the mean TCA is unbiased, the individual errors will cancel, leaving an excellent estimate of the mean infiltration for a given storm intensity.

In Figure 2.9 the same analysis is made under the deep water table conditions for exfiltration. For this case one-hundred post storm moisture profiles ($s_{pi}(z)$) are used as initial conditions and the potential evaporation (e_p) is used as the forcing. Here the approximation is less accurate though still reasonable for mean water balance estimation. For water balance studies it is not the absolute deviation between the ensemble mean exfiltration curve and the "mean" TCA solution that is critical, but rather the difference between the cumulative integral under the curves up to the end of the interstorm event. For this case, much of the interstorm event is climate controlled and the soil capacity rates are not relevant during this fraction of time.

As before the variation caused by the differences in initial condition profile is largest for intermediate times. Note that the kink in the flux rate curve has been completely smoothed out in this case. Again, this is caused by differences in the drying time, t_d, for each of the realizations. A similar analysis for the shallow water table case showed no soil controlled evaporation events. This is because the exfiltration capacity curve for the shallow water table is always larger than the potential evaporation forcing. This result is consistent with the water balance for the twenty year simulation (Table 2.2), which showed

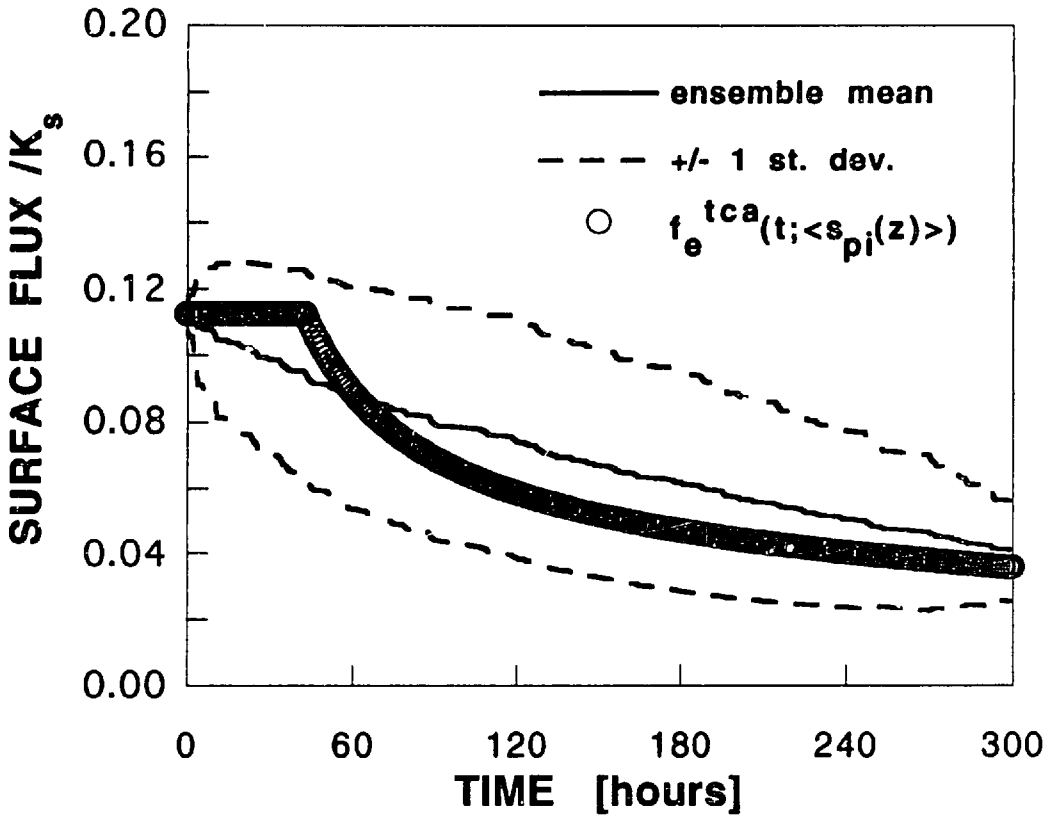

Figure 2.9 Test of time compression approximation for exfiltration using mean initial conditions: Deep water table case

actual evaporation equal to potential evaporation.

2.d.3 Test of the TCA under Equivalent Steady State Initial Conditions

While the results with the mean initial condition profile are interesting from a theoretical point of view, they are still partly impractical from the point of view of equilibrium water balance modeling. In general, one does not know these mean non-uniform pre-storm and pre-interstorm moisture profiles. Previously, however, it was demonstrated that the equivalent steady moisture profile $s_s(z; q_{st}=<q>)$ formed a reasonable estimate of these mean initial condition profiles, with the estimate improving deeper in the soil. Summarizing the earlier results, this improvement is due to the damping out of the surface induced perturbations with depth and the corresponding reduction in the variance and covariance terms (Equation 2.12) that biased the equivalent steady estimate of the mean moisture profile.

If the infiltration and exfiltration capacity curves are not too sensitive to the near surface initial condition profile, one might then expect that the equivalent steady profile $s_s(z; q_{st}=<q>)$ could be used as the initial condition in place of the means ($<s_{ps}(z)>$, and $<s_{pi}(z)>$). The utility of this further approximation is that the equivalent steady profile is dependent only on the mean column flow and water table depth. Methods for estimating these two parameters of the steady flow profile are discussed at the end of this chapter.

To test this further simplifying approximation, the infiltration and exfiltration capacities are simulated again, this time using the equivalent steady profiles (see Figures 2.1 and 2.3) as the initial condition. The resulting equivalent steady TCA solutions are plotted as the circles in Figures 2.10, 2.11 and 2.12. Using this estimate of the pre-event initial conditions introduces some bias to the estimation of the mean surface fluxes for the deep water table infiltration and exfiltration.

For infiltration (Figure 2.10), the "equivalent steady" TCA expressions underestimate the mean infiltration, particularly at intermediate times. This underestimation occurs because the equivalent steady profile overestimates the moisture content of the mean pre-storm profile (Figure 2.1). For exfiltration (Figure 2.11), the approximation leads to an overestimation of the mean flux, consistent with the fact that equivalent steady profile also overestimates the mean post-storm moisture profile (Figure 2.1).

As mentioned previously, the cumulative rather than the instantaneous infiltration

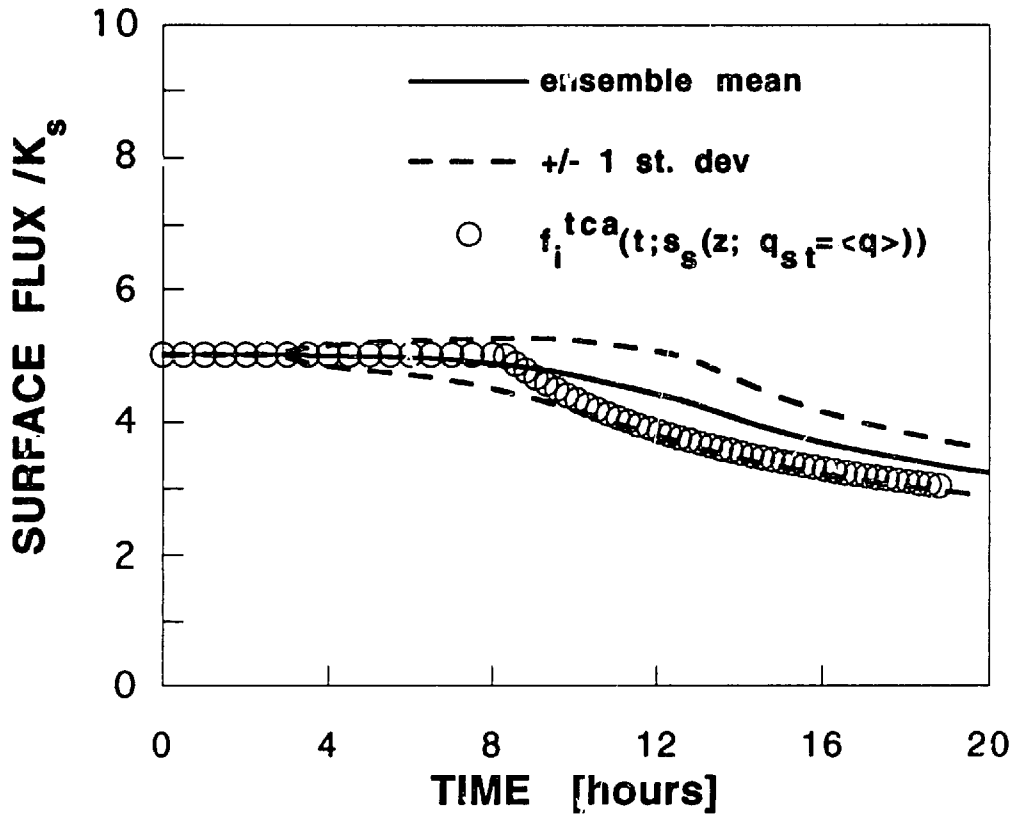

Figure 2.10 Test of time compression approximation for infiltration using equivalent steady state initial conditions: Deep water table case

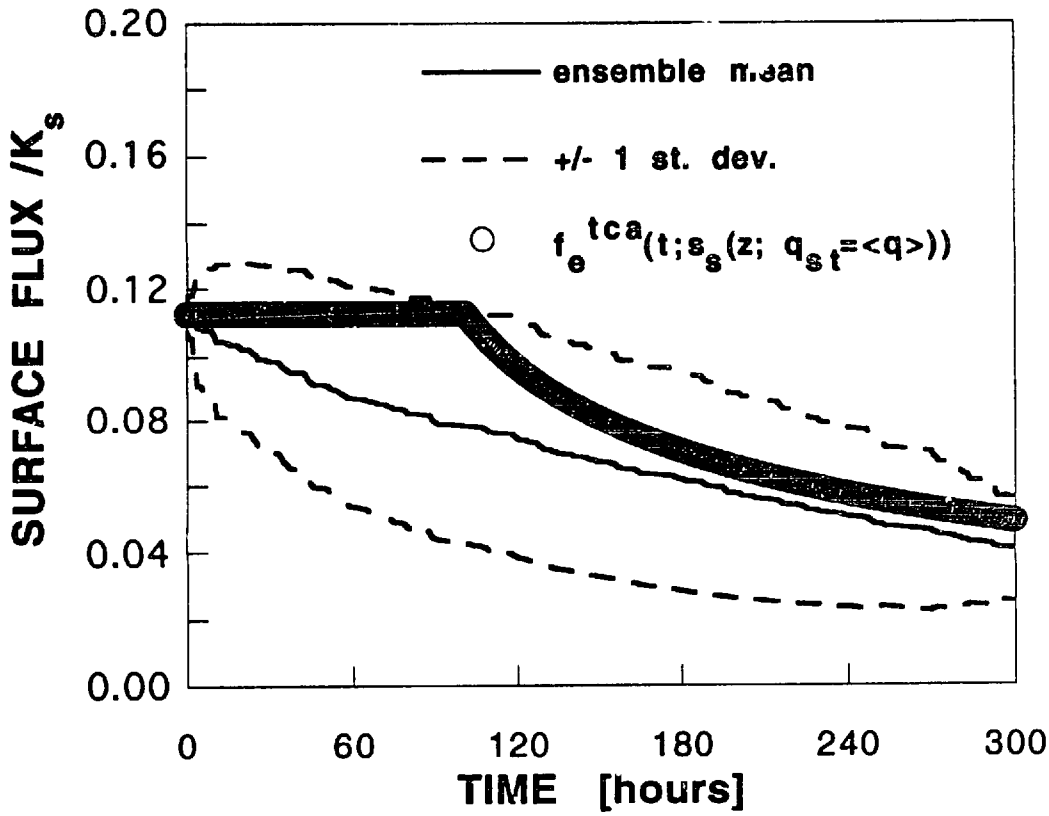

Figure 2.11 Test of time compression approximation for exfiltration using equivalent steady state initial conditions: Deep water table case

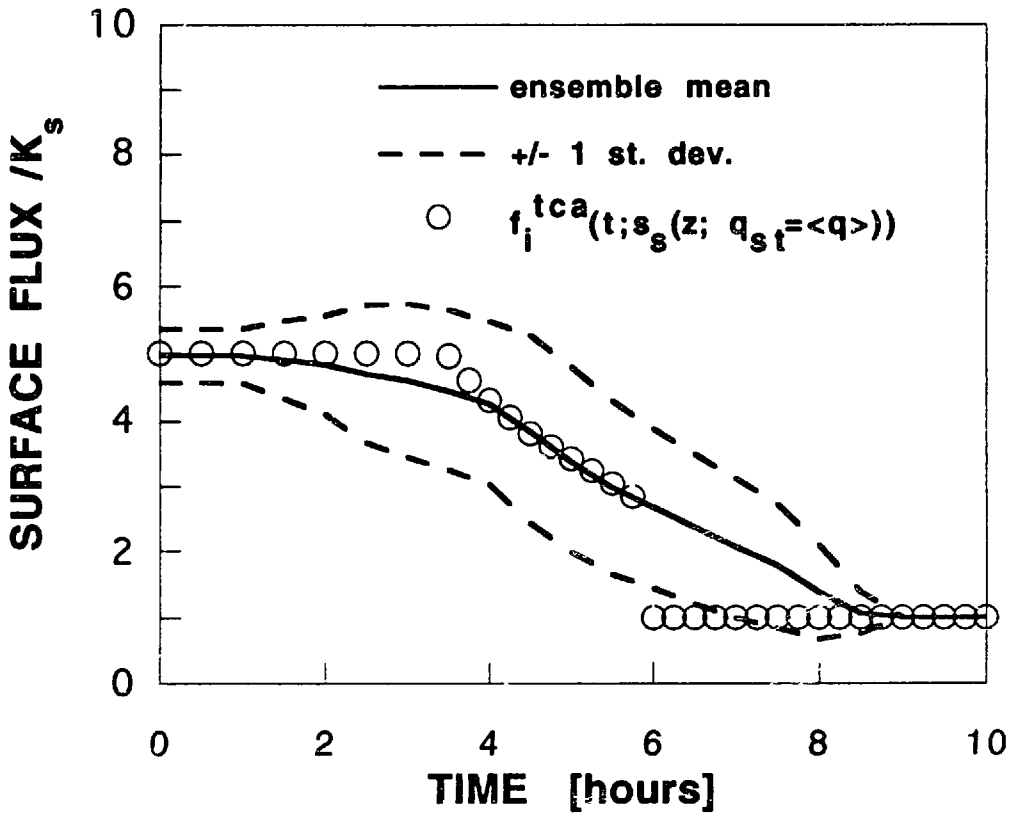

Figure 2.12 Test of time compression approximation for infiltration using equivalent steady state initial conditions: Shallow water table case

and exfiltration are the important quantities. It is thus significant that in both cases the long time behavior (which corresponds to the largest deviations from climate control) is predicted well.

Considering infiltration excess runoff for example, the errors associated with using the equivalent steady profile to initialize flux capacities are least for the largest runoff events, assuming (reasonably) that these events are caused by high intensity-long duration storms. The long time behavior, and thus the large soil controlled cumulative moisture exchanges, are predicted well because the role of the highly variable near surface initial condition is gradually diminished as the event progresses. This is because at long durations the infiltration front penetrates deeper in the soil, leaving infiltration excess runoff generation more dependent on penetration velocities in the deeper and less variable moisture profile where the equivalent steady profile best estimates the actual initial condition. This may be the reason why in traditional engineering approaches to initializing basins for rainfall-runoff transformation, methods that use correlations with the deep moisture state (e.g. the Antecedent Precipitation Index (A.P.I) give a good indication of the infiltration capacity.

For the shallow case (Figure 2.12), the TCA estimation using the equivalent steady state profile as the initial condition gives slightly better estimates than using the mean initial conditions. This is contradictory to the TCA operation being linear. Apparently the overestimation of the wetness of the mean pre-storm moisture profile by the equivalent steady profile compensates for second-order nonlinearity in TCA operation.

In summary, the steady-state initialized TCA yields an adequate and simple means to estimate the event exchanges of moisture which occur under combinations of climate and soil controlled boundary conditions. The robustness of the approximation derives from a combination of: 1) the fact that the TCA behaves in an approximately linear fashion with respect to initial conditions; and 2) the fact that by the time the surface flux rate comes under soil control (i.e. t_p or t_d), the wetting (or drying) front has usually penetrated comparatively deep into the soil, where the moisture state is relatively steady and thus is well estimated by the equivalent steady moisture profile.

In the above analysis, useful characteristics of the TCA have been demonstrated for a given soil type (clay) and a given rainstorm intensity and potential evaporation rate. The subject of Chapter 3 is the testing of an equilibrium water balance model whose performance is based, in a large part, on the validity of the use of the TCA and the

equivalent steady-state profile. The tests are conducted for various soil textures and climate types; they provide support for the use of the TCA and for the use of the equivalent steady-state profile as an indicator of mean initial conditions under broader conditions than are demonstrated here.

2.e Implications for Event Based Water Balance Models

The major focus of this work is on long-term equilibrium water balance modeling and the implications of this study on long time scale water balance are discussed in the following chapter (3). Some of the results nonetheless have relevance to short range event based water balance modeling and rainfall-runoff transformation.

A common problem in this type of modeling is specification of the initial moisture state of the watershed. The role of the initial condition is handled differently in various models, mostly depending on the type of model. Physically-based distributed models such as TOPMODEL [*Beven and Kirkby*, 1979] and the model presented by *Cabral et al.* [1993] specify the moisture state over the spatial domain.

The average streamflow of a given watershed and its contributing area characteristics could be used to estimate the spatial distribution of soil moisture, given assumptions are made concerning the dynamics of the saturated flow domain. For example, *Sivapalan et al.* [1987] use the contributing area methodology of TOPMODEL and an assumption that the baseflow before a storm results from a basin-wide spatially uniform recharge to derive the spatial distribution of the water table depth relative to the basin average water table depth. This mean depth can also be related base flow, either using the flow equations of TOPMODEL [*Sivapalan et al.*, 1987], or assuming Boussinesq flow [*Troch et al.*, 1993]. These methods incorporate the spatial effects, discussed by *Penman* [1951, referenced in *Kuhnel et al.*, 1991] of "riparian" near channel zones, where the evaporation is usually potential and runoff production significant, and "non-riparian" zones where evaporation may be soil controlled.

Also remotely sensed data of the near surface moisture state and some assumptions of how the profile is distributed from the surface to the water table may be used [*Famiglietti and Wood*, 1991b, referenced in *Troch et al.*, 1993]. Likewise, one may use the position of the water table in conjunction with assumptions on the moisture profile gradient from the water table up to the surface [*Sivapalan et al.*, 1987; *Troch et al.*, 1993]. In each of the

la'ter studies, the profile was assumed to be hydrostatic. This assumption will be discussed shortly.

In the absence of measurements of the moisture profile at the modeled locations in the field, the equivalent steady moisture profile should provide a reasonable, though partly biased, estimate of the initial condition for determining infiltration and exfiltration capacities. For homogeneous soils, this equivalent steady moisture profile can be found exactly for linear soils [*Gardner*, 1958]. *Salvucci* [1993] derived an approximate expression for soils with Gardner type power law conductivities. In Chapter 4 the derivation of this expression is re-derived and extended to apply to Brooks-Corey soils. For heterogeneous soils, it may be determined numerically (e.g. *Warrick and Yeh* [1990]). In all cases, the depth to the water table and steady flow rate (recharge or capillary rise) must be known.

Assuming that one of the above methods can be used to determine the water table depth and equivalent steady flow rate, the equivalent steady profile should form a better initial condition for initializing infiltration and exfiltration capacities than the hydrostatic profile assumed by *Sivapalan et al.* [1987], *Famiglietti and Wood* [1991a,b] and *Troch et al.* [1993]. The degree of improvement will depend, in both cases, on the depth to the water table.

For shallow water tables near channels, the steady profile is close to hydrostatic (see Figure 2.4). For deep water tables however, the hydrostatic assumption may lead to serious underestimation of the wetness of the moisture profile (see Figure 2.1), while the equivalent steady profile would only slightly overestimate the profile's moisture content.

If used to estimate infiltration capacities from which infiltration excess runoff is being calculated, the hydrostatic assumption is probably sufficient, since much of this runoff is created in the areas of high water table near the channels. For storage excess runoff, where the generation is partly dependent on downslope redistribution of infiltration from uphill areas, the hydrostatic assumption could be problematic, as it would overestimate the infiltration capacity of these uphill areas. If used to estimate exfiltration capacities, as in *Famiglietti and Wood* [1991a], it could be especially problematic since the departures of evaporation from potential will occur mostly in the drier uphill areas where the water table is deeper.

These effects are illustrated for the deep water table condition in Figures 2.13 and 2.14. The circles in these figures represent the TCA approximated solution using a

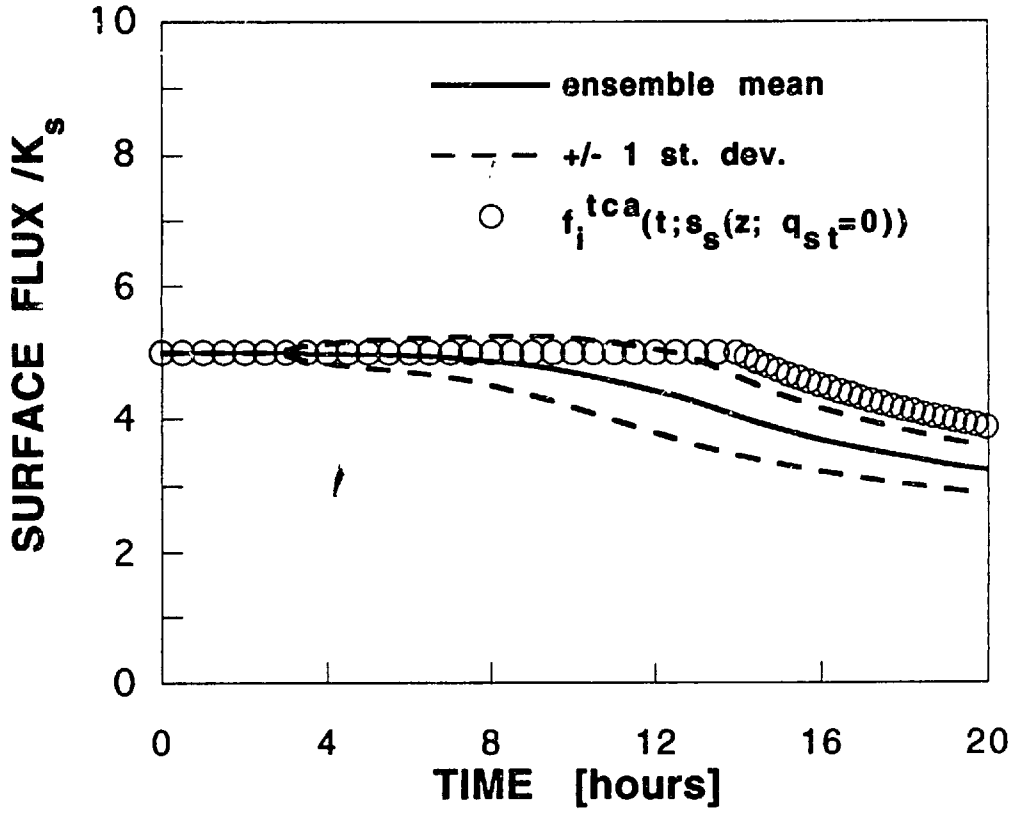

Figure 2.13 Test of time compression approximation for infiltration using hydrostatic initial conditions: Deep water table case

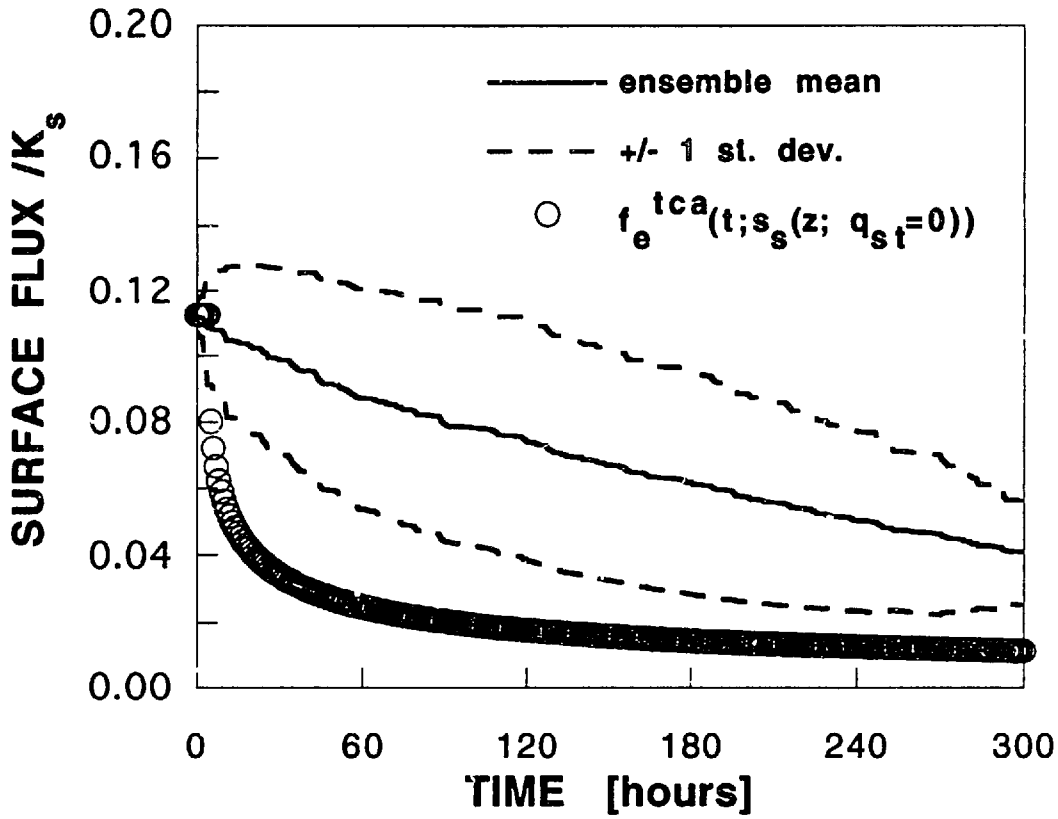

Figure 2.14 Test of time compression approximation for exfiltration using hydrostatic initial conditions: Deep water table case

hydrostatic initial profile in the flux capacity determination. The effect on infiltration is rather small. The impact on the exfiltration solution however, is significant and could cause large underestimation of evaporation. The direction of the effect is consistent with the relative wetness of the hydrostatic profile in comparison with the mean initial condition profiles (Figure 2.1).

2.f Conclusions

The definition of pre-event soil moisture profile and time compression analysis are critical components in water balance models that are based on realistic infiltration/exfiltration relations and include profile-redistribution of vadose zone moisture. Detailed analysis of these two fundamental components of water balance modeling are presented. Numerical integration of the governing equations for liquid moisture flow in the unsaturated zone are used in simulations designed to illustrate the role of temporal variability in the system. The simulations consist of forcing the surface of a one-dimensional soil column, bounded at its base by a fixed water table, with the output of a stochastic event-based model of precipitation and potential evaporation. The simulations are run until (and beyond when) an equilibrium condition is reached between the long term mean values of surface and bottom fluxes. For situations with deep water table, two distinct zones develop: a near-surface highly-unsteady zone, and a deeper quasi-steady zone. The equivalent steady moisture profile, i.e. the steady profile corresponding to the mean of the simulated column flow, is found to reasonably approximate the temporal mean, mean pre-storm, and mean post-storm moisture profiles, particularly in the deeper zone. In the upper zone, the equivalent steady profile forms a biased estimate of the temporal mean. The bias is shown, through perturbation analysis, to lead to overestimation of the wetness of the mean moisture profile. For shallow water tables, the distinction between the two zones collapses. In this case, both the equivalent steady profile and the mean profile are close to the hydrostatic profile.

The simulations are also used to test the utility of the time compression approximation (TCA) in modeling surface fluxes under temporally variable initial conditions. It is demonstrated that the use of the mean pre- and post- storm event moisture profiles as initial conditions for the infiltration and exfiltration flux capacities does not produce major bias in TCA predicted surface fluxes. In this sense the TCA behaves as a

linear operator. Furthermore, it is shown that the estimation of these mean initial condition profiles by the equivalent steady state soil moisture profile is an adequate approximation for determining mean landsurface response to event-based atmospheric forcing.

In summary, the time compression approximation (TCA) provides an adequate description of the nonlinear, state dependent transition of surface flux from climate to soil control. It is dependent on the specification of an initial soil wetness profile, and is nearly linear in that the mean of surface flux histories for an ensemble of events is well reproduced by the TCA flux expression evaluated at the mean of the initial conditions of the ensemble of events. Because the mean initial condition is well approximated by the equivalent steady profile defined by the temporal mean flux (<q>) through the soil column, the equivalent steady profile and the TCA approximation may be combined to form a tractable closure to the land surface water balance equation subject to intermittent storm and interstorm events.

Chapter 3: Modification and Testing of a Statistical-Dynamical Model of the Equilibrium Water Balance for Soils Bounded by Deep Water Tables

3.a Background

Chapter 2 reported on the results of a numerical study of soil moisture profile dynamics. Two essential tools for partitioning precipitation and potential evaporation forcing were discussed: the equivalent steady profile and the time compression approximation. Comments were made on how these tools may be used in running water balance modeling. Here the concepts are applied to the analysis of the equilibrium water balance.

As a starting point the analytic framework of the hydro-climatic system put forth by *Eagleson* [1978a] is reviewed. This framework establishes a systematic approach to the modeling of equilibrium water balance, expressing the most essential dynamical processes and their couplings in a manner amenable to statistical-dynamical analysis. The approximate analytic solution of the water balance partitioning [*Eagleson* ,1978b-g] by a soil column bounded by a deep water table is described.

Mean water balance estimates found with this approximate analytic solution are compared here with the results of a monte-carlo numerical integration of the governing conservation and flow equations. The comparisons are made for an inclusive range of characteristic soil-climate combinations, leading to situations characterized by diverse hydrologic response regimes, and thus forming a robust test of the model's capabilities. The comparisons are not meant to imply that the numerical simulation model fully represents the hydrology of real systems. Rather the comparisons are made to test the ability of the equilibrium model to represent, in a simple manner, some of the complicating features of real hydrologic processes. The complexities include: 1) the nonlinearity of the hydraulic properties; 2) the formation of surface boundary conditions by the interaction of the atmospheric forcing and the surface moisture state; and 3) the temporal variability of the soil moisture profile as induced by the atmospheric forcing.

The comparisons with simulation results are also used to further support the general conclusions of Chapter 2. In that chapter it was demonstrated, for a limited number of characteristic soil-climate combinations, that the equivalent steady moisture profile (the

steady profile which transmits the mean vertical recharge) forms an adequate surrogate for the moisture profile prior to storm and interstorm (evaporation) events. In particular it was shown that the infiltration and exfiltration capacities could be initialized with this moisture profile and then used with the time compression approximation (TCA) to predict the mean response of the surface fluxes to atmospheric forcing. The analytic equilibrium model tested here utilizes the TCA and a related moisture profile assumption, and its performance is based, in large part, on their validity. In the conclusion of this chapter the framework is established for extending the Eagleson model to account for near surface water table effects.

3.b Model review

3.b.1 General Framework

Eagleson [1978a] represents the physical processes of the hydro-climatic system as in Figure 3.1 (reproduced from Figure 4, *Eagleson* [1978a]). In this framework, the climate exists as an independent system which, through interaction with static surface parameters (e.g. roughness and albedo characteristics), forms atmospheric forcing of the soil hydrologic system in the form of precipitation and potential evaporation events. In response to this forcing, the land surface as governed by the diffusive soil moisture processes infiltrates, exfiltrates, transpires through vegetation, drains and stores moisture. The long-term average of these responses form the mean water balance partitioning of precipitation into evapotranspiration and yield (surface and groundwater runoff).

3.b.2 Climate Forcing

The atmospheric forcing denoted in Figure 3.1 is modeled as the Poisson arrival process of rectangular rain pulses with exponentially distributed intensity (i) and duration (t_r), between which are periods (t_b) of constant potential evaporation (e_p). This representation of the atmospheric forcing captures the essential features of the intermittency of precipitation events. Because this study focuses on temporal variability, this choice is critical and warrants further discussion.

Note first that in relation to the water balance, the critical soil moisture processes are

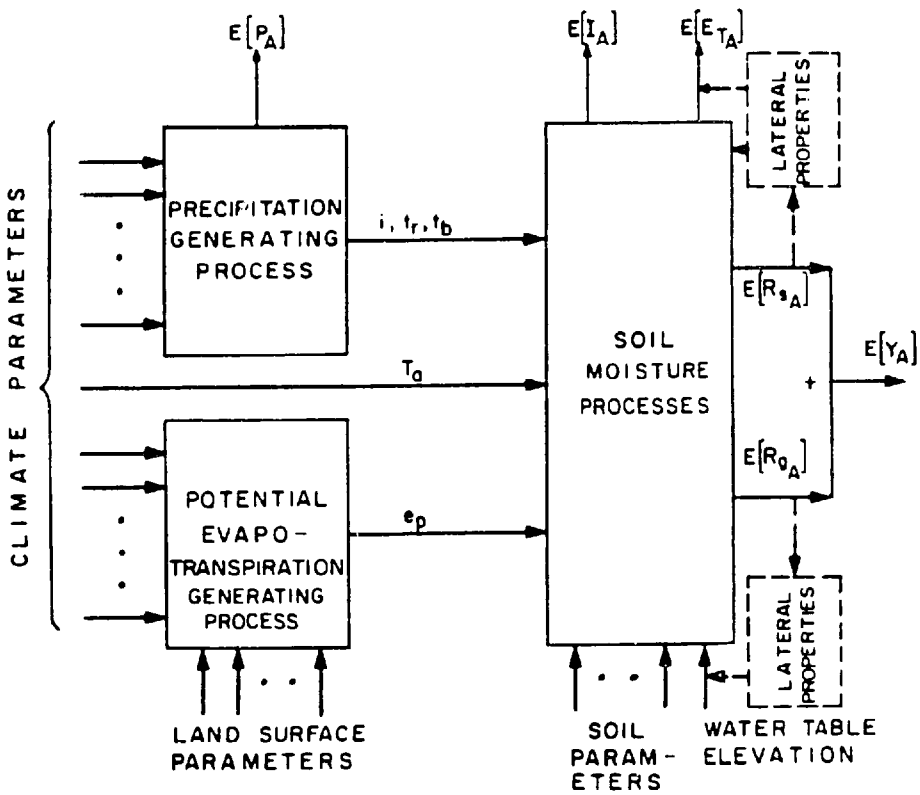

Figure 3.1 Simplified hydro-climate system [*Eagleson*, 1978a]

those which determine whether or not the soil can infiltrate water at the rate it is supplied (i.e. the rainfall intensity, i) and evaporate it at the rate demanded (i.e. the potential evaporation rate, e_p). When the soil can absorb or supply at these rates, the situation is referred to as climate controlled, and when it cannot the situation is soil controlled. As discussed in the Chapter 2 it is the latter case, the existence of which follows directly from the physics of moisture flow, which complicates the determination of water balance.

Secondly, note that the time scales of these processes (switches between the soil controlled and climate controlled regimes), found for example through TCA analysis by comparing flux-capacity relationships to atmospheric forcing rates, are often on the order of hours to days (e.g. ponding and drying times). The critical time scales in the dynamics of water balance are thus at the same time scales at which the atmospheric forcing contains great variability (i.e. weather dominated storm and interstorm durations). The large variability of the forcing at the time scales critical to the dynamics demands that the representation of atmospheric forcing retain its highly intermittent variability.

3.b.3 Soil moisture processes

The major assumptions concerning the representation of the soil moisture processes are discussed in detail in Chapter 2. In summary, the unsaturated zone hydrology is represented by the one dimensional mass conservation of the Darcy flux throughout a homogeneous soil column represented by the *Brooks and Corey* [1966] hydraulic parameterization. The top of this representative column is forced by the above described stochastic event-based atmospheric forcing, and the surface boundary conditions are formed by the dynamic interaction of this forcing with the surface moisture state. They are taken as flux boundary conditions, equal to the atmospheric forcing, as long as the surface is not saturated or very dry. If and when the surface becomes saturated or very dry, the surface fluxes come under soil control, and the boundary conditions are specified as the surface concentration conditions. The bottom of the soil column is bounded by a water table at a fixed position for all time. The model includes a distributed root sink, but this feature is not tested in this work. In addition, the model incorporates the role of surface retention in both the evaporation and infiltration processes, but this feature also is not tested.

In forming an approximate analytic solution for the resulting evaporation and yield

(recharge and surface runoff), *Eagleson* [1978a-g] takes the event-based derived distribution approach. In this approach he makes four critical assumptions:

1. The solution to the surface flux during a single event (storm infiltration or interstorm evaporation) under a sequence of flux and then concentration boundary conditions can be approximated using time compression. A test of this approximation, along with a review of its derivation, is discussed in Chapter 2. The approximation is found to be rather accurate.

2. The soil column can be conceptually separated into an upper, unsteady boundary layer, within which the surface-induced forcing is dominant, and a deeper quasi-steady zone, and the fluxes in each can be determined independently. This assumption is supported (for conditions of deep water table) in Chapter 2 where the rapid filtering of the higher frequency (event scale) flux variability with depth is reported.

3. The solution for the fluxes into and out of a soil column bounded by a water table can be approximated by adding the capillary rise that would occur from the water table to a dry surface to the fluxes that would occur if the medium were semi-infinite. This assumption will not be tested here, as the water table in the test cases will be positioned deep enough to preclude its effect on the surface moisture dynamics. Accounting for the effects of a near surface water table is discussed in the final section of this chapter and in the remaining chapters of this thesis.

4. The final and most critical assumption is that the near-surface moisture profile at the beginning of each storm and interstorm event can be approximated by the depth- and time-averaged soil moisture and that its magnitude can be found by equating the long term mean of the fluxes into and out of the soil column. *Eagleson* [1978a] refers to this as the equilibrium soil moisture, s_0, and emphasizes its role as the primary variable in partitioning the land surface moisture fluxes.

With these assumptions, Eagleson finds analytic expressions for the expected value of the event-integrated surface fluxes into the boundary layer and the mean bottom flux out of the quasi-steady zone, all in terms of the equilibrium soil moisture. Details of these

derivations are found in *Eagleson* [1977] and *Eagleson* [1978a-g]. Here, only the methodology is presented.

3.b.4 Mean Annual Infiltration

For infiltration, determination of the mean annual flux requires integrating the lesser of the rainfall intensity (i) or infiltration capacity (f_i^*) (viz. the time compression approximation) over all possible storm durations and intensities. Multiplying each possible duration - intensity combination by its joint probability of occurrence, summing these to find the mean event flux, and then multiplying this mean event infiltration by the mean number of storms per year (m_v) yields the annual infiltration volume.

The expected value operation (<·>) described above may be written:

$$\langle I_A \rangle = m_v \int_0^\infty \int_0^\infty \left(\int_0^\tau MIN\left[f_i^*(t), \xi \right] dt \right) f_{t_r}(\tau) f_i(\xi) d\tau d\xi \qquad (3.1)$$

where $f_{t_r}(\tau)$ and $f_i(\xi)$ are the probability distributions of storm duration and storm intensity (respectively).

For the infiltration capacity, *Eagleson* [1978c] uses the *Philip* [1957a] equation series solution for infiltration into a semi-infinite and uniform soil moisture profile:

$$f_i^* = \frac{1}{2} S_i t^{-1/2} + A_o \qquad (3.2)$$

where $S_i(s_{ps})$ is the sorptivity and $A_o(s_{ps})$ primarily (but not exclusively) reflects the effects of gravity. The dependence of these terms on the soil parameters for an assumed semi-infinite soil at uniform initial soil saturation (s_{ps}, soil moisture *p*rior to *s*torm) is given by *Eagleson* [1978e] as:

$$S_i = 2(1 - s_{ps}) \left[\frac{5 n_e K_s |\Psi_s| \phi_i(d, s_{ps})}{3 m \pi} \right]^{1/2} \qquad (3.3)$$

$$A_o = \frac{1}{2} K_s (1 + s_{ps}^c) \tag{3.4}$$

In the above, n_e is the porosity, K_S is the saturated hydraulic conductivity, and m, c and Ψ_S are parameters of the *Brooks and Corey* [1966] unsaturated soil hydraulic model (the pore size distribution index, the pore disconnectedness index, and the bubbling pressure head, respectively; see Appendix A for review). The function $\phi_t(d,s_{ps})$ appearing in (3.3) is the dimensionless sorption diffusivity, a weighted average of the (moisture dependent) diffusivity. It was derived by *Crank* [1956] on the basis of numerical experimentation, and is given by *Eagleson* [1978e] as:

$$\phi_i(d, s_{ps}) = (1 - s_{ps})^{-5/3} \int_{s_{ps}}^{1} s^d (s - s_{ps})^{2/3} ds \tag{3.5}$$

where d is related to m and c by:

$$d = c - \frac{1}{m} - 1 \tag{3.6}$$

Utilizing equations (3.2) through (3.4) and assuming i and t_r distributed exponentially, *Eagleson* [1978e] integrates (3.1) to find (with some analytic approximation):

$$\langle I_A(s_{ps}) \rangle = \langle P_A \rangle \left\{ 1 - exp\left(-\eta A_o - \left[\eta^2 \delta S_i^2 \right]^{1/3} \right) \cdot \right.$$
$$\left. \Gamma\left(1 + \frac{1}{2}\left[\eta^2 \delta S_i^2 \right]^{1/3} \right) \cdot \left(\frac{1}{2}\left[\eta^2 \delta S_i^2 \right]^{1/3} \right)^{-\frac{1}{2}\left[\eta^2 \delta S_i^2 \right]^{1/3}} \right\} \tag{3.7}$$

where δ and η are equal to the reciprocals of the mean storm duration and intensity, $\langle P_A \rangle$ is the mean annual precipitation, and $\Gamma(\cdot)$ is the Gamma function.

3.b.5 *Mean Annual Bare Soil Evaporation*

To find the mean annual bare soil evaporation ($<E_{s_A}>$), *Eagleson* [1978d] uses the time compression approximation to integrate the lesser of the potential evaporation rate (e_p) and the exfiltration capacity (f_e^*) over all possible interstorm durations. He then multiplies each of these event-integrated fluxes by the probability of the interstorm duration, sums these weighted amounts, and again multiplies by the mean number of storms (interstorms) per year (m_v) yielding (for the case of no vegetation, no surface retention, and infinite water table depth):

$$\left\langle E_{s_A} \right\rangle = m_v \int_0^\infty \left(\int_0^\tau MIN\left(f_e^*, e_p\right) dt \right) f_{t_b}(\tau) d\tau \tag{3.8}$$

Here $f_{t_b}(\tau)$ is the probability distribution of time between storms and f_e^* is approximated by *Eagleson* [1978d] as:

$$f_e^* = \frac{1}{2} S_e t^{-1/2} \tag{3.9}$$

In the above, S_e is the exfiltration desorptivity:

$$S_e = 2 s_{pi}^{1+d/2} \left[\frac{n_e K_s |\Psi_s| \phi_e(d, s_{pi})}{m\pi} \right]^{1/2} \tag{3.10}$$

where s_{pi} is the soil saturation prior to interstorm. The dimensionless exfiltration diffusivity ($\phi_e(d,s_{pi})$), also a weighted mean derived by *Crank* [1956], is given by Eagleson (1978d) as:

$$\phi_e\left(d, s_{pi}\right) = 1.85 \cdot s_{pi}^{-d-1.85} \int_0^{s_{pi}} s^d \left(s_{pi} - s\right)^{0.85} ds \tag{3.11}$$

Taking the expected value expressed in (8) for exponentially distributed time between storms, *Eagleson* [1978d] finds the mean annual bare soil evaporation (again under

conditions of no vegetation, infinite water table depth, and no surface retention):

$$\left\langle E_{s_A}\left(s_{pi}\right)\right\rangle = \left\langle E_{p_A}\right\rangle \cdot \left\{1 - \left(1+\sqrt{2E}\right)e^{-E} + \sqrt{2E}\cdot\left(\Gamma\left(\frac{3}{2}\right) - \gamma\left[\frac{3}{2}, E\right]\right)\right\} \tag{3.12}$$

Here $\Gamma(\cdot)$ is the gamma function, $\gamma(\cdot,\cdot)$ is the incomplete gamma function, $<E_{pA}>$ is the mean annual potential evaporation:

$$\left\langle E_{p_A}\right\rangle = \frac{e_p m_v}{\beta} \tag{3.13}$$

and E is the evaporation effectiveness:

$$E = \frac{\beta S_e^2}{2e_p^2} \tag{3.14}$$

where β is the reciprocal of the mean time between storms (t_b).

3.b.6 Recharge

The (quasi-steady) deep soil flux, for infinite water table condition, is given by *Eagleson* [1978c] as the gravitational percolation at the quasi-steady soil saturation (s_s), yielding a mean annual recharge ($R_{gA}(s_s)$) of

$$\left\langle R_{g_A}\right\rangle = K_s s_s^c T \tag{3.15}$$

where T is the time interval of one year. Equation (3.15) is derived by applying equation (A.2) to (2.11) (and changing sign to define recharge as a positive addition to the saturated zone) under the assumption of uniform soil moisture distribution in the soil column.

3.b.7 Equilibrium Water Balance Partitioning

To determine the mean water balance partitioning, *Eagleson* [1978f] approximates

the (temporally variable) boundary layer soil moisture values prior to all storms (s_{ps}) and interstorms (s_{pi}), and the quasi-steady soil moisture below the boundary layer (s_s), by a single effective soil moisture, the so called equilibrium soil moisture (s_o) for which the inputs and outputs to the soil column are in balance. Mathematically this equilibrium soil moisture is defined implicitly by:

$$\left\langle I_A\left(s_{ps}=s_o\right)\right\rangle-\left\langle E_{s_A}\left(s_{pi}=s_o\right)\right\rangle=\left\langle R_{g_A}\left(s_s=s_o\right)\right\rangle \tag{3.16}$$

This last step, which follows from assumption (4) in the beginning of this section (Analytic Approach) and which is the essence of the equilibrium water balance method, will be discussed at length in relation to the statistical analysis of the soil moisture profile of Chapter 2.

3.c Modifications

Detailed analyses and careful implementation of the *Eagleson* [1978a-g] model reveal that it ought to include two simple modifications in order to maintain internal consistency. Here two changes are introduced to the model equations and hereafter the modified model is used for all comparisons.

1. By definition, the diffusivity is:

$$D(s)=\frac{1}{n_e}K(s)\frac{d\Psi}{ds} \tag{3.17}$$

Using the K(s) and Ψ(s) relations given by Brooks-Corey (reviewed in the Appendix A) *Eagleson* [1978c] derives the diffusivity as:

$$D(s)=\frac{K_s\left|\Psi_s\right|}{mn_e}s^d \tag{3.18}$$

This however applies only for soil saturation (s) less than one and capillary tension head (Ψ) less, in magnitude, than the bubbling pressure head, Ψ_s. For tension head between Ψ_s and zero, the soil is so called tension saturated, and the diffusivity is, by definition,

infinite, i.e.:

$$D(s=1)=\infty \tag{3.19}$$

For the exfiltration capacity, neglecting the tension saturated zone has no effect, since the initial soil saturation and boundary condition are both less than one. For infiltration, however, the tension saturated zone will develop (for soils displaying this characteristic) prior to ponding, and thus must be modeled in the derivation of infiltration capacity. *Philip* [1957b], noted that its effect is equivalent to that of ponded water of depth $|\Psi_s|$ at the soil surface, and showed that its effect on infiltration capacity could be accounted for by modifying the sorptivity as:

$$S_{i,mod}=\left(S_i^2+2n_eK_s|\Psi_s|\cdot\left(1-s_{ps}\right)\right)^{1/2} \tag{3.20}$$

The exact same result can be arrived at by applying the Crank weighting integral to the corrected diffusivity form (equations 3.18 and 3.19). *Haverkamp et al.* [1990] and *Zimmerman and Bodvarsson* [1991] found equivalent dependence of sorptivity on the magnitude of the tension saturated pressure head.

In the following tests, this substitution (Equation 3.20) is made in the expression for mean annual infiltration (Equation 3.7).

2. In deriving an exfiltration capacity (f_e^*) for vegetated soils, *Eagleson* [1978c] finds:

$$f_e^*=\frac{1}{2}S_e t^{-1/2}-\frac{1}{2}K\left(s_{pi}\right)-Me_v \tag{3.21}$$

where $K(s_{pi})$ is the unsaturated hydraulic conductivity at soil saturation s_{pi}, M is the fractional vegetation coverage and e_v is the transpiration rate. He then simplifies this expression by dropping the $K(s_{pi})$ term, noting that for early times it will be much less than the first term (which is proportional to $t^{-1/2}$). However, in using the time compression approximation, the actual flux is always taken as the lesser of the capacity (f_e^*) and the forcing (e_p). A better rationale for excluding the $K(s_{pi})$ term is thus its magnitude relative to e_p. Assuming that in some conditions the mean recharge and potential evaporation rates

are of the same order, the 0.5 $K(s_{pi})$ term must then be kept, because under equilibrium conditions (e.g. Equation 3.16) it may be of the same order as the mean recharge ($K(s_s)$).

Re-inserting this term into the exfiltration capacity, the modified expected value of bare soil evaporation becomes:

$$\left\langle E_{s_{A,mod}}(s_{pi})\right\rangle = \left\langle E_{p_A}\right\rangle \cdot \left\{1 - \left(1 + \sqrt{2\Lambda}E + (2\Omega)^{-1/2}\right)e^{-\Lambda E} + \left((2\Omega)^{-1/2} + \sqrt{2\Omega}E\right)e^{-\Omega E} + \sqrt{2E}\cdot\left(\gamma\left[\frac{3}{2}, \Omega E\right] - \gamma\left[\frac{3}{2}, \Lambda E\right]\right)\right\} \tag{3.22}$$

where:

$$\Lambda = \frac{1 + \dfrac{K_s s_{pi}^c}{4e_p}}{\left(1 + \dfrac{K_s s_{pi}^c}{2e_p}\right)^2} \tag{3.23}$$

and

$$\Omega = 2\left(\frac{K_s s_{pi}^c}{e_p}\right)^{-2} \tag{3.24}$$

Note that for $K(s_{pi}) << e_p$, as might occur in an area with little recharge and high potential evaporation (e.g. arid climate, clay soil), Λ approaches one and Ω approaches infinity. In this limit, Equation (3.22) reverts back to (3.12).

While the two modifications described above are important, they do not signify a departure from the basic model structure and philosophy as given by *Eagleson* [1978a-g].

3.d Tests and Discussion

In order to test the expressions for the mean water balance partitioning, approximately twenty years of unsaturated flow are simulated using the numerical finite element program developed by *Milly* [1982]. This model integrates the governing flow

and conservation equations (Richard's Equation) over a discretized soil column. The surface boundary conditions are formed, at each time step, by the interaction of the atmospheric forcing (a realization of the stochastic model) and surface state, as described in Chapter 2. The bottom boundary condition is taken as a water table at fixed position. The mean annual water balance is found by integrating the surface and bottom fluxes throughout the duration of the simulation, and then dividing the totals by duration.

In all, nine simulations were performed by combining three soil types, ranging from clay to sand-loam (Table 3.1), with three climate regimes, ranging from humid to arid (Table 3.2). For each simulation, the water table was located at five meters below the surface. Sensitivity analysis revealed this to be effectively semi-infinite, as raising or lowering it had little to no impact on the mean water balance.

Table 3.1: Representative Brooks-Corey Soil Parameters

	clay	silt-loam	sand-loam
K_s (cm/sec)	3.4 E-05	3.4 E-04	3.4 E-03
Ψ_s (cm)	-90	-45	-25
n_e (dimensionless)	0.45	0.35	0.25
m (dimensionless)	0.44	1.2	3.3

Source: *Bras* [1990]

Table 3.2: Representative Climate Parameters

	humid	semi-humid	arid
$\langle i \rangle$ (cm/day)	1.61	5.07	2.99
$\langle t_r \rangle$ (days)	0.72	0.25	0.48
$\langle t_b \rangle$ (days)	3.77	3.44	6.46
e_p (cm/day)	0.19	0.33	0.41
E_{pA} (cm/yr)	58.2	112.3	139.3
P_A (cm/yr)	94.2	125.4	75.5

Source: *Hawk and Eagleson* [1992]

Table 3.3 and Figure 3.2 compare these simulated water balance results (written as a percentage of the mean annual precipitation), with the analytic results of the (modified) equilibrium model (i.e. Equation 3.16). The correspondence is remarkable. The equilibrium model reasonably predicts the partitioning for such varied hydrologic regimes as the arid clay example, which is dominated by evaporation (84%) and yields little recharge (14%) or surface runoff (2%), and the humid sand-loam example, which is dominated by recharge (95%) and yields little evaporation (5%). The ability of the model to predict such distinct partitioning under the same forcing reveals that the model is truly capturing the soil-controlled events that are so critical to estimating water balance. The equilibrium model is not merely reflecting the partitioning implicit in the forcing, e.g. the potential evaporation and mean precipitation.

Table 3.3: Comparison of Simulated Mean Water Balance and Analytic Equilibrium Model Estimates

	% Evaporation		% Runoff		% Recharge	
	Sim	Equil	Sim	Equil	Sim	Equil
arid,clay	84.4	84.6	1.9	1.6	13.7	13.8
arid, silt-loam	29.2	36.3	0.0	0.0	70.8	63.7
arid, sand-loam	4.5	2.5	0.0	0.0	95.5	97.5
semi-humid, clay	71.4	74.8	3.8	4.2	24.8	21.0
semi-humid, silt-loam	31.6	35.5	0.0	0.0	68.4	64.5
semi-humid, sand-loam	5.3	2.9	0.0	0.0	94.7	97.1
humid,clay	58.0	60.8	0.3	0.4	41.7	38.8
humid, silt-loam	30.2	33.5	0.0	0.0	69.8	66.5
humid, sand-loam	5.0	2.9	0.0	0.0	95.0	97.1

Note also the skill with which the equilibrium model captures the mean surface runoff production for the clay soil runs, even though the runoff is a small fraction of the

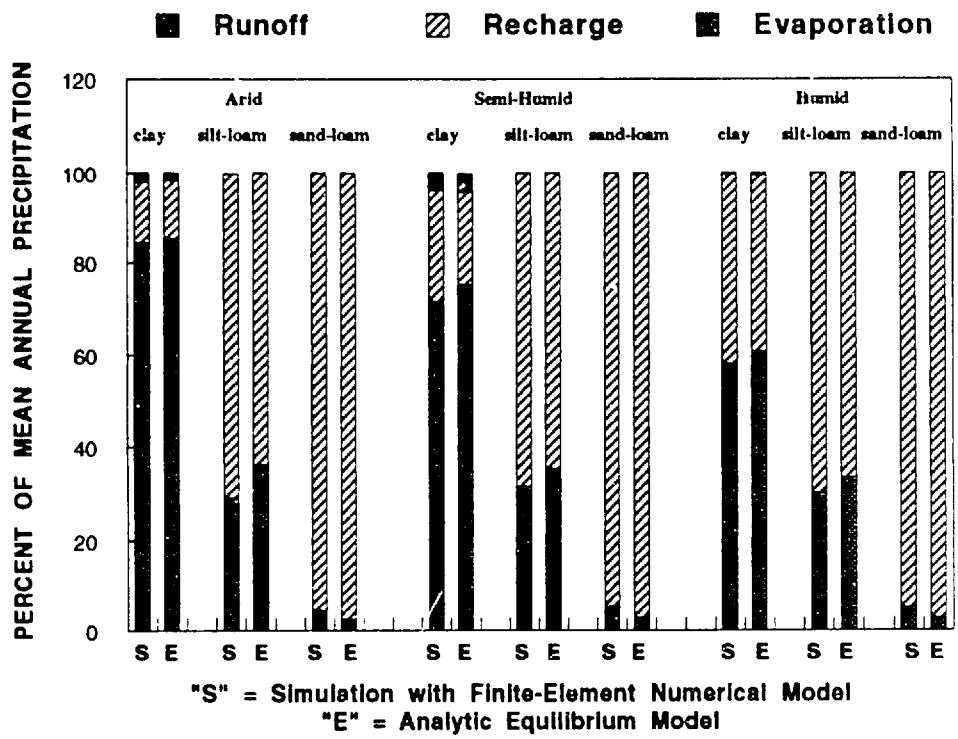

Figure 3.2 Comparison of finite-element simulated mean water balance and analytic equilibrium model results

rainfall and is produced by extreme conditions (large i, t_r)

For the six cases run with silt-loam or sand-loam soils textures, the partitioning is seen to depend primarily on the soil type, as opposed to climate forcing. For example the three silt-loam cases show no surface runoff and approximately one third of the precipitation being evaporated. The lack of runoff is the result of the saturated conductivities being much larger than mean rainfall intensities, precluding Horton type infiltration excess runoff. The relative constancy of the evaporation fraction, despite the large difference in potential evaporation among the three climates, is due to dominance of soil controlled evaporation regime for these cases. In the limit where most of the interstorm of most evaporation events is spent under soil control, the magnitude of the potential evaporation is unimportant, leaving the interstorm duration characteristics as the only important climate characteristic.

While the regimes dominated by soil controlled events are clearly the most difficult to predict, note also that the model does correctly capture the climate controlled events. For example, for the humid climate clay soil case, the equilibrium model yields approximately 60% evaporation and the ratio the annual potential evaporation to the mean annual precipitation is 62% (Table 3.2). It is still significant from a modeling point of view that the equilibrium model predicts few soil control events when indeed there are few (e.g. in humid climates).

As stated previously, this comparison of the analytic equilibrium model with the numerical simulations is not to be taken as a surrogate for field validation. The successful comparison does, however, have many implications for the understanding and modeling of water balance, particularly with respect to the role of temporal variability in the forcing and in the moisture profile.

The ability of the equilibrium model to represent such a complex system as was simulated in the case studies implies that the model's approximation of the moisture fluxes and the underlying assumptions regarding the moisture profile are reasonable. The former is not surprising. The dynamic models of infiltration and exfiltration, and the steady state models of percolation utilized in the equilibrium model, are all based in rigorous derivations from the governing equation of moisture flow. In fact, the particular choices made in this model's construction (e.g. a *Philip* [1957a] type infiltration equation), are rather unimportant. The infiltration equation could, for example, be replaced with other physically based equations (e.g. *Haverkamp et al.* [1990]), though such a substitution

might complicate the mathematics involved in determining expected values. What is significant is how the time compression approximation (TCA) is applied to these components and, most importantly, how the components are coupled using the concept of an equilibrium soil moisture (s_o). In the following, these concepts are explored with respect to the analysis in Chapter 2.

3.d.1 The Equilibrium Soil Moisture and the Equivalent Steady State Moisture Profile

Eagleson [1978a] introduces the equilibrium soil moisture (s_o) as a simplified zeroth-order representation of the actual time varying, near surface spatial average soil moisture. This representation is illustrated in Figure 3.3 (reproduced from *Eagleson* [1978a], Figure 7). Note that to find the mean infiltration and exfiltration exactly would require knowledge of the obability distributions (p.d.f.'s) of soil moisture profiles prior to storm and interstorm e s. A first order approximation of the means would require that the expectations (equations 3.7 and 3.22) be taken at the mean of the initial condition moisture profiles (i.e. the mean of $s_{ps}(z)$ and $s_{pi}(z)$, respectively) [*Eagleson*, 1978c]. A zeroth-order representation approximates the ensemble of event-based initial conditions ($s_{ps}(z)$ and $s_{pi}(z)$), which in reality vary from event to event and are related with decreasing correlation to all previous events, by a single "effective" depth averaged value. By the equilibrium method, the magnitude of this effective soil moisture is determined by requiring that the mean annual additions to and subtractions from the soil moisture balance, invoking a long-term stationarity of soil moisture. That a single effective equilibrium soil moisture value (s_o) may be used to represent the ensemble of initial condition profiles ($s_{ps}(z)$ and $s_{pi}(z)$) across such a range of soil-climate scenarios as demonstrated in Table 3.3 can be understood in terms of the following four observations:

1. The event-integrated infiltration and exfiltration fluxes are nonlinearly dependent on the initial condition moisture profile (due to both the nonlinear dependence of the Darcy flux on soil moisture and the nonlinearity of the state-dependent boundary condition). However, as discussed in Chapter 2, the nonlinearity is weak enough, with respect to the inter-event variability of the moisture profile, that the mean response of the soil column under an ensemble of initial moisture profiles may be well approximated by the response under the mean initial moisture profile condition.

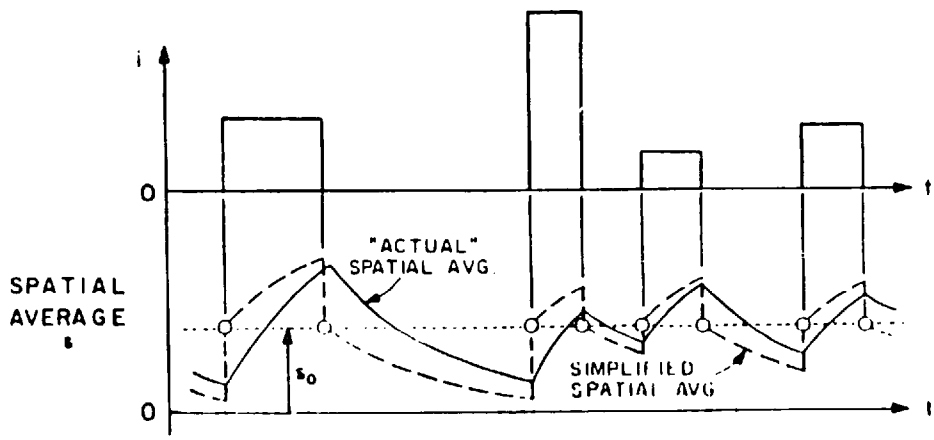

Figure 3.3 Soil moisture representation [*Eagleson*, 1978a]

Note that this quasi-linearity requirement is on the dependence of the event integrated flux on the initial soil moisture profile and not on the dependence of the instantaneous flux on the instantaneous soil moisture profile. For example, so-called linear soils (see Appendix A), which yield linear dependence of the Darcy flux on the soil moisture and its gradient, can still undergo switches from flux boundary conditions (i.e. climate-control) to concentration conditions (i.e. soil-control). Thus even for linear soils, the event integrated flux which depends on both the governing equation and the interaction of the forcing and the surface state to form the boundary condition can be nonlinearly dependent on the initial soil moisture profile.

This quasi-linearity of both the event infiltration and exfiltration with respect to initial moisture content implies that the first-order approximation of their means (taking the expected values at $\langle s_{ps}(z) \rangle$ and $\langle s_{pi}(z) \rangle$) will yield a good approximation to the exact means (the determination of which requires the probability density function of $s_{ps}(z)$ and $s_{pi}(z)$).

Mathematically :

$$\left\langle E_{s_A}\left(s_{pi}(z)\right)\right\rangle \cong \left\langle E_{s_A}\left(\left\langle s_{pi}(z)\right\rangle\right)\right\rangle \tag{3.25}$$

$$\left\langle I_A\left(s_{ps}(z)\right)\right\rangle \cong \left\langle I_A\left(\left\langle s_{ps}(z)\right\rangle\right)\right\rangle \tag{3.26}$$

2. With respect to the sensitivity of the mean event infiltration and exfiltration to the mean initial conditions ($\langle s_{ps}(z) \rangle$ and $\langle s_{pi}(z) \rangle$), these mean pre-storm and pre-interstorm moisture profiles, which are conditional means of the moisture profile, do not differ significantly from the overall (i.e. unconditional) mean moisture profile ($\langle s(z) \rangle$) given the random arrival of events. Furthermore, as discussed in Chapter 2, the steady moisture profile which transmits the mean recharge is identical to the temporal mean moisture profile for linear soils and forms an adequate zeroth-order estimate of the mean for nonlinear soils. The initial condition profiles may thus be approximated by the equivalent steady profile. Mathematically:

$$\left\langle s_{ps}(z)\right\rangle \approx \left\langle s_{pi}(z)\right\rangle \approx \langle s(z)\rangle \approx s_s\left(z; q_{st} = \langle q\rangle\right) \tag{3.27}$$

In Chapter 2 it is demonstrated that the nature of the nonlinear dependence of the Darcy flux on soil moisture is such that the equivalent steady profile will always overestimate the moisture content of the mean profile (Equation 2.12). Note also that the mean profile prior to interstorm ($<s_{pi}(z)>$) must be more wet than both the mean prior to storm ($<s_{ps}(z)>$) and the overall mean ($<s(z)>$). The approximation in (3.27) therefore holds better for $<s_{pi}(z)>$ than $<s_{ps}(z)>$. This behavior is important because, as will be shown shortly, the mean bare soil evaporation is more sensitive to initial condition ($<s_{pi}(z)>$) than the mean infiltration.

For deep water tables, the equivalent steady profile becomes near-uniform away from the water table, and (3.27) may be further simplified:

$$\langle s_{ps} \rangle \approx \langle s_{pi} \rangle \approx \langle s \rangle \approx s_s(q_{st} = \langle q \rangle) \tag{3.28}$$

An example of the relation of the mean pre-storm, pre-interstorm, overall mean, and equivalent steady profiles is given in Chapter 2 (Figure 2.1) for a clay soil semi-humid climate case. In Figure 3.4 the relation for the silt-loam soil with arid climate forcing is illustrated. As with the clay semi-humid case, the equivalent steady profile appears to offer a good estimate of the other three. As discussed above, $s_s(z;q_{st}=<q>)$ consistently overestimates the mean ($<s(z)>$) and mean pre-storm ($<s_{ps}(z)>$), and better estimates the mean prior to interstorm ($<s_{pi}(z)>$). The sufficiency of the approximations (3.27 or 3.28), however, must be judged in the context of their application. It was found in Chapter 2 that for the purpose of initializing flux capacities for the clay semi-arid case, the approximations were indeed sufficient.

4. At equilibrium soil moisture, the relative sensitivity of the steady flux to the equivalent steady soil moisture is very large in comparison with the sensitivity of the mean infiltration and exfiltration to the initial soil moisture content, i.e:

$$\frac{s_s}{\langle q \rangle} \cdot \frac{\partial \langle q \rangle}{\partial s_s} \gg \frac{s_{pi}}{\langle E_{s_A} \rangle} \cdot \frac{\partial \langle E_{s_A} \rangle}{\partial s_{pi}} \tag{3.29}$$

$$\frac{s_s}{\langle q \rangle} \cdot \frac{\partial \langle q \rangle}{\partial s_s} \gg \frac{s_{ps}}{\langle I_A \rangle} \cdot \frac{\partial \langle I_A \rangle}{\partial s_{ps}} \tag{3.30}$$

This disparity of sensitivity is recorded in table 3.4 for the nine soil-climate combinations. This relative high sensitivity of the steady flux to soil moisture effectively restricts the possible range of equilibrium soil moisture to a band over which the mean infiltration and bare soil evaporation vary relatively less, lending accuracy to the equilibrium method.

Table 3.4: Sensitivity of Mean Hydrologic Fluxes to Soil Moisture at Equilibrium
(expressed as elasticity (%))

	recharge	evaporation	runoff
arid,clay	834	230	-3
arid, silt-loam	466	73	0
arid, sand-loam	357	34	0
semi-humid, clay	783	123	-8
semi-humid, silt-loam	466	53	0
semi-humid, sand-loam	358	29	0
humid,clay	773	22	-1
humid, silt-loam	466	51	0
humid, sand-loam	358	42	0

The magnitude of the water balance equilibrium soil moisture is thus, in the large part, determined by the steady flux component. The equilibrium soil moisture (s_o) defined implicitly by (3.16) is not the temporal mean moisture, but is the equivalent steady soil moisture ($s_s(q_{st}=<q_{est}>)$) corresponding to an implicit *estimate* of the mean recharge (i.e. the recharge estimated by requiring equilibrium between the estimated mean surface flux and the mean deep soil flux). Mathematically, this interpretation of the equilibrium soil moisture is:

$$s_o \equiv s_s\left(q_{st} = \langle q \rangle_{est}\right) \tag{3.31}$$

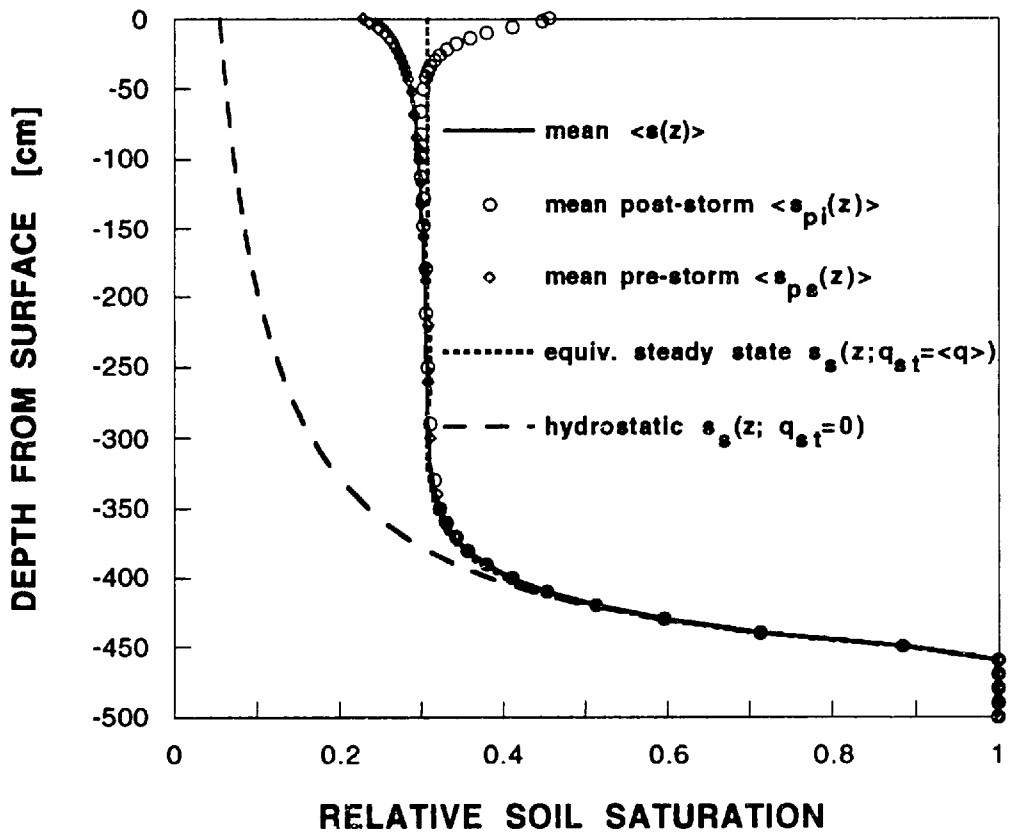

Figure 3.4 Characteristic soil moisture profiles for silt-loam, arid climate case study

In Table 3.5 the equilibrium soil moisture (s_0) for the equilibrium model and the equivalent steady soil moisture ($s_s(q_{st}=<q>)$) from the numerical simulations (i.e. the steady profile which transmits the *actual* mean recharge) are compared. Again, the correspondence is very high.

Table 3.5: Equilibrium and Equivalent Steady Soil Moistures

	equilibrium (analytic model)	equivalent steady (numerical model)
arid,clay	0.54	0.54
arid, silt-loam	0.31	0.32
arid, sand-loam	0.13	0.13
semi-humid, clay	0.61	0.62
semi-humid, silt-loam	0.35	0.35
semi-humid, sand-loam	0.15	0.15
humid,clay	0.64	0.65
humid, silt-loam	0.63	0.64
humid, sand-loam	0.14	0.14

Without the disparity of sensitivity expressed in (3.29) and (3.30), the equilibrium method would not be as robust, and the errors introduced by the approximations (3.25) through (3.28) would be reflected in a large discrepancy between the equilibrium (s_0) and the equivalent steady ($s_s(q_{st}=<q>)$) soil moistures and thus large errors in the predicted equilibrium partitioning

The close relation between the equilibrium soil moisture's role in the water balance and the use of the equivalent steady soil moisture ($s_s(q_{st}=<q>)$) to initialize flux capacities, supports the validity of the latter under a wider range of climate-soil combinations than explicitly tested in Chapter 2.

3.e Requirements for Extension to Near Surface Water Table Conditions

In Chapter 2 it was demonstrated that the equivalent steady profile formed a sufficient estimate of the mean pre-storm moisture profile under both deep and shallow

water table conditions. Given the similarity between the equilibrium water balance method and the use of the equivalent steady moisture profile for initializing flux capacities, it may be expected that the equilibrium concept can be applied to shallow water table conditions as well. Just as the equilibrium soil moisture was shown to correspond to an implicit estimate of the equivalent steady soil moisture, it is expected (and will be shown in Chapter 5) that the model may be extended by finding the "equilibrium" equivalent steady profile which, when used to initialize the infiltration and exfiltration capacity, balances the long term mean column flow.

The difficulty however lies in the determination of the infiltration and exfiltration capacities under steady, bounded, shallow water table conditions. For the deep water table case (i.e. under practically semi-infinite conditions), the steady initial condition corresponds to a uniform moisture profile for which there are many analytic infiltration and exfiltration capacity functions (e.g. the expressions used herein). For shallow water tables and steady initial condition moisture profile, the only infiltration capacity functions available in the literature are for so-called linear soils. Analytic infiltration and exfiltration capacity functions for realistic nonlinear soils under bounded conditions could thus have great utility if implemented in such an equilibrium model, as this would yield a direct connection between the location of the water table and the mean recharge (or capillary rise).

Salvucci [1993] has derived an approximate analytic expression for the equivalent steady moisture profile. This derivation is reviewed in Chapter 4. Following that review, an infiltration capacity function which uses the equivalent steady initial condition is derived and a shallow water table exfiltration capacity function proposed by *Eagleson* [1978c] is reviewed. When set in the equilibrium framework discussed herein, these expressions form the teleconnection between the water table and surface fluxes.

3.f Conclusions

The equilibrium water balance model of *Eagleson* [1978a-g] is modified and tested under conditions of deep water table, no vegetation and no surface retention. The model, after minor modification, yields excellent estimates of mean evaporation, infiltration and recharge partitioning as compared with the results of a monte-carlo numeric simulation of moisture flow in a deep, homogeneous soil column. Testing over an inclusive range of soil textures and climate forcings indicate that the model is robust in that it successfully captures

both soil controlled and climate controlled hydrologic behavior.

In conjunction with the results of Chapter 2, the results of this chapter indicate that simple characterization of the soil moisture profile, in particular the equivalent steady state moisture profile, may be sufficient for modeling the long-term water balance.

The results of Chapters 2 and 3 also indicate that the model of *Eagleson* [1978a-g] may be extended to shallow water table conditions. This extension requires the derivation of the infiltration and exfiltration capacity of soils in steady-state equilibrium with the water table. These shallow water table processes are the subject of Chapter 4.

Chapter 4: Process Studies

4.a Background

The last topic discussed in Chapter 3 concerns the extension of the equilibrium water balance model of *Eagleson* [1978a-g] to account for the effects of near-to-surface water table. This requires that the equilibrium soil moisture, which acts as initial condition to the near surface processes and determines the rate of percolation deeper in the soil, be replaced by the equilibrium equivalent steady soil moisture profile. As discussed, this requires analytic expression of the steady moisture profile above a water table. In addition, the infiltration and exfiltration capacities must be modified to reflect this change of surrogate initial condition.

In this chapter the derivation of the steady moisture profile reported by *Salvucci* [1993] is repeated. It is also modified to apply specifically to *Brooks and Corey* [1966] soils so that it may be compatible with the water balance model of *Eagleson* [1978a-g]. Next this profile is integrated (approximately) to yield an expression for the storage capacity of soils in steady state equilibrium with the water table. This expression is used in Chapter 5 in the determination of storage excess runoff. In the following Section (4.d) the steady profile expression is used in the derivation of the wetting fronts and infiltration capacity which result from ponded infiltration into soils at steady equilibrium with the water table. In Section (4.e), it is assumed that the effect of a shallow water table on exfiltration may, as *Eagleson* [1978c] proposed, be accounted for by linear superposition of the exfiltration capacity for unbounded soils with the maximum possible (steady) capillary rise that could occur from a shallow water table. Furthermore it is assumed that the exfiltration capacity may be initialized with the surface value of the steady moisture profile.

4.b The Steady State Moisture Profile

For the steady state condition, the capillary tension head profile $\Psi(z)$, and thus the moisture profile s(z), is determined by the Darcy equation for the (steady) flux q:

$$q = -K(s)\left(\frac{d\Psi(s)}{dz} + 1\right) \tag{4.1}$$

where K(s) is the unsaturated hydraulic conductivity, z is the vertical coordinate (positive up, zero at land surface), and s is the relative soil saturation (equal to the volume of water divided by the pore volume available to moisture flow; $0 \leq s \leq 1$).

The complexity of analytic or numerical solutions to (4.1) depends, as in the unsteady case, on the choice of hydraulic parameterization of K(s) and $\Psi(s)$. *Philip* [1957] derives integral solutions for measured K(s) and $\Psi(s)$ to the coupled heat and moisture flux from the water table. *Gardner* [1958] gives an exact analytic solution for the exponential conductivity relation $K(\Psi) = K_S e^{\alpha\Psi}$ and for an algebraic conductivity relationship of the form $K(\Psi) = a/(\Psi^n + b)$, for certain values of the exponent (n). *Ripple et al.* [1972] uses nondimensionalization and numerical integration to present graphical solutions to (4.1) for the algebraic case. *Anat et al.* [1965] incorporates the *Brooks and Corey* [1966] hydraulic parameterization (a special case of the algebraic function) and developed an approximate solution for $n > 1$. This solution applies only to evaporation and consists of two expressions, one valid for the relatively wet section of the moisture profile, and one for the drier section. *Warrick* [1988] shows that with the proper change of variables, the exact solution for Gardner's algebraic function and the Brooks-Corey case can be written, for any $n > 1$, in terms of the incomplete Beta function. More recently, *Warrick and Yeh* [1990] used analytic and numerical techniques to analyze steady flow in layered soils.

In each of these works, the solution is first posed for the depth, z, as a function of the capillary tension head (Ψ) and the steady flow rate (q). In addition to this form, *Gardner* [1958], *Anat et al.* [1965], *Ripple et al.* [1972] and *Warrick* [1988] invert their solutions (and made certain approximations) to derive expressions for the dependence of evaporation on the water table depth for the limiting case boundary condition of infinite ground surface capillary tension (i.e., infinite dryness). Except for this limiting condition, the solutions incorporating the algebraic or Brooks-Corey hydraulic conductivity functions are not explicitly invertible to the more useful forms $\Psi(z,q)$ and $q(\Psi,z)$.

In this section an approximate solution to Equation (4.1) is posed for a algebraic conductivity function similar to that used by *Gardner* [1958]. While the solution is approximate, it has added utility in that it is: a) explicitly invertible from $z(\Psi,q)$ to $\Psi(z,q)$ and $q(z,\Psi)$; b) applicable to both infiltration and capillary rise; and c) a single expression valid throughout the whole profile. At the conclusion of this section, a minor modification is presented to make the expression applicable for Brooks-Corey soils such that the

solution will be compatible with the water balance model of *Eagleson* [1978a-g].

For comparison, the approximate expressions for the tension head profile and moisture profile are compared against a trapezoidal-rule numerical integration of the governing steady flow equation (Equation (4.1)). In addition the limiting case evaporation is compared with those expressions found in the literature.

4.b.1 Derivation

Steady, vertical flow in the unsaturated zone is governed by Equation (4.1), in which $d\Psi/dz$ represents flow due to gradients in capillary tension and the "1" reflects the gradient of the gravitational head. There are numerous models for representing the dependence of capillary tension head and hydraulic conductivity on soil saturation. Following the derivation of *Salvucci* [1993], the *Gardner* [1958] function is employed to directly relate the capillary tension to the reduction of hydraulic conductivity from its saturated value (K_S):

$$K(\Psi) = \frac{K_s}{1 + \left[\frac{\Psi}{\Psi_1}\right]^n} \tag{4.2}$$

In the dry limit, ($|\Psi|$ large) this representation closely mimics the *Brooks and Corey* [1966] model if Ψ_1 is set equal to the bubbling pressure head (Ψ_S) and n equal to the product of their pore size distribution index (m) and pore size disconnectedness index (c). In the wet limit, Equation (4.2) smoothes out the discontinuity present in Brooks-Corey. Figure 4.1 illustrates the similarity of the two models. In the following, the parameters n and Ψ_1 will be chosen on the basis of this similarity.

Incorporating Equation (4.2) into (4.1), normalizing the flow rate (q) by K_S (notate q') and rearranging, one obtains the following differential equation in Ψ:

$$\frac{d\Psi}{dz} + q'\left(\frac{\Psi}{\Psi_1}\right)^n + (1 + q') = 0 \tag{4.3}$$

subject to the water table boundary condition:

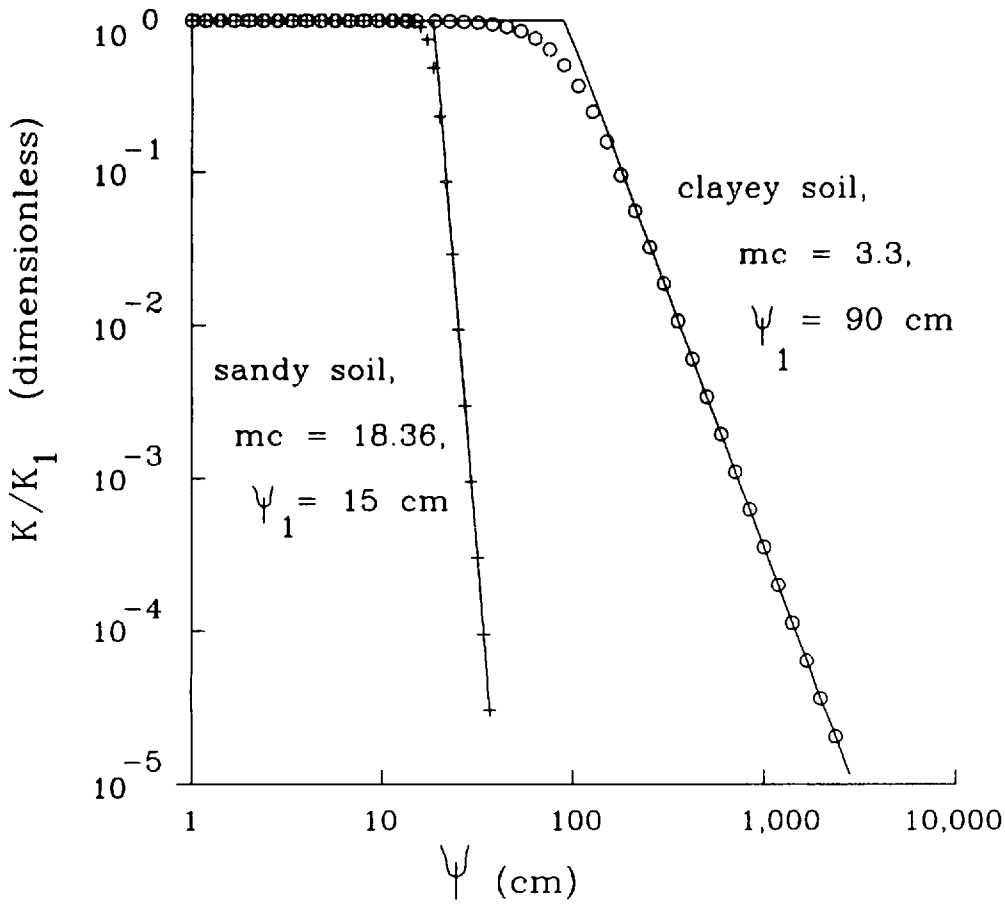

Figure 4.1 Comparison of Brooks-Corey (solid lines) and Gardner type (pluses and circles) models of hydraulic conductivity as a function of capillary tension head

$$\Psi = 0 \qquad at \qquad z = Z_w \tag{4.4}$$

Note that the normalized flow rate q' will take on values considerably less than one when this analysis is applied in the "equivalent steady" sense discussed in Chapter 2. For example, for a clay soil q' would be approximately bounded by the limiting cases corresponding to annual potential evaporation (e.g. +50 cm/yr) and annual precipitation (e.g. -100 cm/yr) divided by the soil saturated conductivity (e.g. 1072 cm/yr):

$$\frac{-100\ cm/yr}{1072\ cm/yr} \cong -0.09 < q' < \frac{+50\ cm/yr}{1072\ cm/yr} \cong +0.05 \tag{4.5}$$

Values of K_1 , Ψ_1 , n and the approximate range of q' (calculated as they are above) are listed for three soil textures in Table 4.1.

Table 4.1

Representative Values of the Brooks-Corey Soil Parameters and Representative Climatic Limits of Normalized Flow Rate (q')

	K_S (cm/sec)	Ψ_S (cm)	n =m c	q' +	q'-
Clay	3.4E-05	-90	3.3	-0.1	0.05
Silt Loam	3.4e-04	-45	5.64	-0.01	0.005
Sand Loam	3.4e-03	-25	11.88	-0.001	0.0005

Source: *Bras* [1990]

Numerical integration of Equation (4.3) reveals that most of the curvature of the solution for both infiltration and exfiltration occurs before $\Psi/\Psi_1 = |q'/(1 + q')|^{-1/n}$ (i.e., the limiting pressure head at which $d\Psi/dz = 0$ for a given q'). Accordingly, the

nondimensional variables Ψ' and z' are defined:

$$\Psi' = \frac{\Psi/\Psi_1}{|q'/(1+q')|^{-1/n}} \tag{4.6}$$

$$z' = \frac{z/\Psi_1}{|q'/(1+q')|^{-1/n}} \tag{4.7}$$

With the above, the solution of Equation (4.3) subject to boundary condition (4.4) is equivalent to evaluating the definite integral:

$$z' = \frac{1}{1+q'} \int_0^{\Psi'} \frac{dx}{1+f \cdot x^n} \tag{4.8}$$

where

$$f \equiv sgn(q') = \frac{q'}{|q'|} \tag{4.9}$$

This integral is solved exactly for integer values of the exponent (n) in *Gradshteyn and Ryzhik* [1980, eqs. 2.144, 2.146]. The solution, however, may not be generalized since its form changes for different values of the exponent and it is only invertible for particular values of n. Through a change of variables, *Warrick* [1988] expresses the integral in terms of the incomplete Beta function. While for real n > 1 this form is general, it too is not easily inverted.

The overriding concern in the derivation of presented by *Salvucci* [1993] is that the final dimensional solution be: a) invertible from z(Ψ,q) to Ψ(z,q) and q (Ψ,z); b) valid for both infiltration and exfiltration (f = +/-1); and c) consistent with the limiting behavior for Ψ approaching infinity (the maximum capillary rise condition), z approaching infinity (the limiting gravitational percolation) , and q' approaching zero (the hydrostatic case)

To approximate the integral (4.8), *Salvucci* [1993] makes the change of variables:

$$\Phi = f + \Psi'^{-n} \tag{4.10}$$

in Equation (4.8), yielding:

$$z' = \frac{-1}{n(1+q')} \int_{\infty}^{\Phi} \frac{(y-f)^{-1/n}}{y}\, dy \qquad (4.11)$$

Upon expanding the binomial in (4.11), term by term integration becomes possible. Note that for evaporation f = +1, and thus y >1 for all Ψ' (viz. Equation (4.10)). Expanding the binomial around y thus leads to a converging approximation for evaporation.

For infiltration however, f = -1 and thus y will be greater than one for the range $0 < \Psi' < 2^{-1/n}$, while for $2^{-1/n} < \Psi' < 1$, y will be less than one. Expanding the integrand around y will therefore yield a divergent approximation near $\Psi' = 1$. The first term of such an expansion is $y^{-1-1/n}$, while expanding around f (which should be done for y < f) will yield y^{-1}. When n is large (as for sands and silt-loams), the difference is negligible and the limiting behaviors are identical. For infiltration therefore, the first term (and only the first term) of the expansion around y may be taken to uniformly approximate the integrand. In summary, higher order terms may be retained for the (convergent) exfiltration case, but a solution applicable to both infiltration and exfiltration is limited to a one term expansion.

Expanding the numerator around y, integrating term by term, applying the boundary condition, back-substituting Equation (4.10) and re-dimensioning yields:

$$z \equiv Z_w - \frac{\Psi_1}{1+q'}\left[\frac{q'}{1+q'} + \left(\frac{\Psi}{\Psi_1}\right)^{-n}\right]^{-1/n} \qquad (4.12)$$

In Figures 4.2 through 4.4, the depth-tension head profile as calculated using Equation (4.12) is compared with the numerical solution for the typical soils (n ranges from 3.3 to 11.88) and flow conditions (-.1 < q' < .05) listed in Table 4.1. For all three soil types, the approximation under infiltration conditions (negative q') is good, though there is a slight bias towards overestimating the depth (z), especially for the clay soil. That the bias is less for sandy soils than clays results from the expansion of the integrand of (4.11), which, as discussed previously, is best for large n. Under evaporation conditions, the approximation underestimates the tension head, particularly in the dry limit asymptote (i.e.

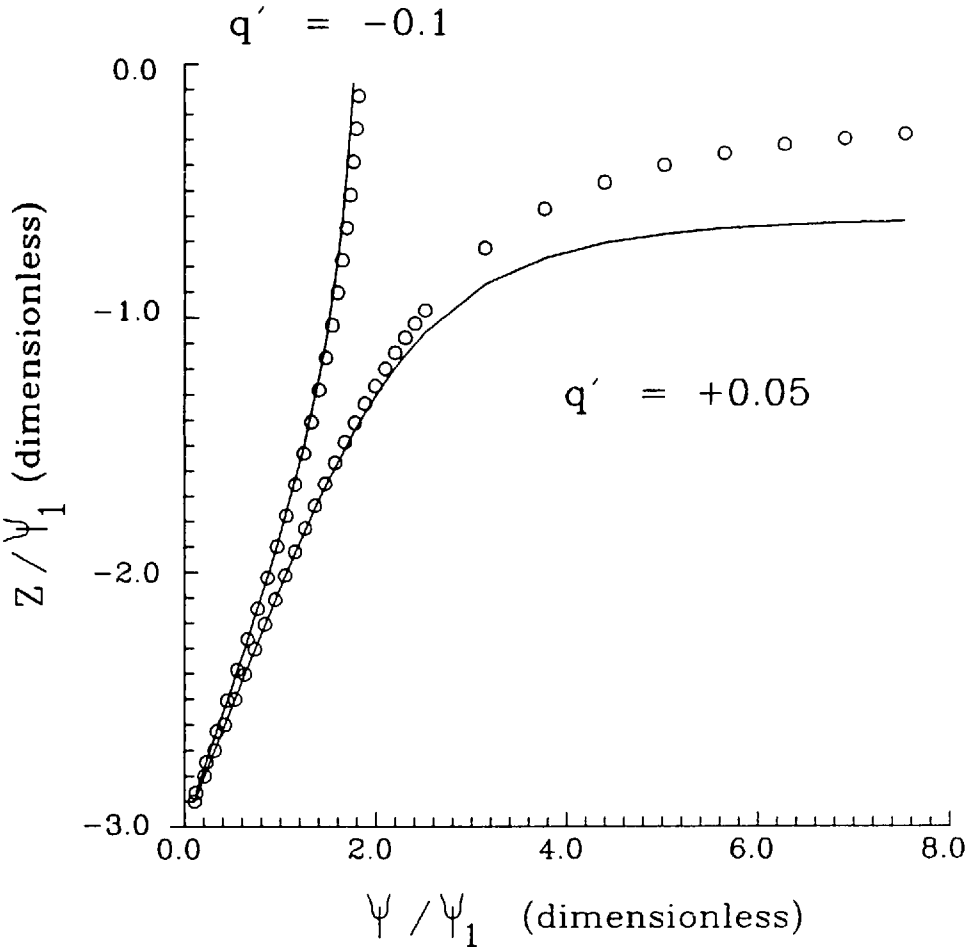

Figure 4.2 Comparison of approximate capillary tension head profiles (solid lines) and numerical solution (circles) for clay (n=3.3)

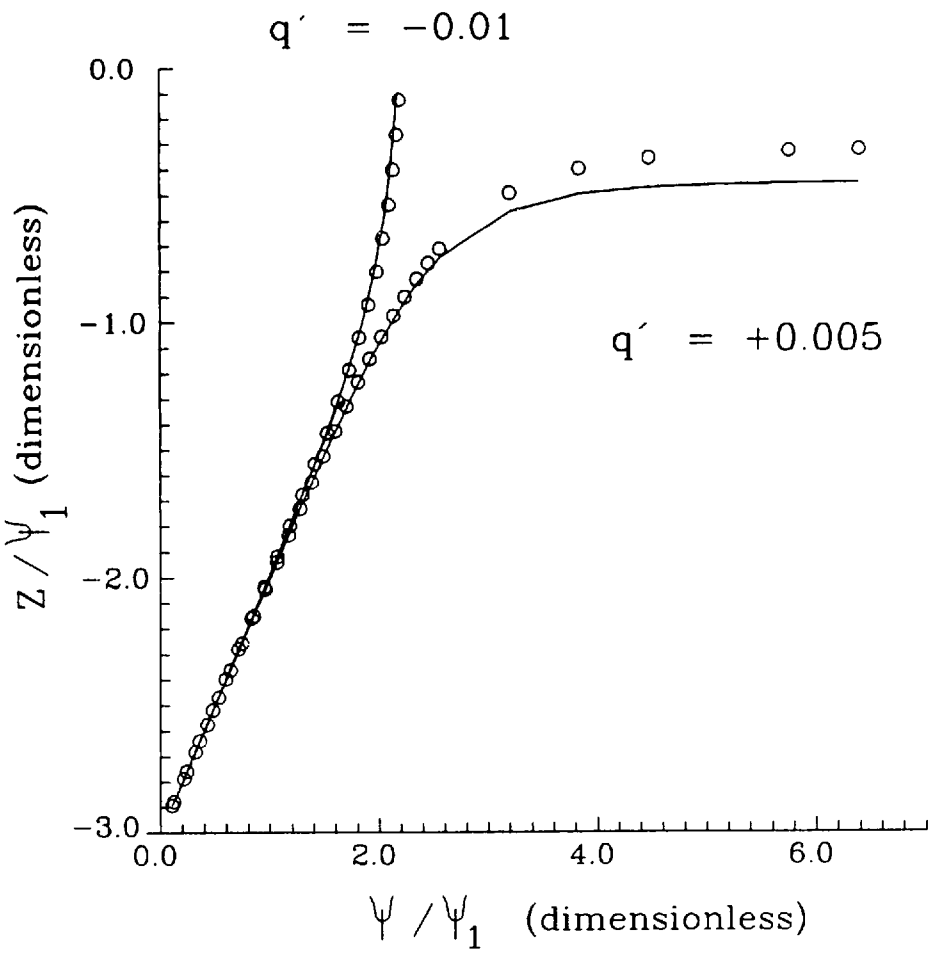

Figure 4.3 Comparison of approximate capillary tension head profiles (solid lines) and numerical solution (circles) for silt-loam (n=5.64)

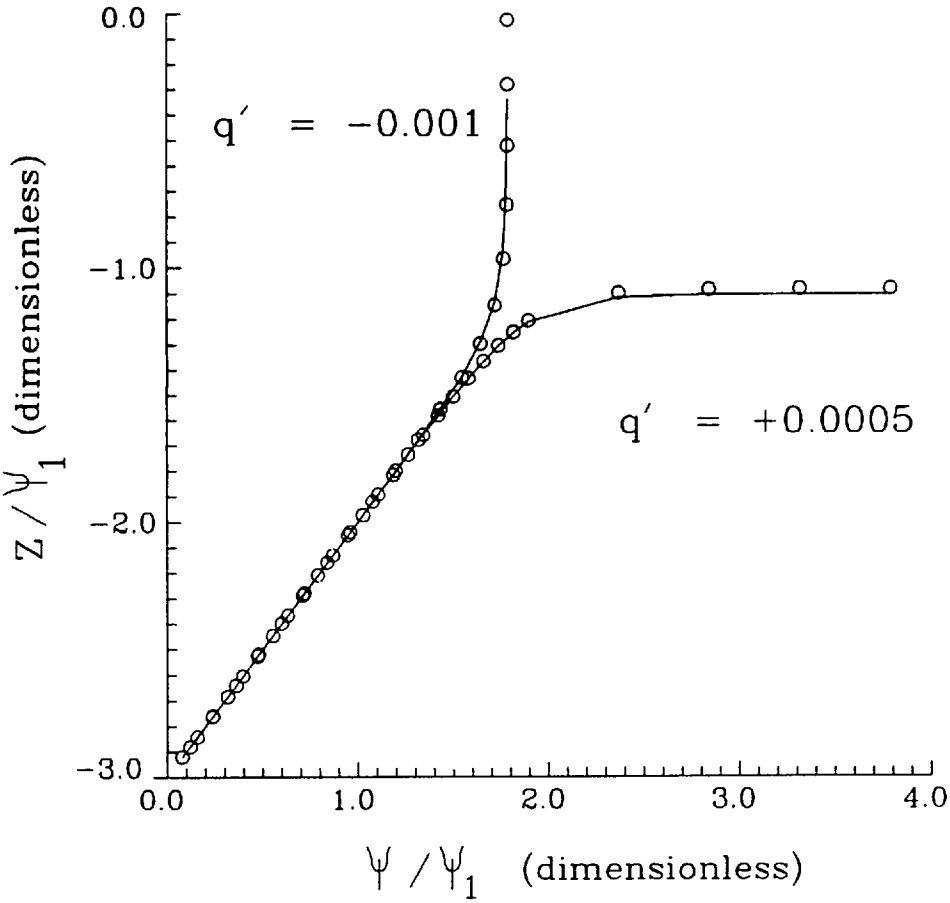

Figure 4.4 Comparison of approximate capillary tension head profiles (solid lines) and numerical solution (circles) for sand-loam (n=11.88)

the horizontal part of the profile). Again, for the clayey lower valued r soils (Figure 4.2), the approximation error is larger than for the sandy soils. (Figure 4.4).

4.b.2 Inversion

Equation (4.12) can be directly inverted to give $\Psi(z,q')$, and with a model relating the moisture content to tension head, the moisture profile, $s(z,q')$. To obtain an explicit expression for $q'(\Psi,z)$, however, the term $(1+q')^{1-n}$ must be expanded. The pairs of values of q' and n in Table 4.1 indicate that as n increases, the magnitude of q' decreases (i.e. high values of n correspond to sandy soils with large hydraulic conductivity), such that the expansion will introduce little additional error. Carrying out this expansion and solving for q' yields:

$$q' = \frac{\left(\frac{Z_w - z}{\Psi_1}\right)^{-n} - \left(\frac{\Psi}{\Psi_1}\right)^{-n}}{1 + \left(\frac{\Psi}{\Psi_1}\right)^{-n} + (n-1)\left(\frac{Z_w - z}{\Psi_1}\right)^{-n}} \qquad (4.13)$$

Note that the influence of the water table depth depends on how dry the surface is and the soil type. Capillary rise from a "shallow" water table and percolation to a "deep" water table are often treated as separate phenomena. This formulation (Equation (4.13)) explicitly demonstrates that "shallow" and "deep" are relative to surface moisture state and yields a rational method to discriminate between the two conditions.

Equation (4.13) exhibits the following limiting behavior: a) for $\Psi = -(z-Z_W)$, the flux is zero (i.e. hydrostatic); b) for the water table at negative infinity ($Z_W = -\infty$), the flux for a given Ψ at the surface (z=0) is $-K(\Psi)/K_S$. This corresponds to a condition of water table decoupling in which the only gradients near the surface are gravitational. This condition is commonly referred to as the "unit gradient" case or the limit of free percolation; c) for Ψ at the surface (z=0) infinitely dry, the flux is given by:

$$q' = \frac{\left(\frac{Z_w}{\Psi_1}\right)^{-n}}{1-(n-1)\left(\frac{Z_w}{\Psi_1}\right)^{-n}} \tag{4.14}$$

For the first two limiting conditions, the approximation is exact. For the last condition, which represents the maximum rate of evaporation from a water table, the approximation is not exact. The exact (implicit) solution for this limiting case is given by *Ripple et al.* [1972] and *Warrick* [1988] as:

$$q' = (1+q')^{1-n}\left[\frac{\pi}{n\ \sin\left(\frac{\pi}{n}\right)}\right]^n \left(\frac{Z_w}{\Psi_1}\right)^{-n} \tag{4.15}$$

In Table 4.2, the limiting case approximate solution (i.e., Equation 4.14) is compared with the exact (implicit) solution (4.15) and with the following approximate, but explicit limiting case evaporation formulae:

Anat et al. [1965]:

$$q' = \left(1+\frac{1.886}{1+n^2}\right)^n \left(\frac{Z_w}{\Psi_1}\right)^{-n} \tag{4.16}$$

Eagleson [1978] based upon the work of *Gardner* [1958]:

$$q' = \left(1+\frac{3}{2(n-1)}\right)^n \left(\frac{Z_w}{\Psi_1}\right)^{-n} \tag{4.17}$$

Ripple et al. [1972] and *Warrick* [1988]:

$$q' = \left(\frac{\pi}{n \sin\left(\frac{\pi}{n}\right)} \right)^{n} \left(\frac{Z_w}{\Psi_1} \right)^{-n} \tag{4.18}$$

The relative error is calculated (with the exact implicit expression (Equation 4.15) as a reference case) using:

$$rel.\ error = \left| \frac{q_{approx} - q_{exact}}{q_{exact}} \right| \tag{4.19}$$

Overall, Equation (4.14) performs worse, in this limiting case, than the existing solutions.

Table 4.2

Comparison of Relative Error of Limiting Evaporation Formulae

	n = m c	q'	Gardner Eagleson	Anat	Ripple/ Warrick	This Work Eq 4.14.
Clay	3.3	0.05	0.11	0.09	0.12	0.38
Silt Loam	5.64	0.005	0.01	0.04	0.02	0.25
Sand Loam	11.8	0.0005	0.00	0.02	0.01	0.13

In summary, for soils characterized by Gardner-type hydraulic properties, an analytically simple approximation has been found for: a) the steady state flow rate in an unsaturated soil in terms of the capillary tension at some distance from the water table, and b) the steady state tension head profile ($z(\Psi,q)$ or $\Psi(z,q)$). The approximations work well over a wide range of soil types. They correctly capture the limiting behaviors of percolation to an infinitely deep water table and evaporation to an infinitely dry surface. In addition, the new solution is valid for the intermediate case when the magnitude and direction of flow are sensitive to both the water table depth and capillary tension.

For use in extending the water balance model of *Eagleson* [1978a-g] however, this

solution must apply to Brooks-Corey soils. Figure 4.1 demonstrates that the Gardner and Brooks-Corey soil retention curves are similar, especially at the dry end. As they are not exactly the same, however, simply making the substitutions $\Psi_1=\Psi_S$ and n=m*c will necessarily introduce some error. It was found, through simple trial and error, that in addition to the above substitutions, modifying Equation 4.12 as follows reduces the error:

$$z \equiv Z_w - \Psi_s \left[\left(\frac{1}{1+q'} \right) \left(q' + \left(\frac{\Psi}{\Psi_s} \right)^{-m \cdot c} \right) \right]^{-1/(m \cdot c)} \tag{4.20}$$

Using the Brooks-Corey expressions for relating soil moisture and capillary tension head (Appendix A, Equation A.1), the steady soil moisture profile ($s_S(z)$) becomes:

$$s_s(z) \equiv \begin{cases} \left[-q' + (1+q') \left(\frac{Z_w - z}{\Psi_s} \right)^{-m \cdot c} \right]^{1/c} & z \geq Z_w - \Psi_s \\ 1 & z < Z_w - \Psi_s \end{cases} \tag{4.21A}$$

In this modified form, the limiting case of infinite water table percolation through Brooks-Corey soils is exact, i.e. $q=-K_S s^c$. The accuracy of expression (4.21A) is illustrated in the figures of the section describing the wetting front model (Section 4.d, Figures 4.8,4.9 and 4.10).

For use in later chapters, the limiting case capillary rise rate for Brooks-Corey soils may be found by solving Equation (4.21A) for q' under the condition that the surface is dry (i.e. s=0 at z=0), yielding:

$$q' = \frac{\left(\frac{Z_w}{\Psi_s} \right)^{-mc}}{1 - \left(\frac{Z_w}{\Psi_s} \right)^{-mc}} \tag{4.21B}$$

4.c The Storage Capacity of the Unsaturated Zone at Equilibrium with a Water Table

In situations where the water table is near the ground surface the available unsaturated zone storage may be very small. In these cases precipitation in excess of this storage will not infiltrate; there will be surface ponding and runoff. Unlike infiltration excess runoff, this type of runoff can occur regardless of whether or not the storm intensity exceeds the infiltration capacity rate. Thus storage excess runoff may be produced by long, low intensity storms occurring on conductive soils, a situation in which infiltration excess runoff is unlikely to occur.

In order to model this runoff generation, it is useful to have an analytic expression for the storage capacity of the soil prior to the rainfall event. As discussed previously, the moisture profile prior to storm may be approximated by the equivalent steady moisture profile. A simple expression for the storage capacity may thus be found by integrating the storage capacity of the steady profile expression derived in the previous Section (4.b).

Denoting this capacity by $\forall_e$, it may be expressed as:

$$\forall_e = \int_{Z_w}^{0} n_e\left(1 - s_s(z)\right)dz \tag{4.22}$$

Substituting Equation (4.21A) into (4.22) yields an integral which is not solved in closed form. It may be simply approximated, however, by linearly expanding $s_s(z)$ at the surface and at the tension saturated zone, and then integrating 4.22 piecewise as illustrated in Figure 4.5. This simple approximation yields:

$$\forall_e = -n_e(1 - s_*)Z_j + \frac{1}{2}n_e\phi Z_j^2 + \frac{1}{2}n_e\lambda\left(Z_w - Z_j - \Psi_s\right) \tag{4.23}$$

where s_* is the surface saturation:

$$s_* \equiv \left(-q' + (1+q')\left(\frac{Z_w}{\Psi_s}\right)^{-mc}\right)^{1/c} \tag{4.24}$$

λ and ϕ are the slopes of the profile at the surface and tension saturated zone:

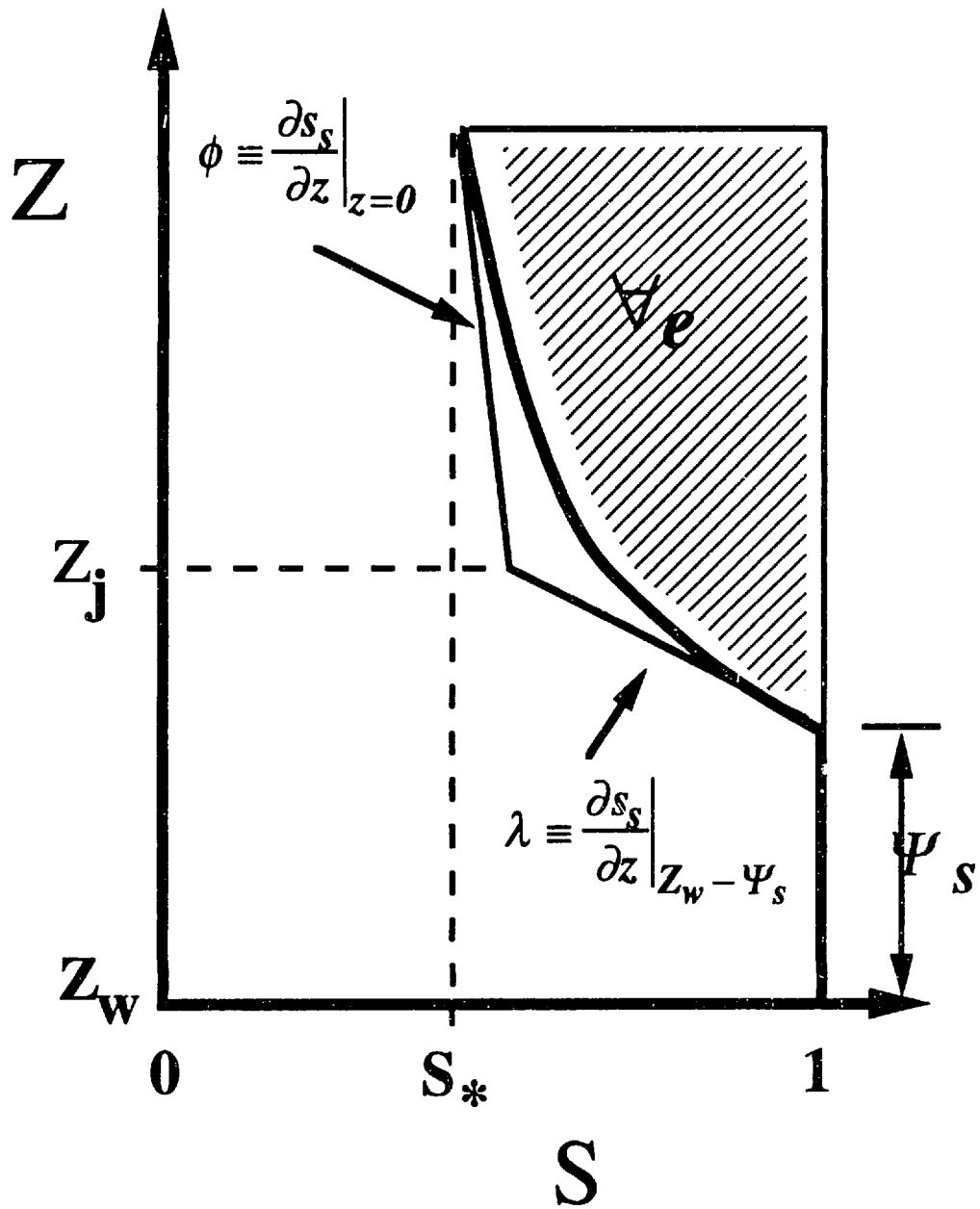

Figure 4.5 Definition sketch for approximating the storage capacity of the steady state soil moisture profile

$$\lambda \equiv \frac{m(1+q')}{\Psi_s} \tag{4.25}$$

$$\phi \equiv \frac{m(1+q')\left(s_*^{1-c}\right)}{\Psi_s}\left(\frac{Z_w}{\Psi_s}\right)^{-mc-1} \tag{4.26}$$

and Z_j is the depth at which the two linear expansions meet:

$$Z_j \equiv \frac{(1-s_*)-\lambda(Z_w-\Psi_s)}{\lambda+\phi} \tag{4.27}$$

4.d Infiltration into Soils Bounded by a Water Table

Simple and realistic modeling of the process of infiltration is of great importance and utility for many fields including hydrology, agronomy, and geomorphology. A wide range of exact and approximate solutions to infiltration problems (and the related zero gravity sorption problem) exist in the literature. Some of the characteristics that distinguish various problems and their solutions are the treatment of boundary conditions, initial conditions and soil hydraulic properties. As *Bouwer* [1969] points out, there is a trade-off in many solutions between the exactness of the solution and the restrictions on its application due to assumptions made concerning, for example, the initial condition moisture profile. *Bouwer* [1969] argues that the simple and demonstrably inexact Green-Ampt model [*Green and Ampt*, 1911] is in some ways more useful than others because it can treat variability in the initial soil moisture profile and soil texture.

In this section a balance is struck concerning this trade-off. An infiltration capacity solution is derived which is similar in form and utility to the Green-Ampt model, but which more accurately describes the moisture profile dynamics and the wetting front. The critical attribute of this solution with respect to the water balance model developed in this thesis is that it is applicable to soils bounded by (and at steady-state equilibrium with) a water table.

Existing analyses of the general problem of (one dimensional) infiltration organize into

five general classes: 1) Linearized solutions (e.g. *Warrick* [1975], *Braester* [1973], *Philip* [1991], *Warrick et al.* [1991], *Srivastava and Yeh* [1991]) in which the soil hydraulic properties' dependence on moisture content are taken such that the governing equation is linear (see Appendix A). These solutions are general in terms of their ability to incorporate complex initial and boundary conditions (including bounded soil columns), but are ill-suited to application because the required assumptions on the soil hydraulic properties are restrictive and unrealistic; 2) Green and Ampt type solutions (e.g. *Green and Ampt* [1911], *Philip* [1954], *Philip* [1993], *Govindaraju and Kavvas* [1993]) which make *a priori* assumptions about the shape of the wetting front. These are generally flexible solutions in terms of their ability to incorporate various initial and boundary conditions but the *a priori* wetting front assumptions introduce error and also confusion over the physical meaning and measurement of model parameters ; 3) Perturbation analyses which typically involve a Boltzman transformation (e.g. *Philip* [1957b], *Brutsaert* [1977]). These solutions are very accurate and simple to use, but they typically apply only for short times and the use of the Boltzman transformation restricts the applicability of the solutions to situations of unbounded soils with uniform initial moisture content; 4) Successive steady state solutions (e.g. *Macey* [1959], *Parlange* [1971]). These solutions are also restricted to cases of uniform initial soil moisture conditions; and 5) Boundary layer solutions (e.g. *Zimmerman and Bodvarsson* [1989] and [1991]). These solutions are analytically simple but also require the use of the Boltzman transformation and therefore are of restricted applicability.

In the *Eagleson* [1978a-g] model, the infiltration capacity is derived in similar fashion to *Philip* [1957b] (class #3 above). As mentioned above, this type of solution applies only to unbounded soils at uniform initial moisture content. To make the solution applicable to bounded soils, *Eagleson* [1978c] proposes that the effect of a shallow water table on the infiltration capacity can be approximated by subtracting the potential capillary rise rate (the capillary rise that would occur from a water table to a dry surface) from the infiltration rate that would occur into a semi-infinite (i.e. unbounded) soil column. This approximation is derived by analogy to the technique of superposing sources and sinks in linear diffusion equations. The technique is assumed to be valid so long as the water table is not so close to the surface that the infiltrating moisture fronts reach the capillary fringe.

In this section a set of approximate solutions (valid for all water table depths) of varying analytic complexity and accuracy are derived. At the end of this section the

solutions are compared with each other and with the superposition method. Despite the strong nonlinearity of the governing diffusion equation, the method proposed by *Eagleson* [1978c] works about as well as the simpler of the new solutions, though not as well as the most complex solution.

4.d.1 Derivation of Approximate Solution

Consistent with the *Eagleson* [1978a-g] water balance model, the approximate solution for infiltration under bounded soil conditions is derived for the *Brooks and Corey* [1966] representation of soil hydraulic properties. This representation relates the moisture retention and unsaturated hydraulic conductivity properties of soil (Appendix A).

The initial and boundary conditions of the infiltration solution derived in this section describe the infiltration capacity of a homogenous soil in steady equilibrium with a water table. As such, the initial condition soil moisture profile is approximated by the equivalent steady moisture profile expression derived earlier in this chapter (Equation 4.21A) and the surface boundary condition is one of zero head (free water). Unlike in the previous sections, the coordinate system throughout this derivation is positioned with the vertical coordinate (z) positive downward and zero at the surface. This simplifies notation considerably for the case of infiltration.

The solution follows directly from exploiting one exact mathematical property and three assumed approximate mathematical properties concerning the dynamics of infiltration. In summary, the procedure is to assume that to zeroth order the wetting front profile preserves similarity (which is the key assumption of *Green and Ampt* [1911] and *Philip* [1954]), and then use this assumption to solve for the deviation of the profile from similarity. The necessary assumptions are the following:

1) Application of a zero head boundary condition at the surface of a soil displaying the properties of a tension saturated zone will create a wetting front profile comprised of a tension saturated zone from the surface to some depth (z_{ts}) followed by a smooth profile (of length z_c) over which the moisture decreases from saturation to the initial condition soil moisture value ($s_s(z_{ts}+z_c)$). This characteristic is illustrated in Figure 4.6. *Philip* [1969] points out that if the capillary pressure is zero at the surface and (by definition) Ψ_s at the front of the tension saturated zone (z_{ts}), then the moisture flux throughout the tension

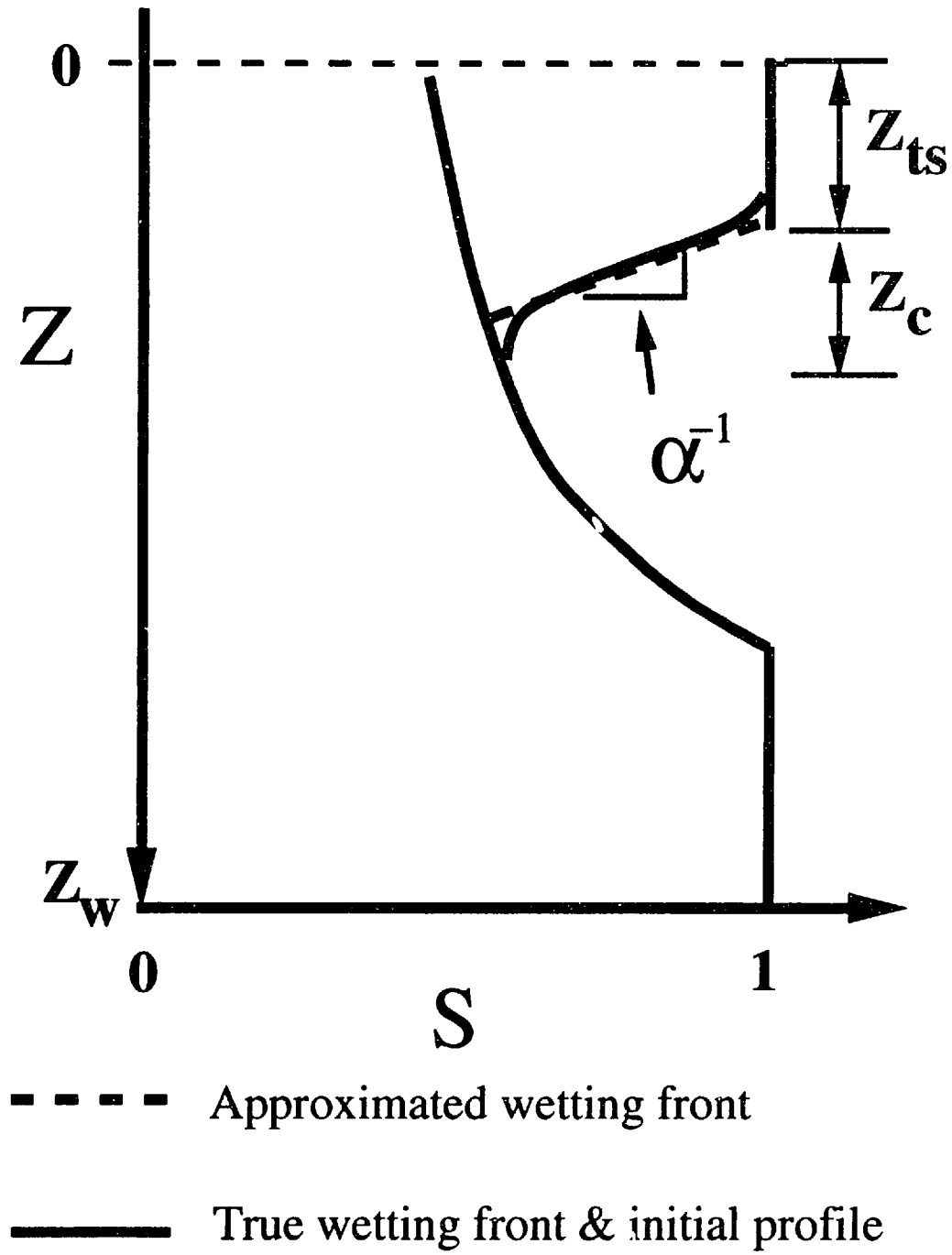

Figure 4.6 Definition sketch for linear wetting front model

saturated zone may be expressed by Darcy's law as:

$$q = K_s\left(\frac{-\Psi_s}{z_{ts}} + 1\right) \tag{4.28}$$

2) The profile in front of the tension saturated zone (i.e. $z_{ts} < z < z_{ts} + z_c$) may be approximated, at any given time, by a linear segment with slope α^{-1} (see Figure 4.6).

3) The profile in front of the tension saturated zone (i.e. $z_{ts} < z < z_{ts} + z_c$) approximately preserves similarity while it advects downward through the soil column. This allows the time rate of change of moisture in the wetting front (pore velocity) to be approximated by:

$$\frac{\partial s}{\partial t} \equiv -v_f \frac{\partial s}{\partial z} \tag{4.29}$$

where v_f is the velocity of the wetting front at its trailing edge (z_{ts}), i.e.

$$v_f \equiv \frac{dz_{ts}}{dt} \tag{4.30}$$

4) In approximating v_f, only the tension saturated portion ($z<z_{ts}$), and not the gradual portion ($z_{ts} < z < z_{ts} + z_c$) of the wetting front is accounted for in (4.30). The velocity of the wetting front (v_f) may then be approximated by: 1) taking the pore space between the soil surface and the depth of tension saturation (z_{ts}) as a control volume; and 2) dividing the rate of infiltration (f_i^*) into the control volume minus the steady flux out of the control volume (the flux corresponding to the initial condition (q_{st})) by the available pore space at z_{ts}:

$$v_f \equiv \frac{dz_{ts}}{dt} \equiv \frac{f_i^* - q_{st}}{n_e\left(1 - s_s(z_{ts})\right)} \tag{4.31}$$

This approximation is equivalent to assuming that the *approximated* wetting front (the straight line segment) advects but does not "rotate" (i.e. $d\alpha/dt = 0$). This assumption is equivalent to that made by *Green and Ampt* [1911] in their piston front model. Here

however, it is made only at this intermediate step. The final infiltration model fully accounts for the "rotation" of the approximated wetting front.

With these four properties, solution of the process of the wetting front profile evolution is broken up into two simpler problems: 1) analysis of flow processes within the tension saturated zone ($z<z_{ts}$) and any associated growth of the tension saturated zone; 2) analysis of flow processes along the approximated wetting front and any associated rotation of this front. Requiring conservation of mass for the two zones provides the final closure to the problem. In the following, these three aspects of the problem are analyzed.

The first of these three analyses is the simplest. Within the tension saturated zone property #1 may be used to relate the infiltration capacity (f_i^*) to the extent of the tension saturated zone (z_{ts}):

$$f_i^* = K_s\left(\frac{-\Psi_s}{z_{ts}(t)} + 1\right) \tag{4.32}$$

Note that Equation (4.32) is expressed in terms of a time varying depth of tension saturated soil ($z_{ts}(t)$).

The second analysis is considerably more complex. Along the wetting front ($z>z_{ts}$), application of the conservation of mass yields:

$$n\frac{\partial s}{\partial t} = -\frac{\partial q}{\partial z} \tag{4.33}$$

where q is the (unsaturated) Darcy flux. For soils represented by the *Brooks and Corey* [1966] model, this flux may be written (similar to Equation (2.11) but for z positive downward):

$$q = \frac{K_s \Psi_s}{m} s^{\frac{c+1}{2}} \frac{\partial s}{\partial z} + K_s s^c \tag{4.34}$$

Substituting Equation (4.29) (i.e. property #3) into Equation (4.33) and integrating from z_{ts}, where the soil is saturated (s=1) and the flux rate equals the infiltration rate ($q=f_i^*$), yields:

$$v_f(1-s) = \frac{f_i^*}{n_e} - \frac{q(s)}{n_e} \tag{4.35}$$

Solving (4.34) for $\frac{\partial s}{\partial z}$ and substituting (4.35) for q(s) and (4.31) for v_f yields:

$$\frac{\partial s}{\partial z} = \frac{\left(f_i^* - q_{st}\right)\left(\frac{1-s}{1-s_s(z_{ts})}\right) - f_i^* + K_s s^c}{\left(\frac{-K_s \Psi_s}{m}\right) s^{\frac{c+1}{2}}} \tag{4.36}$$

Application of Equation (4.36) to the center of the wetting front gives the following simple expression for α, the inverse of the approximate wetting front profile slope:

$$\alpha = \frac{-(c-3)\Psi_s \hat{s}^{\frac{c+1}{2}}}{\left(2\hat{s}^c - q'\right) - f'} \tag{4.37}$$

In the above

$$f' \equiv \frac{f_i^*}{K_s} \tag{4.38}$$

$$q' \equiv \frac{q_{st}}{K_s} \tag{4.39}$$

and

$$\hat{s} \equiv \frac{1}{2}\left(1 + s_s(z_{ts})\right) \tag{4.40}$$

Equation (4.37) may also be written (for future analytic convenience) in terms of z_{ts} by substituting for f' using Equations (4.32) and (4.38):

$$\alpha = \frac{-(c-3)\Psi_s \hat{s}^{\frac{c+1}{2}}}{\left(2\hat{s}^c - q'\right) - \left(1 - \frac{\Psi_s}{z_{st}}\right)} \tag{4.41}$$

Derivation of Equation (4.41) requires the zeroth order approximation that the wetting front preserves geometric similarity (assumption #3). Now this assumption may be dropped, i.e. the wetting front may rotate according to equation (4.41) or (4.37).

In summary, Equation (4.32) describes the infiltration capacity in terms of the extent of the tension saturated zone ($z_{ts}(t)$) and Equation (4.37) describes the slope of the approximate wetting front profile in terms of the infiltration rate. Given these two approximations of the moisture dynamics, finding the time evolution of the wetting front profile and infiltration rate is accomplished by requiring mass conservation.

First define a volume ($\forall$) as the cumulative water added to the soil (since the onset of infiltration) between the surface and the penetration depth (z_{ts}+ z_c):

$$\forall \equiv n_e \int_0^{z_{ts}+z_c} \left(s(\zeta;t) - s_s(\zeta)\right) d\zeta \tag{4.42}$$

The approximation of the wetting front as a straight line segment allows the volume of moisture between z_{ts} and z_c (cross-hatched, Figure 4.7) to be approximated by the area of a triangle of height z_c and a base of width 1-$s_s(z_{ts})$. Making this approximation and noting that for z less than z_{ts} the soil is saturated, (4.42) may be expressed as

$$\forall = \int_0^{z_{ts}} n_e \left(1 - s_s(\zeta)\right) d\zeta + \frac{1}{2} n_e \left(1 - s_s(z_{ts})\right) z_c \tag{4.43}$$

The depth z_{ts} + z_c is defined as the intersection of the wetting front and the (nonlinear) initial moisture profile (Equation (4.21A)). Analytic expression of this depth for use in Equation (4.43) would thus be implicit. As is illustrated in Figure 4.7, the depth may be approximated explicitly by linearly expanding the initial condition moisture profile ($s_s(z)$) around the depth z_{ts}, and then solving for the intersection of this expansion and the wetting front, yielding for z_c:

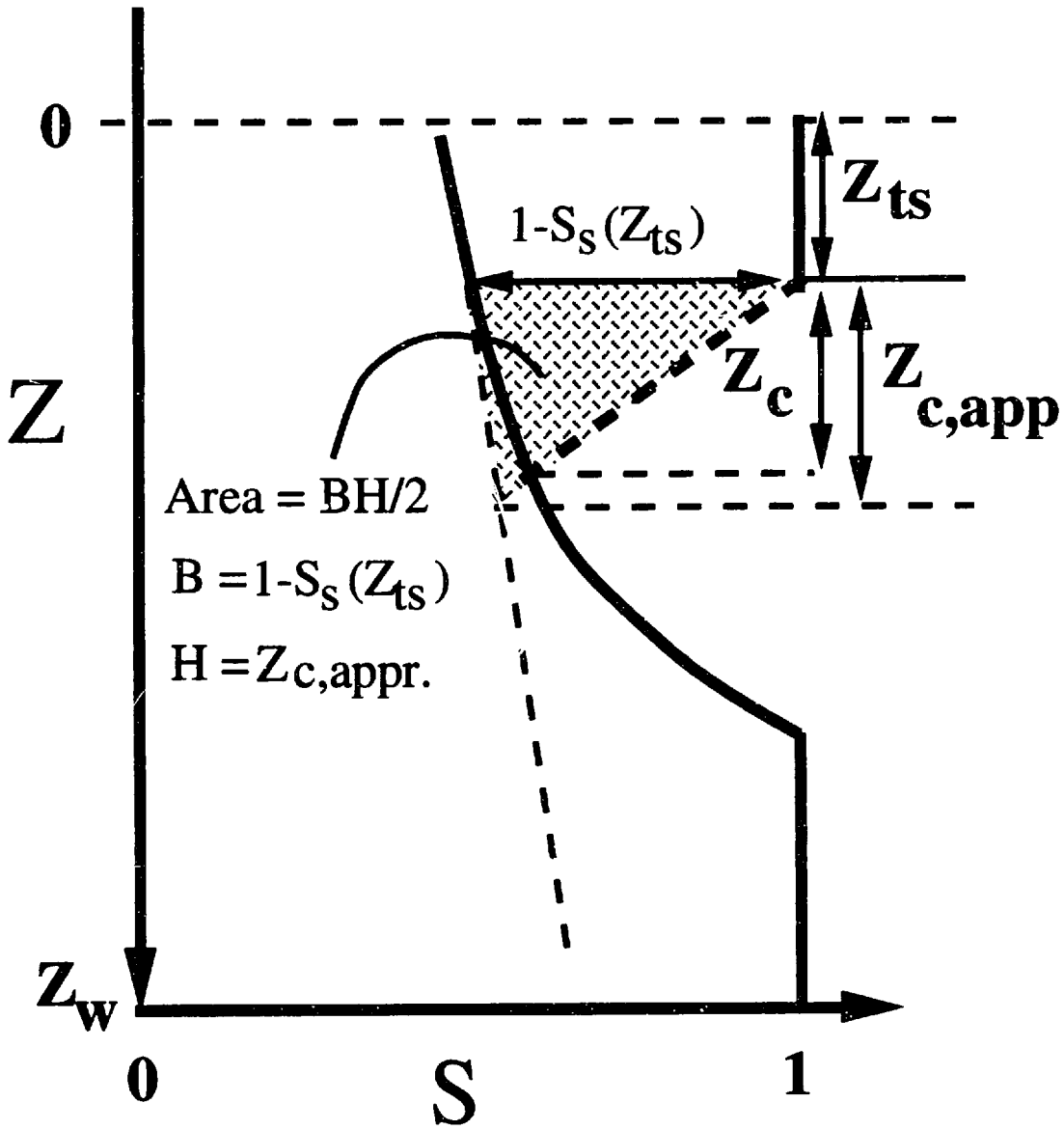

Figure 4.7 Definition sketch for wetting front control volume

$$z_c \equiv \frac{-\alpha\left(1 - s_s(z_{ts})\right)}{1 - \alpha \left.\frac{\partial s}{\partial z}\right|_{z_{ts}}} \tag{4.44}$$

Substitution of Equation (4.44) into (4.43) leaves the added volume ($\forall$) dependent only on the depth z_{ts}:

$$\forall = \int_0^{z_{ts}} n_e\left(1 - s_s(\zeta)\right) d\zeta - \frac{\alpha n_e \left(1 - s_s(z_{ts})\right)^2}{2\left(1 - \alpha \left.\frac{\partial s}{\partial z}\right|_{z_{ts}}\right)} \tag{4.45}$$

The rate of change of this volume of moisture is equal to the flux into the soil surface (f_i^*) minus the steady state initial condition flux (q_{st}) at $z_{ts} + z_c$:

$$\frac{d\forall}{dt} = f_i^* - q_{st} \tag{4.46}$$

Because the only time varying variable in the expression for $\forall$ is z_{ts}, the derivative in Equation (4.46) may be expanded by the chain rule as:

$$\frac{d\forall}{dt} = \frac{\partial \forall}{\partial z_{ts}} \frac{dz_{ts}}{dt} \tag{4.47}$$

Differentiating Equation (4.45) with respect to z_{ts} gives:

$$\frac{\partial \forall}{\partial z_{ts}} = n_e \Bigg\{ \left[1 - s_s(z_{ts})\right] - \left[\frac{1}{2}\left(1 - s_s(z_{ts})\right)^2 \frac{\partial \alpha}{\partial z_{ts}} + \alpha \frac{\partial s_s}{\partial z}\Big|_{z_{ts}} \left(1 - s_s(z_{ts})\right) \right] \left(1 - \alpha \frac{\partial s_s}{\partial z}\Big|_{z_{ts}} \right)^{-1} - \left[\frac{1}{2}\alpha\left(1 - s_s(z_{ts})\right)^2 \left(\frac{\partial \alpha}{\partial z}\Big|_{z_{ts}} \cdot \frac{\partial s_s}{\partial z}\Big|_{z_{ts}} + \alpha \frac{\partial^2 s_s}{\partial z^2}\Big|_{z_{ts}} \right) \right] \left(1 - \alpha \frac{\partial s_s}{\partial z}\Big|_{z_{ts}} \right)^{-2} \Bigg\} \tag{4.48}$$

Substituting Equations (4.36) and (4.47) into Equation (4.46) and integrating with respect to time yields the following integral relating the position of the tension saturated zone (z_{ts}) to the time since the onset of infiltration:

$$t = \frac{1}{K_s} \int \frac{z_{ts} \dfrac{\partial \forall}{\partial z_{ts}}}{\left(1 - \dfrac{q_{st}}{K_s}\right) z_{st} + \Psi_s} dz_{ts} \tag{4.49}$$

The above equation may be integrated numerically by substituting Equations (4.41) and (4.21A) into Equation (4.48), taking the necessary derivatives of s_s and α (analytically), and then substituting the result (i.e. $\dfrac{\partial \forall}{\partial z_{ts}}(z_{ts})$) into Equation (4.49).

The infiltration rate (f_i^*) at any time may then be found in terms of z_{ts} using Equation (4.32), and the approximate wetting front profile may be constructed using Equation (4.41) for α. In summary, for a given infiltration rate (f_i^*), the depth of the tension saturated zone is (from 4.32):

$$z_{ts}(t) = -\Psi_s \left(\frac{f_i^*}{K_s} - 1 \right)^{-1} \tag{4.50}$$

The time at which the infiltration rate occurs is found by integrating (4.49) from z_{ts} equals zero to the value given by (4.50). Like the *Green and Ampt* [1911] solution, this solution

is implicit. In fact, the solution presented here collapses to the *Green and Ampt* [1911] solution in the limit corresponding to very sandy soils. For sandy soils, the limiting value of the pore disconnectedness index (c) is three, and the wetting front becomes rectangular (α=0, see Equation 4.41). For α constant and equal to zero, Equation (4.48) states that the rate of change of the control volume ($\forall$) with z_{ts} collapses to $n_e(1-s_s(z_{ts}))$. In this limit, Equation (4.49) is identical to that found by *Green and Ampt* [1911] and used by *Bouwer* [1969] in the analysis of infiltration into soils with nonuniform initial moisture profile.

4.d.2 Example Applications of Approximate Infiltration Equations

To test the accuracy of the approximate infiltration model three infiltration cases have been simulated using *Milly's* [1982] numerical finite element unsaturated flow simulation code. The cases are simulated for a clay soil, a silt loam and a sand loam (for Brooks-Corey parameter values see Table 3.1). In each case the soil column is bounded by a water table at a depth of 150 centimeters and it recharges the saturated zone at a steady rate of 30 centimeters per year. These soil textures, recharge rates and water table positions test the infiltration model under moisture conditions ranging from effectively semi-infinite and uniform (for sand) to highly nonuniform (for clay). The three Figures (4.8, 4.9 and 4.10) compare the predicted and simulated wetting front profiles. The open circles in the figures are finite-element simulation results and the solid lines are the approximate analytic model results using equation (2.3) and (A.1-A.4).

As noted above, the initial condition moisture profile corresponds to the same water table depth and steady initial flow rate for each case, yet the initial moisture profiles vary greatly due to the different moisture retention and conductivity characteristics of the three soils. For example, note that the existence of a tension saturated zone, which causes the soils to be saturated for $-\Psi_s$ centimeters (the bubbling pressure head) above the water table, makes the water table be positioned, on the basis of saturation levels, at higher levels in the clay case (Figure 4.8) than the silt (Figure 4.9) and sand (Figure 4.10) cases. The clay and silt soils have a much larger tension saturated zone at the water table due to their larger bubbling pressure heads (-90 and -45 cm. respectively versus -10 cm. for sand). The clay and silt soils also have a gradual increase of moisture content from the water table to the surface; the profiles are clearly nonuniform.

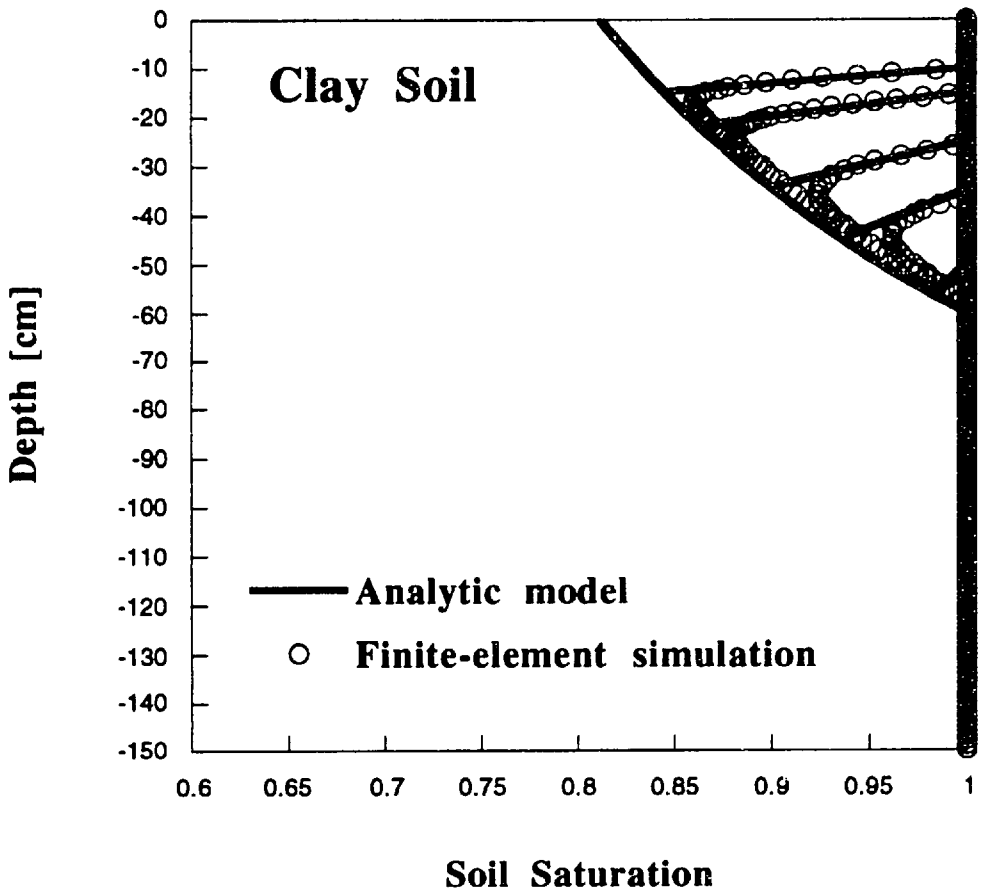

Figure 4.8 Wetting fronts in clay soil: analytic model vs. finite-element simulation

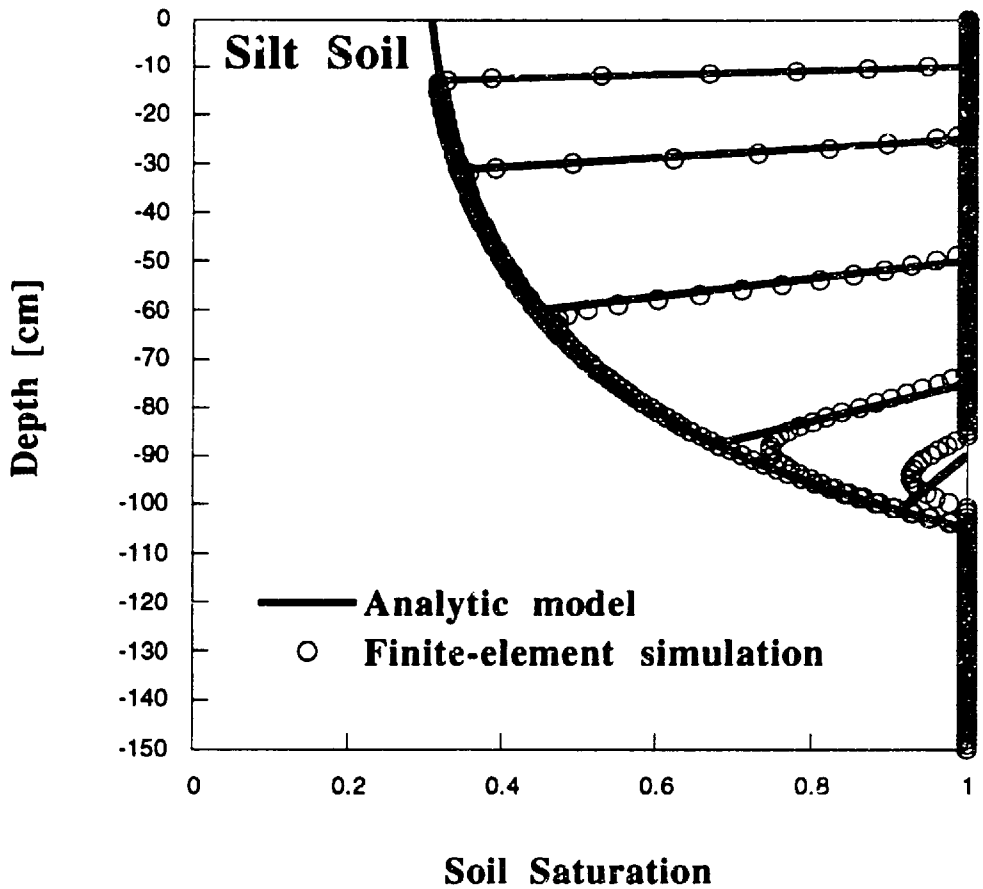

Figure 4.9 Wetting fronts in silt soil: analytic model vs. finite-element simulation

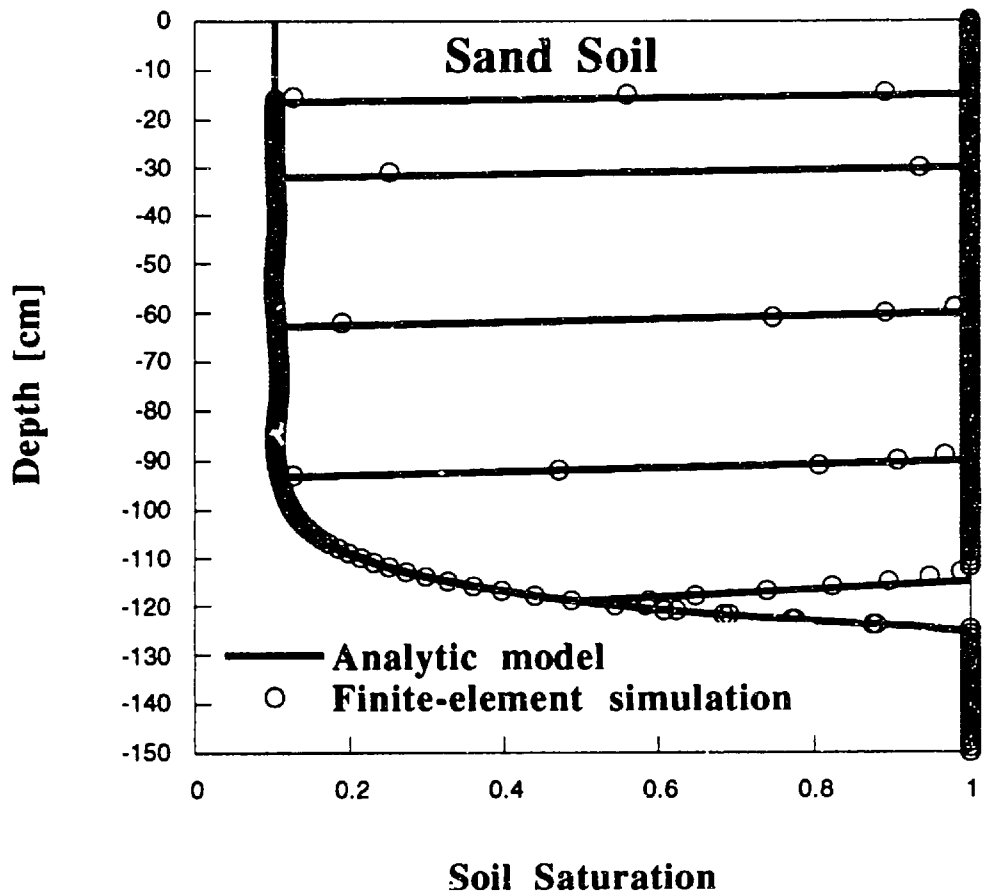

Figure 4.10 Wetting fronts in sand soil: analytic model vs. finite-element simulation

In all three cases the accuracy of the approximate wetting front model is very good. The position and slope of the wetting front as predicted by the analytic model are in close agreement with the numerical simulations, particularly at early times. As is illustrated by the figures, the approximations are best for the sandy soils and decrease as the soil characteristics tend to those representative of clay (i.e. as the saturated matric potential (Ψ_s) and the pore disconnectedness index (c) increase). Note also the accuracy with which the approximate analytic expression of the steady initial moisture profile (Equation 4.21A) captures the numerically simulated initial condition (the finite element model is initialized by requiring steady recharge).

The "increased sandyness-increased accuracy" characteristic of the approximate model is related to the fact that for the sand soil, as compared with silt or clay, the unsaturated moisture diffusivity that applies along the wetting front is small relative to the potential for flow through the tension saturated zone (N.B., the saturated hydraulic conductivity (K_s) and bubbling pressure head (Ψ_s) affect the potential for flow in both the unsaturated and tension-saturated zones, but the large pore distribution index (m) reduces only the unsaturated zone flow potential (i.e. the diffusivity, Equation A.6)). In order to compensate for this small relative diffusivity, the wetting front gradient is forced to be very large at all times. This sharpness (α small) leads to increased accuracy both because the wetting front was assumed to be rectangular (α =0) in the estimation of the velocity of the wetting front (property # 4), and because the "rotation" of the approximated wetting front ($d\alpha/dt$) was assumed negligible in the approximation of the rate of change of soil moisture (property #3). As would be expected, the accuracy of the overall approximation increases as the assumed conditions are more closely realized (i.e. for smaller α).

The sharpness of the wetting front for sandy soils is reflected in the form of the equation for the wetting front slope α^{-1} (e.g. Equation (4.41)). As Ψ_s and c decrease, the inverse of the slope decreases, and the wetting fronts become more piston-like (Green-Ampt). In fact, in the sand-limit of the Brooks-Corey soil hydraulic representation, the pore disconnectedness index (c) approaches the value three, the unsaturated diffusivity approaches zero (see Equations (A.4) and (A.6)), and α approaches zero. In this limit the approximate model derived here becomes exact and also identical to the model of *Green and Ampt* [1911] and *Philip* [1954].

Even though some details of the wetting front profile are lost because of the assumed

linear shape of the wetting front (property # 2), integral features such as the infiltration capacity are well preserved. The accuracy of these integral properties, which is the critical issue for water balance modeling, is illustrated by the infiltration rate (f_i^*) comparisons in Figures 4.11, 4.12 and 4.13. Again the open circles plot the finite-element simulation results and the solid lines plot the approximate analytic model. The analytic model is labeled the "implicit integral" approximation (for future comparison) because it is implicit in the infiltration rate (i.e. $t(z_{ts}(f_i^*))$ in Equation (4.49)) and application of the model involves evaluating an integral (Equation 4.49).

Note that in all three cases there is a sudden drop in infiltration rate to the saturated conductivity limit. This is due to column saturation (i.e. the wetting front reaching the water table). In general the analytic model closely approximates the numerically simulated results. Again the most error is incurred in the clay soil case (Figure 4.11), for which the time to column saturation is overestimated by about five percent. This result is consistent with the overall relation of the accuracy of the approximate model to the sand content of the soil.

In order to illustrate the impact of the water table presence on the infiltration rate (and thus potentially the runoff generation), the infiltration capacity of an unbounded soil at uniform initial moisture content (equal to the surface moisture content value of the bounded cases) is also plotted (dash-dotted lines, Figures 4.11-4.13). The derivation for this solution is given shortly. At this point, note that the difference in predicted rates is on the order of one half to twice the saturated hydraulic conductivity. More importantly, the unbounded solution by definition never saturates the column. After the predicted column saturation, the error that would be incurred by using a standard "unbounded" or "semi-infinite" infiltration capacity is even larger.

4.d.3 Explicit Approximation of the Infiltration Capacity

The approximate analytic equations for describing the wetting fronts and infiltration rate represent a significant simplification as compared with full numerical simulation procedures, but are still too unwieldy to be used in a derived distribution approach to estimating the expected value of infiltration for a given water table depth and distribution of storm conditions. The complicating attributes of the solution are that the solution still requires numerical evaluation of an integral (i.e. Equation (4.49)) and that the solution

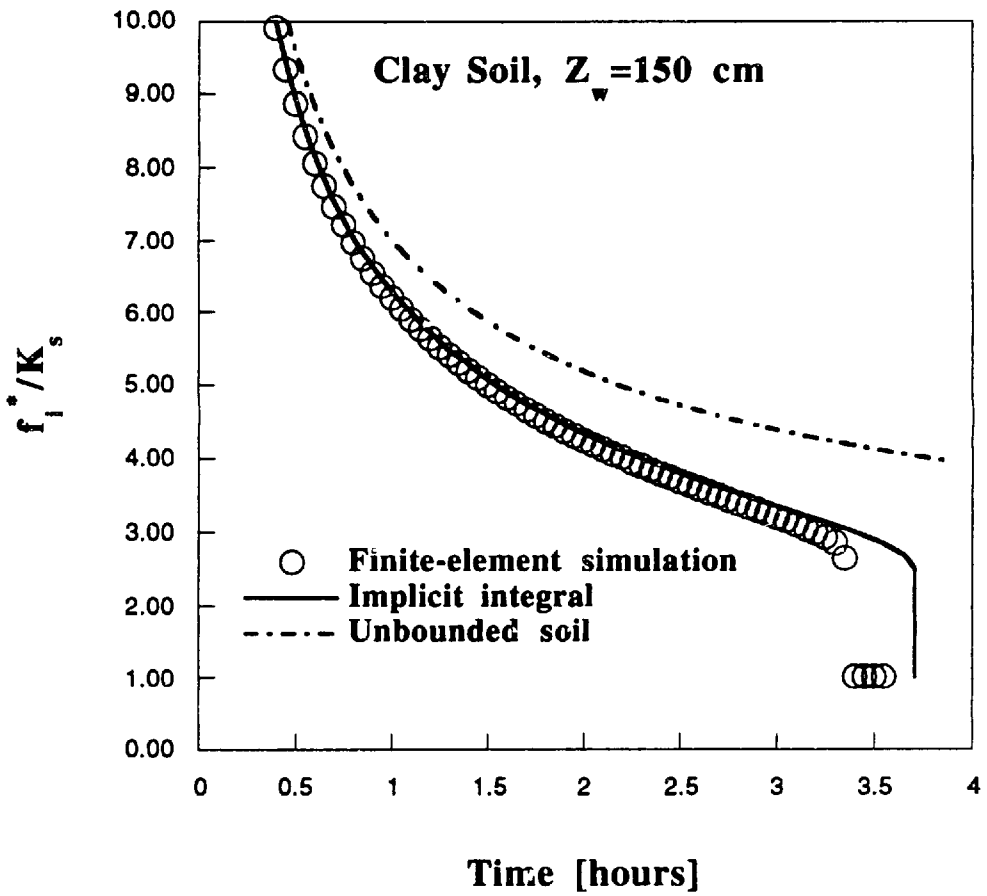

Figure 4.11 Infiltration capacity into clay soil: analytic model vs. finite-element simulation

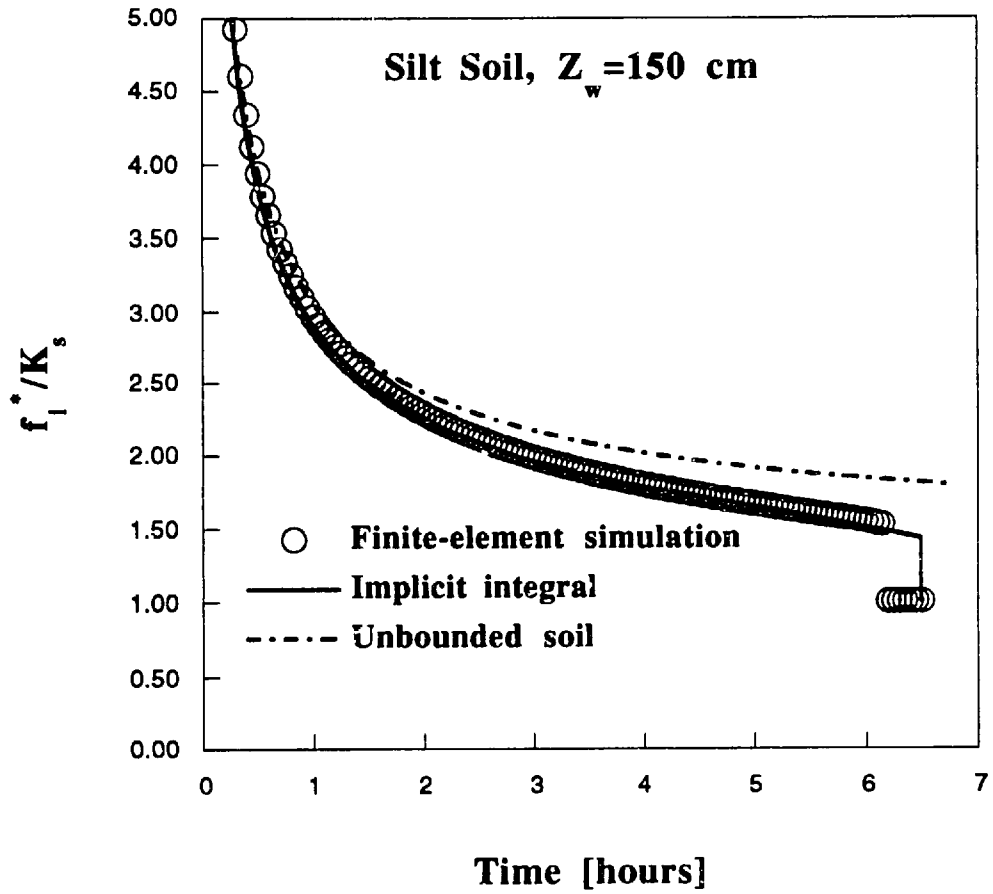

Figure 4.12 Infiltration capacity into silt soil: analytic model vs. finite-element simulation

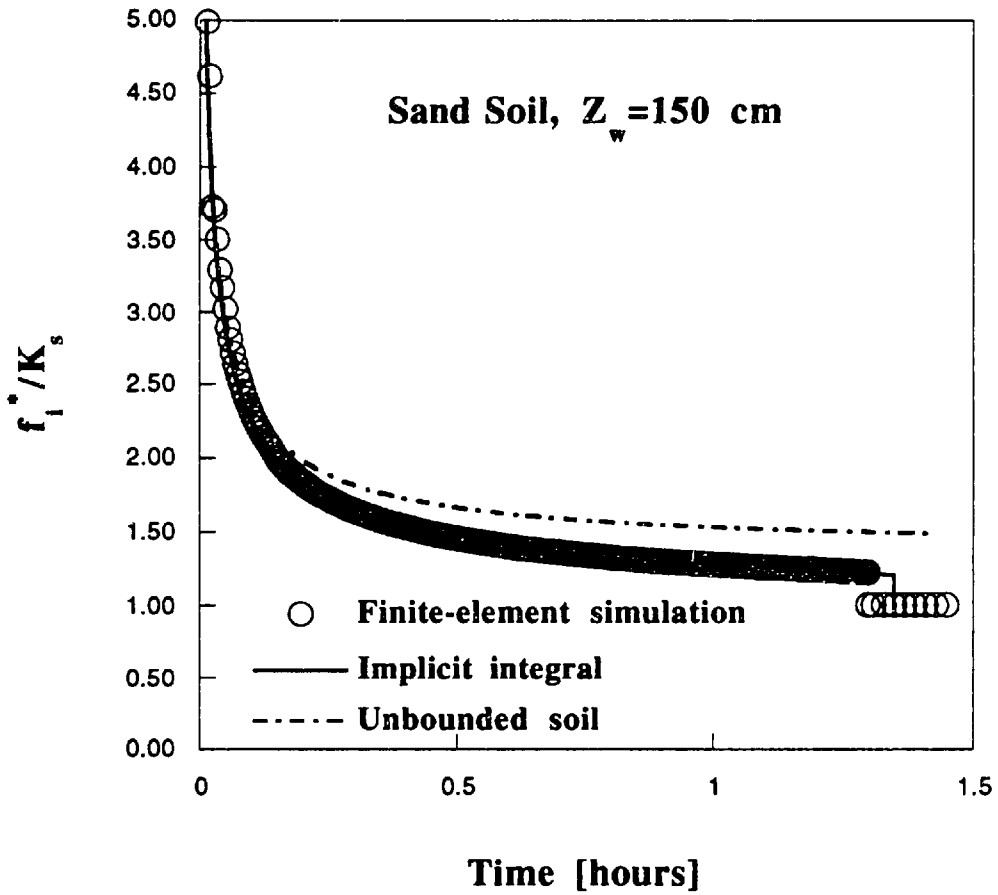

Figure 4.13 Infiltration capacity into sand soil: analytic model vs. finite-element simulation

expresses the infiltration rate implicitly (i.e. the solution expresses $t(z_{ts}(f_i^*))$).

In order to obtain a simple explicit expression for the infiltration rate, further approximation must be made. The necessary approximations are: 1) that the initial moisture profile be approximated by a linear expansion around the surface; 2) that the expression for α be modified slightly (discussed below); 3) that the slope of the initial condition moisture profile be assumed small in comparison with the wetting front slope; and 4) that the ratio q_{st}/K_s be assumed negligible in comparison with unity. In addition it is necessary to deal directly with the normalized infiltration rate (f'), rather than the depth of the tension saturated zone (z_{ts}), and to nondimensionalize time. These approximations are discussed below.

The first approximation is straight-forward and has already been carried out in the previous section when deriving the approximate storage capacity of the steady-state profile (Figure 4.5). Using the same notation as previously, the initial soil moisture profile (Equation (4.21A)) may be expanded as follows:

$$s_s \cong s_* + \phi z \tag{4.51}$$

where s_* is the soil moisture at the surface (Equation (4.24), but for z positive downward) and ϕ is the slope of the moisture profile evaluated at the surface (Equation (4.26), but for z positive downward). Because this approximation deteriorates with depth, the approximation error of the explicit infiltration capacity expression will be largest as the wetting front penetrates deeper at larger times. Thus the infiltration expression will be most valid for short times.

The second approximation involves modifying the expression for α (Equation (4.37)). For most initial conditions, the first term of the denominator $\left(2\hat{s}^c - q'\right)$ will be of order one (taken to be unity), while the normalized infiltration capacity (f') will, at early time, be much larger than one (e.g. see Figure 4.11). Thus for small times, α (Equation (4.41)) may be approximated, for analytic convenience, by:

$$\alpha \cong \frac{-(c-3)\Psi_s \hat{s}^{\frac{c+1}{2}}}{1-f'} \tag{4.52}$$

The assumption that the slope of the initial moisture profile is much smaller than the slope

of the wetting front profile allows Equation (4.45) to be simplified to:

$$\forall = \int_0^{z_{ts}} n_e\left(1 - s_s(\zeta)\right)d\zeta - \frac{1}{2}\alpha n_e\left(1 - s_s(z_{ts})\right)^2 \tag{4.53}$$

The rate of change of this volume with z_{ts} (Equation (4.48)) then simplifies to:

$$\frac{\partial \forall}{\partial z_{ts}} = n_e\left\{\left[1 - s_s(z_{ts})\right] - \left[\frac{1}{2}\left(1 - s_s(z_{ts})\right)^2 \frac{\partial \alpha}{\partial z_{ts}} + \alpha \left.\frac{\partial s_s}{\partial z}\right|_{z_{ts}} \left(1 - s_s(z_{ts})\right)\right]\right\} \tag{4.54}$$

The requirement that the analysis be expressed in terms of f' rather than z_{ts} is accomplished by substituting f' for z_{ts} (e.g. in Equation (4.54)) through Equations (4.32) and (4.38):

$$z_{ts} = \frac{-\Psi_s}{f' - 1} \tag{4.55}$$

Removing dependence on z_{ts} also requires that all derivatives taken with respect to z_{ts} (e.g. in Equation (4.54)) be multiplied by the derivative of z_{ts} with respect to f', i.e.:

$$\frac{\partial}{\partial f'} = \frac{dz_{ts}}{df'} \cdot \frac{\partial}{\partial z_{ts}} = \left(\frac{\Psi_s}{(f' - 1)^2}\right)\frac{\partial}{\partial z_{ts}} \tag{4.56}$$

With the above change of variables and approximations (i.e. Equations (4.51), (4.52), (4.54) and the assumption that q_{st}/K_s is small), and neglecting terms of order $(f'-1)^{-1}$, the mass balance Equations (4.46) yields:

$$f'(f' - 1)^3 + \chi(f' - 1 + \Gamma)\frac{df'}{dt} = 0 \tag{4.57}$$

where:

$$\chi \equiv \frac{-n_e(1-s_*)\Psi_s}{K_s}\left(1+\frac{1}{2}(c-3)(1-s_*)\hat{s}^{\frac{c+1}{2}}\right) \tag{4.58}$$

and

$$\Gamma \equiv \frac{\phi\Psi_s/(1-s_*)}{\left(1+\frac{1}{2}(c-3)(1-s_*)\hat{s}^{\frac{c+1}{2}}\right)} \tag{4.59}$$

The final step is to nondimensionalize the temporal dependence in Equation (4.57) by the following change of variables:

$$\tau \equiv \frac{t}{t+\chi} \tag{4.60}$$

With this change of variables, Equation (4.57) becomes the differential equation:

$$f'(f'-1)^3+(f'-1+\Gamma)(1-\tau)^2\frac{df'}{d\tau}=0 \tag{4.61}$$

An approximate solution of Equation (4.61) may be formed by the method of power series substitution (cf. *Bender and Orzag* [1978]). This method involves assuming a power series solution with undetermined coefficients, substituting this assumed solution into the governing Equation (4.61), and then equating coefficients multiplying like powers of the independent variable (in this case τ) such that the equality of Equation (4.61) is obeyed.

It is well known that the early time behavior of the infiltration rate is proportional to $t^{-1/2}$ (e.g. *Philip*, [1957b]). As t and τ scale linearly for small time (see Equation (4.60)), it seems reasonable to form the power series for f' in half powers of τ starting with $\tau^{-1/2}$:

$$f' \equiv A_0\tau^{-1/2}+A_1\tau^0+A_2\tau^{1/2}+A_3\tau+\ldots \tag{4.62}$$

Substituting this assumed solution into Equation (4.61), expanding the binomial terms and equating coefficients of the highest power of τ yields the following equation for A_0:

$$-\frac{1}{2}A_0^2 + A_0^4 = 0 \tag{4.63}$$

Solving Equation (4.63) and choosing the positive non-zero root as physically plausible gives

$$A_0 = \frac{\sqrt{2}}{2} \tag{4.64}$$

Solving for the next highest power yields an equation in A_0 and A_1. This equation may be solved simultaneously with (4.64) to find for A_1:

$$A_1 = \frac{2}{3} + \frac{\Gamma}{3} \tag{4.65}$$

This procedure may be repeated to find as many coefficients of (4.62) as desired. Here only these first two terms will be kept. Including more higher order terms improves the approximation very little (for this bounded soil case) because these higher order terms are more important only for later times when the solution is already restricted with the use of the initial condition soil moisture expansion (Equation (4.51)). For the case of unbounded soils, however, where the initial steady-state soil moisture is uniform, the higher order terms improve the solution considerably. As the unbounded case is not directly relevant to the model development undertaken in this thesis, this limiting case analysis is restricted to Appendix B. The most interesting conclusion of the analysis is that *unlike* the traditional power series in true time (t) analyses of, for example, *Philip* [1957b], the power series in $\tau=t/(t+\chi)$ actually leads to a uniformly converging solution for all times.

It is interesting to note how the information concerning the water table depth and steady initial flow rate are contained in the bounded soil series solution. Essentially, the information comes in through the dependence of the term χ on the surface soil moisture (s_*, Equation (4.24)) and through the dependence of the term Γ (Equation (4.59)) on the slope of the initial moisture profile (ϕ, Equation (4.26)). Under shallow (small Z_w), wet (large s_*) conditions, χ decreases and Γ becomes more negative, reducing the infiltration

capacity of the soil.

4.d.4 Two Term Solution for Application to Current Model

In order to derive the expected value of infiltration- and storage-excess runoff, it is desirable to approximate the bounded water table solution further such that it is similar in form to the two term *Philip* [1957b] solution, yet retains the water table dependency. To accomplish this Equation (4.62) is truncated at two terms, Equation (4.60) is substituted for τ, and the result is expanded for small time yielding:

$$f_i^* \equiv \frac{\sqrt{2\chi}K_s}{2} t^{\frac{-1}{2}} + \left(\frac{2+\Gamma}{3}\right)K_s \tag{4.66}$$

This final approximation is plotted in the figures (4.14, 4.15 and 4.16) as the dashed curves. While this solution is clearly not nearly as accurate as the more complex approximations (the implicit integral solution), it does reflect the overall reduction of the infiltration rate due to the presence of a shallow water table. This is illustrated by comparing it to the previously mentioned unbounded solution (dot-dashed curves), generated by Equation (4.66) but with Γ set to zero (corresponding to infinite water table). Also plotted in these three figures are the superposition solution (close dots) of *Eagleson* [1978c]. These curves are generated by subtracting the dry soil potential capillary rise (Equation 4.14) corresponding to a water table depth of 150 centimeters from the unbounded solution (the dot-dashed curve). As mentioned previously, the superposition solution works about as well as Equation (4.66) despite the strong nonlinearity of the governing diffusion equation (especially near saturation). Note that one advantage of this new solution (Equation 4.66) over the infiltration equation developed by *Eagleson* [1978c] is that it does not require the evaluation of a diffusion weighting integral (e.g. *Crank* [1956] integral, Equation (3.5)) in order to define an effective diffusivity. Instead the coefficients are simple algebraic expressions (e.g. χ, as given by Equation (4.58)).

For the power series in time cases, the breakdown of the solution at large times (and thus deep wetting fronts) is due to a combination of 1) the breakdown of the linear approximation of the initial soil moisture profile far from the surface, and 2) the inability of

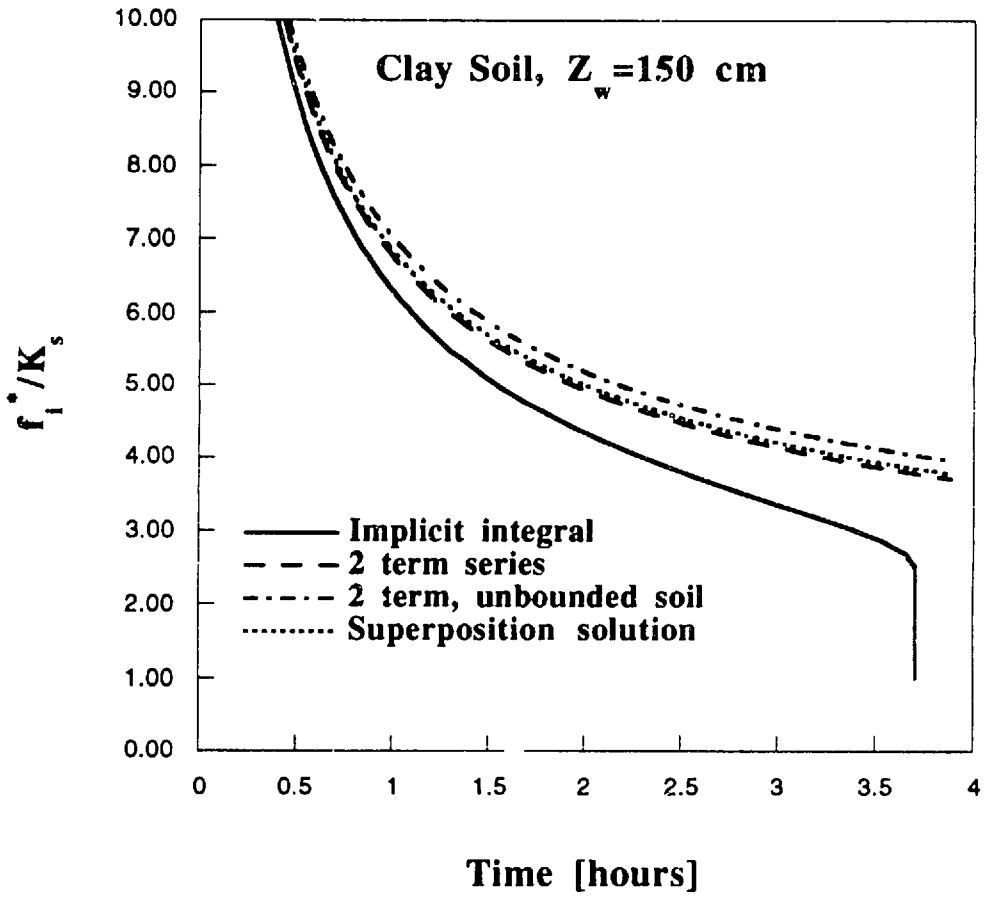

Figure 4.14 Infiltration capacity into clay soil: comparison of approximate analytic models

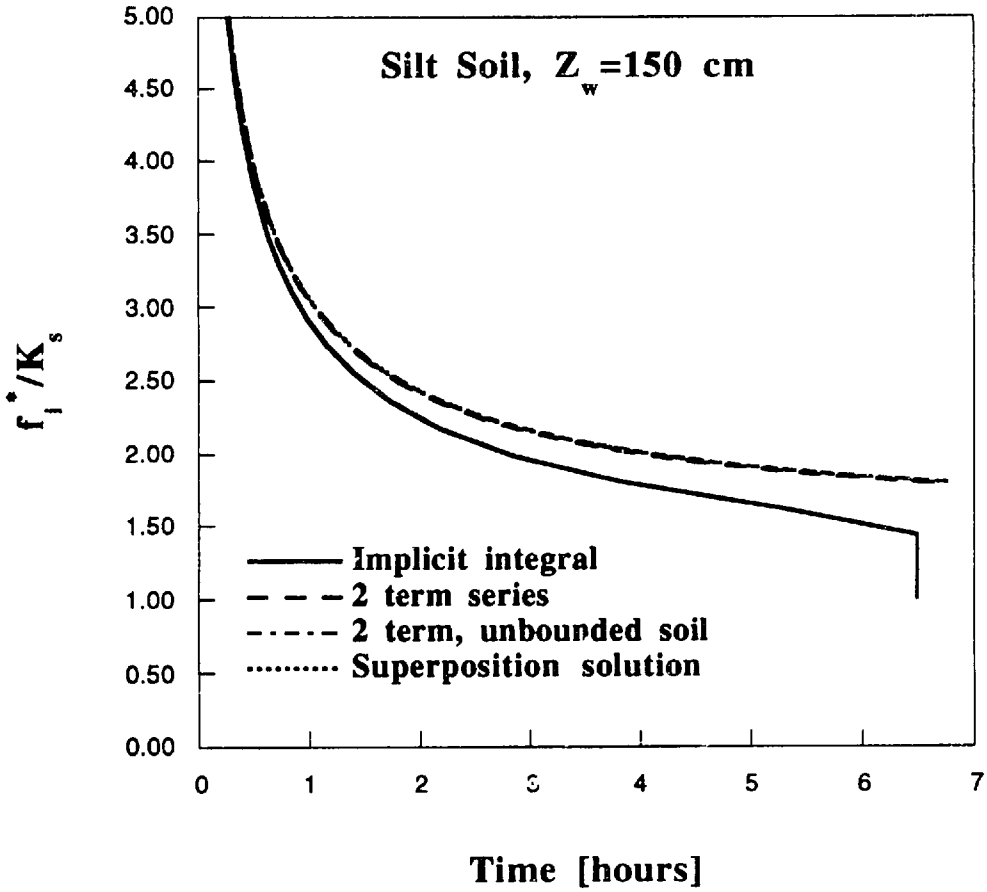

Figure 4.15 Infiltration capacity into silt soil: comparison of approximate analytic models

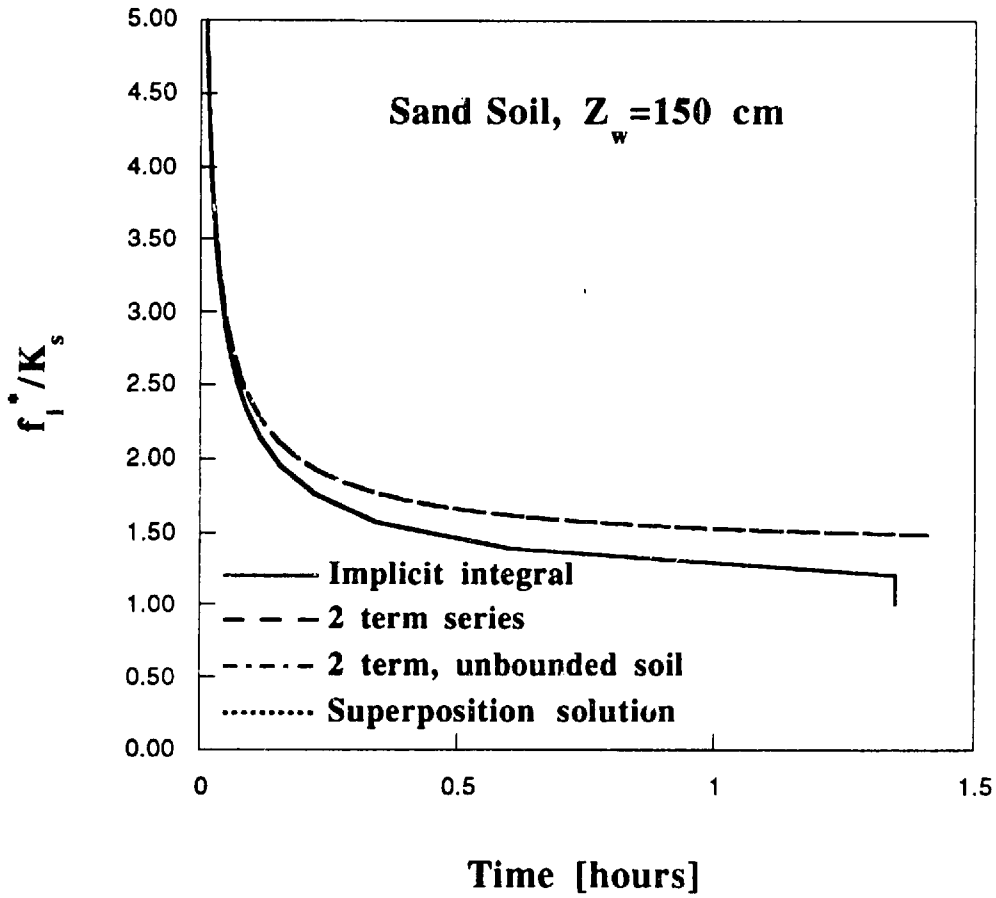

Figure 4.16 Infiltration capacity into sand soil: comparison of approximate analytic models

power series in time to capture the long time infiltration behavior (even of soils of uniform initial moisture content). For the silt and sand soil cases, the error is due mostly to the second source, causing all three power series solutions to diverge so early that they never even reflect the presence of the shallow water table (and thus are practically indistinguishable).

While not the most accurate of the analytical approximations derived in this chapter, the form of Equation (4.66) is simple and thus it is the expression used in the subsequent analysis such as the derivation of the expected value of surface and storage runoff in the presence of a shallow water table. As mentioned previously, the largest errors incurred by using infiltration capacity solutions derived for unbounded soils come from neglecting the sudden drop in infiltration capacity due to column saturation. As this characteristic is accounted for in the expected value analysis, the final equilibrium water balance model produces very good estimates of the runoff despite the inaccuracy of Equation (4.66).

4.e The Exfiltration Capacity from Soils Bounded by a Water Table

Eagleson [1978c] proposes that the exfiltration capacity of a soil column bounded by a water table can be approximated by adding the potential capillary rise rate to the exfiltration capacity of an unbounded soil at uniform initial moisture content. This approximation is based on the theory of superposition in the analysis of linear diffusion equations. As it has been shown for the case of infiltration, the superposition of solutions is an adequate approximation for estimating water balance

For consistency within this thesis, the limiting capillary rise rate derived earlier in the chapter (Equation (4.21B)) will be added to the exfiltration capacity instead of that used by *Eagleson* [1978c] (Equation 4.17). Adding this flux (denoted w) to the exfiltration capacity (as modified to account for gravity effects in Chapter 3), yields:

$$f_e^* = \frac{1}{2} S_e(s_*) t^{-1/2} - \frac{1}{2} K_s s_*^c + w \qquad (4.67)$$

where $S_e(s_*)$ is the desorptivity (Equation 3.10) of a soil at uniform moisture content and s_* is the equivalent steady soil moisture evaluated at the soil surface (Equation 4.24). The depth to the water table effects the exfiltration capacity both through its influence on the surface soil moisture (by way of the equivalent steady profile) and through its influence on

the potential capillary rise rate. Note that if the water table is far from the surface (Z_w large), the potential capillary rise rate approaches zero and the equivalent steady profile becomes uniform. For this condition Equation (4.67) collapses back to the form used in Chapter 3.

In the following chapter, Equation (4.67) is used in conjunction with the time compression approximation (see Chapter 3) to determine the mean bare soil evaporation that results from intermittent interstorm periods.

4.f Summary

Extension of the statistical-dynamical equilibrium water balance model of *Eagleson* [1978a-g] to shallow soils bounded by water table requires enhancements to the three major hydrologic components of the model: characterization of the moisture state, infiltration, and exfiltration. Regarding the moisture state, a simple analytic expression is derived for the steady-state moisture profile. As demonstrated in Chapters 2 and 3, this profile may serve (via the equivalent steady interpretation) as a useful parameterization of the mean initial condition moisture profile prior to storm and interstorm events.

Using the equivalent steady profile expression as a surrogate initial condition, the mean initial storage capacity of the soil is derived. This storage capacity expression is used in the following chapter to derived storage excess runoff from an ensemble of storms. The equivalent steady profile is also used as an initial condition in the derivation of a new water table dependent infiltration capacity and wetting front model. In its general form the model reproduces numerically simulated wetting front profiles, infiltration rates and column saturation times with a high level of accuracy. The general form, however, is awkward to manipulate in that it involves numerical evaluation of an integral and expresses the infiltration rate in an implicit form. For use in expected value analysis a simple two-term *Philip* [1957b]-type equation is derived from the full solution. The two term solution is not as accurate as the full solution, but is considerably simpler to apply. For the exfiltration capacity the superposition method of *Eagleson* [1978c] is applied in conjunction with the equivalent steady profile to derive an expression with explicit dependence on water table depth.

Chapter 5: Expected Value of Hydrologic Fluxes for Soils Bounded by Water Table

5.a Background

In Chapter 4 a set of equations are developed for characterizing the moisture and flux conditions associated with steady recharge or capillary rise, unsteady infiltration and unsteady exfiltration. The equations are more general than many existing models in that they are applicable to conditions of (water table) bounded soils.

In this chapter the expressions for the mean surface runoff and bare soil evaporation derived by *Eagleson* [1978d,e] are modified to account for the new (water table dependent) hydrologic process models. While the infiltration, exfiltration and steady flow components used in the original model (reviewed in Chapter 3) depend on the initial soil moisture state through an assumed uniform initial soil moisture, the new components depend on initial moisture state through the equivalent steady state moisture profile. This profile, which is shown to approximate the temporal mean soil moisture profile in Chapter 2, is parameterized in Chapter 4 (Equation (4.21A)) in terms of soil parameters, the water table depth, and the steady (or temporal mean, equivalent steady) flow rate. Thus instead of all of the fluxes (mean infiltration, exfiltration and recharge) being related by that effective soil moisture for which the fluxes are in equilibrium (the equilibrium soil moisture s_o), they may instead be related by that mean flow (recharge or capillary rise) rate, for a given water table depth, for which the fluxes are in equilibrium. The state variable for this water balance model is a flux rate rather than a volumetric water content variable

For the expected value of bare soil evaporation the modification is very simple. For surface runoff however, the modification is complicated because it involves accounting for the sudden loss of infiltration capacity at the time of column saturation.

At the end of the chapter the equilibrium condition is analyzed for a few climate-soil pairs and a range of water table depths. The quantitative and analytically tractable results illustrate many of the well known qualitative features of hillslope hydrology including, for example: 1) the tendency for areas of near surface water table to discharge saturated zone groundwater in the long term mean, produce evaporation at the potential rate, and yield large amounts of surface runoff; and 2) the tendency of areas with deep water tables to

recharge the saturated zone, produce soil-limited evaporation, and yield little to no surface runoff.

5.b Bare Soil Evaporation

The methodology presented by *Eagleson* [1978d] for finding the mean bare soil evaporation is reviewed in Chapter 3. In summary, it involves integrating the lesser of the moisture dependent exfiltration capacity (f_e^*) or potential evaporation rate (e_p) over the ensemble of exponentially distributed interstorm durations (of mean extent β^{-1}) and multiplying each of these possible interstorm exchanges by the probability of its associated duration. This mean interstorm evaporation is then multiplied by m_v, the mean number of storms (and thus interstorms) per year. In Chapter 3, the expression for the mean evaporation given by *Eagleson* [1978d] is modified to account for the effect of gravity on the exfiltration capacity (assumed to be negligible in *Eagleson* [1978d]). In that chapter the water table is assumed so deep as to preclude its effect on the exfiltration capacity.

Eagleson [1978c] proposes that the potential capillary rise and the exfiltration capacity of a soil with an unbounded and uniform initial soil moisture profile may be added. Reintroducing this assumption to the modified Equations (3.22, 3.23 and 3.24), the final expression for bare soil evaporation becomes:

$$\left\langle E_{s_{A,mod}} \right\rangle = \frac{e_p m_v}{\beta}\left\{1-\left(1+\sqrt{2\Lambda}E+(2\Omega)^{-1/2}\right)e^{-\Lambda E}+\left((2\Omega)^{-1/2}+\sqrt{2\Omega}E\right)e^{-\Omega E}+\sqrt{2E}\cdot\left(\gamma\left[\frac{3}{2},\Omega E\right]-\gamma\left[\frac{3}{2},\Lambda E\right]\right)\right\} \tag{5.1}$$

$$\Lambda = \frac{1+\frac{K_s s_*^c}{4e_p}-\frac{w}{2e_p}}{\left(1+\frac{K_s s_*^c}{2e_p}-\frac{w}{e_p}\right)^2} \tag{5.2}$$

and

$$\Omega = 2\left(\frac{K_s s_*^c}{e_p} - \frac{2w}{e_p}\right)^{-2} \tag{5.3}$$

For completeness, all intermediate equations required to evaluate Equation (5.1) are repeated here:

$$w = \frac{K_s\left(\frac{Z_w}{\Psi_s}\right)^{-mc}}{1-\left(\frac{Z_w}{\Psi_s}\right)^{-mc}} \tag{5.4}$$

$$E = \frac{\beta S_e^2}{2e_p^2} \tag{5.5}$$

$$S_e = 2s_*^{1+d/2}\left[\frac{n_e K_s|\Psi_s|\phi_e(d,s_*)}{m\pi}\right]^{1/2} \tag{5.6}$$

$$\phi_e\left(d,s_*\right) = 1.85\cdot s_*^{-d-1.85}\int_0^{s_*} s^d\left(s_* - s\right)^{0.85} ds \approx \frac{2m^2\pi}{3(1+3m)(1+4m)} \tag{5.7}$$

The approximation to Equation (5.7) is derived in *Entekhabi and Eagleson* [1989]. The surface soil moisture (s_*) appearing in the above equations is (from Equation (4.21A):

$$s_* \equiv \left(\frac{-q}{K_s} + \left(1+\frac{q}{K_s}\right)\left(\frac{Z_w}{\Psi_s}\right)^{-mc}\right)^{1/c} \tag{5.8}$$

For given soil parameters (K_s, Ψ_s, m, c, and n_e), climate parameters (e_p and β) and depth to water table (Z_w), the mean annual bare soil evaporation will depend, through Equations (5.1) through (5.7), on the mean moisture state by way of the mean recharge or discharge q (in Equation (5.8)).

5.c Infiltration Excess Runoff

Modification of the *Eagleson* [1978e] derivation of infiltration excess runoff is significantly more complicated for conditions of shallow water table due to the possibility of column saturation. The approach taken here is to modify *Eagleson's* [1978e] expression to apply to infiltration excess occurring up until column saturation (t_s), and then separately derive an expression for the mean runoff generation after ($t > t_s$) column saturation ("storage excess runoff").

The final infiltration capacity expression (Equation (4.66)) is intentionally simplified to a two term Philip type expression because that is the type of expression used in the *Eagleson* [1978e] model. For notational simplicity, the nomenclature used by *Eagleson* [1978e] is adopted here, i.e. the first coefficient of Equation (4.66) is re-defined as twice the sorptivity (S_i) and the second term is denoted A_o:

$$f_i^* \cong \frac{1}{2} S_i t^{\frac{-1}{2}} + A_o \tag{5.9}$$

$$S_i = \sqrt{2\chi K_s} \tag{5.10}$$

$$A_o = \left(\frac{2+\Gamma}{3}\right) K_s \tag{5.11}$$

In deriving the infiltration excess surface runoff generation, *Eagleson* [1978e] assumes that most of this runoff is made by long, intense storms for which the infiltration capacity is close to its asymptotic value (A_o). With this assumption, he approximates the rate of runoff generation by a storm of intensity i as ($i-A_o$). In order to determine the fraction of the storm duration over which runoff is produced, he needs to evaluate the ponding time (t_p). As this time is critically dependent on the early time behavior of the infiltration capacity, he uses the full infiltration Equation (5.9) and applies the time compression approximation (Equations (2.18) and (2.22)). This approximation of infiltration excess runoff generation is illustrated in Figure 5.1. The cross-hatched area represents the true excess of rainfall intensity over infiltration capacity, while the single hatched rectangular area represents the approximation made by *Eagleson* [1978e]. In addition, the upper time

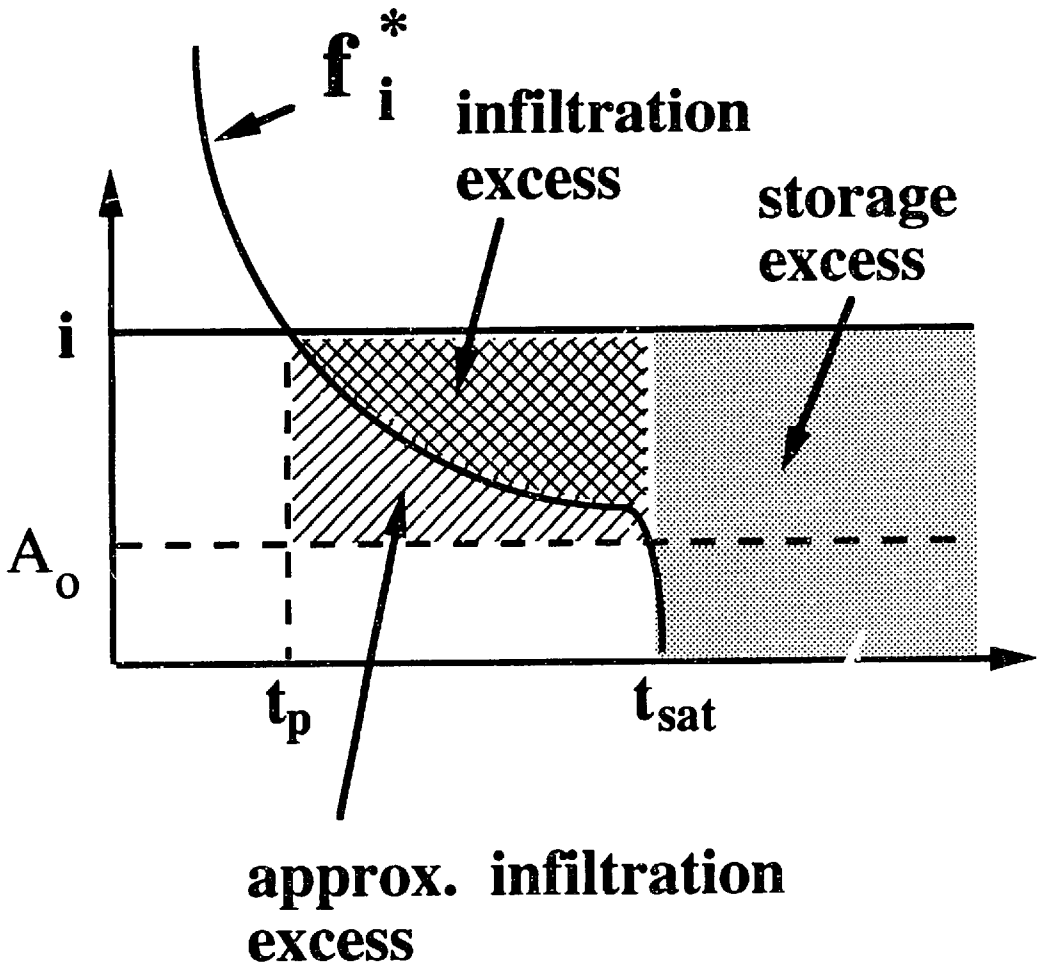

Figure 5.1 Definition sketch for infiltration excess runoff generation

limit due to column saturation (t_S) is illustrated. In the original work, this upper limit is not accounted for, as the model is stated to apply only for water table depths deep enough that the infiltration fronts do not reach the capillary fringe (*Eagleson* [1978c]).

For exponentially distributed storm durations and storm intensities, the expected value of the (approximated) infiltration excess runoff ($\langle R_{ie} \rangle$) illustrated in Figure 5.1 may be written:

$$\langle R_{ie} \rangle = \int_{A_o}^{\infty} \eta e^{-\eta i} di \int_{t_p}^{t_s} \delta e^{-\delta \tau} (i - A_o)(\tau - t_p) d\tau \tag{5.12}$$

Through the simple change variables and integration limits:

$$\tau^* \equiv \tau - t_p \tag{5.13}$$

$$\zeta \equiv i - A_o \tag{5.14}$$

the integral is written as

$$\langle R_{ie} \rangle = e^{-\eta A_o} \int_0^{\infty} \zeta \eta e^{-\eta \zeta - \delta t_p} d\zeta \int_0^{t_s - t_p} \tau^* \delta e^{-\delta \tau^*} d\tau^* \tag{5.15}$$

Evaluating this integral for finite t_S is complicated because both the ponding time (t_p) and the time to column saturation (t_S) that appear in the upper limit of the inner integral are dependent on the rainfall intensity and thus on ζ. The time to saturation depends on intensity in a particularly complex way because it may occur after some combination of climate limited infiltration (before ponding) and soil-limited infiltration (after ponding). If however, the assumption is (again) made that the storms that dominate the production of infiltration excess will have high rainfall intensity, then the actual infiltration rate will be mostly soil controlled. Under this condition the ponding time will be small and the limiting case time to column saturation (t_S^*) will be dependent only on the infiltration capacity and equilibrium unsaturated zone storage ($\forall_e$, Equation (4.23)), i.e.

$$\forall_e = \int_0^{t_s^*} f_i^*(t)dt \tag{5.16}$$

For the infiltration capacity given by Equation (5.9), this integral is readily solved and the solution inverted to give:

$$t_s^* = \left(\sqrt{\frac{S_i^2}{4A_o^2} + \frac{\forall_e}{A_o}} - \frac{S_i}{2A_o} \right)^2 \tag{5.17}$$

Note that in this high storm intensity, soil controlled limit, t_p may approach zero but t_s remains finite and approaches t_s^* (Equation (5.17)). In the limit then, t_s will be independent of intensity (and thus ζ) and will be much larger than t_p. For this case the inner integral of Equation (5.15) may be approximated by evaluating it with upper limit t_s^* and it may be taken outside of the outer integral, yielding:

$$\left\langle R_{ie,bounded} \right\rangle = \left(\frac{1}{\delta} \left(1 - e^{-\delta t_s^*} \right) - t_s^* e^{-\delta t_s^*} \right) \cdot e^{-\eta A_o} \int_0^\infty \zeta \eta e^{-\eta\zeta - \delta t_p} d\zeta \tag{5.18}$$

Note that for unbounded soils where t_s is infinite, the inner integral of Equation (5.15) is also independent of ζ and may be integrated out yielding:

$$\left\langle R_{ie,unbounded} \right\rangle = \frac{1}{\delta} e^{-\eta A_o} \int_0^\infty \zeta \eta e^{-\eta\zeta - \delta t_p} d\zeta \tag{5.19}$$

For this unbounded condition, *Eagleson* [1977 and 1978e] finds, after considerable mathematical manipulation, that the mean annual infiltration excess runoff ($\langle R_{ie_A} \rangle$) may be approximated by:

$$\left\langle R_{ie_{A,unbounded}} \right\rangle = \langle P_A \rangle exp\left(-\eta A_o - \left[\eta^2 \delta S_i^2\right]^{1/3}\right) \cdot$$
$$\Gamma\left(1+\frac{1}{2}\left[\eta^2 \delta S_i^2\right]^{1/3}\right) \cdot \left(\frac{1}{2}\left[\eta^2 \delta S_i^2\right]^{1/3}\right)^{-\frac{1}{2}\left[\eta^2 \delta S_i^2\right]^{1/3}} \quad (5.20)$$

where $\langle P_A \rangle$ is the mean annual precipitation. Comparing Equations (5.18) and (5.19), the mean annual infiltration excess runoff generation for bounded soils may then be approximated as:

$$\left\langle R_{ie_{A,bounded}} \right\rangle = \left\langle R_{ie_{A,unbounded}} \right\rangle \cdot \left(1 - e^{-\delta t_s^*}\left(1+\delta t_s^*\right)\right) \quad (5.21)$$

Note that in the limit of deep soils, the storage capacity ($\forall_e$) and thus time to column saturation (t_s^*) will become very large, and the factor multiplying the unbounded mean annual runoff will tend to unity. For very shallow soils $\forall_e$ and t_s^* become small, in which case the factor multiplying the unbounded runoff value tends to zero. In this case all runoff generation will be storage excess runoff, the subject of the following section.

As in the pervious section, all intermediate equations required to evaluate (5.17), (5.20) and (5.21) are repeated here:

$$S_i = \sqrt{2\chi K_s} \quad (5.22)$$

$$A_o = \left(\frac{2+\Gamma}{3}\right) K_s \quad (5.23)$$

$$\chi \equiv \frac{-n_e(1-s_*)\Psi_s}{K_s}\left(1+\frac{1}{2}(c-3)(1-s_*)\hat{s}^{\frac{c+1}{2}}\right) \quad (5.24)$$

$$\Gamma \equiv \frac{\phi\Psi_s/(1-s_*)}{\left(1+\frac{1}{2}(c-3)(1-s_*)\hat{s}^{\frac{c+1}{2}}\right)} \quad (5.25)$$

$$\forall_e = -n_e(1-s_*)Z_* + \frac{1}{2}n_e\phi Z_*^2 + \frac{1}{2}n_e\lambda(Z_w - Z_* - \Psi_s) \tag{5.26}$$

$$s_* \equiv \left(-\frac{q}{K_s} + \left(1 + \frac{q}{K_s}\right)\left(\frac{Z_w}{\Psi_s}\right)^{-mc} \right)^{1/c} \tag{5.27}$$

$$\lambda \equiv \frac{m(1+q')}{\Psi_s} \tag{5.28}$$

$$\phi \equiv \frac{m(1+q')\left(s_*^{1-c}\right)}{\Psi_s}\left(\frac{Z_w}{\Psi_s}\right)^{-mc-1} \tag{5.29}$$

$$Z_* \equiv \frac{(1-s_*) - \lambda(Z_w - \Psi_s)}{\lambda + \phi} \tag{5.30}$$

5.d Storage Excess Runoff

An important component of the hydrologic balance, especially in near channel areas of near surface water table, is runoff generated after the available unsaturated storage capacity of a soil has been filled. It is commonly accepted that this condition occurs due to a combination of two separate dynamic processes: 1) the soil may become saturated due to local infiltration (from "above") ; or 2) the soil may become saturated due to the lateral convergence of flow on sloped terrains. In this thesis, the saturated flow system is analyzed as a mean, equivalent steady-state system (see Section 1.b.2). Thus the latter effect is not dynamically accounted for *during* storms, even though lateral flow is allowed, in a steady state sense, and does redistribute water in the saturated zone.

Accounting only for the local infiltration mechanism, the quantity of excess generated for a storm of intensity i up to time t is simply $i^*(t-t_s)$. This generation is represented in Figure 5.1 by the shaded region. For exponentially distributed intensity and duration, the mean storage excess runoff per storm ($\langle R_{se} \rangle$) is:

$$\langle R_{se} \rangle = \int_0^\infty \eta e^{-\eta i} di \int_{t_s}^\infty i(\tau - t_s) \delta e^{-\delta \tau} d\tau \tag{5.31}$$

Changing variables and limits of integration, (5.31) may be simplified as:

$$\langle R_{se} \rangle = \int_0^\infty i \eta e^{-\eta i} e^{-\delta t_s} di \int_0^\infty \tau^* \delta e^{-\delta \tau^*} d\tau^* \tag{5.32}$$

where

$$\tau^* \equiv \tau - t_s \tag{5.33}$$

Integrating the inner integral of Equation (5.32) yields:

$$\langle R_{se} \rangle = \frac{1}{\delta} \int_0^\infty i \eta e^{-\eta i} e^{-\delta t_s} di \tag{5.34}$$

As mentioned in the previous section on infiltration excess, the time to saturation (t_s) depends on intensity in a complex way due to the possible switching of infiltration control from climate to soil. Because the focus of the previous section was infiltration excess (a soil-control phenomenon occurring mainly for high-intensity storms), the time to saturation was approximated under the assumption that the infiltration history up to column saturation was mainly soil-controlled. Here the focus is on storage excess generation, which may occur regardless of the soils infiltration capacity and storm intensity, so long as the total storm depth is large. Thus the integral of (5.34) is approximated under the assumption of no previous soil controlled infiltration, in which case the (climate limit) time to saturation (t_s^{**}) is simply:

$$t_s^{**} = \frac{\forall_e}{i} \tag{5.35}$$

Substituting this saturation time into Equation (5.34) and multiplying by the mean number of storms per year (m_v), the integral is readily evaluated [Equation 3.2.9.3 of *Gradshteyn*

and Rhyzik, 1980] to express the mean annual storage excess runoff ($\langle R_{se_A} \rangle$):

$$\left\langle R_{se_A} \right\rangle = 2m_v \forall_e K_2\left(2\sqrt{\forall_e \eta \delta}\right) \tag{5.36}$$

In Equation (5.36), $K_2(\cdot)$ is the Bessel function of the second type. For large depth to water table, the storage capacity ($\forall_e$), which appears linearly in Equation (5.36), is large. The function $K_2(\cdot)$, however, decreases with increasing argument more rapidly. Therefore the storage excess runoff monotonically decreases with increasing storage capacity, as one would expect. The necessary equations for evaluating the storage capacity ($\forall_e$) and thus the storage excess runoff have been repeated in the preceding section of this chapter (Equations (5.26) through (5.30)).

5.e The Equilibrium Water Balance in the Presence of a Water Table

Examination of the final equations for bare soil evaporation (Section 5.b), infiltration excess runoff (Section 5.c) and storage excess runoff (Section 5.d) reveals that the dependence of these surface fluxes on the moisture state of the soil is embodied in the steady flux rate q. As discussed in Chapter 2, setting this steady flux (q) equal to the long term mean flux through the soil column ($\langle q_A \rangle$) provides, by way of the equivalent steady profile, an estimate of the mean initial moisture profile. This mean initial condition profile in turn determines the magnitude of the infiltration capacity, exfiltration capacity, and storage capacity of the soil.

Closure of the long term mean water balance is found requiring long term stationarity of the mean moisture state. Assuming negligible lateral flow in the unsaturated zone and stationarity of mean moisture, the mean flow into the soil from the atmosphere (or out of the soil and into the atmosphere) must balance the mean flow out of the unsaturated zone and into the saturated zone (or into the unsaturated zone from the saturated zone). Emphasizing the dependence of the surface fluxes on the state variable $\langle q_A \rangle$, this condition may be written:

$$\begin{aligned}\langle q_A \rangle = -\Big\{ &\langle P_A \rangle - \left\langle E_{s_A}\left[\langle q_A \rangle; Z_w; climate; soil\right]\right\rangle - \\ &\left\langle R_{ie_A}\left[\langle q_A \rangle; Z_w; climate; soil\right]\right\rangle - \left\langle R_{se_A}\left[\langle q_A \rangle; Z_w; climate; soil\right]\right\rangle\Big\}\end{aligned} \tag{5.37}$$

This (implicit) mathematical statement of the mean annual water balance may be solved by simple root finding procedures (e.g. bisection).

Note that the state variable for this water balance equation is the mean recharge (or capillary rise) rate $\langle q_A \rangle$. Through Equation (4.21A) this rate represents the full soil moisture profile from the surface to the water table. Using the recharge (or capillary rise) rate as the state variable is unlike many water balance models which instead rely on the average soil moisture over some arbitrary depth of soil, e.g.

$$\bar{s} = \frac{1}{L}\int_0^L s(z)dz \tag{5.38}$$

One difficulty with models that depend on equations such as (5.38) is the determination of the appropriate averaging length (L).

To test this (water table dependent) equilibrium water balance model, a series of (approximately) twenty year numerical finite element simulations have been carried out. The simulation procedure is identical to that used for testing the unbounded model under various climate/soil combinations (i.e. the Chapter 3 simulations in which the numerical model is forced by a realization of the stochastic storm model). Here, however, the simulations are carried out for a range of water table depths and a single climate-soil pair.

The climate and soil parameters used in the test case are those used previously to represent clay soil and semi-humid climate. One technical limitation of the numerical finite-element model impairs the ability to compare the analytic equilibrium model as it is derived in this thesis to numerical simulations. The limitation is that the numerical finite element model is incapable of changing the head value of the bottom node (the water table) when the column saturates. Thus when an infiltration front reaches the lowest node and the column saturates, the numerical model predicts downward flow due to gravity at a rate equal to the saturated hydraulic conductivity. A more realistic handling of the numerical model's lower boundary conditions would allow pressure to transmit down through the saturated system, raising the head at the lowest node such that the column becomes hydrostatic. Under this condition, all rainfall applied to the surface would run off, instead of only that rainfall in excess of the saturated hydraulic conductivity.

Instead of attempting to re-program the finite element model used in this thesis [*Milly,*

1982], the analytic expression for storage excess runoff (Equation 5.36) is modified for this analytic vs. finite element simulation comparison (*and only for this comparison)* . The modification is simple: instead of expressing the storage excess runoff production in Equation (5.31) as $i*(t-t_s)$, it is expressed as $(i-K_s)*(t-t_s)$. The modified storage runoff integral becomes:

$$\left\langle R^*_{se_A} \right\rangle = \frac{m_v}{\delta} \int_{K_s}^{\infty} (i - K_s) \eta e^{-\eta i} e^{-\delta t_s} di \qquad (5.39)$$

Unlike the original integral, the modified integral must be evaluated numerically (e.g. by trapezoidal rule integration or quadratures).

While it is not totally satisfactory to test the analytic model under these modified (and unrealistic) conditions, the comparison should suffice because: 1) it still tests the critical assumption that the equivalent steady soil moisture profile may be used as a surrogate for initializing flux capacities; and 2) the modification presents no significant change to the form of the model. The major difference in results due to the storage excess modification used in this comparison is that the unmodified model yields one-hundred percent runoff for water table depths less than the bubbling pressure head. In the modified case the runoff asymptotes to some fraction of the precipitation, as a large portion of post column saturation precipitation is allowed to infiltrate at the saturated hydraulic conductivity.

The results of the comparison are illustrated in Figure 5.2. The analytic equilibrium model estimated fluxes (solid lines) are in remarkably good agreement with the simulated mean fluxes (open circles). The ability of such a simple model to capture the response of such varied physical processes as infiltration, exfiltration and redistribution to such a rich, structured and multi-scaled atmospheric forcing sequence is truly significant. Note again that this is a relatively simple analytic model: it uses a simple equivalent steady parameterization of the complex dynamic soil moisture processes and it uses time compression to approximate the partitioning of atmospheric forcing under a combination of soil- and climate-limited conditions. While this sort of model test is no surrogate for field testing, it is nonetheless useful. This test implies that for the purpose of studying the long term mean of hydrologic fluxes at the point scale, the (simple) analytic equilibrium model may serve as a surrogate for complex finite element simulation of Richard's equation. This test does not imply, on the other hand, that a sufficient simulation of hydrology consists of

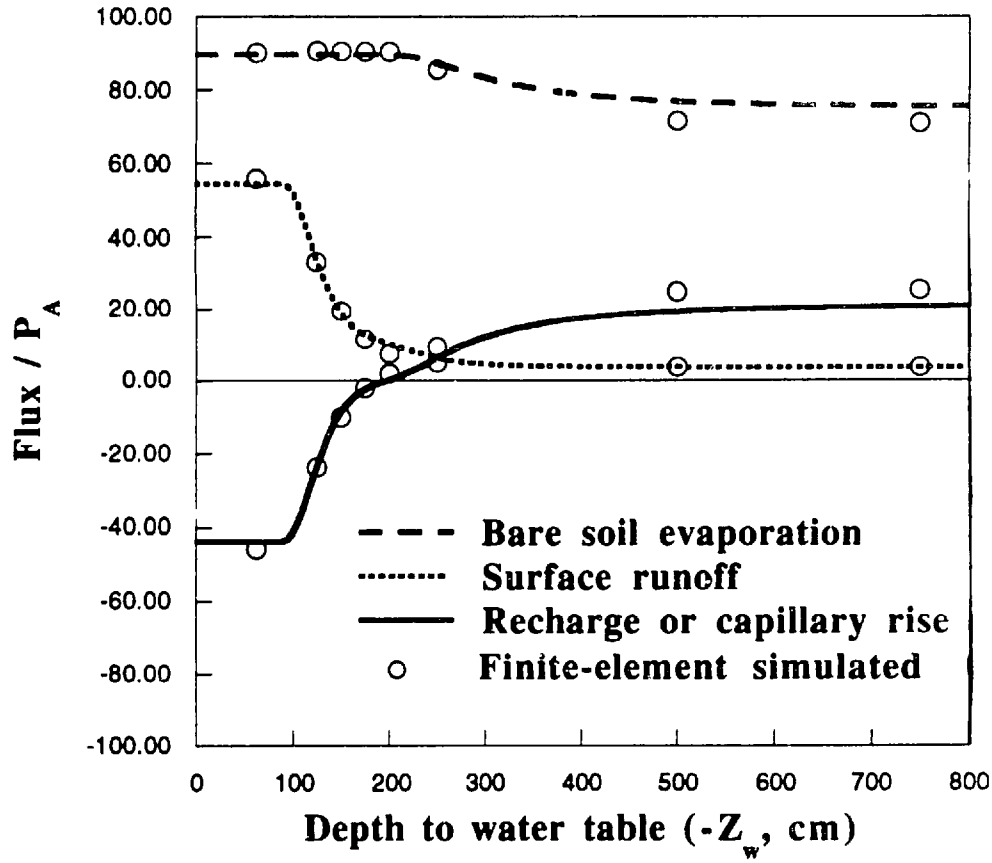

Figure 5.2 Comparison of mean finite-element simulated (circles) and analytic equilibrium estimated (lines) hydrologic fluxes for a range of depths to water table

applying Richard's equation as it is here: i.e. to homogeneous soils described by *Brooks and Corey* 's [1966] non-hysteritic model of moisture retention and conductivity. Heterogeneities in soil hydraulic properties, preferential flowpaths, and other complications are often present.

Also note that in Figure 5.2, for large depth to water table, the sensitivity of all hydrologic fluxes to the water table depth disappears. With respect to the surface forcing, the system is semi-infinite (unbounded). For moderate depths there is a very strong water table influence. As anticipated, the surface runoff production increases and the evaporation becomes more climate controlled with decreasing depth to water table. Note especially that for deep water tables the surface runoff is small and the evaporation is under considerable soil control, yielding net recharge to the saturated zone. Conversely for shallow water table, most of the rainfall becomes runoff and the evaporation is at potential, creating a situation in which the evaporated unsaturated zone losses are replenished by a net flux of water form the saturated zone into the unsaturated zone (a capillary rise flux). The ability of the equilibrium model to capture this propensity for the unsaturated zone to act as a source or sink depending on the water table depth is the exact criteria required to create the type of hillslope circulation found in the field studies described in the introduction of this thesis (Chapter 1).

5.f Summary

The previously derived enhanced process models which describe steady flow, infiltration capacity, storage capacity and exfiltration capacity are used to derive the expected value of the long term water balance components subject to intermittent precipitation events. Randomness at the "weather" time scale is incorporated in the mean value analysis by integrating the event fluxes over probability distributions of storm intensity, duration and intermittency. The approach follows the methodology of *Eagleson* [1978d,e] and, with the exception of the derived expression for storage excess runoff, leads to simple analytic modifications of the expressions derived in that work. Here the additional presence of a water table results in the mean fluxes being dependent not just on a (scalar) value of soil moisture, but on the whole equivalent steady moisture profile. This profile is characterized by the water table depth, Z_w, and the mean column flow $\langle q \rangle$. Taking the water table depth as a fixed parameter, the state variable is $\langle q \rangle$. Thus instead

of solving for the equilibrium moisture content (s_o), the long term mean water balance condition is solved by finding the mean unsaturated zone flux <q> which may , depending on the water table depth, represent long term mean recharge (percolation) or discharge (capillary rise).

Chapter 6: The Spatial Structure of Surface Hydrologic Fluxes under the Influence of Saturated-Unsaturated Zone Coupling, Climate Forcing and Geological Constraints

6.a Background

In the previous chapter the water table dependent hydrologic process models developed in this thesis are incorporated into an analytic model of equilibrium water balance. The model expresses the long-term mean infiltration, bare soil evaporation, storage- and infiltration-excess runoff, and recharge to or capillary rise from the saturated zone. The model represents a one-dimensional column of soil bounded by a water table at arbitrary depth. Allowing the position of the water table to influence and be influenced by the flows within the unsaturated and saturated zones opens the possibility to couple saturated and unsaturated flow systems over sloped terrains (at the climatic time scale) in a simple and efficient way. Full numerical modeling of the coupled system, while introduced as early as the 1970's (e.g. *Freeze* [1971]), remains very complex and computer intensive. In fact many of the programs described in a recent survey of available "off the shelf" programs (*Van der Heijde and Elnawawy* [1993]), contain numerous caveats as to the applicability of the models, particularly for the unsaturated zone. Part of the problem is that to capture infiltration fronts reliably, very fine resolution is required near the soil surface (on the order of centimeters).

In this chapter a preliminary example of a potential use of this statistical-dynamical approach is described. An attempt is made to recreate some of the observed characteristic spatial features of hillslope hydrologic fluxes. The relatively large lateral conductivity of saturated soils (in comparison with unsaturated soils) provides the ability and the teleconnection to redistribute the unsaturated zone fluxes over complex terrains. At equilibrium, in which the water table is positioned such that there is a statistical steady state between the recharge/discharge from the unsaturated zone and the divergence of flow in the saturated zone, familiar spatial patterns and circulations emerge. Depending on the particular climate, soil and geologic representation, distinct areas dominated by percolation and soil-limited evaporation (near the hillslope divide), discharge and runoff production (near the stream/valley), and midline (areas with little to no recharge) are identified.

As is discussed in the survey of related research (in Chapter 1), a similar equilibrium of

saturated and unsaturated flow systems has been analyzed by *Miller and Eagleson* [1982]. The research reported in this thesis and most especially in this chapter represents an important extension of that work. The differences include the following: 1) the unsaturated zone flow in *Miller and Eagleson* [1982] is modeled after *Eagleson* [1978a-g] without the modifications incorporated here, the most quantitatively significant of which is the inclusion of storage excess runoff calculated by way of the equivalent steady profile; 2) the systems analyzed in *Miller and Eagleson* [1982] are at a larger scale and do not include topographical variation or the effects of topographically driven convergence and divergence; 3) the analysis here focuses on both the spatial structure and area average fluxes while for the analysis of *Miller and Eagleson* [1982], the focus is mainly on the area averaged water balance; and 4) in this thesis the equivalent steady moisture profile is identified as the critical teleconnection between the saturated and unsaturated system, is analytically related to the mean moisture profile, and is approximated by a simple power function (Equation 4.21A).

In the final section of this chapter, a parallel analysis of the coupled system is carried out which leads to a simple index for identifying the dominance of geological, climatic or soil controls on the spatial average and spatial patterns of the hydrologic fluxes. In addition some preliminary comments are made on the implications of both the full model and the derived index to such topics as the areal scaling and the relation of geomorphology to hydrology.

6.b Coupling the Saturated and Unsaturated Zones

Flow in saturated zone is assumed to obey the Darcy law:

$$\vec{q} = -K_s \nabla \Phi \tag{6.1}$$

where Φ is the total head and K_S is saturated hydraulic conductivity (here assumed isotropic and homogeneous). For this type of gradient flow system, the steady state head distribution is determined by substituting (6.1) into a mass conservation statement, which implies that the Laplacian of the head must be zero:

$$\nabla^2 \Phi = 0 \tag{6.2}$$

With the head field determined, the associated flow field is found by application of Equations (6.1). There are numerous methods available to solve Equation (6.2), for example finite-element, finite-difference, relaxation, over-relaxation, electric analog and graphical techniques. Many of these are reviewed by *Bear* [1988]. For all methods, solution of (6.2) requires specification of the boundary conditions over the saturated flow domain.

The analysis in this chapter focuses on three types of idealized hillslopes. The most simple is illustrated in Figure 6.1. It consists of a parallelogram of soil underlain by impermeable bedrock. The soil depth (H) is constant throughout, as is the slope angle (θ). The overall hillslope length is denoted L. This hillslope is assumed to form half of a symmetrical valley, such that the lower vertical boundary (A-A' in Figure 6.1) may be taken as a no flow boundary. The higher vertical boundary (C-C') occurs at the hillslope divide, and thus also represents a no flow boundary, as does the (assumed impermeable) bedrock (D-D'). The hillslope shown in Figure 6.1 also contains a water table (dashed line). Note that the seepage face is included near the channel where the water table coincides with the ground surface. It is assumed in this analysis that all surface runoff and the discharge occurring through the seepage face is removed by the channel network and that there is no significant depth of water maintained over the base of the hillslope.

Strictly defined, the water table is the locus of points at which the pressure head is equal to zero such that the total potential (Φ) is equal to the elevation. For soils which create a tension saturated zone, it is useful to redefine the water table to include this part of the saturated zone, as the hydraulic conductivity in this zone is saturated and thus capable of transmitting significant flow (these issues are discussed by *Freeze and Cherry* [1979, p. 44] and *Freeze* [1969]). With this modification, the water table, which forms the mathematical upper boundary to the saturated flow domain, is defined such that the head (Φ) boundary condition is equal to the water table elevation minus the bubbling pressure head. Note that this boundary, being governed by a "concentration" condition, allows vertical flow to pass through it. The vertical flow that passes through it (the percolation or capillary rise) is determined by application of Equation (6.1) at the water table location.

The numerical method chosen to solve Equation (6.1) is simple successive over-relaxation over a discretized grid with all derivatives evaluated by finite difference (see *Bear*

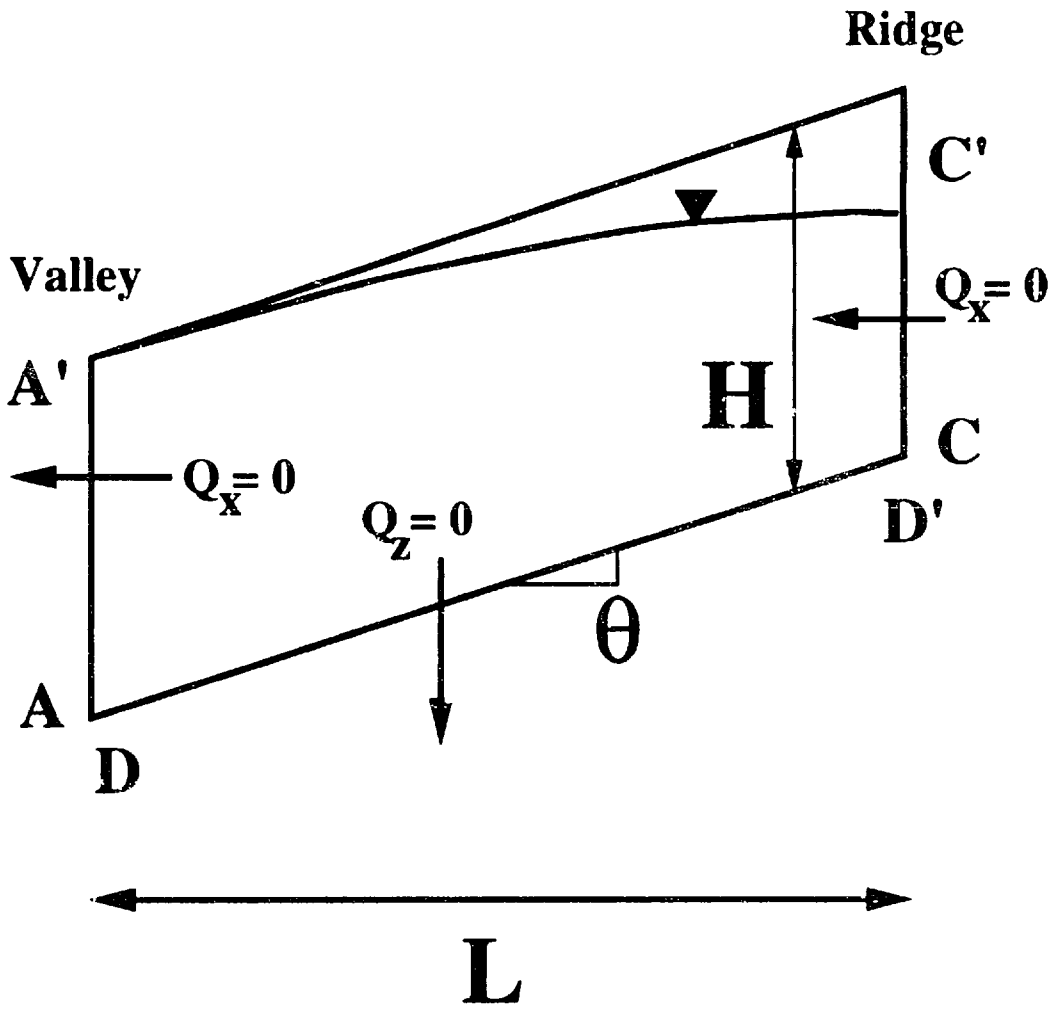

Figure 6.1 Definition sketch of simple planar hillslope for analysis of coupled saturated-unsaturated flow analysis

[1988], pp. 345-346).

Thus mathematical evaluation of the two separate flow systems is rather simple. For each position along the hillslope the unsaturated (vertical) mean flow ($<q_A>$) is found, for a given climate, soil and depth from surface to water table, using Equation (5.37). The saturated flow field is found, for a given spatial distribution of the water table depth (e.g. $Z_w(x)$), by simple over-relaxation methods. The key to finding the equilibrium solution to the *coupled* system is to find the spatial distribution of the water table for which the vertical flow through the boundary of the two systems (the water table) are equal. As discussed in the introduction (Section 1.b.2) this water table distribution may be considered as the equivalent steady water table, i.e. it is the water table for which the *mean* fluxes of the saturated and unsaturated system are in a steady-state equilibrium.

In Chapter 2 the rational for defining and using an equivalent steady moisture profile, and the errors it introduces, were discussed. A similar exploration of the relation between the mean of the dynamically varying water table and the equivalent steady state water table is planned for future research. The perturbation methods used in Chapter 2 could be applied to the analysis. At this point, note that despite the linearity of the equation governing saturated flow (6.1), the water table represents a nonlinear boundary condition. It is therefore expected that, similar to the moisture profile analysis, covariance terms will exist which introduce bias between the mean and equivalent steady water table positions.

As mentioned previously, there are two other hillslope types considered. They are illustrated in Figure 6.2. The upper hillslope is meant to characterize, in the simplest way, a converging hillslope (e.g. converging toward a channel head), and the lower a diverging hillslope (e.g. diverging from a highland into a valley). These types of terrain are also often termed spurs and hollows. The methods used to analyze these are essentially similar to the planar hillslope (Figure 6.1) in that the vector equations are identical (Equations (6.1) and (6.2)). The only differences are that cylindrical coordinates are used in their numerical evaluation and that the vertical fluxes (both saturated and unsaturated) must be weighted by the planar surface area through which they flow. One additional parameter is required to define the domain for these cases, the convergence ratio (R_c) which is defined as the ratio of the contour length at the divide to that at the channel. As illustrated in the Figure (6.2), the ratio is greater than one for converging hillslopes and less than one for diverging hillslopes.

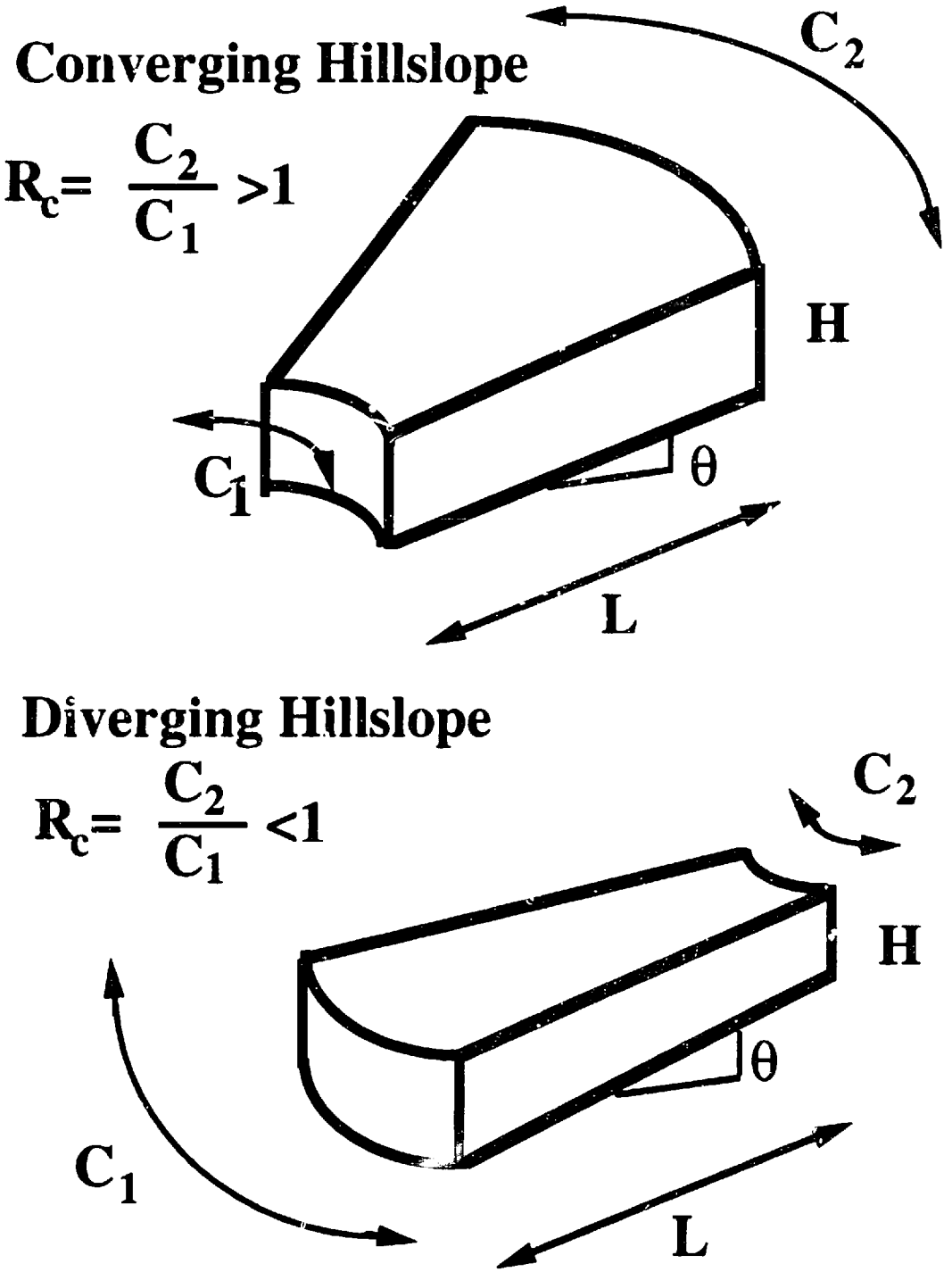

Figure 6.2 Definition sketch of simple converging and diverging hillslopes for coupled saturated-unsaturated flow analysis

6.c Case Studies and Field Evidence

Seven case studies have been solved for the purpose of analyzing the ability of the coupled model to reproduce observed spatial hydrologic response characteristics. The case studies consist of a base case which uses a certain climate-soil-geology set of parameters and six cases in which some of these parameters are varied. The studies illustrate the sensitivity of the system to variations in the hydrologeologic, climatic and geomorphologic parameters.

A summary of the input parameters required by the model is shown in Figure 6.3. In review they are the following: for climate, the potential evaporation (e_p), the inverse of the mean time between storms (β), the inverse of the mean storm duration (δ), and the inverse of the mean storm intensity (α); for soil, the saturated hydraulic conductivity (K_s), the bubbling pressure head (Ψ_s), the pore size distribution index (m), and the effective porosity (n_e); for geology, the overall soil depth to bedrock (H), the overall hillslope angle (θ), and the length of the hillslope (L). In the case studies, the soil and climate parameters are chosen according to the same named groupings as are used throughout this thesis (for values, see Tables 3.1 and 3.2).

6.c.1 Equilibrium Coupled Saturated-Unsaturated Flow on Inclined Surfaces

The base case consists of a silt soil, semi-humid climate, ten percent hillslope angle, two meter soil depth, and seventy-five meter hillslope length. Sensitivity of the point equilibrium water balance, for this climate and soil, to depth to the water table (from Equation (5.37)) is illustrated in Figure 6.4. Note that there is a strong dependence of the equilibrium partitioning to water table depth down to approximately one and one-half meters, and that for depths greater than approximately one meter, there is strong soil control on the evaporation (dashed line). For water tables at depths of more than two meters below the surface, the system is effectively semi-infinite. As will be seen shortly, this characteristic reduces the two-way coupling between the saturated and unsaturated zones to one way coupling (i.e. changes of water table elevation effect the saturated flow system but not the recharge). For surface runoff (dotted line) there is no soil control until the water table is less than about one meter. Most importantly, note that the net flux

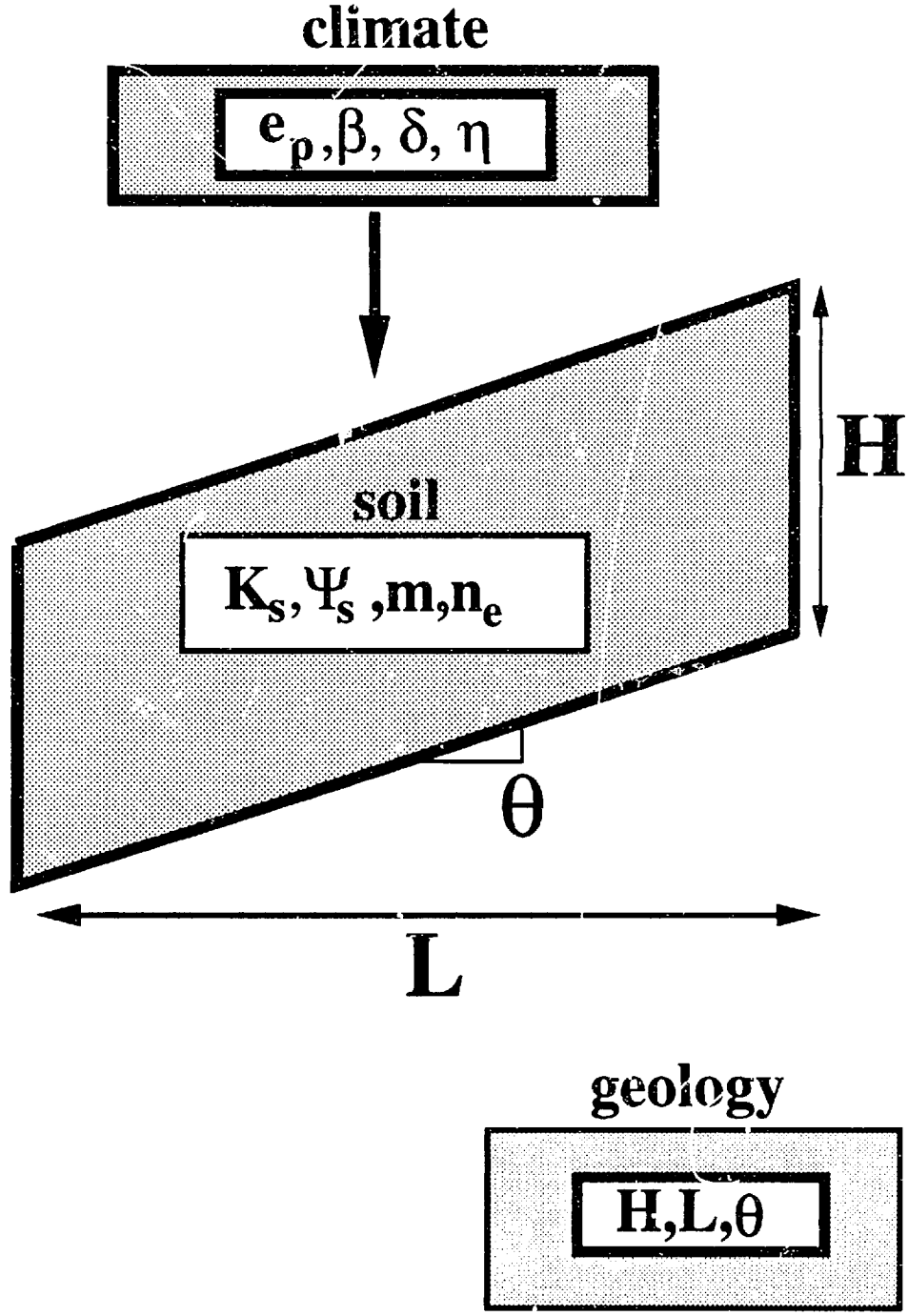

Figure 6.3 Schematic showing required climate, soil and geology parameters

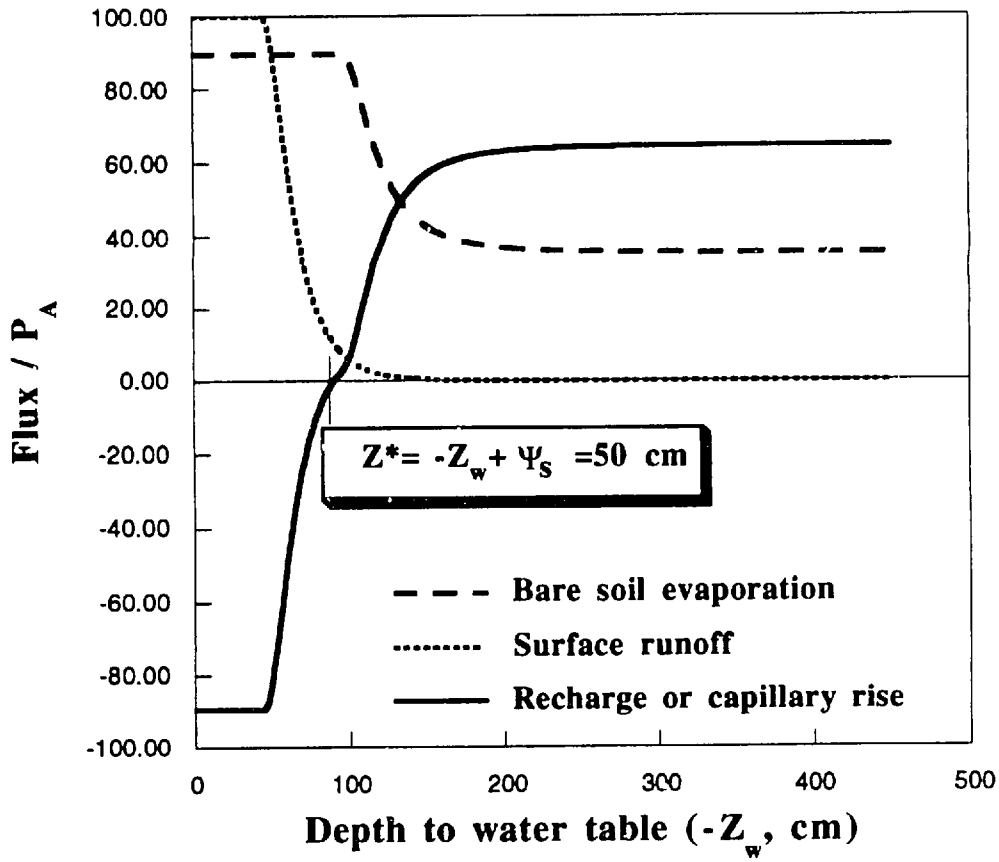

Figure 6.4 Sensitivity of point equilibrium water balance to distance to water table for silt soil and semi-humid climate

between the unsaturated and saturated zone ($<q_A>$, solid line) switches from recharge to capillary rise for a distance to the saturated zone ($-Z_w + \Psi_s$) of about fifty centimeters. This depth is labeled Z* for future reference.

The hillslope circulation which results when the profile unsaturated zone is allowed to equilibrate with the saturated zone is illustrated by the series of panels in Figure 6.5. The top panel shows the magnitude of the surface hydrologic fluxes of storage excess runoff (solid line), bare soil evaporation (dashed line), and infiltration excess runoff (dotted line, though there is none in this case) along the hillslope. All fluxes are normalized by the mean annual precipitation. The next panel shows a plot of the net recharge or capillary rise, also normalized by $<P_A>$, between the saturated and unsaturated zone. The third panel shows the hillslope, the equilibrium water table (dotted line), stream lines of flow and contours of head (solid lines). Finally, the stacked bar graph shows the water balance partitioning of precipitation, averaged over the hillslope for this climate.

Note that for this base case the hillslope organizes itself into three distinct regions which together define a hillslope circulation. Near the divide (extending downslope about fifteen meters), there is a recharge zone. Here the water table is relatively deep (a requirement if the unsaturated zone-atmosphere interaction is to allow recharge, see Figure 6.4) and the saturated zone flow lines have a strong downward component to them. In this region, the evaporation (top graph, dashed lines) is under considerable soil control (i.e., the mean evaporation rate is approximately forty percent of the precipitation, while the potential evaporation rate is about ninety percent of precipitation). Also note that the saturated and unsaturated zones are just about decoupled near the divide. This can be inferred from the observation that the recharge (solid line, second graph down) and evaporation have reached asymptotic values, while the water table depth (dotted line, third graph down) is located further and further from the surface when moving in the direction of the divide.

The recharge is laterally redistributed downslope through a midline area which begins at approximately sixty meters and ends at twenty meters. Throughout this region, water table closely follows (and is almost parallel to) the surface at a depth for which the mean recharge is zero (Z* is approximately fifty centimeters, see Figure 6.4). The fact that the net recharge along this region is approximately zero should not be interpreted to mean that this zone is hydrologically inactive. Throughout there is considerable infiltration, evaporation and surface runoff being generated, but over the long term mean these fluxes

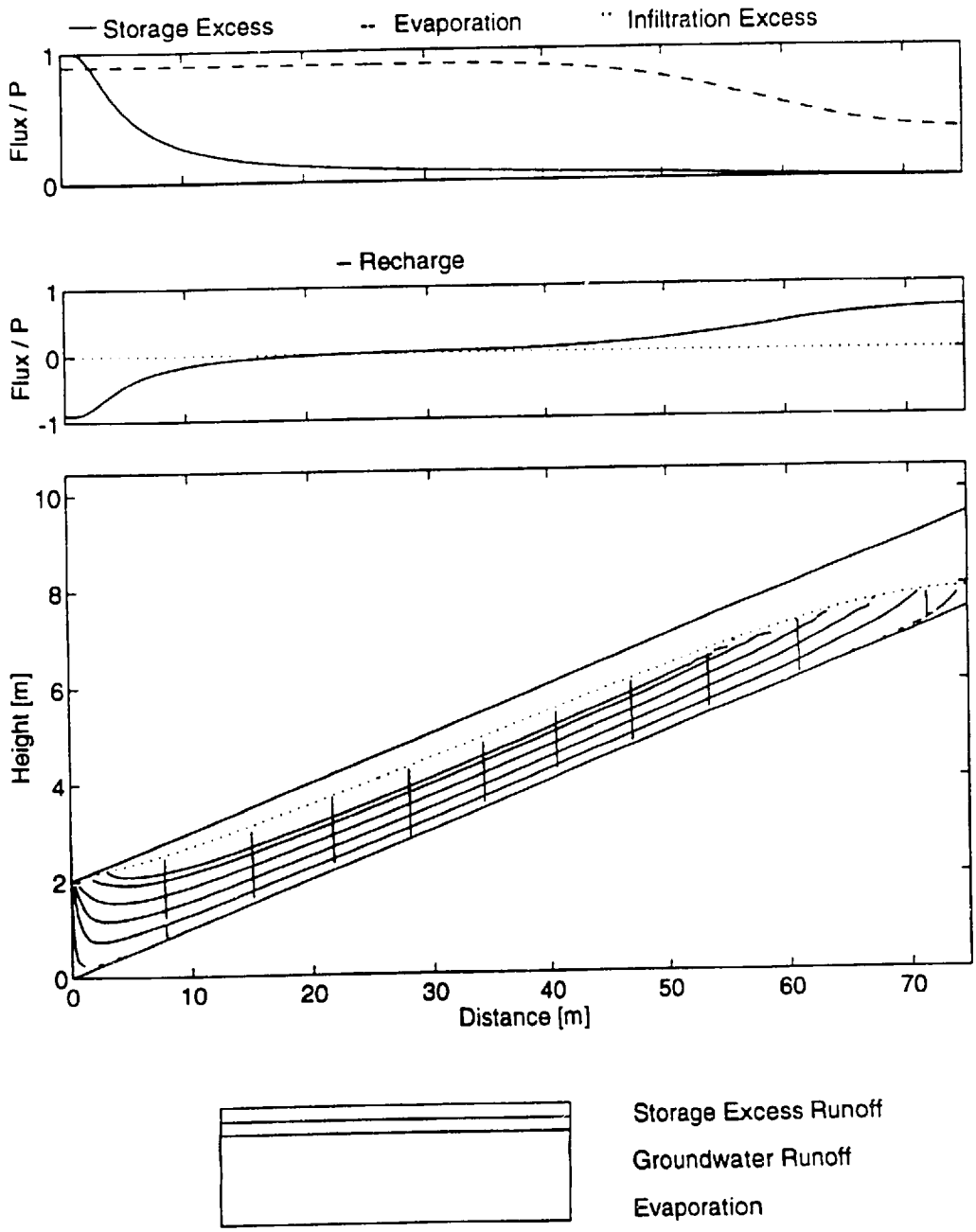

Figure 6.5 Modeled equilibrium hillslope fluxes: Base case

balance and the net exchange between the saturated and unsaturated zones is zero. This midline zone is the result of a limited effective transmissivity which itself results from the interaction of climate, soil and geologic boundaries by way of hillslope saturated-unsaturated zone coupling. The potential soil transmissivity, K_S*H, is reduced by the critical zero-recharge depth-to-saturated zone (Z^*) to $K_S*(H-Z^*)$, while the maximum water table gradient is bounded by hillslope angle. These concepts are analyzed more rigorously and developed into an index of hydrologic control in the following section.

These flow conditions in the midline act to restrict the extent and strength of the recharge area, i.e. the midline grows uphill until the net recharge is no more than the midline is able to transmit within the saturated zone. Over this midline the surface hydrology is relatively constant and is set by the partitioning that occurs for zero recharge, i.e. any rainfall in excess of the soil storage capacity given the depth Z^* is forced to become runoff, while at the same time the depth Z^* is that for which the mean stored water (infiltration) may be, in the mean, evaporated.

The final hydrologically distinct region along this hillslope is the first ten to twenty meters near the channel. Here the water table gets close to the surface, inducing significant surface runoff and climate limited evaporation (i.e. potential evaporation). As discussed previously, this leads to a condition of net evaporation from the water table (capillary rise). Again, this is due to the fact that there is so little storage capacity in the moist near-channel soils that little water infiltrates during storms, but large amounts of water evaporate during interstorms. It is very interesting that a significant portion of the water recharged uphill is lost to evaporation in this region *before* it ever reaches the channel and becomes streamflow.

For this base case, an (equilibrium) seepage face develops at approximately one meter from the valley bottom. Over this region considerable saturated flow is directly discharged to the surface. Over this length, there is no unsaturated zone, and thus no pointwise equilibrium water balance. The only constraint on this zone is that the total vertical discharge through this seepage face (which is taken to represent baseflow even though a "standing" stream is not allowed to develop) be equal to the net recharge of the hillslope. This is not a prescribed boundary condition. The location of this equilibrium seepage face is determined in conjunction with the equilibrium water table. Experience thus far indicates that there is always only one equilibrium water table and associated seepage face for which the whole system is in equilibrium.

Note that the seepage face shown as part of the equilibrium hillslope does not imply that the seepage face never dynamically grows (as with partial area runoff production). In fact for every place along the hillslope where there is storage excess runoff (dominant in the first ten or so meters from the channel in this case; see top panel in Figure 6.5), the surface saturates for some fraction of storm durations. The equilibrium seepage face and water table, like the equivalent steady moisture profile, are indicative of the mean initial condition before a storm occurs, not the water table distribution during a particular runoff event. One planned extension of this research (discussed in Chapter 7) is to derive the probability distribution of the seepage face extending to various lengths up the hillslope.

The final panel in Figure 6.5 shows the partitioning of precipitation as averaged over the hillslope (but excluding the seepage face). For this particular case, most of the precipitation is evaporated and the remainder (the yield) is approximately evenly split between base flow contributions and surface runoff. The saturated flow through the seepage face is the groundwater contribution to baseflow.

A critical facet of this research can be understood by comparing this result with the equilibrium water balance calculation computed in Chapter 3 under assumptions of infinite water table depth (no saturated-unsaturated coupling). As illustrated by Figure 3.2, the silt soil, semihumid water balance for deep water table shows no surface runoff and twice as much recharge as evaporation, values not at all representative of the case analyzed here. This simple comparison illustrates the strong influence of these saturated-unsaturated interactions.

6.c.2 Influence of Hydrogeologic and Climatic Factors on Hillslope Hydrologic Fluxes

To further illustrate the mechanisms through which climatic, soil and geologic conditions affect the hillslope hydrologic cycle, various parameters may be varied, alone or in combination with others, and the results analyzed. The next series of graphs illustrate the role of the key geologic parameters.

In Figure 6.6 the overall soil depth (H) is decreased to one meter, half of the base case. All other parameters are identical to the base case. The most notable effect is that the midline area has grown significantly. As discussed previously, the midline tends to grow at the expense of the recharge area until the net recharge can be transmitted under the midline. As the critical zero recharge depth Z^* is determined solely by climate-soil

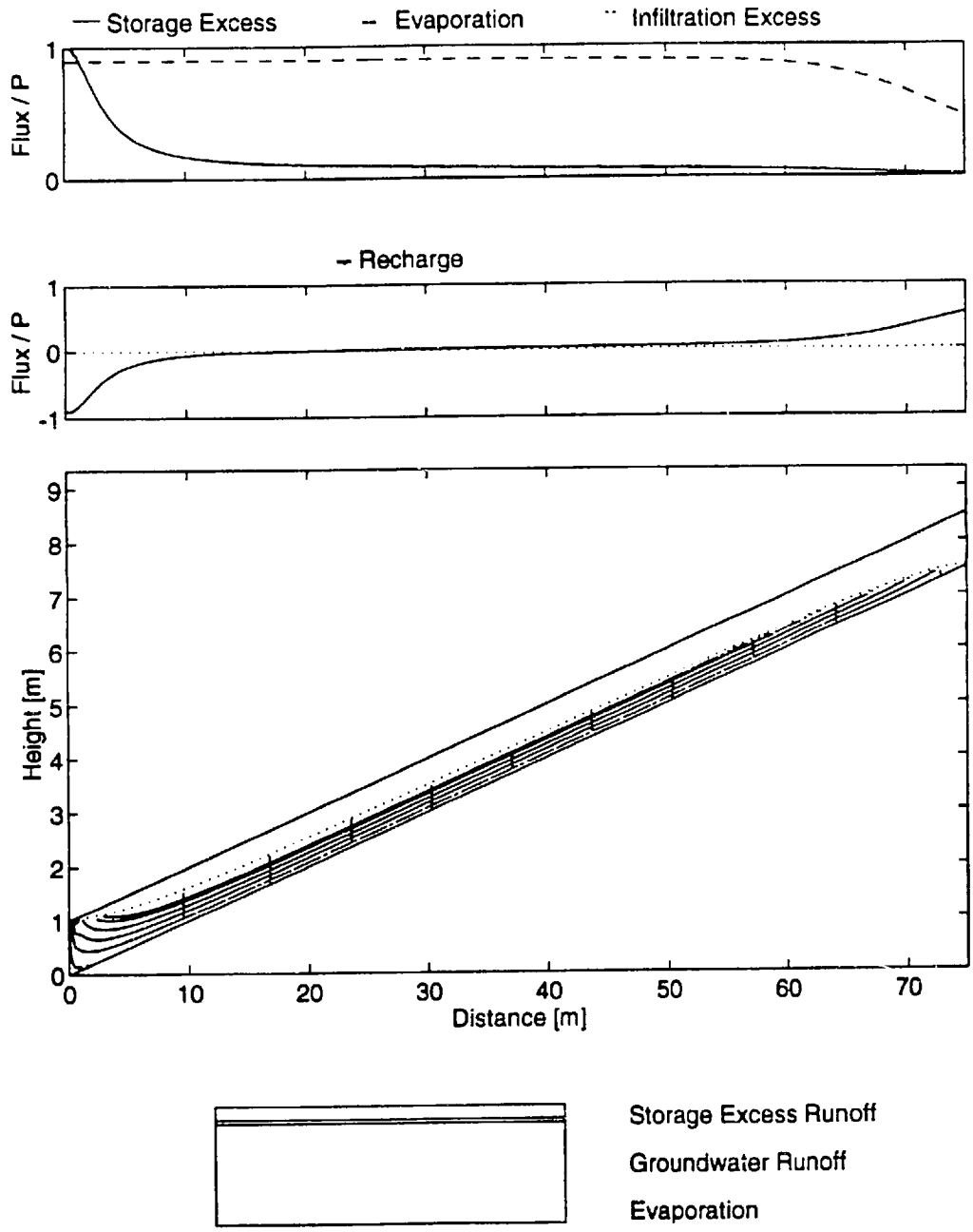

Figure 6.6 Modeled equilibrium hillslope fluxes: Effect of reduced soil depth

interaction (i.e. by solution of Equation (5.37)), the reduction of overall depth of soil reduces the effective transmissivity of the midline (e.g. from K_S*(200 cm - 50 cm) to K_S*(100 cm - 50 cm)). Note that in this case the saturated and unsaturated zones do not decouple, as they do near the divide in the base case. Most importantly, note in the bar graph (Figure 6.6) that the reduction of soil depth has led to much less baseflow ("groundwater runoff") and that this reduction has come at the expense of the evaporation, which has increased significantly. Also note that even for this one meter deep case there is still a very small saturated zone near the divide. This is partly an artifact of the neglect of lateral unsaturated flow, i.e. even close to the divide where recharge has accumulated for small horizontal distances, the only way to laterally redistribute this recharge is through the saturated zone.

In Figure 6.7 the base case is altered by increasing the soil depth (H) to five meters, over twice the base case. The effects are dramatic. The midline has all but disappeared. The transition from recharge area to discharge area has collapsed almost to a point, a location which the hydrogeological literature refers to as a "hinge point". The mechanism which causes the midline to collapse is exactly the same one that causes it to grow in the one meter case: a balance between the extent of the recharge area and the ability to transmit this recharge laterally. In this case the transmissivity is so high that the recharge area extends almost all the way down to the valley.

For this high-transmissivity case the saturated-unsaturated systems near the divide are fully decoupled and the recharge to the groundwater table occurs at the maximum rate allowed by the climate-soil interactions. The saturated zone adjusts itself to discharge the cumulative recharge from above and upslope, but does not influence the magnitude of the recharge. The region over which this decoupling occurs has water table-to-surface distances in excess of approximately one meter, consistent with the point water balance sensitivity illustrated in Figure 6.4. Also note the larger extent over which the bare soil evaporation is under soil control. The overall effect of this (soil depth induced) high transmissivity hillslope is that the water table can be positioned, on the spatial average, further from the surface. For deeper average water table, more of the interstorm evaporation events are governed by the soil-limited regime, thus limiting evaporation and (indirectly) increasing recharge. This effect is clearly seen in the spatial average water balance depicted in the stacked bar graph panel. The groundwater runoff has almost doubled, almost entirely at the expense of evaporation. Note that this case has partitioning

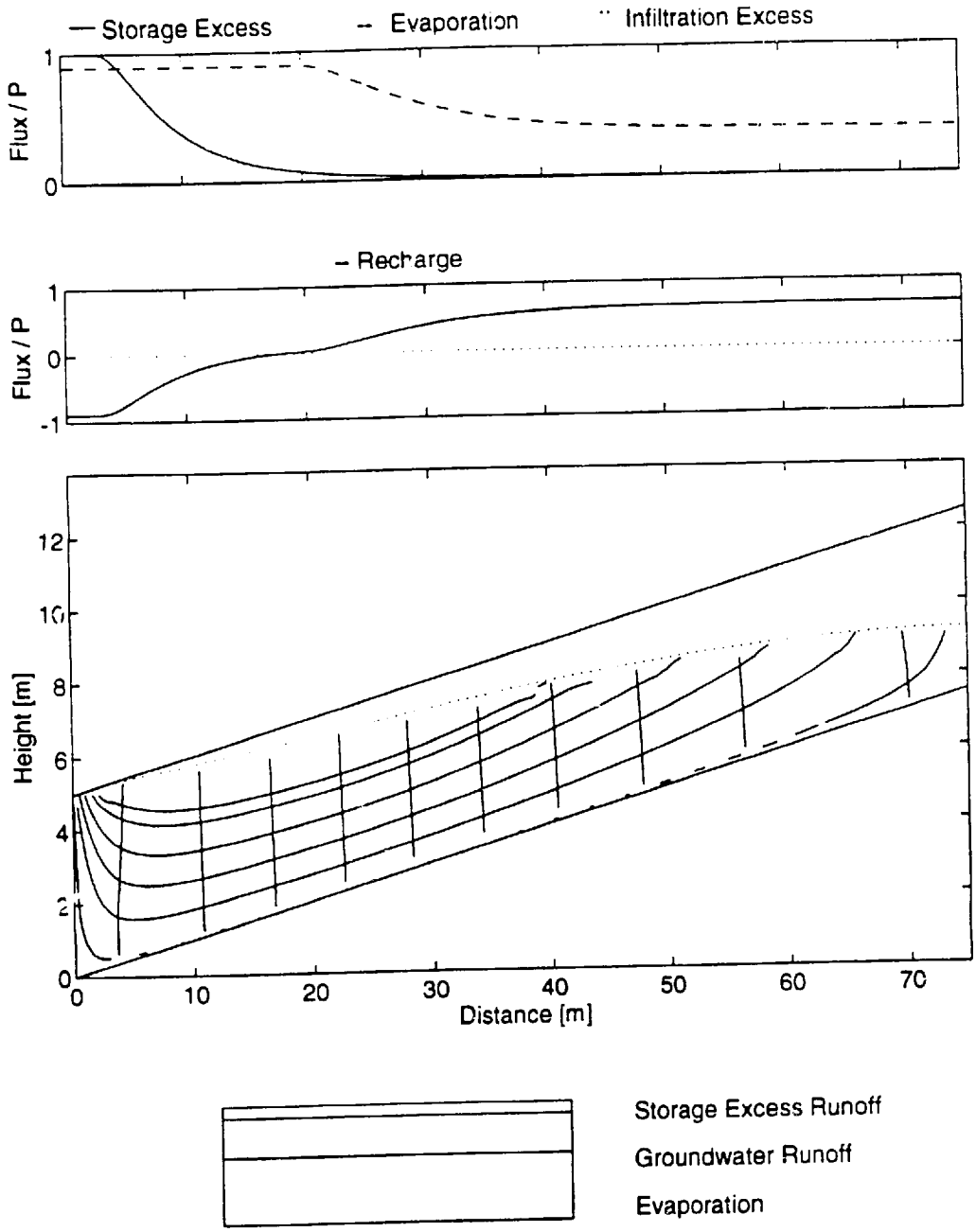

Figure 6.7 Modeled equilibrium hillslope fluxes: Effect of increased soil depth

much closer to the simple semi-infinite point balance reported in Chapter 3 (Figure 3.2).

The surface values of the equilibrium (equivalent steady) soil moisture profile associated with the water balance at each location along the hillslope is not plotted in the figures. The qualitative moisture distribution, however, roughly follows the bare soil evaporation. Thus for the five meter soil case (Figure 6.7), the surface equilibrium soil moisture (which by the analysis of Chapter 2 can be presumed representative of the temporal mean moisture), is constant over much of the hillslope, and then increases rapidly near the channel.

In Figure 6.8 the hillslope length is increased to two-hundred and fifty meters (L over twice the base case). As expected from the previous discussion, the midline extends over most of the hillslope. The extent of the recharge area at the divide is not dependent, in this limit, on the length of the hillslope. It is only dependent on the transmissivity of the hillslope. In this limit the area averaged groundwater component of the water balance scales inversely with length, as can be seen by comparing the stacked bar panels of Figures 6.8 and 6.5.

In the next figure (6.9) the average slope of the hillslope is reduced to five percent. This is seen to have roughly the same effect as decreasing the soil depth (i.e. increased midline, decreased groundwater runoff), but for a different reason. Here the transmissivity under the midline is the same, but the maximum hydraulic gradient of the water table has been greatly reduced. Again the effect is that the midline advances up the hill to reduce the net recharge to an amount which can be laterally drained.

The effect of doubling the hillslope angle (to twenty percent) is shown in Figure 6.10. Now the ability of the saturated zone to transmit water laterally has been greatly increased. The water table can thus reside lower, which increases recharge from the unsaturated zone. When the water table is lower the transmissivity is reduced, but large hydraulic gradients have "room" to develop and compensate for the lost transmissivity. Again the result is that the total area average groundwater runoff has dramatically increased.

The role of climate is explored in Figure 6.11. Here the same soil and geologic description are used as in the base case, but the climate forcing is characteristic of humid regions. This climate, with lower ratio of potential evaporation to precipitation, causes more of the interplay to occur between recharge and surface runoff. For example, with the bare soil evaporation relatively fixed at its potential rate over the hillslope, and the ability to transmit water laterally roughly the same (not exactly because Z^* is different for the silt-

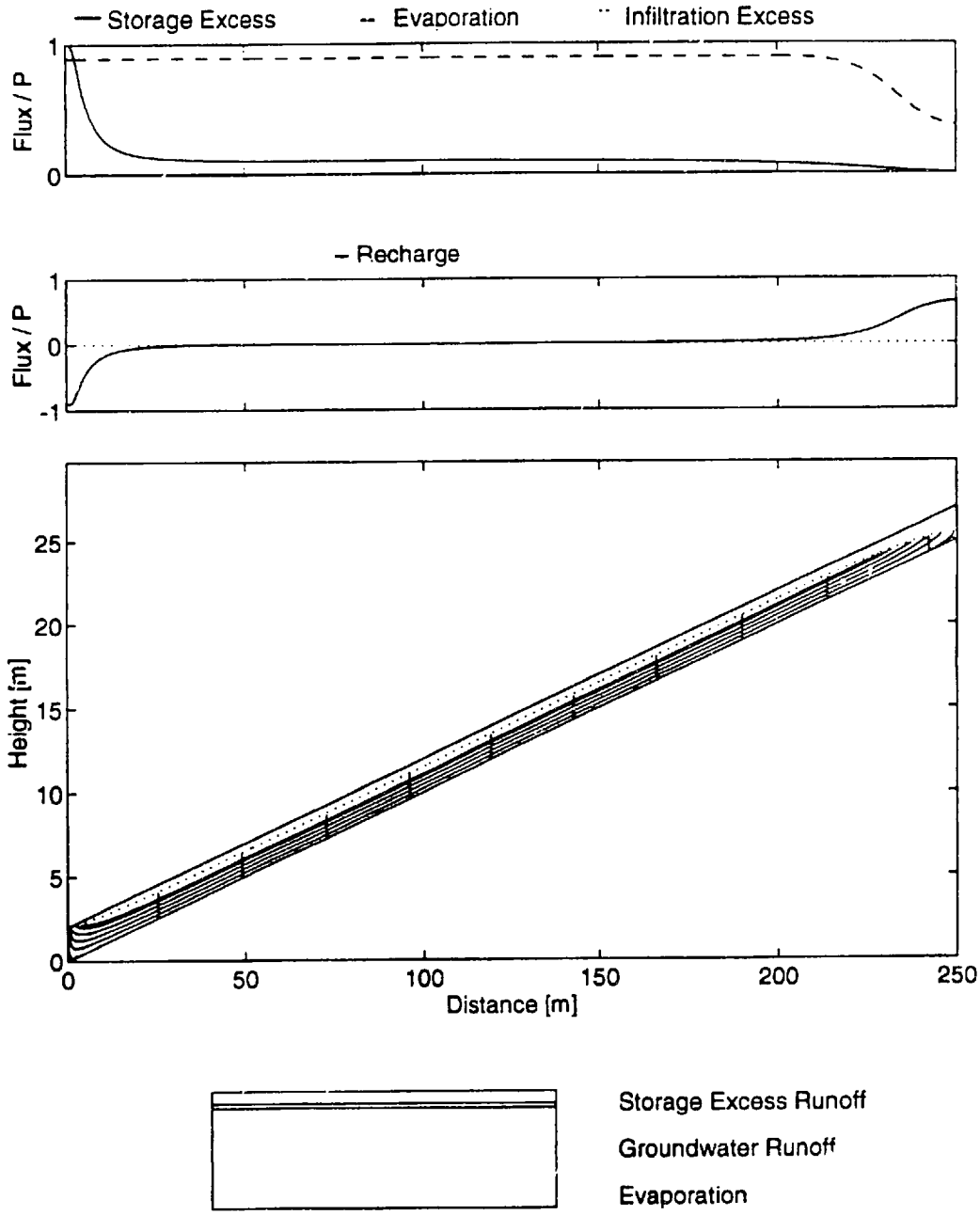

Figure 6.8 Modeled equilibrium hillslope fluxes: Effect of increased hillslope length

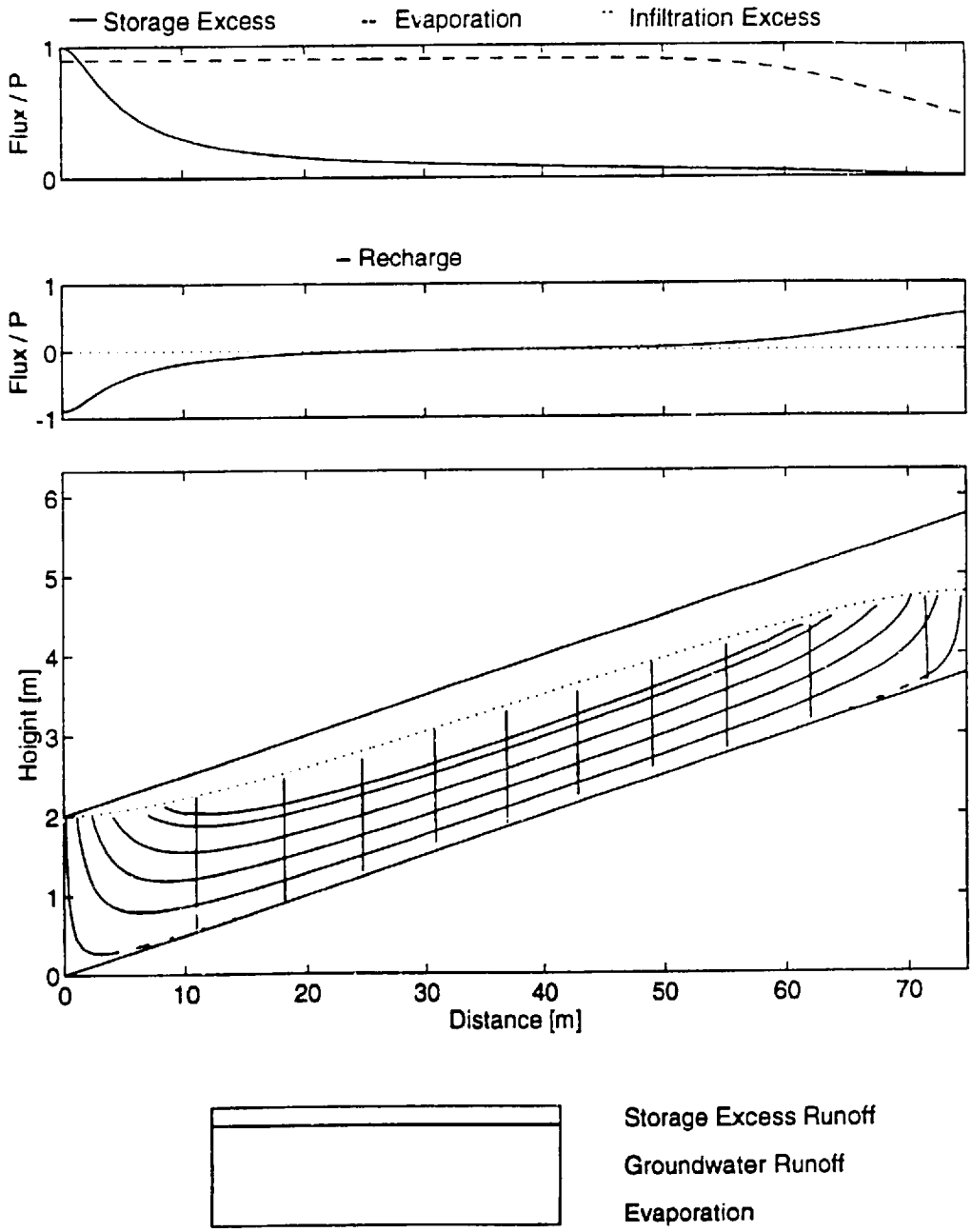

Figure 6.9 Modeled equilibrium hillslope fluxes: Effect of reduced slope

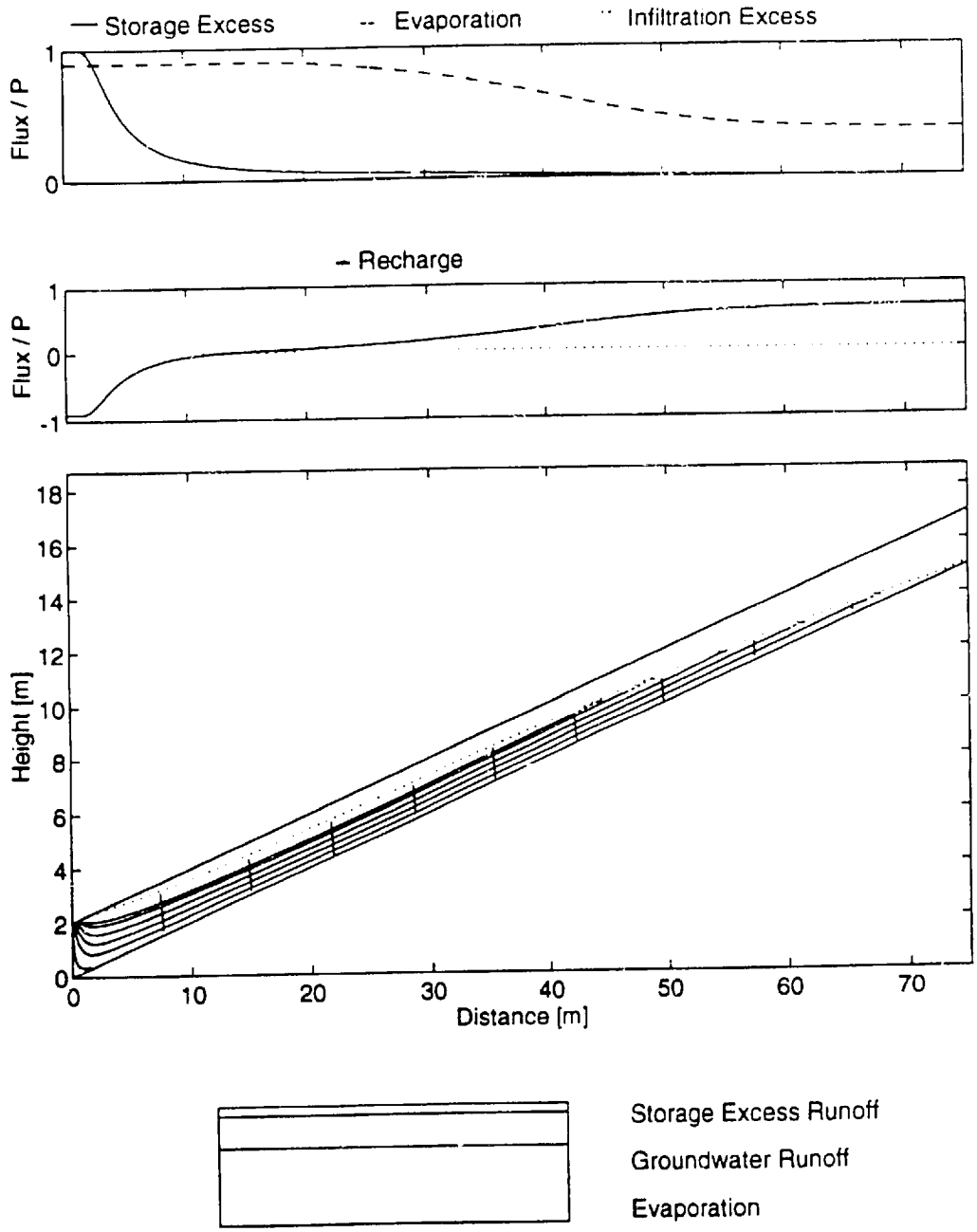

Figure 6.10 Modeled equilibrium hillslope fluxes: Effect of increased slope

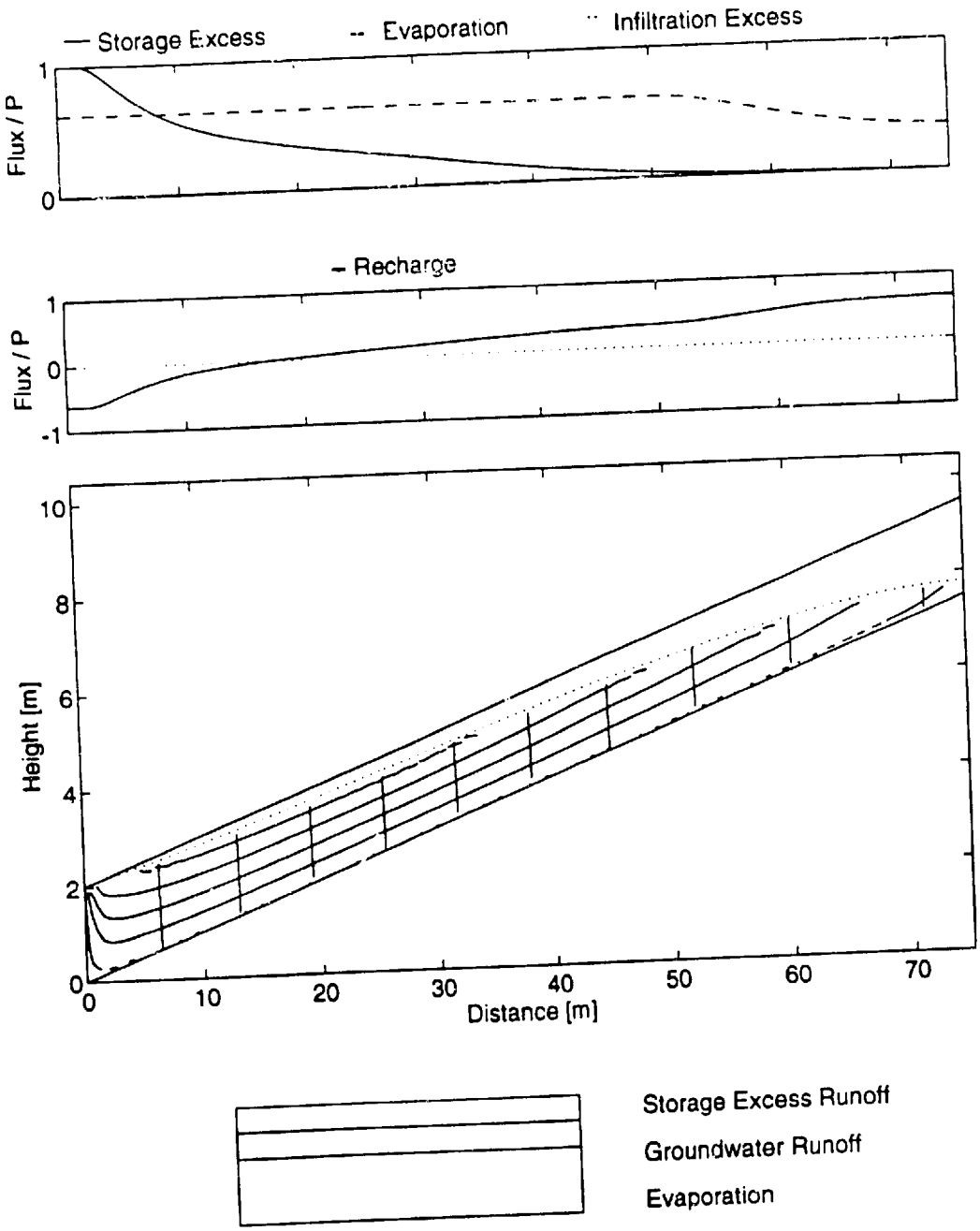

Figure 6.11 Modeled equilibrium hillslope fluxes: Humid climate

humid combination), the surface runoff increases dramatically. In particular note that large quantities of runoff are produced even twenty to thirty meters uphill of the valley. An example with arid climate forcing is given in Figure 6.12. Note here that the water table resides deeper in the midline area than it does for the semi-humid case. This is because Z* is larger for arid climates, as can be seen by comparing the depth-to-saturated zone at the exact hinge points of Figures 6.12 and 6.5. The transmissivity-reducing effect of Z* being larger, combined with the much larger evaporation rates near the channel (the potential evaporation is almost twice the annual precipitation rate), both act to reduce the total yield in this case.

In Figure 6.13, the effect of changing the soil type is demonstrated. Again, all parameters are held the same as the base case, except that here the soil is clay. There are many significant changes in the behavior induced by this change in conductivity and moisture retention characteristics. First, this is the only case which yields infiltration excess runoff. In fact, the infiltration excess runoff is of the same magnitude as the storage excess runoff, though they dominate at opposite ends of the hillslope. The infiltration excess runoff occurs dominantly away near the ridge, while the storage excess dominates near the channel. This is because the storage excess is very dependent on the water table depth, while the infiltration excess is rather insensitive to water table depth and moisture content. Note also that for this case the "stream" implied the hillslope equilibrium is ephemeral. There is no baseflow and no equilibrium seepage face. All of the small amount of water recharged near the divide is evaporated in the valley. The presence of storage excess runoff is evidence for the intermittent appearance of streams draining the hillslope during storm events. One reason for the lack of recharge in this case is that the water table has to be very deep before significant recharge can develop (see Figure 6.14), but the maximum allowed in this case is the two meters of available soil. Another reason is that Z* is larger for this case (110 cm.), which reduces the the transmissivity and causes the midline to extend uphill. Both of these reasons are the effect of the rather strong unsaturated-saturated zone coupling which occurs for clay soils.

In Figures 6.15 and 6.16 the dramatic effects on the spatial structure of fluxes caused by converging and diverging conditions are illustrated. The case plotted in Figure 6.15 corresponds to a seventy five meter long hillslope converging practically to a point, as might represent the support area of a first order stream. The convergence ratio (R_c) in this case is seventy five, which is rather large and represents an extreme case. Note how this

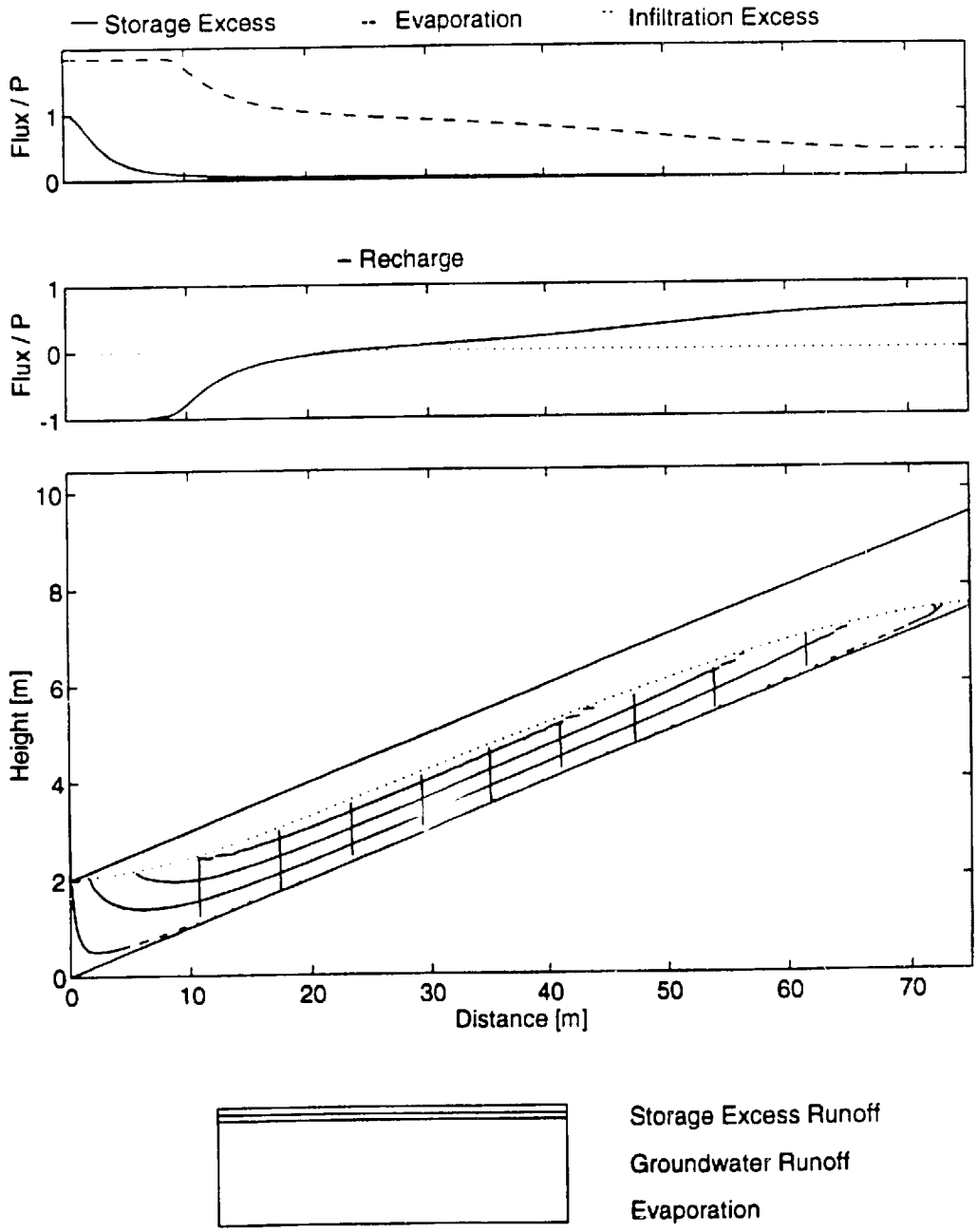

Figure 6.12 Modeled equilibrium hillslope fluxes: Arid climate

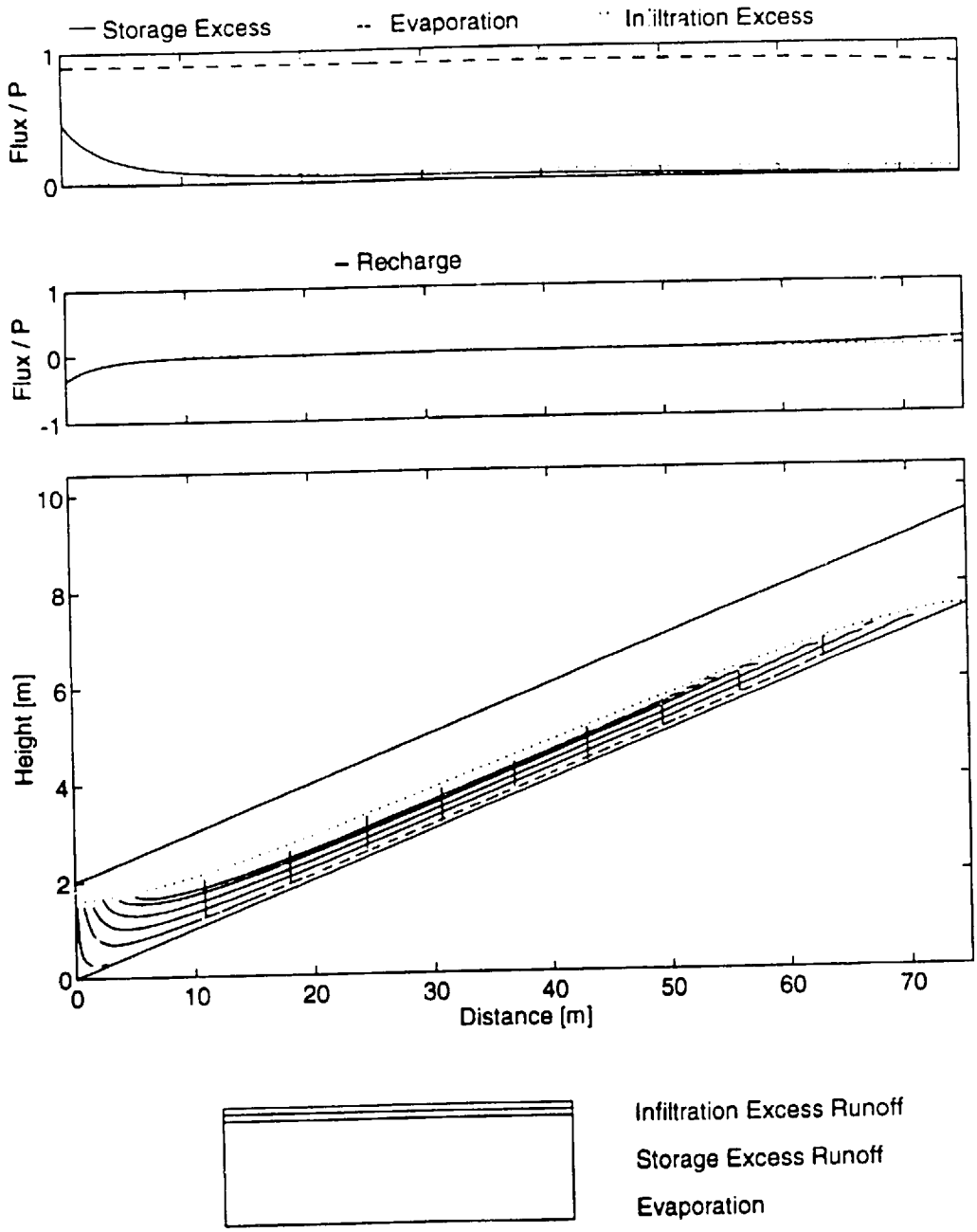

Figure 6.13 Modeled equilibrium hillslope fluxes: Clay soil

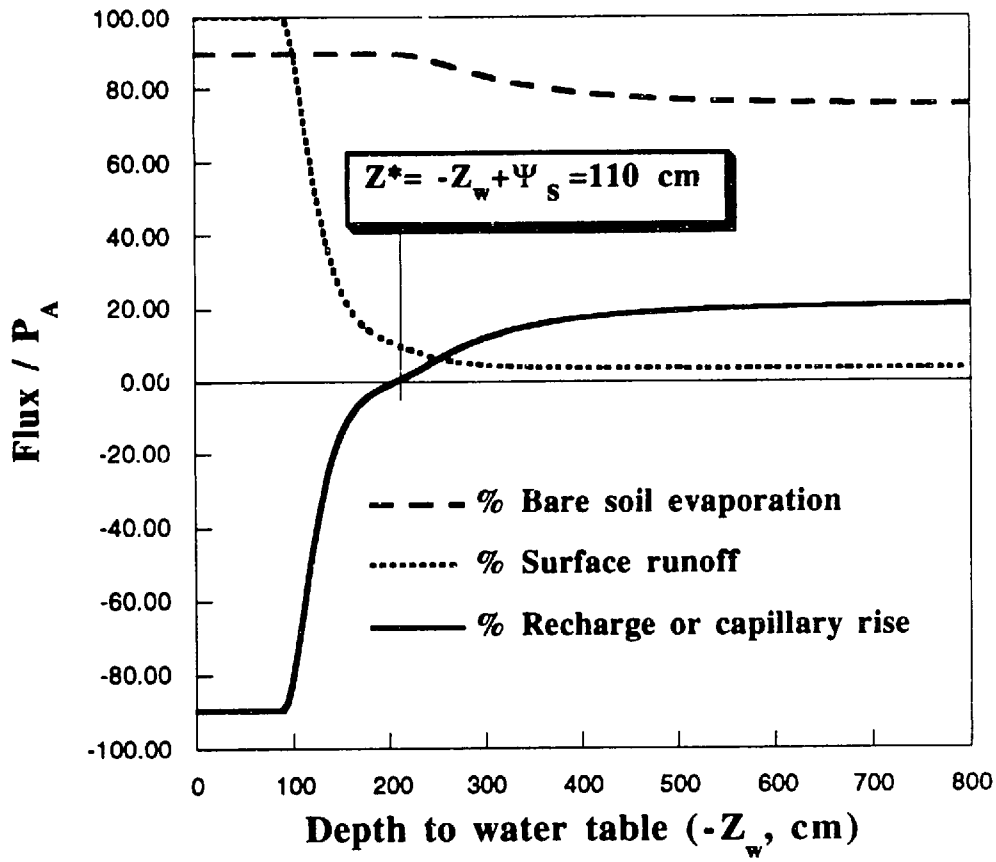

Figure 6.14 Sensitivity of point equilibrium water balance to distance to water table for clay soil and semi-humid climate

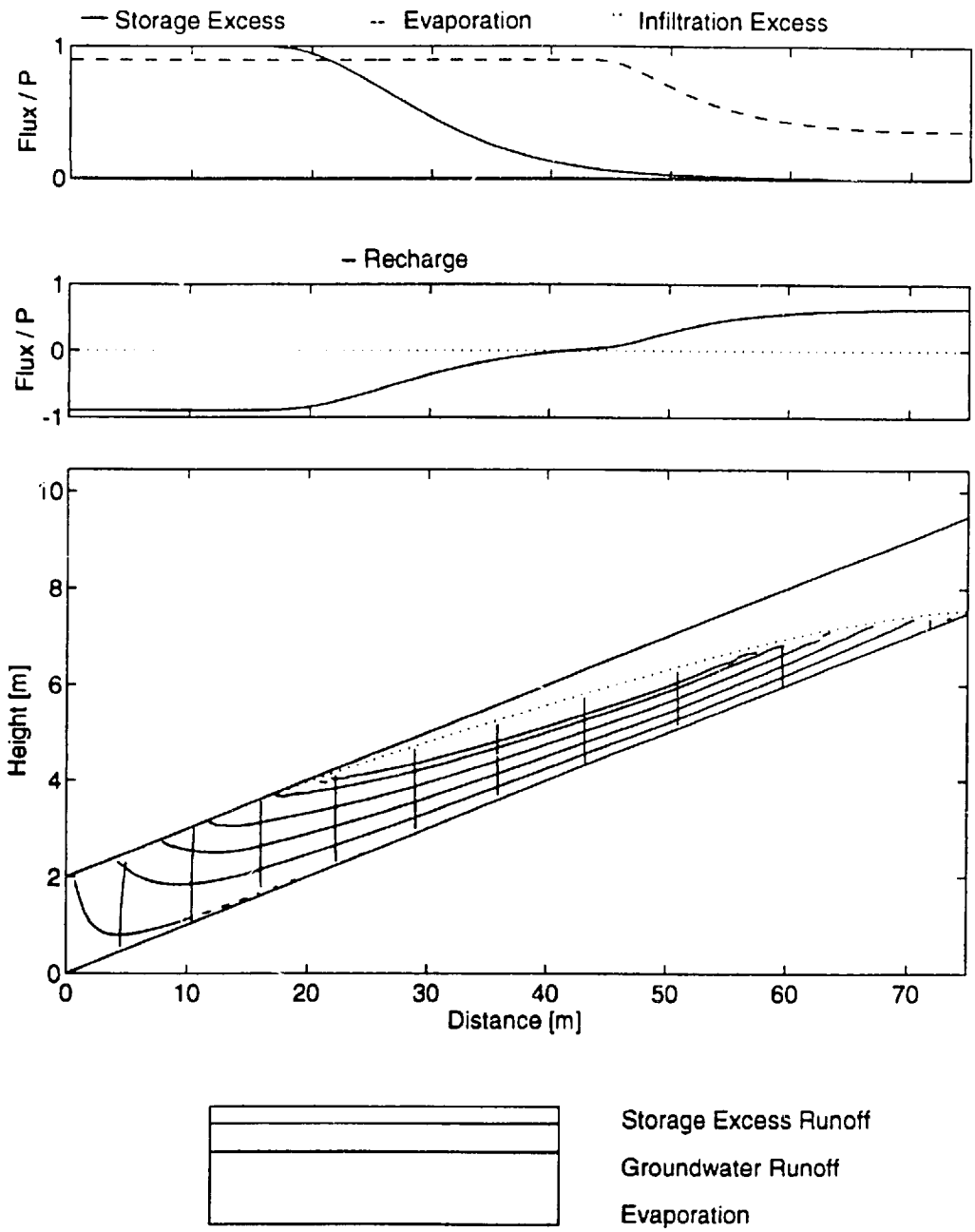

Figure 6.15 Modeled equilibrium hillslope fluxes: Effect of hillslope convergence

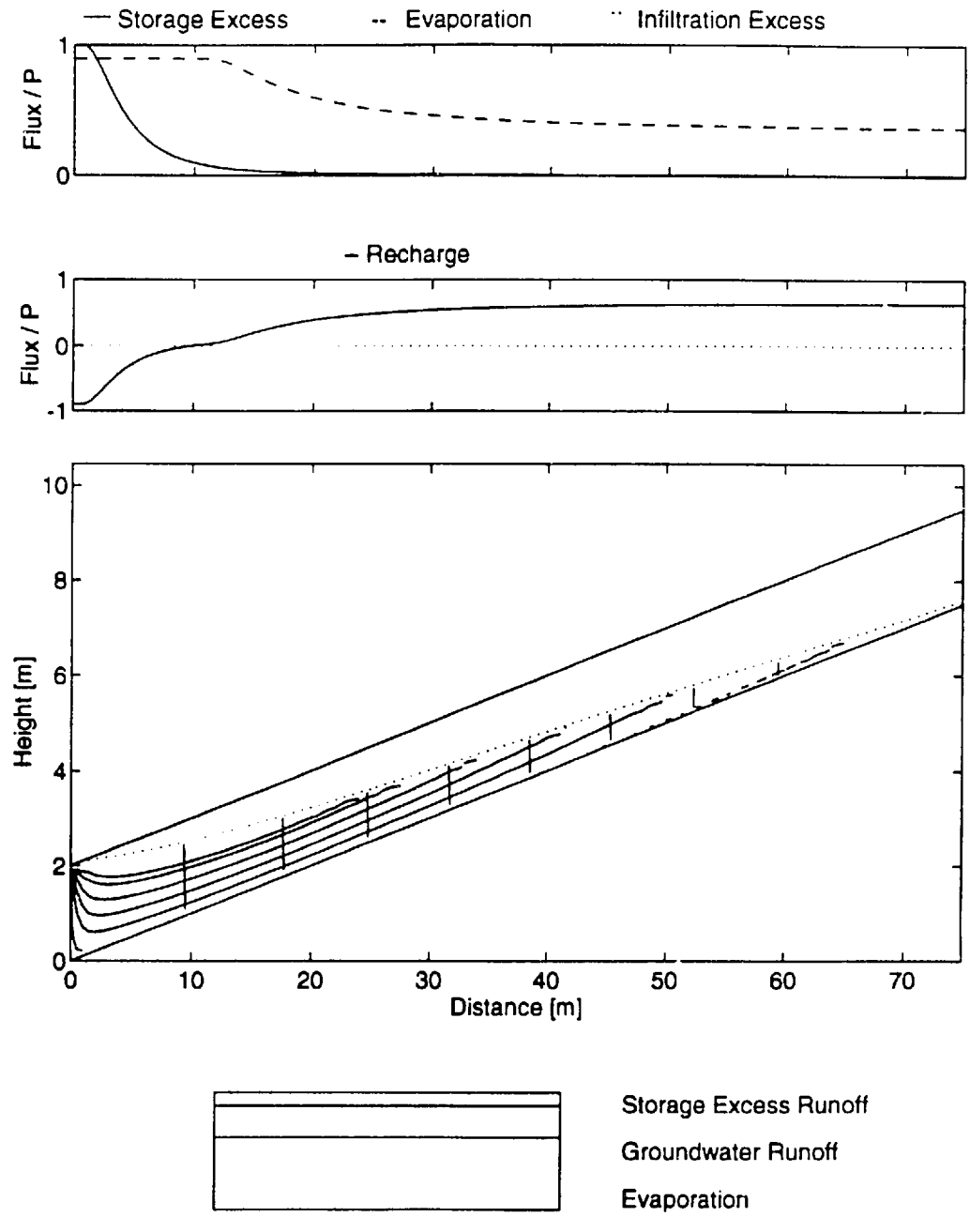

Figure 6.16 Modeled equilibrium hillslope fluxes: Effect of hillslope divergence

convergence takes the seepage face uphill to approximately twenty meters as compared to two meters with the base case. The runoff production both over the seepage face and throughout most of the hillslope are greatly augmented. These effects are the result of the water table requirement to rise in order to increase transmissivity and drain an increasing large amount of flow as it nears the stream head. Note however, that despite the large change in the spatial structure, (e.g. increased runoff near the channel head), the area averaged partitioning changes little. This is partly because the areas near the channel head represent very little of the overall area.

The divergent case (Figure 6.16, this time a 1/75 ratio for R_c), shows the opposite effect. The length over which recharge takes place (and evaporation is soil controlled) is much larger, and the runoff producing length is diminished. For this case the increasing area available for laterally transmitting accumulated recharge allows the water table to be positioned far from the surface, thus enhancing recharge and diminishing runoff. As with the converging case, the overall area averaged effect is less dramatic, again because weighted area averaging tends to diminish the importance of the most effected locations.

6.c.3 Supporting Field Evidence

The model derived in this thesis and applied in the previous section has not been field tested or calibrated to any specific site. This remains as an important area of intended research (see Chapter 7). The overall, qualitative features which arise from the model analyses however, are in broad agreement with many reported field observations.

The most striking similarity is the reproduction of distinct areas of recharge, discharge (capillary rise), and midline. As discussed in the introduction, *Toth* [1966] reports on an extensive field study of the long term climatic mean structure of recharge and discharge over a region of Canadian prairie. He uses a variety of techniques to infer hydrologic response, including interpretation of geochemical (e.g. salt deposits) and geobotanical (e.g. willow rings) evidence. Information derived from these type of observations are particularly well suited for comparison with the work of this thesis because they are natural "integrators" over time and thus reveal the long term mean climatic condition, i.e. those simulated here.

Two figures from *Toth* [1966] are reproduced as Figure 6.17. On the left is a map showing areas of recharge (down arrows), midline (dashes) and discharge (up arrows). It

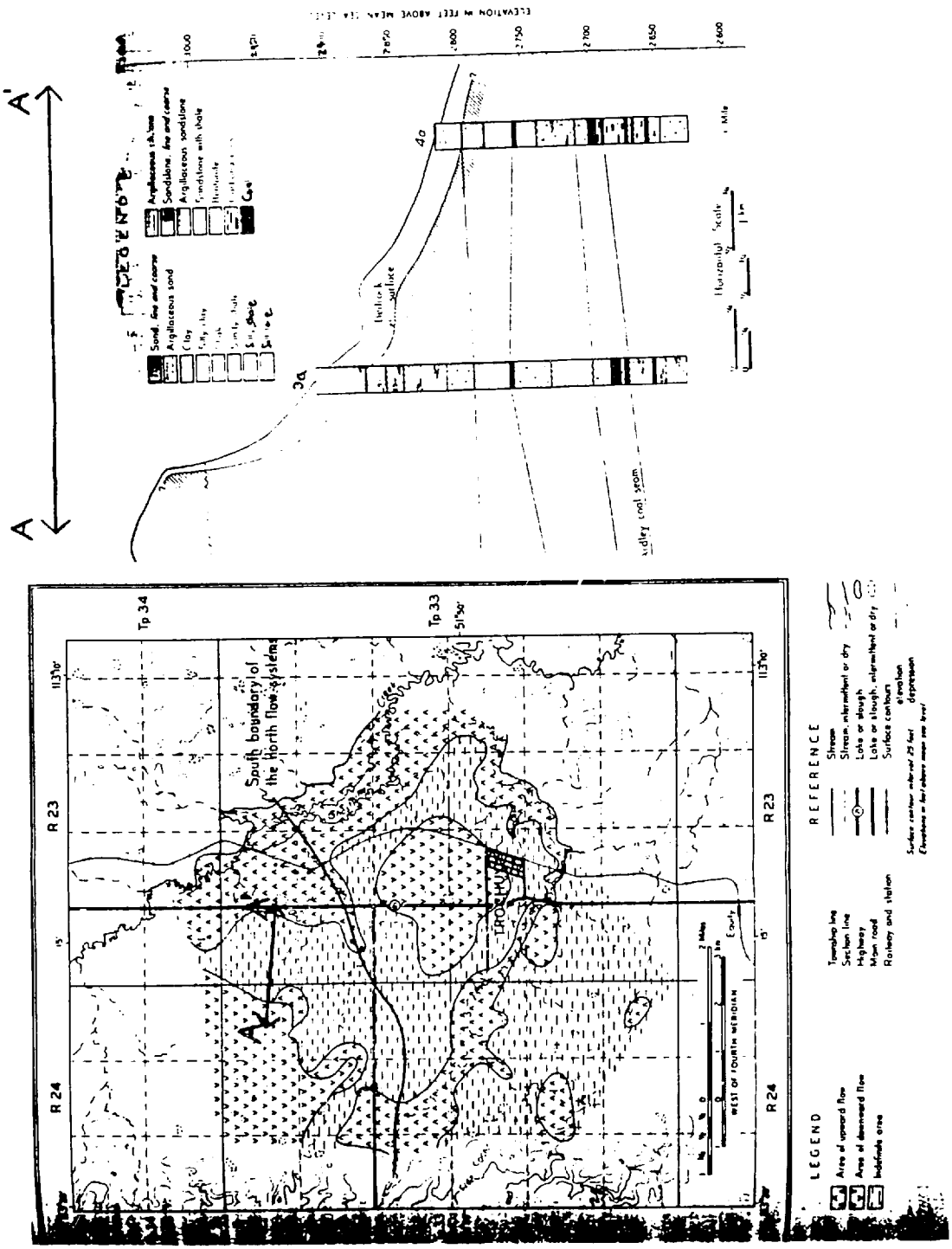

Figure 6.17 Spatial structure of recharge and discharge within a prairie environment [*Toth*, 1966]

is, unfortunately, difficult to discern topography and drainage network on this map, though a careful inspection and reading of *Toth's* [1966] comments do indicate, as one would expect, that the recharge areas occur dominantly on local highlands and the discharge areas near streams. On the right is a lithographic cross-section showing the transect labeled "A-A'". Here the topography is clear. The average slope is approximately four percent, the soil depth averages two meters and the overall length is two-thousand meters. The corresponding recharge-discharge profile (from the arrows along transect A-A') is consistent with the model results presented earlier: a small recharge area near the ridge, an extended midline, and a discharge (net evaporation) area dominating the valley. As demonstrated in the previous analysis (especially Figures 6.6, 6.8 and 6.9), the coupled model developed here predicts extended midlines especially when the soil depth is small in comparison with the hillslope length scale and when the overall slope is small, all of which reduce lateral redistribution potential and all of which are characteristics of the transect A-A. Overall *Toth* [1966] estimates that the following breakdown of distinct hydrologic zones: 26 % recharge, 42 % midline, and 32 % discharge. Also *Toth* [1966] notes that the groundwater flows parallel to the water table along the midline, consistent with the midline region streamlines plotted in all of the previous figures.

Similar highly-structured recharge-discharge maps derived from field observations are reported in *Freeze and Cherry* [1979, p. 202]. Also, *Freeze and Witherspoon* [1968] find qualitatively similar spatial patterns in recharge, midline and discharge by combining measurements of water table elevation and soil permeability with three-dimensional steady flow modeling. Consistent with the data-driven model results, the field observations of *Toth* [1966] and those reported in *Freeze and Cherry* [1979], and the equilibrium model results presented here, *Freeze and Cherry* [1979] state that on average, five to thirty percent of catchment areas discharge water in the mean (both in the sense of seepage and, more pertinent to this work, in the sense of an excess of evaporation over infiltration). *Freeze and Cherry* [1979] also state that the hinge point tends to occur closer to the valley than the midpoint. All of the previous cases studied demonstrate this behavior.

Other corroborating field evidence that the coupled saturated-unsaturated equilibrium model is capturing important hydrologic characteristics are found in the comments of *Helvey et al.* [1972]. *Helvey et al.* [1972] carried out a three year field study of soil moisture profiles on deep soils on the slopes of the Southern Appalachians is North Carolina. The soils in their study averaged eight meters deep. One characteristic they

report is that the moisture variance attenuated rapidly with depth. This lends support to the definition and utility of the equivalent steady profile discussed in Chapter 2. Furthermore they report that there is a strong lateral soil moisture gradient for only twenty to thirty percent of the distance from stream to the watershed divide. This could be an example of the decoupling of saturated and unsaturated zones which was found to be particularly prevalent in the deep soil case (Figure 6.7). Figure 6.18 contains a reproduction of their regression based model results for the predicted interstorm evapotranspiration as a function of distance from the stream. Their model results, which being based on regression to field data may be assumed to be representative of that field data, are qualitatively very similar to the equilibrium model results in that the evaporation monotonically decreases with distance from the channel (e.g. Figure 6.7).

Further corroborating evidence is found in *Chorley* [1978], which, in summarizing many field studies of runoff, reports on the development of bulb-like contributing (and growing) runoff areas at channel heads. The approximate radial symmetry of these observed partial areas and their strong runoff potential support the results of the converging hillslope studies of this thesis.

In summary, a brief survey of reported field evidence tends to corroborate both the underlying assumptions and the results (particularly regarding spatial structure) of the simple analytic model developed in this thesis. While this does not surrogate for comprehensive field tests that include model parameter estimation, it does give strong qualitative support for continuing this approach to hillslope hydrologic modeling.

6.d Conclusions and an Index of Geological, Climatic and Soil Control

In the analysis of many climate-soil-hillslope configurations, an extended midline is found to develop and, to a certain degree, control the spatial structure of the hillslope response. In this section a limiting-case partial-analysis is outlined to identify and quantify this effect.

First note that in order to have water balance in the closed hillslopes (i.e. impermeable bedrock, symmetric valleys) studied previously, a hinge point must exist somewhere along the hillslope. At this point, or along this line if it is an extended midline, the equilibrium depth-to-saturated zone must be Z^*, i.e. the depth at which the point unsaturated zone water balance analysis predicts zero net recharge (see Figures 6.4 and 6.14). Also note that

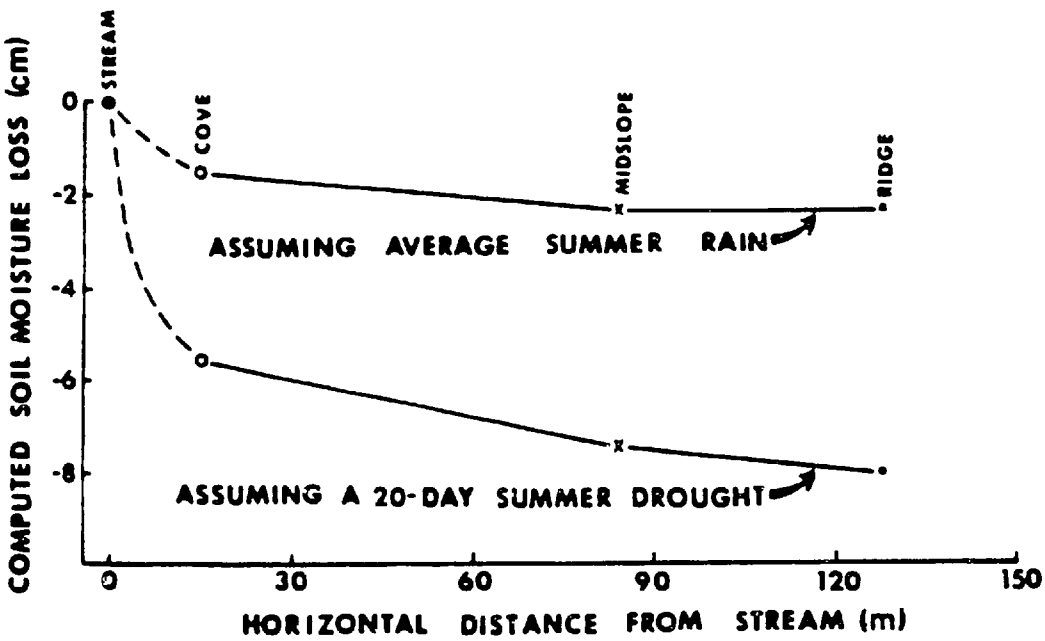

Figure 6.18 Relation of hillslope evapotranspiration to distance from channel [*Helvey et al.*, 1972]

at this point, the water table can not have a greater slope than the surface, because if it did the equilibrium model would predict recharge *downhill* of the hinge and capillary rise *uphill* of the hinge. Thus the maximum possible lateral flow under a hinge point (or midline) may be written (assuming Dupuit flow) as:

$$Q_{max} \approx K_s\left(H - Z^*\right)\theta \tag{6.3}$$

Note that in this simple equation, Z^* is determined solely by climate and soil interaction (by way of Equation 5.37), while H and θ are geologic parameters.

The constrained hillslope circulation which can occur assuming this limiting-case analysis of the saturated zone is sketched schematically in Figure 6.19. In essence the length of the recharge zone near the divide is constrained by the fact that the cumulative uphill recharge has to pass under the midline and thus cannot exceed Q_{max}. Note that as seen in the case studies, shallow, clay-soil, flat, arid conditions all tend to reduce Q_{max} and thus increase "geologic" control over the spatial structure and the spatial average water balance, while deep, conductive, humid and steep conditions increase Q_{max}, leaving the hydrology largely determined by climate-soil interaction and independent of topography. Under the former case full account must be taken of topography, while under the latter the semi-infinite point model of Chapter 3 could be simply scaled (i.e. linearly scaled with area) to estimate regional watershed fluxes.

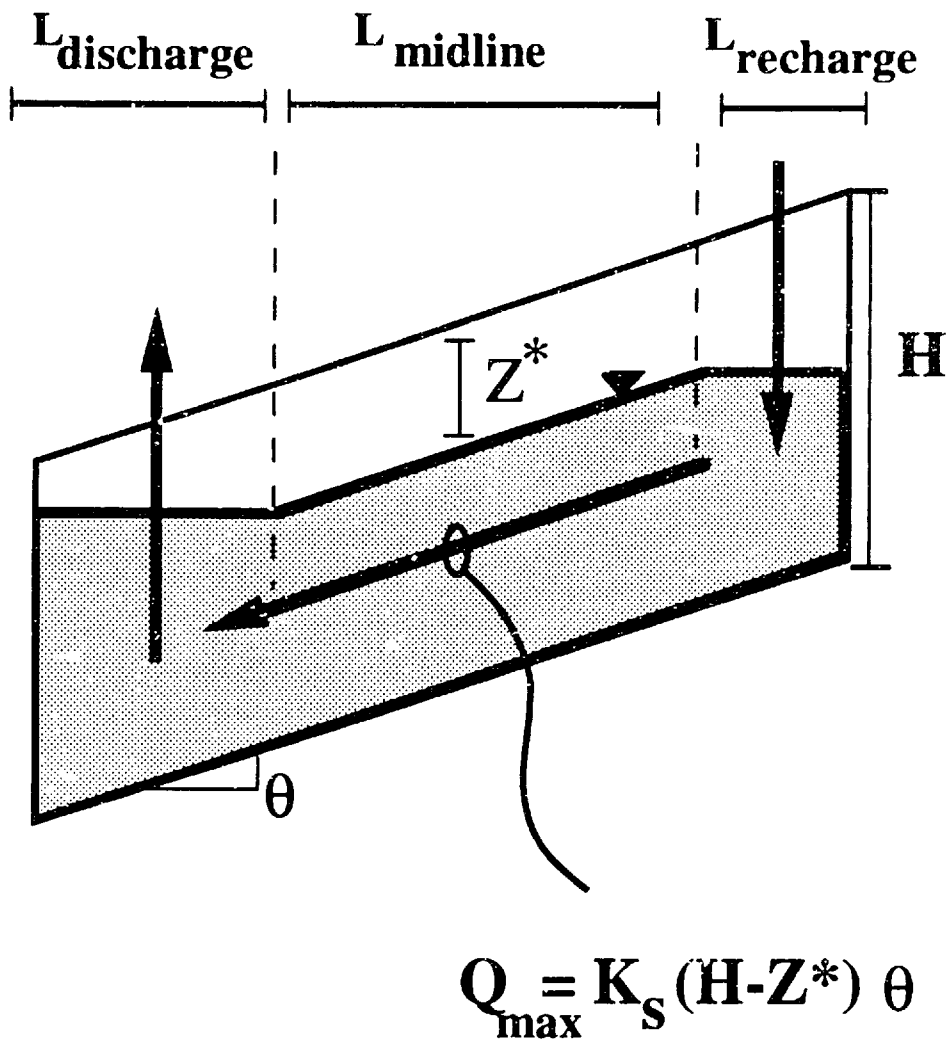

Figure 6.19 Simplified spatial structure of hydrologic fluxes and an index of climatic and geologic control

Chapter 7: Key Findings and Planned Research Extensions

7.a Key Findings

Research into a few critical aspects of water balance, including process based modeling, parameterization of initial conditions on the soil moisture state, and the role of saturated-unsaturated zone coupling in determining hydrologic response (hillslope circulations and flux patterns), are reported in this thesis. These analyses culminate in an analytic model which, given the depth to the water table, determines the temporal mean surface water balance for a given climate forcing and soil properties. When this model is coupled to the equations describing saturated flow, the spatial structure of the mean hydrologic surface fluxes and the circulation of water throughout the hillslope domain may be found. Application of this analysis to simple planar, converging and diverging hillslopes produces patterns and circulations in good qualitative agreement with observation.

The following list highlights the key findings of this research effort:

- The equivalent steady moisture profile, defined as the steady profile which transmits the temporal mean unsaturated zone flow, provides a useful and simple parameterization of the soil moisture state for the purpose of initializing the soil infiltration and exfiltration capacities. This parameterization is sufficient for use in determining mean hydrologic response.

- The time compression approximation, which relates the solution of infiltration and exfiltration under constant concentration boundary conditions to situations of switching flux (atmospheric) and concentration (ponded or dry) boundary conditions, is shown to apply under nonuniform initial moisture profile conditions (such as those in equilibrium with a shallow water table) as well as uniform moisture profiles.

- Estimated temporal mean fluxes given by the analytic equilibrium model are in good agreement with those found by long time finite-element numerical simulation.

- The coupled saturated-unsaturated hillslope equilibrium model qualitatively reproduces observed spatial features of hillslope hydrologic fluxes.

- The water table over a hillslope adjusts to a position that is characterized by three hydrologically distinct segments: the net recharge region near the topographic divide; the net discharge region near the valley drainage area; and an important midline segment, the extent of which depends on hydrogeologic and climatic conditions in a simple way, that has no net exchange with the unsaturated zone and in which the flow lines run parallel to the water table.

7.b Planned Research Extensions

During the course of this research, a number of necessary and interesting extensions to the work were identified. To further substantiate and firmly establish some of the hypotheses and results of this thesis, we are proceeding with many of the extensions discussed below. A number of these investigations are nearing completion.

Planned research extensions related to this thesis fall under two general categories: those involving further application and extension of the saturated-unsaturated zone coupling for multidimensional systems, and those involving smaller scale individual hydrologic processes. The former are discussed under the heading "Hillslope Studies" and the latter under "Process Studies". The former are mostly related to the findings of Chapter 6, while the latter are ideas related to the analysis procedures of Chapter 2 and the modeling techniques of Chapter 4.

Hillslope Studies

The analytic results of this work need to be compared with observed long term mean soil moisture distributions and hydrologic response patterns under a variety of geologic and climatic settings. If the basic model results are validated, a study of the scaling of hydrologic response with area may be guided by the findings herein, in particular those of the partial analysis in Chapter 6. Such a study may also be extended to explore the relation of geomorphological descriptors to hydrologic response.

For practical application, the feasibility of utilizing the equivalent steady profile as a tool

for coupling the saturated and unsaturated zones under seasonal conditions should be explored. In addition, the potential of using of field-measured or numerically simulated infiltration and exfiltration capacities under heterogeneous soil conditions should be studied.

Process Studies

Process studies which could be incorporated into the framework established in this thesis include the derivation of analytic steady moisture profiles and infiltration/exfiltration capacities for heterogeneous soils with distributed root sink. One particularly useful approach would be to develop these functions in the framework of variable but geometrically scaled soil properties, such that most of the spatial heterogeneity would be contained in a single scaling parameter. The "alpha" model of infiltration derived in Chapter 4 may be amenable to such an analysis, and may also be extended to describe exfiltration. Two other important processes which are neglected in this work but which should be included in future extensions are reinfiltration of surface runoff and snowmelt-type recharge events. Both of these issues should be approached in an "event" based statistical-dynamical manner such that they may be incorporated into the general framework discussed here.

APPENDIX A: SOIL HYDRAULIC MODELS

The *Brooks-Corey* [1966] model relates the effective soil saturation (s), the capillary tension head (Ψ) and the unsaturated hydraulic conductivity (K(s)) by the following relationships:

$$s(\Psi) = \begin{cases} \left(\frac{\Psi}{\Psi_s}\right)^{-m} & \Psi \le \Psi_s \\ 1 & \Psi \ge \Psi_s \end{cases} \tag{A.1}$$

$$K(s) = K_s \cdot s^c \tag{A.2}$$

In the above:

$$s = \frac{\Theta - \Theta_r}{n_t - \Theta_r} \tag{A.3}$$

where Θ is the volumetric moisture content, Θ_r is the residual moisture content, and n_t is the total porosity. In addition, Ψ_s is the bubbling pressure head, which is the largest tension head at which the soil remains saturated, m is the pore size distribution index, and c is the pore disconnectedness index . On the basis of theory and experiment for a wide range of soil types, *Brooks and Corey* [1966] show that these two exponents can be related by:

$$c = \frac{2 + 3m}{m} \tag{A.4}$$

Note that for the soil moisture diffusivity (D) defined as:

$$D(\Theta) = K(\Theta) \cdot \frac{d\Psi}{d\Theta} \tag{A.5}$$

the Brooks-Corey relation gives the following dependence of D on s:

$$D(s) = \begin{cases} \left(\frac{-K_s \Psi_s}{m n_e}\right) \cdot s^{(c+1)/2} & s < 1 \\ \infty & s = 1 \end{cases} \tag{A.6}$$

The exponential soil model [*Gardner*, 1958] relates the soil hydraulic properties by:

$$K(\Psi) = K_s \cdot e^{\alpha \Psi} \tag{A.7}$$

$$s(\Psi) = e^{\alpha \Psi} \tag{A.8}$$

which yields:

$$K(s) = K_s \cdot s \tag{A.9}$$

and

$$D = \frac{K_s}{\alpha n_e} \tag{A.10}$$

In the above, α is a (positive) scaling parameter with units of inverse length. While exponential relations such as (A.7) and (A.8) can reasonably represent $s(\Psi)$ and $K(\Psi)$ separately, it is not necessarily the case that the length scale (α) would be the same for each relationship. This assumption is often made as it yields the above constant diffusivity and linear dependence of conductivity on moisture, thus simplifying mathematical analysis. The term linear soils is used to describe this (exponential) model because it yields a linear diffusion equation.

Appendix B: Infiltration into Unbounded Soils

This solution for the infiltration capacity of bounded Brooks-Corey soils has limiting behavior for deep water tables which is not directly relevant to the overall water balance model developed in this thesis, but has relevance to water balance modeling in general.

Note that when the water table becomes deep in Equation (4.26), the slope of the profile approaches zero (the "unit gradient" limit), and thus Γ approaches zero. In the limit where the depth to the water table is infinite, the initial condition moisture profile is uniform, and the infiltration capacity equation evaluated to four terms simplifies to:

$$f'_{z_w \to \infty} \cong \frac{\sqrt{2}}{2}\tau^{-1/2} + \frac{2}{3} - \frac{\sqrt{2}}{6}\tau^{1/2} - \frac{4}{135}\tau \qquad \text{(B.1)}$$

Note that at infinite time, the variable τ is equal to one, and Equation (B.1) gives a limiting normalized infiltration rate of approximately 1.11. The correct limiting normalized infiltration rate is unity, since the limiting rate of infiltration for large penetration depth is the saturated conductivity (K_s). As the above procedure for evaluating the coefficients of the assumed power series is carried out to include more terms, the coefficients decrease. The contribution of these higher order terms thus decreases. The decrease is due both to the smaller coefficients and to the fact that for τ less than one (which it is by definition), the terms decrease as the power which τ is raised to increases. Carrying out this procedure to sixteen terms gave a limiting infiltration rate less than one percent higher than the true value. It appears then, though it cannot be stated for certain, that the power series in one half powers of τ forms a converging solution to the governing differential Equation (4.61).

This is the only solution known by the author which explicitly and uniformly approximates the infiltration capacity into a soil of uniform initial moisture content over all time. The solution of *Philip* [1957b] for example, is comprised of an early time and late time solution. Comparing his approach to that taken in this thesis, it appears that the critical step in obtaining a uniformly converging solution is the change of variable to $\tau=t/(t+\chi)$.

Instead of including a large number of terms to improve the long time behavior of (B.1), one may chose the last coefficient (in this case A3) to force the expression to asymptote to unity. This distributes some of the late time error to early times, but may be

worthwhile due to the simplicity of the result. Carrying this out and redimensioning the result yields:

$$f^*_{i\,z_w\to\infty} \cong \frac{\sqrt{2}K_s}{2}\left(\frac{t}{t+\chi}\right)^{-1/2} + \frac{2}{3}K_s - \frac{\sqrt{2}K_s}{6}\left(\frac{t}{t+\chi}\right)^{1/2} - \frac{\left(1-\sqrt{2}\right)K_s}{3}\left(\frac{t}{t+\chi}\right) \quad \text{(B.2)}$$

In Figure B.1 this solution is compared with numerical simulation results for the silt soil (used previously) with uniform initial moisture content corresponding to thirty centimeters per year of recharge. The value of χ for this case is 10.7 hours. Thus for small time, τ is roughly equal to the time divided by 10.7 hours. For τ equal to one half, t is equal to 10.7 hours and as τ approaches one, time rapidly approaches infinity. The numerical simulation (open circles) was carried out to one-hundred hours.

In many applications, it is also useful to have an expression for the cumulative infiltration (F_i^*). This is accomplished simply by integrating Equation (B.2) with time:

$$F \cong K_s\left\{\left(1-\frac{\sqrt{2}}{3}\right)t + \left(\frac{\sqrt{2}}{3}\right)\sqrt{\chi t + t^2} + \left(\frac{\sqrt{2}-1}{3}\right)\chi\left(\ln[t+\chi]-\ln[\chi]\right) + \left(\frac{\sqrt{2}}{3}\right)\chi\left(\ln\left[t+\frac{\chi}{2}+\sqrt{\chi t+t^2}\right]-\ln\left[\frac{\chi}{2}\right]\right)\right\} \quad \text{(B.3)}$$

Equations (B.2) and (B.3) strike a useful balance between accuracy and utility for water balance modeling. As is noted in Chapter 4, these τ based equations do not require any evaluation of diffusivity weighting integrals (such as the one proposed by *Crank* [1959], i.e. equation 3.5 of this thesis) and they are parameter efficient, with all soil and initial condition information contained simply (i.e., algebraically) in parameters K_S and χ.

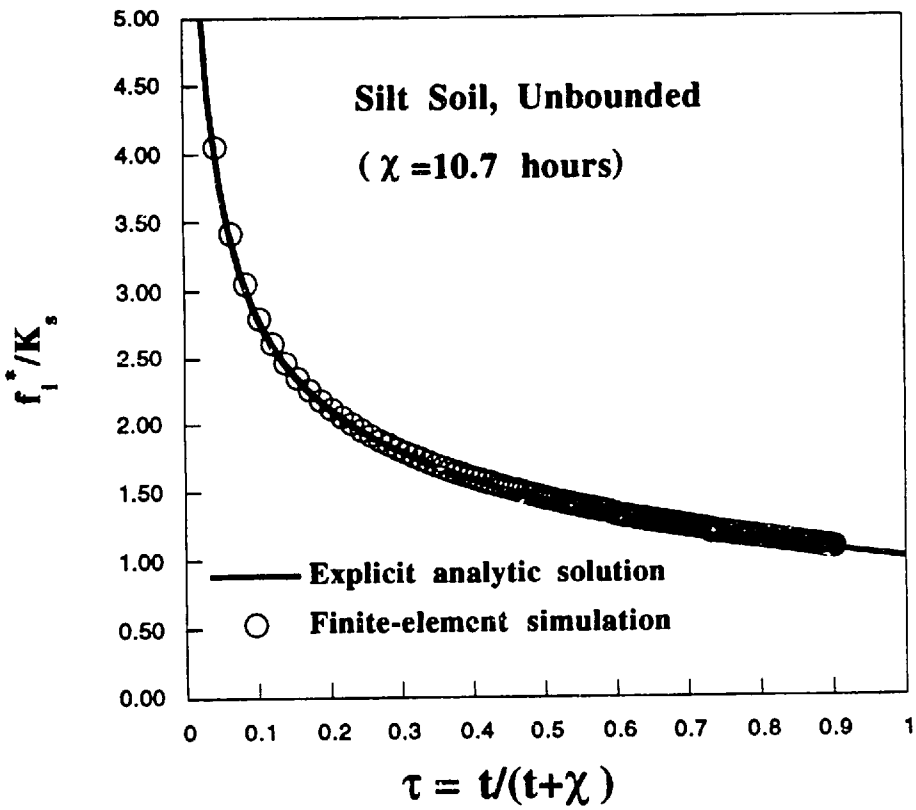

Figure B.1 Infiltration capacity of an unbounded silt soil: comparison of four term explicit expression and finite-element simulation

REFERENCES

Abbot, M.B., J.C. Bathurst, J.A. Cunge, P.E. O'Connel, and J. Rasmussen, An introduction to the European Hydrological System-Systeme hydrologique Europeen, "SHE",2, Structure of a physically-based, distributed modeling system, *J. Hydrol.*, *87*, pp. 61-77, 1986.

Alley, W.M., On the treatment of evapotranspiration, soil moisture accounting, and aquifer recharge in monthly water balance models, *Water Resources Res*earch, 20(8), pp. 1137-1149, 1984.

Anat, A., H. R. Duke, and A. T. Corey, Steady upward flow from water table, *Hydrology Papers, CSU 7,* 1965.

Bakr, A.A., L.W. Gelhar, A.L.Gutjahr, and J.R. MacMillan, Stochastic analysis of spatial variability in subsurface flows, 1, comparison of one and three-dimensional flow, *Water Resources Research, 14,* pp. 263-271, 1978.

Band, L.E., Distributed parameterization of complex terrain, in *Land Surface-Atmosphere Interaction observations, models and analysis,* E. Wood (ed.), Kluwer Academic Publishers, Norwood MA, pp. 249-270, 1991

Bear, J. *Dynamics of Fluids in Porous Media,* Dover Publications Inc., Mineola, 1988

Bender, C. M., and S. A. Orszag, *Advanced Mathematical Methods for Scientists and Engineers,* McGraw-Hill Book Company, New York, 1978

Beven, K., Changing ideas in hydrology-the case of physically-based models, *J. Hydrol.*, *105*, pp. 157-72, 1989.

Beven, K., A. Calver, and E.M. Morris, *The Institute of Hydrology distributed model, Rep. 98,* Inst. of Hydrol., Wallingford, Oxon, United Kingdom, 1987.

Beven, K.J., and M.J. Kirkby, A physically based. variable contributing area model of basin hydrology, *Hydrologic Sciences-Bulletin, 24*, pp. 43-69, 1979.

Binley, J. Elgy, and A., K. Beven , A physically based model of heterogeneous hillslopes: 1. Runoff production, *Water Resources Research, 25(6)*, pp. 1219-1226, 1989.

Binley, A., K. Beven, and J. Elgy, A physically based model of heterogeneous hillslopes: 2. Effective hydraulic conductivities, *Water Resources Research, 25(6)*, pp. 1227-1233, 1989.

Blain, C.A., and P.C.D. Milly, Development and application of a hillslope hydrologic model, *Adv. in Water Resources, 14(4)*, pp.168-174, 1991.

Bouwer, H. Infiltration of water into nonuniform soil, Journal of the Irrigation and Drainage Division, ASCE, Vol. 95, No. IR4, pp. 451-562, 1969

Braester, C. Moisture variations at the soil surface and the advance of the wetting front infiltration at constant flux, *Water Resources Research, 9(3)*, pp. 687-694, 1973.

Bras, R. L.,*Hydrology: an introduction to hydrologic science* , Addison-Wesley Publishing Company, Inc., Reading, Massachusetts, 1990.

Bresler, E. and G. Dagan, Unsaturated flow in spatially variable fields, 2, application of water flow models to various fields, *Water Resources Research, 19(2)*, pp. 421-428, 1983.

Brooks, R. H. and A.T. Corey, Properties of porous media affecting fluid flow, *J. Irrig. Drain. Div. Am. Soc. Civ. Eng., 92(IR2)*, 61-88, 1966.

Brutsaert, W., Vertical infiltration into dry soil, *Water Resources Research, 13(2)*, 363-368, 1977.

Budyko, M.I., *Klimat i zhizn, Gidrometeor.,Izdat.*, Leningrad. Trans. by D.H Miller as Climate and Life, Academic Press, New York, 1974.

Cabral, M.C., L.Garrote, R.L. Bras, and D. Entekhabi, A Kinematic model of infiltration and runoff generation in layered and sloping soils, *Advances in Water Resources, 15,* 311-324, 1993

Carlston, C.W., Drainage density and streamflow, *U.S. Geol. Surv. Prof. Pap., 422-C,* 1963

Carlston, C.W., The effect of climate on drainage density and streamflow, *Int. Assoc. Hydrol. Sci., Bull., 11(3),* pp. 62-69, 1966

Chan, S.O., and P.S. Eagleson, Water balance studies of the Bahr el Ghazal Swamp, *Mass. Inst. of Technol., Dept of Civ. Eng., R. M. Parsons Lab Rept. No. 261*, 317 pp., 1980.

Chorley, R. J., The hillslope hydrologic cycle, in *Hillslope Hydrology,* M.J. Kirkby (ed.), John Wiley and Sons, Ltd., New York, 1978.

Cordova, J.R., and R.L. Bras, Physically based probabilistic models of infiltration, soil moisture, and actual evapotranspiration, *Water Resources Research, 17(1),* pp. 93-106, 1981.

Crank, J., *The mathematics of diffusion, 2nd ed.,* Oxford University Press, New York, 1959.

Dagan, G. and E. Bresler, Unsaturated flow in spatially variable fields, 1, derivation of models for infiltration and redistribution, *Water Resources Research, 19(2),* pp. 413-420, 1983.

Dingman, S.L., Drainage density and streamflow: A closer look, *Water Resources Research, 14(6),* pp. 1183-1187, 1978.

Dooge, J.C.I., and Q.J. Wang, Comment on "An investigation of the relation between ponded and constant flux rainfall infiltration: by A. Poulovassilis et al.", *Water Resour. Res., 29(4)*, 1335-1337, 1993

Eagleson, P.S., Climate soil and vegetation, 1, Introduction to water balance dynamics, *Water Resour. Res., 14(5)*, 705-712, 1978a.

Eagleson, P.S., Climate soil and vegetation, 2, The distribution of annual precipitation derived from observed storm sequences,*Water Resour .Res. ,14(5)*, 713-721, 1978b

Eagleson, P.S., Climate soil and vegetation, 3, A simplified model of soil moisture movement in the liquid phase, *Water Resour. Res., 14(5)*, 722-730, 1978c

Eagleson, P.S., Climate soil and vegetation, 4, The expected value of annual evapotranspiration, *Water Resour. Res., 14(5)*, 731-740, 1978d

Eagleson, P.S., Climate soil and vegetation, 5, A derived distribution of storm surface runoff, *Water Resour. Res., 14(5)*, 741-748, 1978e

Eagleson, P.S., Climate soil and vegetation, 6, Dynamics of the annual water balance, *Water Resour. Res., 14(5)*, 749-764, 1978f

Eagleson, P.S., Climate soil and vegetation, 7, A derived distribution of annual water yield, *Water Resour. Res., 14(5)*, 765-776, 1978g

Eagleson, P.S., Climate, soil and the water balance: A framework for their analytic coupling, *Lecture notes for the Tenth Annual John R. Freeman Memorial Lecture,* Massachusetts Institute of Technology, Cambridge, Mass, 1977

Eagleson, P.S. Ecological optimality in water-limited natural soil-vegetation systems: 1., Theory and Hypothesis, *Water Resources Research, 18(2)*, pp. 325-340, 1982.

Eagleson, P.S. and S. A. Miller, Water table depression in the Gezira region, *Proc. Conf. on Water Resource Dev. in Egypt*, (edited by I.M. Elassiouti, D.H. Marks and M.A. Abu-Zeid), Egyptian Ministry of Irrigation, Cairo, pp. 201-212, 1983.

Eagleson, P.S. and R.I. Segarra, Water-limited equilibrium of savanna vegetation systems, *Water Resources Research, 21(11)*, pp. 1483-1493, 1985.

Engman, E.T. and A.S. Rogowski, A partial area model for storm flow synthesis, *Water Resources Research, 10(3)*, pp. 464-472, 1974.

Entekhabi, D., I. Rodriguez-Iturbe and R.L. Bras, Variability in large-scale water balance with land-atmosphere interactions, *J. of Climate, 5(8)*, 798-813, 1993

Entekhabi, D., and P.S. Eagleson, Land surface hydrology parameterization for atmospheric general circulation models including subgrid scale variability, *J. of Climate, 2(8)*, 816-831, 1989

Entekhabi, D. and P.S. Eagleson, Climate and the equilibrium state of land surface hydrology parameterization, in *Landsurface-atmosphere interaction: observations, models and analysis*, E. Wood (ed.), Kluwer Academic Publishers, Norwood MA, pp. 205-220, 1991.

Famiglietti, J.S. and E.F. Wood, Evapotranspiration and runoff from large land areas, in *Landsurface-atmosphere interaction: observations, models and analysis*, E. Wood (ed.), Kluwer Academic Publishers, Norwood MA, pp. 179-204, 1991a

Famiglietti, J.S. and E.F. Wood, Comparison of passive microwave and model derived estimates for soil moisture fields, paper presented at 5th International Colloquium, Physical Measurements and Signatures in Remote Sensing, Courchevai, France, 1991b

Fox, J.D., Incorporating freeze-thaw calculations into a water balance model, *Water Resources Research, 28(9)*, pp. 2229-2244, 1992.

Freeze, R.A., The mechanism of natural groundwater recharge and discharge: 1. One dimensional, vertical, unsteady, unsaturated flow above a recharging or discharging groundwater flow system, *Water Resources Research, 5(1)*, pp. 153-171, 1969.

Freeze, R.A., Three dimensional transient saturated-unsaturated flow in a groundwater basin, *Water Resources Research, 7(2)*, pp. 347-366, 1971.

Freeze, R.A., Role of subsurface flow in generating runoff: 1. Base flow contributions to channel flow, *Water Resources Research, 8(3)*, pp. 609-623, 1972a.

Freeze, R.A., Role of subsurface flow in generating runoff: 1. Upstream source areas, *Water Resources Research, 8(5)*, pp. 1272-1283, 1972b.

Freeze, R.A., and P.A. Witherspoon., Theoretical analysis of regional groundwater flow: 1. Analytical and numerical solutions to the mathematical model, *Water Resources Research, 2(4)*, pp. 641-656, 1966.

Freeze, R.A., and P.A. Witherspoon., Theoretical analysis of regional groundwater flow: 3. Quantitative interpretation, *Water Resources Research, 4(43*, pp. 581-590, 1968.

Freeze, R.A. and J.A. Cherry, *Groundwater*, -Hall, Inc., Englewood Cliffs, NJ, 1979

Gardner, W. R., Some steady state solutions of the unsaturated moisture flow equation with application to evaporation from a water table, *Soil Science, 85(4)*, pp. 228-232, 1958

Gardner, W.R., Solutions of the flow equations for the drying of soils and other porous media, *Soil Science Society Proceedings*, 183-187, 1959

Gleick, P.H., The development and testing of a water balance model for climate impact analysis: Modeling the Sacramento basin, *Water Resources Research, 23(6)*, pp. 1049-1061, 1987.

Gradshteyn, I. S. and I. M. Ryzhik, *Table of Integrals, Series, and Products,* Academic Press, Inc., New York, 1980

Green, W.H. and G.A. Ampt, Studies on soils physics: I. Flow of air and water through soils, *J. Agr. Sci., 4,* 1-24, 1911

Govindaraju, R.S. and M.L. Kavvas, Development of an approximate model for unsaturated flow with root water uptake under rectangular water content profiles assumptions, *Journal of Hydrology, 146,* 321-339, 1993.

Haverkamp, R. J.-Y Parlange, J.L. Starr, G.Scmhitz and C. Fuentes, Infiltration under ponded conditions: 3. A predictive equation based on physical parameters, *Soil Science, 149(5),* 292-300, 1990

Hawk, K.L. and P.S. Eagleson, *Climatology of station storm rainfall in the continental United States: Parameters of the Bartlett-Lewis and Poisson rectangular pulses models,* Mass. Inst. of Technol., Dept. of Civ, Eng., R.M. Parsons Lab Rept. No. 336, 1992

Helvey, J.D., J.D. Hewlett, and J.E. Douglas, Predicting soil moisture in the Southern Appalachians, *Proc. Soil Sci. Am., 36,* pp. 954-959, 1972

Hillel, D., *Applications of Soil Physics,* Academic Press, Inc., New York, 1980

Horton, R.E , Drainage-basin characteristics, *Eos Trans. A.G.U., 13,* pp. 350-361, 1932.

Jacob, C.E., Correlation of groundwater levels and precipitation on Long Island, N.Y.: Pt. 1, Theory, *Trans. A.G.U., 24,* pp. 564-573, 1943.

Kirkby, M.J., Implications for sediment transport, in *Hillslope Hydrology,* M.J. Kirkby (ed.), John Wiley and Sons, Ltd., New York, 1978.

Kuhnel, V., J.C.I. Dooge, J.P.J O'Kane, and R.J. Romanowicz, Partial analysis applied to scale problems in surface moisture fluxes, in *Landsurface-atmosphere interaction:*

observations, models and analysis, E. Wood (ed.), Kluwer Academic Publishers, Norwood MA, pp. 221-247, 1991.

Lettau, H., Evaporation climatonomy - A new approach to numerical prediction of monthly evapotranspiration, runoff, and soil moisture storage, *Monthly Weather Review, 97(10)*, pp. 691-699, 1969.

Lettau, H., and M.W. Baradas, Evaporation climatonomy: II: Refinement of parameterization, exemplified by application to the Mabacan watershed, *Monthly Weather Review, 101*, pp. 636-649, 1973.

Linsley, R.K. and J.B. Franzini, *Water Resources Engineering. Third Ed.*, McGraw-Hill Book Co., New York, 1979.

Macey, R.I., A quasi-steady -state approximation method for diffusion problems: I. Concentration dependent diffusion coefficients., *Bull. Math. Biophys. 21*, 19-32, 1959.

Miller, S.A. and P.S. Eagleson, Interaction of the saturated and unsaturated moisture zones 1. Analytic solutions of the linearized Richard's equation, 2. The role of climate in shaping the phreatic surface, *Mass. Inst. of Technol., Dept of Civ. Eng., R. M. Parsons Lab Rept. No.284* , 1982.

Milly, P.C.D., Moisture and heat transport in hysteritic, inhomogeneous porous media: A matric head-based formulation and a numerical model, *Water Resour. Res., 18(3)*, 489-498, 1982

Milly, P.C.D., An event-based simulation model of moisture and energy fluxes at a bare soil surface, *Water Resour. Res., 22(12)*, 1680-1692, 1986

Milly, P.C.D., Advances in modeling of water in the unsaturated zone,*Transport in Porous Media,3*, 491-514, 1988

Milly, P.C.D. and P.S. Eagleson, Infiltration and evaporation at inhomogeneous land surfaces, *Mass. Inst. of Technol.. Ralph M. Parsons Lab., Dep. of Civ. Eng.,R. M. Parsons Lab Rep. No. 278* , 1982.

Milly, P.C.D. and P.S. Eagleson, Effects of spatial variability on annual average water balance, *Water Resources Research, 23(11)*, pp. 2135-2142, 1987.

Moore. W.L. and C.W. Morgan, eds, *Effects of watershed changes on streamflow*, University of Texas Press, Austin, 1969

Montgomery, D.R., and W.E. Dietrich, Source areas, drainage density, and channel initiation, *Water Resources Research, 25(8)*, pp. 1907-1918, 1989.

Ol'dekop, E.M., Ob isparenii s poverkhonsti rechnykh basseinov, *Trans. Meteorol. Observ. Iurevskovo., Univ. Tartu, 4*, 1911.

Palmer, W.C., Meteorological drought, *Res. Pap. U.S. Weather Bur.,45*, 58 pp., 1965.

Parlange, J. -Y., Theory of water movement in soils: 2. One-dimensional infiltration, *Soil Science, 112*, 313-317, 1971.

Parlange, M.B., G.G. Katul, R.H. Cuenca, M. Levant Kavvas, D.R. Nielsen, and M. Mata., Physical basis for a time series model of soil water content, *Water Resources Research, 28(9)*, pp. 2437-2446, 1992.

Penman, H.L. Vegetation and hydrology, *Technical Communication No. 53*, Commonwealth Bureau of Soils, Harpenden, 1951.

Philip, J.R. An infiltration equation with physical significance, *Soil Science, 77*, 153-157, 1954.

Philip, J. R., Evaporation, moisture and heat fields in the soil, *Journal of Meteorology,14(1)*, 354-366, 1957a.

Philip, J.R., The theory of infiltration: 4. Sorptivity and algebraic infiltration equations, *Soil Science, 84*, 257-264, 1957b

Philip, J.R., The theory of infiltration: part 7, *Soil Science, 83*, 435-448, 1957c

Philip, J.R., Theory of infiltration, in Advances in Hydroscience, vol. 5, ed. Ven Te Chow, pp. 215-296 ,Academic Press, New York, 1969

Philip, J.R., Constant rainfall infiltration into bounded soil profiles, *Water Resour. Res., 27(12),* pp. 3265-3270, 1991.

Philip, J.R., Variable-head ponded infiltration under constant or variable rainfall, *Water Resour. Res., 29(7),* pp. 2155-2165, 1993

Pike, J.G., The estimation of annual runoff from meteorological data in a tropical climate, *J. Hydrol. 2*, pp. 116-123, 1964.

Pinker, R.T. and L.A. Corio, Estimating monthly water and energy budgets over the central U.S. Great Plains. Part I: Evapoclimatonomy model formulation, *Monthly Weather Review*, 115, pp. 1,140-1,152, 1987.

Poulovassilis, A. P. Kerkides, S. Elmaloglou, and I. Argyrokastritis, An investigation of the relation between ponded and constant flux rainfall infiltration, *Water Resour. Res., 27(7),* 1403-1409, 1991

Protopapas, A.L. and R.L Bras, The one-dimensional approximation for infiltration into heterogeneous soils, *Water Resources Research, 27(6)*, pp. 1019-1027, 1991a.

Protopapas, A.L. and R.L Bras, Analytic solutions for unsteady multidimensional infiltration in heterogeneous soils, *Water Resources Research, 27(6)*, pp. 1029-1034, 1991b.

Ramirez, J.A. and R.L. Bras, Conditional distributions of Neyman-Scott models for storm arrivals and their use in irrigation scheduling, *Water Resources Research, 21(3)*, pp. 317-330, 1985.

Reeves, M. and E.E. Miller, Estimating infiltration for erratic rainfall,*Water Resour. Res., 11(1)*, 102-110, 1975

Richards, L.A. Capillary conduction of liquids through porous mediums, *J. Phys. 1*, pp. 318-333, 1981.

Ripple, C. D., J. Rubin and T. E. A. van Hylckama, Estimating steady state evaporation rates from bare soils under conditions of high water table, *Geological Survey Water Supply Paper 2019A*, 1972

Rodriguez-Iturbe, I., D. Entekhabi, and R.L Bras, Nonlinear dynamics of soil moisture at climate scales, *Water Resources Research, 27(8)*, 1991.

Rodriguez-Iturbe, I., and J.B. Valdes, The geomorphic structure of hydrologic response, *Water Resources Research, 15(6)*, pp. 1407-1420, 1979.

Salvucci, G.D., An approximate solution for the steady vertical flux of moisture through an unsaturated homogeneous soil, *Water Resources Research, 29(11)*, pp. 3749-3753, 1993.

Salvucci, G.D. and P.S. Eagleson, A test of ecological optimality for semiarid vegetation, *Mass. Inst. of Technol., Dept of Civ. Eng., R. M. Parsons Lab Rept. No. 335*, 195 pp., 1992.

Schreiber, P.: 1904, Uber die Beziehungen zwischen dem niederschlag und der Wasserfuhrung der Flusse in Mitteleuropa, *Z. Meteorol., 21 (10)*, 1904.

Sherman, L.K., Comparison of F-curves derived by the method of Sharp and Holtan and of Sherman and Mayer, *Trans. Am. Gephys. Union, 24*, 465-467, 1943

Sivapalan, M., K.J. Beven, and E.F. Wood, On hydrologic similarity, 2, A scaled model of storm runoff production, *Water Resour. Res., 23(12)*, 2266-2278, 1987

Sivapalan, M., and P.C.D. Milly, On the relation between the time condensation approximation and the flux-concentration relation, *Journal of Hydrology,105*, 357-367, 1989

Smith, R.E. and R.H.B. Hebert, Mathematical simulation of interdependent surface and subsurface hydrologic processes, *Water Resour. Res., 19(4)*, 987-1001, 1983

Smith, R.E., C. Corradini and F. Melone, Modeling infiltration for multistorm runoff events, *Water Resour. Res., 29(1)*, 133-144, 1993

Srivastava, R., and T, -C. J. Yeh, Analytical solutions for one-dimensional, transient infiltration toward the water table in homogenous and layered soils, *Water Resources Research, 27(5),* 753-762, 1991

Stagnitti, F., J.Y. Parlange, T.S. Steenhius, M.B. Parlange, and C.W. Rose, A mathematical model of hillslope and watershed discharge, *Water Resources Research, 28(8)*, pp. 2,111-2,122, 1992.

Tarboton, D.G., R.L. Bras, and I. Rodriguez-Iturbe, Scaling and elevation in river networks, *Water Resources Research, 25(9)*, pp. 2037-2051, 1989.

Thomas, H.A., Improved methods for National Water Assessment, *report contract WR15249270, U.S. Water Resour. Council.*, Washington, D.C., 1981.

Thornthwaite, C.W., The moisture-factor in climate, *Trans. A.G.U., 27(1)*, pp. 41-48, February 1946.

Thornthwaite, C.W., An approach to the rational classification of climate, *Geogr. Rev., 38(1)*, pp. 55-94, 1948.

Thornthwaite, C.W., and J.R. Mather, The water balance, *Publ. Climatol. Lab. Climatol. Drexel Inst. Technol., 8(1)*, pp. 1-104, 1955.

Toth, J., A theory of groundwater motion in small drainage basins in central Alberta, *J. Geophys. Res., 67,* pp. 4375-4387, 1962.

Toth, J., A theoretical analysis of groundwater flow in small drainage basins, *J. Geophys. Res., 68,* pp. 4795-4812, 1963.

Toth, J., Mapping and interpretation of field phenomena for groundwater reconnaissance in a prairie environment, Alberta Canada., *Intern. Assoc. Sci. Hydrol. Bull., 11, No. 2,* pp. 1-49, 1966.

Troch, P.A., F.P. De Troch, and W. Brutsaert, Effective water table depth to describe initial conditions prior to storm rainfall in humid regions, *Water Resour. Res., 29(2),* 427-434, 1993

Van der Heijde, P.K.M., and O.A. Elnawawy, *Compilation of Ground-Water Models,* United States Environmental Protection Agency, Office of Research and Development, Oklahoma, 1993

Warrick, A.W. Analytical solutions to the one-dimensional linearized moisture flow equation for arbitrary input, *Soil Sci., 120(2)* , pp 79-84, 1975.

Warrick, A. W., Additional solutions for steady-state evaporation from a shallow water table, *Soil Sci., 146(2),* pp. 63-66, 1988.

Warrick, A. W. and T.-C. Jim Yeh, One-dimensional, steady vertical flow in a layered soil profile, *Adv. Water Resources, 13(4),* pp. 207-210, 1990

Warrick, A.W., A. Islas, and D.O. Lomen, Analytical solution to Richards equation for time-varying infiltration, *Water Resour. Res, 27(5),* pp. 763-766, 1991

Willgoose, G.R., R.L. Bras, and I. Rodriguez-Iturbe, A coupled channel network growth and hillslope evolution model, 1, theory, *Water Resources Research, 27(2)*, pp. 1671-1684, 1991.

Wood, E.F., M. Sivapalan, K. Beven, and L. Band, Effect of spatial variability and scale with implications to hydrologic modeling, *J. of Hydrol., 102*, pp. 29-47, 1988.

Yevjevich, V.M., Fluctuations of wet and dry years, I. Research data assembly and mathematical models, *Hydrol. Pap. 1*, 55 pp., Colo. State Univ., Fort Collins, 1963.

Zimmerman, R.W., and G.D. Bodvarsson, An approximate solution for the one-dimensional absorption in unsaturated porous media, *Water Resources Research, 25,* 1422-1428, 1989.

Zimmerman, R.W., and G.D. Bodvarsson, A simple approximate solution for horizontal infiltration in a Brooks-Corey medium, *Transport in Porous Media, 6,* 195-205, 1991